Electromagnetic Field Interaction with Transmission Lines

From Classical Theory to HF Radiation Effects

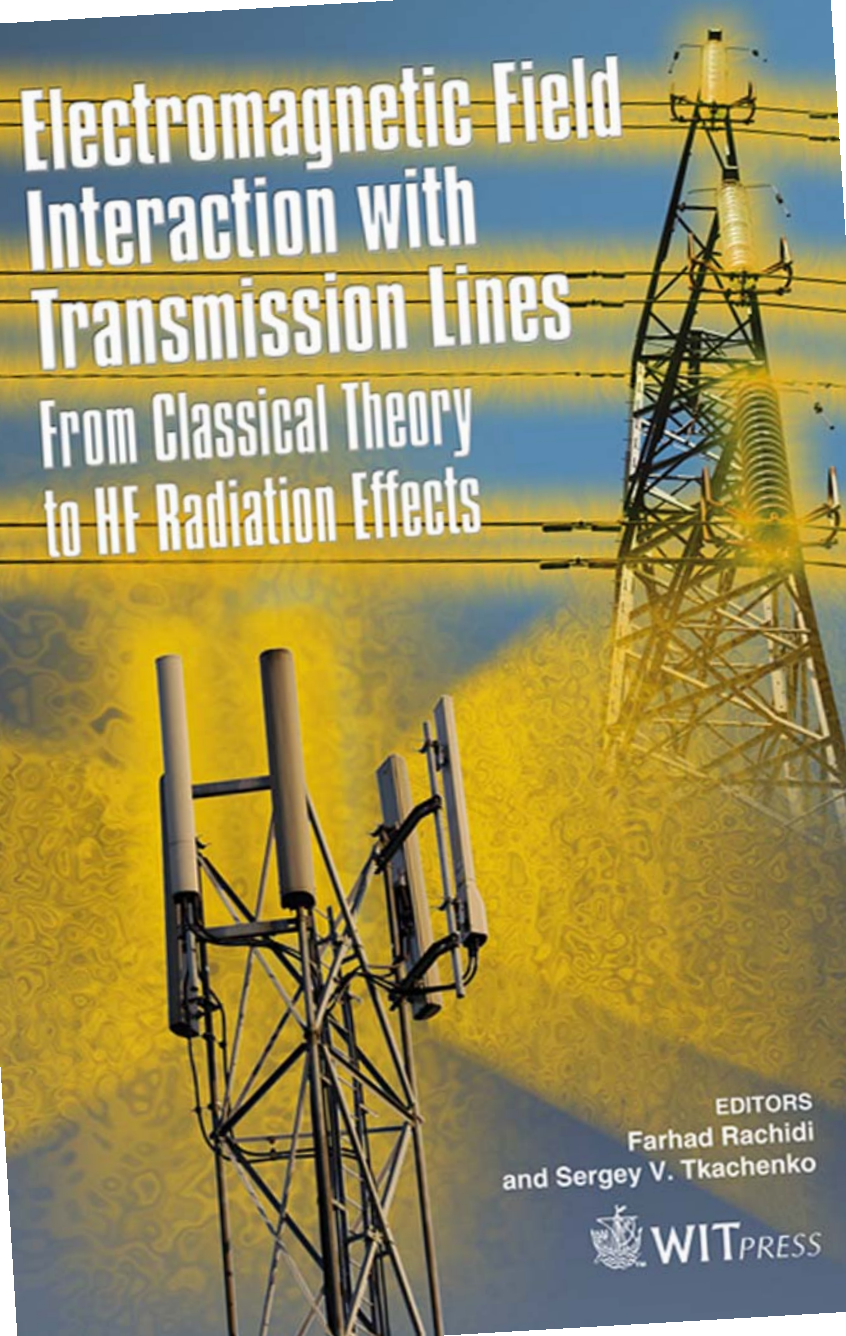

EDITORS
Farhad Rachidi
and Sergey V. Tkachenko

WIT PRESS

Electromagnetic Field Interaction with Transmission Lines

WIT*PRESS*

WIT Press publishes leading books in Science and Technology.
Visit our website for the current list of titles.
www.witpress.com

WIT*eLibrary*

Home of the Transactions of the Wessex Institute, the WIT electronic-library provides the international scientific community with immediate and permanent access to individual papers presented at WIT conferences. Visit the WIT eLibrary at
http://library.witpress.com

Advances in Electrical Engineering and Electromagnetics

Associate Editors

R. Belmans
Katholieke Universiteit Leuven
Belgium

A.R. Bretones
University of Granada
Spain

R. Gomez Martin
University of Granada
Spain

K. Hameyer
Katholieke Universiteit Leuven
Belgium

L. Haydock
Newage International Limited
UK

A. Konrad
University of Toronto
Canada

A. Kugi
Johannes Kepler University
Austria

F. Lattarulo
Politecnico di Bari
Italy

G. Manara
University of Pisa
Italy

E.K. Miller
Lincoln
USA

T. Miyoshi
Kobe University
Japan

O.A. Mohammed
Florida International University
USA

G. Molinari
University of Genoa
Italy

B. Notaros
University of Massachusetts
USA

G. Pelosi
University of Florence
Italy

D. Poljak
University of Split
Croatia

F. Rachidi
EMC Group
Switzerland

T. Rang
Tallinn Technical University
Estonia

B. Ribas
Ministry of Health
Spain

K. Richter
Graz University of Technology
Austria

V. Roje
University of Split
Croatia

S. Russenchuck
European Laboratory for Particle Physics
Switerland

H. Ryssel
Fraunhofer Institute for Integrated Circuits
Germany

A. Savini
Universita de Pavia
Italy

N. Takahashi
Okayama University
Japan

C.Y. Tham
Tunku Abdul Rahman University
Malaysia

A.G. Tijhuis
Technische Universiteit Eindhoven
The Netherlands

S. Tkachenko
Otto-von-Guericke-University of Magdeburg
Germany

T. Tsiboukis
Aristotle University of Thessaloniki
Greece

P. Vas
Unversity of Aberdeen
Scotland

S. Walker
Imperial College London
UK

K. Zakrzewski
Politechnika Lodzka
Poland

This page intentionally left blank

Electromagnetic Field Interaction with Transmission Lines

From classical theory to HF radiation effects

Edited by

F Rachidi & S Tkachenko

WIT*PRESS* Southampton, Boston

Editors:

F. Rachidi
Swiss Federal Institute of Technology, Switzerland

S.V. Tkachenko
Otto-von-Guericke-University, Germany

Published by

WIT Press
Ashurst Lodge, Ashurst, Southampton, SO40 7AA, UK
Tel: 44 (0) 238 029 3223; Fax: 44 (0) 238 029 2853 E-Mail: witpress@witpress.com http://www.witpress.com

For USA, Canada and Mexico

WIT Press
25 Bridge Street, Billerica, MA 01821,
USA Tel: 978 667 5841; Fax: 978 667 7582 E-Mail: infousa@witpress.com
http://www.witpress.com

British Library Cataloguing-in-Publication Data

A Catalogue record for this book is available from the British Library

ISBN: 978-1-84564-063-7
ISSN: 1742-3783

Library of Congress Catalog Card Number: 2007922339

The texts of the papers in this volume were set individually by the authors or under their supervision.

No responsibility is assumed by the Publisher, the Editors and Authors for any injury and/ or damage to persons or property as a matter of products liability, negligence or otherwise, or from any use or operation of any methods, products, instructions or ideas contained in the material herein. The Publisher does not necessarily endorse the ideas held, or views expressed by the Editors or Authors of the material contained in its publications.

© WIT Press 2008

Printed in Great Britain by Athenaeum Press Ltd.

All rights reserved. No part of this publication may be reproduced, stored in a retrieval system, or transmitted in any form or by any means, electronic, mechanical, photocopying, recording, or otherwise, without the prior written permission of the Publisher.

To Mojgan

To Victoria, Natalie and Anna

This page intentionally left blank

Contents

Chapter 2
Surge propagation and crosstalk in multiconductor transmission lines above ground 23
Nelson Theethayi & Rajeev Thottappillil

This page intentionally left blank

Preface

The evaluation of electromagnetic field coupling to transmission lines is an important problem in electromagnetic compatibility. Customarily, use is made of the transmission line (TL) approximation which applies to uniform transmission lines with electrically-small cross-sectional dimensions, where the dominant mode of propagation is transverse electromagnetic (TEM). Antenna-mode currents and higher-order modes appearing at higher frequencies are neglected in the classical TL theory.

Since the development of the TL theory and the derivation of the so-called telegrapher's equations by Oliver Heaviside in the late 19th century, significant progress has been achieved in the understanding of wave propagation along transmission lines. In 1965, Taylor, Satterwhite and Harrison extended the classical TL equations to include the presence of an external electromagnetic field. Their field-to-transmission coupling equations – as well as their equivalent formulations derived later – have been successfully applied to solve a large range of problems dealing with EMP and lightning interaction with power and telecommunication lines.

The unabated increase in the operating frequency of electronic products and the emergence of sources of disturbances with higher frequency content (such as High Power Microwave and Ultra-Wide Band systems) have led to a breakdown of the TL approximation's basic assumptions for a number of applications. In the last decade or so, the generalization of the TL theory to take into account high frequency effects has emerged as an important topic of study in electromagnetic compatibility. This effort resulted in the elaboration of the so-called 'generalized' or 'full-wave' TL theory, which incorporates high frequency radiation effects, while keeping the relative simplicity of TL equations.

This book covers both the classical transmission line theory as well as its recent enhancements. It is intended for graduate students, researchers and engineers interested in the transmission line theory and electromagnetic field interaction with transmission lines, with special emphasis on high frequency effects. The text is organized in two main parts containing a total of seven chapters.

Part I presents the consolidated knowledge of classical transmission line theory and different field-to-transmission line coupling models.

Chapter 1 discusses the assumptions of the TL theory and presents the derivation of the field-to-transmission line coupling equations. Three different but

completely equivalent approaches that have been proposed to describe the coupling of electromagnetic field coupling to transmission lines are also presented and discussed. Chapters 2 and 3, deal, respectively, with the specific cases of overhead multiconductor lines and buried cables. Various factors influencing the pulse propagation and crosstalk along multiconductor systems are discussed, and methods for the calculation of the line longitudinal and transverse line parameters are presented.

Part II presents different approaches developed to generalize the TL theory in order to include high frequency effects.

In Chapter 4, a TL-like pair of equations is derived under the thin-wire approximation for evaluating currents and potentials induced by external electromagnetic fields on a wire of a given geometric form above a perfect conducting ground. Based on perturbation theory, an iterative procedure is proposed to solve the derived coupling equations, where the zero-iteration term is determined by using the classical TL approximation. Chapter 5 presents an efficient hybrid method to compute high frequency electromagnetic field coupling to long, loaded lines including lumped discontinuities. Chapter 6 shows that the classical TL theory may be included in a more general model based on an integral formulation of the general full-wave problem. The derived general model is applied to conventional high-speed microelectronics, as well as to nanoelectronics applications. Chapter 7 deals specifically with high frequency electromagnetic field coupling to buried wires. Two approaches, one in the frequency domain based on the Pocklington's integral equation, and the other in the time domain using the Hallen integral equation, are proposed and discussed.

Although the chapters follow a logical order and a novice reader is advised to read the book sequentially, an effort has been made to make each chapter as independent of the others as possible. Therefore, readers interested in a particular aspect of the subject dealt with in one chapter do not need to consult other chapters of the book.

This book is the result of the authors' activities in the area of electromagnetic field-to-transmission line interactions. The authors are indebted to many individuals for their support, advice, and guidance. Special thanks are due to Michel Ianoz, Juergen Nitsch and Fred M. Tesche, and to all the authors of the chapters for their precious contributions.

Farhad Rachidi and Sergei Tkachenko

PART I

Classical Transmission Line Theory

This page intentionally left blank

CHAPTER 1

Derivation of telegrapher's equations and field-to-transmission line interaction

C.A. Nucci[1], F. Rachidi[2] & M. Rubinstein[3]
[1]*University of Bologna, Bologna, Italy.*
[2]*Swiss Federal Institute of Technology, Lausanne, Switzerland.*
[3]*Western University of Applied Sciences, Yverdon, Switzerland.*

Abstract

In this chapter, we discuss the transmission line theory and its application to the problem of external electromagnetic field coupling to transmission lines. After a short discussion on the underlying assumptions of the transmission line theory, we start with the derivation of field-to-transmission line coupling equations for the case of a single wire line above a perfectly conducting ground. We also describe three seemingly different but completely equivalent approaches that have been proposed to describe the coupling of electromagnetic fields to transmission lines. The derived equations are extended to deal with the presence of losses and multiple conductors. The time-domain representation of field-to-transmission line coupling equations, which allows a straightforward treatment of non-linear phenomena as well as the variation in the line topology, is also described. Finally, solution methods in frequency domain and time domain are presented.

1 Transmission line approximation

The problem of an external electromagnetic field coupling to an overhead line can be solved using a number of approaches. One such approach makes use of antenna theory, a general methodology based on Maxwell's equations [1]. Different methods based on this approach generally use the thin-wire approximation, in which the wire's cross section is assumed to be much smaller than the minimum significant wavelength.

When electrically long lines are involved, however, the antenna theory approach requires prohibitively long computational times and high computer resources. On the

other hand, the less resource hungry quasi-static approximation [1], in which propagation is neglected and coupling is described by means of lumped elements, can be adopted only when the overall dimensions of the circuit are smaller than the minimum significant wavelength of the electromagnetic field. For many practical cases, however, this condition is not satisfied. As an example, let us consider the case of power lines illuminated by a lightning electromagnetic pulse (LEMP). Power networks extend, in general, over distances of several kilometers, much larger than the minimum wavelengths associated with LEMP. Indeed, significant portions of the frequency spectrum of LEMP extend to frequencies up to a few MHz and beyond, which corresponds to minimum wavelengths of about 100 m or less [2].

A third approach is known as transmission line theory. The main assumptions for this approach are as follows:

1. Propagation occurs along the line axis.
2. The sum of the line currents at any cross section of the line is zero. In other words, the ground – the reference conductor – is the return path for the currents in the n overhead conductors.
3. The response of the line to the coupled electromagnetic fields is quasi-transverse electromagnetic (quasi-TEM) or, in other words, the electromagnetic field produced by the electric charges and currents along the line is confined in the transverse plane and perpendicular to the line axis.

If the cross-sectional dimensions of the line are electrically small, propagation can indeed be assumed to occur essentially along the line axis only and the first assumption can be considered to be a good approximation.

The second condition is satisfied if the ground plane exhibits infinite conductivity since, in that case, the currents and voltages can be obtained making use of the method of images, which guarantees currents of equal amplitude and opposite direction in the ground.

The condition that the response of the line is quasi-TEM is satisfied only up to a threshold frequency above which higher-order modes begin to appear [1]. For some cases, such as infinite parallel plates or coaxial lines, it is possible to derive an exact expression for the cutoff frequency below which only the TEM mode exists [3]. For other line structures (i.e. multiple conductors above a ground plane), the TEM mode response is generally satisfied as long as the line cross section is electrically small [3].

Under these conditions, the line can be represented by a distributed-parameter structure along its axis.

For uniform transmission lines with electrically small cross-sectional dimensions (not exceeding about one-tenth of the minimum significant wavelength of the exciting electromagnetic field), a number of theoretical and experimental studies have shown a fairly good agreement between results obtained using the transmission line approximation and results obtained either by means of antenna theory or experiments [4]. A detailed discussion of the validity of the basic assumptions of the transmission line theory is beyond the scope of this chapter. However, it is worth noting that, by assuming that the sum of all the currents is equal to zero, we are

considering only 'transmission line mode' currents and neglecting the so-called 'antenna-mode' currents [1]. If we wish to compute the load responses of the line, this assumption is adequate, because the antenna mode current response is small near the ends of the line. Along the line, however, and even for electrically small line cross sections, the presence of antenna-mode currents implies that the sum of the currents at a cross section is not necessarily equal to zero [1, 3]. However, the quasi-symmetry due to the presence of the ground plane results in a very small contribution of antenna mode currents and, consequently, the predominant mode on the line will be transmission line [1].

2 Single-wire line above a perfectly conducting ground

We will consider first the case of a lossless single-wire line above a perfectly conducting ground. This simple case will allow us to introduce various coupling models and to discuss a number of concepts essential to the understanding of the electromagnetic field coupling phenomenon. Later in this chapter (Sections 4 and 5), we will cover the cases of lossy and multiconductor lines. The transmission line is defined by its geometrical parameters (wire radius a and height above ground h) and its terminations Z_A and Z_B, as illustrated in Fig. 1, where the line is illuminated by an external electromagnetic field. The problem of interest is the calculation of the induced voltages and currents along the line and at the terminations.

The external exciting electric and magnetic fields $\vec{E}^e$ and $\vec{B}^e$ are defined as the sum of the incident fields, $\vec{E}^i$ and $\vec{B}^i$, and the ground-reflected fields, $\vec{E}^r$ and $\vec{B}^r$, determined in absence of the line conductor. The total fields $\vec{E}$ and $\vec{B}$ at a given point in space are given by the sum of the excitation fields and the scattered fields from the line, the latter being denoted as $\vec{E}^s$ and $\vec{B}^s$. The scattered fields are created by the currents and charges flowing in the line conductor and by the corresponding currents and charges induced in the ground.

Three seemingly different but completely equivalent approaches have been proposed to describe the coupling of electromagnetic fields to transmission lines. In what

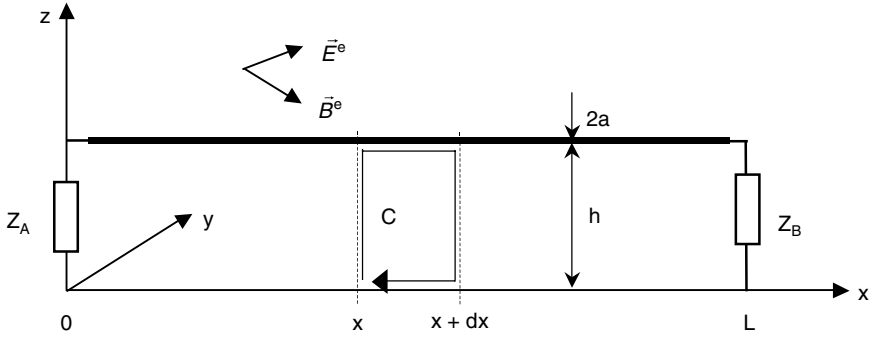

Figure 1: Geometry of the problem.

follows, we will present each one of them in turn. We will first derive the field-to-transmission line coupling equations (which are sometimes referred to as generalized telegrapher's equations) following the development of Taylor *et al.* [5].

2.1 Taylor, Satterwhite and Harrison model

2.1.1 Derivation of the first field-to-transmission line coupling (generalized telegrapher's) equation

Consider the single conductor transmission line of height h in Fig. 1. Applying Stokes' theorem to Maxwell's equation $\nabla\vec{E} = -j\omega\vec{B}$ for the area enclosed by the closed contour C yields

$$\oint_{\mathrm{C}} \vec{E}\cdot \mathrm{d}\vec{l} = -j\omega \iint_{S} \vec{B}\cdot\vec{e}_y \mathrm{d}S \tag{1}$$

Since the contour has a differential width Δx, eqn (1) can be written as

$$\int_0^h [E_z(x+\Delta x,z) - E_z(x,z)]\,\mathrm{d}z + \int_x^{x+\Delta x} [E_x(x,h) - E_x(x,0)]\,\mathrm{d}x = -j\omega \int_0^h \int_x^{x+\Delta x} B_y(x,z)\,\mathrm{d}x\,\mathrm{d}z \tag{2}$$

(The coordinate y will be implicitly assumed to be 0 and, for the sake of clarity, we will omit the y-dependence unless the explicit inclusion is important for the discussion.) Dividing by Δx and taking the limit as Δx approaches zero yields

$$\frac{\partial}{\partial x}\int_0^h E_z(x,z)\,\mathrm{d}z + E_x(x,h) - E_x(x,0) = -j\omega \int_0^h B_y(x,z)\,\mathrm{d}z \tag{3}$$

Since the wire and the ground are assumed to be perfect conductors, the total tangential electric fields at their respective surfaces, $E_x(x,h)$ and $E_x(x,0)$, are zero. Defining also the total transverse voltage $V(x)$ in the quasi-static sense (since $h << \lambda$) as

$$V(x) = -\int_0^h E_z(x,z)\,\mathrm{d}z \tag{4}$$

Equation (3) becomes

$$\frac{\mathrm{d}V(x)}{\mathrm{d}x} = -j\omega \int_0^h B_y(x,z)\,\mathrm{d}z = -j\omega \int_0^h B_y^{\mathrm{e}}(x,z)\,\mathrm{d}z - j\omega \int_0^h B_y^{\mathrm{s}}(x,z)\,\mathrm{d}z \tag{5}$$

where we have decomposed the B-field into the excitation and scattered components.

The last integral in eqn (5) represents the magnetic flux between the conductor and the ground produced by the current $I(x)$ flowing in the conductor.

Now, Ampère–Maxwell's equation in integral form is given by

$$\oint_{C'} \vec{B}^{\mathrm{s}} \cdot \mathrm{d}\vec{l} = I + j\omega \iint \vec{D} \cdot \mathrm{d}\vec{s} \tag{6}$$

If we define a path C' in the transverse plane defined by a constant x in such a manner that the conductor goes through it, eqn (6) can be rewritten as

$$\oint_{C'} \vec{B}^{\mathrm{s}}_{\mathrm{T}}(x,y,z) \cdot \mathrm{d}\vec{l} = I(x) + j\omega \iint \vec{D}_x(x,y,z) \cdot \vec{a}_x \, \mathrm{d}s \tag{7}$$

where the subscript T is used to indicate that the field is in the transverse direction, $\vec{a}_x$ is the unit vector in the x direction, and where we have explicitly included the dependence of the fields on the three Cartesian coordinates.

If the response of the wire is TEM, the electric flux density D in the x direction is zero and eqn (7) can be written as

$$\oint_{C'} \vec{B}^{\mathrm{s}}_{\mathrm{T}}(x,y,z) \cdot \mathrm{d}\vec{l} = I(x) \tag{8}$$

Clearly, $I(x)$ is the only source of $\vec{B}^{\mathrm{s}}_{\mathrm{T}}(x,y,z)$. Further, it is apparent from eqn (8) that $\vec{B}^{\mathrm{s}}_{\mathrm{T}}(x,y,z)$ is directly proportional to $I(x)$. Indeed, if $I(x)$ is multiplied by a constant multiplicative factor which, in general, can be complex, $\vec{B}^{\mathrm{s}}_{\mathrm{T}}(x)$ too will be multiplied by that factor. Further, the proportionality factor for a uniform cross-section line must be independent of x.

Let us now concentrate on the y component of $\vec{B}^{\mathrm{s}}_{\mathrm{T}}(x,y,z)$ for points in the plane $y = 0$. Using the facts we just established that $I(x)$ and $\vec{B}^{\mathrm{s}}_{\mathrm{T}}(x)$ are proportional and that the proportionality factor is independent of x, we can now write

$$B^{\mathrm{s}}_y(x, y = 0, z) = k(y = 0, z) I(x) \tag{9}$$

where $k(y, z)$ is the proportionality constant.

With this result, we now go back to the last integral in eqn (5),

$$\int_0^h B^{\mathrm{s}}_y(x,z) \, \mathrm{d}z$$

Note that, although the value of y is not explicitly given, $y = 0$. The integral represents the per-unit-length magnetic flux under the line. Substituting eqn (9) into it, we obtain

$$\int_0^h B^{\mathrm{s}}_y(x,z) \, \mathrm{d}z = \int_0^h k(y = 0, z) I(x) \, \mathrm{d}z \tag{10}$$

We can rewrite eqn (10) as follows

$$\int_0^h B_y^{\mathrm{s}}(x,z)\,\mathrm{d}z = I(x)\int_0^h k(y=0,z)\,\mathrm{d}z \tag{11}$$

Equation (11) implies that the per-unit-length scattered magnetic flux under the line at any point along it is proportional to the current at that point. The proportionality constant, given by $\int_0^h k(y=0,z)\mathrm{d}z$, is the per-unit-length inductance of the line L'.

This results in the well-known linear relationship between the magnetic flux and the line current:

$$\int_0^h B_y^{\mathrm{s}}(x,z)\mathrm{d}z = L'I(x) \tag{12}$$

Assuming that the radius of the wire is much smaller than the height of the line ($a << h$), the magnetic flux density can be calculated using Ampere's law and the integral can be evaluated analytically, yielding $L' \cong (\mu_0/2\pi)\ln(2h/a)$ [1].

Inserting eqn (12) into eqn (5), we obtain the first generalized telegrapher's equation

$$\frac{\mathrm{d}V(x)}{\mathrm{d}x} + j\omega L'I(x) = -j\omega\int_0^h B_y^{\mathrm{e}}(x,z)\,\mathrm{d}z \tag{13}$$

Note that, unlike the classical telegrapher's equations in which no external excitation is considered, the presence of an external field results in a forcing function expressed in terms of the exciting magnetic flux. This forcing function can be viewed as a distributed voltage source along the line.

Attention must be paid to the fact that the voltage $V(x)$ in eqn (13) depends on the integration path since it is obtained by integration of an electric field whose curl is not necessarily zero (eqn (4)).

2.1.2 Derivation of the second field-to-transmission line coupling equation

To derive the second telegrapher's equation, we will assume that the medium surrounding the line is air ($\varepsilon = \varepsilon_0$) and we will start from the second Maxwell's equation, $\nabla \times \vec{H} = \vec{J} + j\omega\varepsilon_0\vec{E}$, also called Ampère–Maxwell's equation. Rearranging the terms and writing it in Cartesian coordinates for the z-component:

$$j\omega E_z(x,z) = \frac{1}{\varepsilon_0\mu_0}\left[\frac{\partial B_y(x,z)}{\partial x} - \frac{\partial B_x(x,z)}{\partial y}\right] - \frac{J_z}{\varepsilon_0} \tag{14}$$

The current density can be related to the E-field using Ohm's law, $\vec{J} = \sigma_{\mathrm{air}}\vec{E}$, where σ_{air} is the air conductivity. Since the air conductivity is generally low, we

will assume here that $\sigma_{air} = 0$ and will therefore neglect this term (which will eventually result in an equivalent parallel conductance in the coupling equation (see Section 5)).

Integrating eqn (14) along the z axis from 0 to h, and making use of eqn (4), we obtain

$$-j\omega V(x) = \frac{1}{\varepsilon_0\mu_0}\int_0^h \left[\frac{\partial B_y^{\mathrm{e}}(x,z)}{\partial x} - \frac{\partial B_x^{\mathrm{e}}(x,z)}{\partial y}\right] \mathrm{d}z + \frac{1}{\varepsilon_0\mu_0}\int_0^h \left[\frac{\partial B_y^{\mathrm{s}}(x,z)}{\partial x} - \frac{\partial B_x^{\mathrm{s}}(x,z)}{\partial y}\right] \mathrm{d}z \tag{15}$$

in which we have decomposed the magnetic flux density field into the excitation and scattered components.

Since the excitation fields are the fields that would exist if the line were not present, they must satisfy Maxwell's equations. Applying Maxwell's equation (14) to the components of the excitation electromagnetic field and integrating along z from 0 to h directly under the line yields

$$\frac{1}{\varepsilon_0\mu_0}\int_0^h \left[\frac{\partial B_y^{\mathrm{e}}}{\partial x} - \frac{\partial B_x^{\mathrm{e}}}{\partial y}\right] \mathrm{d}z = j\omega \int_0^h E_z^{\mathrm{e}}\, \mathrm{d}z \tag{16}$$

Using eqns (12) and (16) and given that the line response is assumed to be TEM, $B_x^{\mathrm{s}} = 0$, eqn (15) becomes

$$\frac{\mathrm{d}I(x)}{\mathrm{d}x} + j\omega C' V(x) = -j\omega C' \int_0^h E_z^{\mathrm{e}}(x,z)\, \mathrm{d}z \tag{17}$$

where C' is the per-unit-length line capacitance related to the per-unit-length inductance through $\varepsilon_0\mu_0 = L'C'$. Equation (17) is the second field-to-transmission line coupling equation.

For a line of finite length, such as the one represented in Fig. 1, the boundary conditions for the load currents and voltages must be enforced. They are simply given by

$$V(0) = -Z_{\mathrm{A}} I(0) \tag{18}$$

$$V(L) = Z_{\mathrm{B}} I(L) \tag{19}$$

2.1.3 Equivalent circuit

Equations (13) and (17) are referred to as the *Taylor* model. They can be represented using an equivalent circuit, as shown in Fig. 2. The forcing functions (source

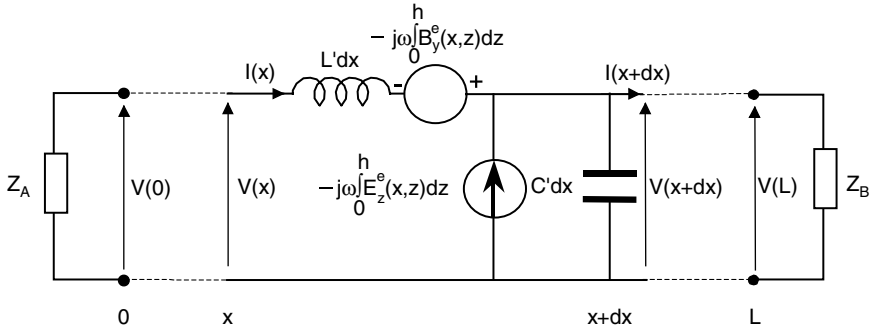

Figure 2: Equivalent circuit of a lossless single-wire overhead line excited by an electromagnetic field (Taylor *et al.* model).

terms) in eqns (13) and (17) are included as a set of distributed series voltage and parallel current sources along the line.

2.2 Agrawal, Price and Gurbaxani model

An equivalent formulation of the field-to-transmission line coupling equations was proposed in 1980 by Agrawal *et al.* [6]. This model is commonly referred to as the Agrawal model. We will call it the *model of Agrawal et al.* hereafter.

The basis for the derivation of the Agrawal *et al.* model can be described as follows: The excitation fields produce a line response that is TEM. This response is expressed in terms of a scattered voltage $V^{\mathrm{s}}(x)$, which is defined in terms of the line integral of the scattered electric field from the ground to the line, and the total current $I(x)$.

The total voltage can be obtained from the scattered voltage through

$$V(x) = V^{\mathrm{s}}(x) + V^{\mathrm{e}}(x) = V^{\mathrm{s}}(x) - \int_0^h E_z^{\mathrm{e}}(x,z)\,\mathrm{d}z \tag{20}$$

The field-to-transmission line coupling equations as derived by Agrawal *et al.* [6] are given by

$$\frac{\mathrm{d}V^{\mathrm{s}}(x)}{\mathrm{d}x} + j\omega L' I(x) = E_x^{\mathrm{e}}(x,h) \tag{21}$$

$$\frac{\mathrm{d}I(x)}{\mathrm{d}x} + j\omega C' V^{\mathrm{s}}(x) = 0 \tag{22}$$

Note that, in this model, only one source term is present (in the first equation) and it is simply expressed in terms of the exciting electric field tangential to the line conductor $E_x^{\mathrm{e}}(x,h)$.

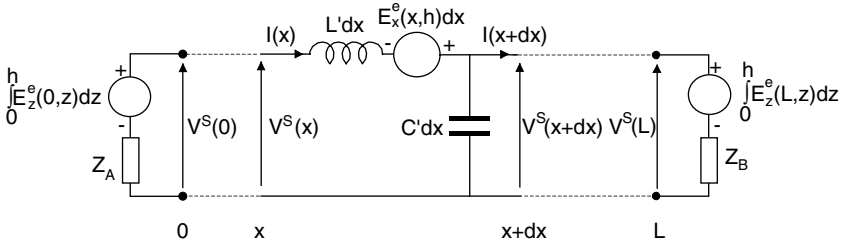

Figure 3: Equivalent circuit of a lossless single-wire overhead line excited by an electromagnetic field (Agrawal *et al.* model).

The boundary conditions in terms of the scattered voltage and the total current as used in eqns (21) and (22), are given by

$$V^{\mathrm{s}}(0) = -Z_{\mathrm{A}} I(0) + \int_0^h E_z^{\mathrm{e}}(0,z)\,\mathrm{d}z \tag{23}$$

$$V^{\mathrm{s}}(L) = Z_{\mathrm{B}} I(L) + \int_0^h E_z^{\mathrm{e}}(L,z)\,\mathrm{d}z \tag{24}$$

The equivalent circuit representation of this model (eqns (21)–(24)) is shown in Fig. 3. For this model, the forcing function (the exciting electric field tangential to the line conductor) is represented by distributed voltage sources along the line. In accordance with boundary conditions (23) and (24), two lumped voltage sources (equal to the line integral of the exciting vertical electric field) are inserted at the line terminations.

It is also interesting to note that this model involves only electric field components of the exciting field and the exciting magnetic field does not appear explicitly as a source term in the coupling equations. As we will see in the next section where we present the Rachidi model [7], it is also possible to represent the coupling model in terms of magnetic fields only.

2.3 Rachidi model

Another form of the coupling equations, equivalent to the Agrawal *et al.* and to the Taylor *et al.* models, has been derived by Rachidi [7]. In this model, only the exciting magnetic field components appear explicitly as forcing functions in the equations:

$$\frac{\mathrm{d}V(x)}{\mathrm{d}x} + j\omega L' I^{\mathrm{s}}(x) = 0 \tag{25}$$

$$\frac{dI^{s}(x)}{dx} + j\omega C' V(x) = \frac{1}{L'}\int_{0}^{h} \frac{\partial B_x^{e}(x,z)}{\partial y}\,dz \tag{26}$$

in which $I^{s}(x)$ is the so-called scattered current related to the total current by

$$I(x) = I^{s}(x) + I^{e}(x) \tag{27}$$

where the excitation current $I^{e}(x)$ is defined as

$$I^{e}(x) = -\frac{1}{L'}\int_{0}^{h} B_y^{e}(x,z)\,dz \tag{28}$$

The boundary conditions corresponding to this formulation are

$$I^{s}(0) = -\frac{V(0)}{Z_A} + \frac{1}{L'}\int_{0}^{h} B_y^{e}(0,z)\,dz \tag{29}$$

$$I^{s}(L) = \frac{V(L)}{Z_B} + \frac{1}{L'}\int_{0}^{h} B_y^{e}(L,z)\,dz \tag{30}$$

The equivalent circuit corresponding to the above equivalent set of coupling equations is shown in Fig. 4. Note that the equivalent circuit associated with the Rachidi model could be seen as the dual circuit – in the sense of electrical network theory – of the one corresponding to the Agrawal *et al.* model (Fig. 3).

3 Contribution of the different electromagnetic field components

Nucci and Rachidi [8] have shown, on the basis of a specific numerical example that, as predicted theoretically, the total induced voltage waveforms obtained using the three coupling models presented in Sections 2.1–2.3 are identical. However,

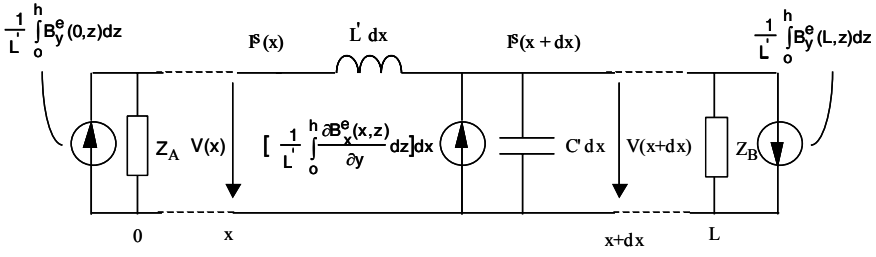

Figure 4: Equivalent circuit of a lossless single-wire overhead line excited by an electromagnetic field (Rachidi model).

the contribution of a given component of the exciting electromagnetic field to the total induced voltage and current varies depending on the adopted coupling model. Indeed, the three coupling models are different but fully equivalent approaches that predict identical results in terms of total voltages and total currents, in spite of the fact that they take into account the electromagnetic coupling in different ways. In other words, the three models are different expressions of the same equations, cast in terms of different combinations of the various electromagnetic field components, which are related through Maxwell's equations.

4 Inclusion of losses

In the calculation of lightning-induced voltages, losses are, in principle, to be taken into account both in the wire and in the ground. Losses due to the finite ground conductivity are the most important ones, and they affect both the electromagnetic field and the surge propagation along the line [9].

Let us make reference to the same geometry of Fig. 1, and let us now take into account losses both in the wire and in the ground plane. The wire conductivity and relative permittivity are σ_w and ε_{rw}, respectively, and the ground, assumed to be homogeneous, is characterized by its conductivity σ_g and its relative permittivity ε_{rg}. The Agrawal *et al.* coupling equations extended to the present case of a wire above an imperfectly conducting ground can be written as (for a step by step derivation see [1])

$$\frac{\mathrm{d}V^{\mathrm{s}}(x)}{\mathrm{d}x} + Z'I(x) = E_x^{\mathrm{e}}(x,h) \tag{31}$$

$$\frac{\mathrm{d}I(x)}{\mathrm{d}x} + Y'V^{\mathrm{s}}(x) = 0 \tag{32}$$

where Z' and Y' are the longitudinal and transverse per-unit-length impedance and admittance respectively, given by [1, 9] (in [1], the per-unit-length transverse conductance has been disregarded)

$$Z' = j\omega L' + Z'_{\mathrm{w}} + Z'_{\mathrm{g}} \tag{33}$$

$$Y' = \frac{(G' + j\omega C')Y'_{\mathrm{g}}}{G' + j\omega C' + Y'_{\mathrm{g}}} \tag{34}$$

in which

- L', C' and G' are the per-unit-length longitudinal inductance, transverse capacitance and transverse conductance, respectively, calculated for a lossless wire above a perfectly conducting ground:

$$L' = \frac{\mu_0}{2\pi}\cosh^{-1}\left(\frac{h}{a}\right) \cong \frac{\mu_0}{2\pi}\ln\left(\frac{2h}{a}\right) \quad \text{for } h >> a \tag{35}$$

$$C' = \frac{2\pi\varepsilon_0}{\cosh^{-1}(h/a)} \cong \frac{2\pi\varepsilon_0}{\ln(2h/a)} \quad \text{for } h >> a \tag{36}$$

$$G' = \frac{\sigma_{\text{air}}}{\varepsilon_0} C' \tag{37}$$

- Z'_{w} is the per-unit-length internal impedance of the wire; assuming a round wire and an axial symmetry for the current, the following expression can be derived for the wire internal impedance [10]:

$$Z'_{\text{w}} = \frac{\gamma_{\text{w}} \text{I}_0(\gamma_{\text{w}} a)}{2\pi a \sigma_{\text{w}} \text{I}_1(\gamma_{\text{w}} a)} \tag{38}$$

  where $\gamma_{\text{w}} = \sqrt{j\omega\mu_0(\sigma_{\text{w}} + j\omega\varepsilon_0\varepsilon_{\text{rw}})}$ is the propagation constant in the wire and I_0 and I_1 are the modified Bessel functions of zero and first order, respectively;
- Z'_{g} is the per-unit-length ground impedance, which is defined as [11, 12]

$$Z'_{\text{g}} = \frac{j\omega \int_{-\infty}^{h} B_y^{\text{s}}(x,z)\,\text{d}x}{I} - j\omega L' \tag{39}$$

  where B_y^{s} is the y-component of the scattered magnetic induction field.

Several expressions for the ground impedance have been proposed in the literature ([13], see also Chapter 2). Sunde [14] derived a general expression for the ground impedance which is given by

$$Z'_{\text{g}} = \frac{j\omega\mu_0}{\pi} \int_0^{\infty} \frac{\text{e}^{-2hx}}{\sqrt{x^2 + \gamma_{\text{g}}^2} + x}\,\text{d}x \tag{40}$$

where $\gamma_{\text{g}} = \sqrt{j\omega\mu_0(\sigma_{\text{g}} + j\omega\varepsilon_0\varepsilon_{\text{rg}})}$ is the propagation constant in the ground.

As noted in [13], Sunde's expression (40) is directly connected to the general expressions obtained from scattering theory. Indeed, it is shown in [1] that the general expression for the ground impedance derived using scattering theory reduces to the Sunde approximation when considering the transmission line approximation. Also, the results obtained using eqn (40) are shown to be accurate within the limits of the transmission line approximation [1].

The general expression (40) is not suitable for a numerical evaluation since it involves an integral over an infinitely long interval. Several approximations for the ground impedance of a single-wire line have been proposed in the literature (see [11] for a survey). One of the simplest and most accurate was proposed by Sunde himself and is given by the following logarithmic function:

$$Z'_{\text{g}} \cong \frac{j\omega\mu_0}{2\pi} \ln\left(\frac{1+\gamma_{\text{g}} h}{\gamma_{\text{g}} h}\right) \tag{41}$$

It has been shown [11] that the above logarithmic expression represents an excellent approximation to the general expression (40) over the frequency range of interest.

Finally, Y'_g is the so-called ground admittance, given by [1]

$$Y'_g \cong \frac{\gamma_g^2}{Z'_g} \tag{42}$$

5 Case of multiconductor lines

Making reference to the geometry of Fig. 5, the field-to-transmission line coupling equations for the case of a multi-wire system along the x-axis above an imperfectly conducting ground and in the presence of an external electromagnetic excitation are given by [1, 4, 15]

$$\frac{\mathrm{d}}{\mathrm{d}x}[V_i^s(x)] + j\omega[L'_{ij}][I_i(x)] + \left[Z'_{g_{ij}}\right][I_i(x)] = [E_x^e(x,h_i)] \tag{43}$$

$$\frac{\mathrm{d}}{\mathrm{d}x}[I_i(x)] + [G'_{ij}][V_i^s(x)] + j\omega[C'_{ij}][V_i^s(x)] = [0] \tag{44}$$

in which

- $[V_i^s(x)]$ and $[I_i(x)]$ are frequency-domain vectors of the scattered voltage and the current along the line;

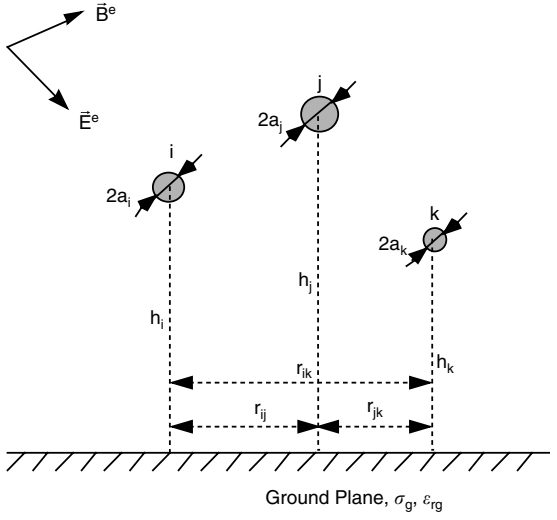

Figure 5: Cross-sectional geometry of a multiconductor line in the presence of an external electromagnetic field.

- $[E_x^e(x,h_i)]$ is the vector of the exciting electric field tangential to the line conductors;
- [0] is the zero-matrix (all elements are equal to zero);
- $[L'_{ij}]$ is the per-unit-length line inductance matrix. Assuming that the distances between conductors are much larger than their radii, the general expression for the mutual inductance between two conductors *i* and *j* is given by [1]

$$L'_{ij} = \frac{\mu_0}{2\pi} \ln\left(\frac{r_{ij}^2 + (h_i + h_j)^2}{r_{ij}^2 + (h_i - h_j)^2} \right) \tag{45}$$

- The self-inductance for conductor *i* is given by

$$L'_{ii} = \frac{\mu_0}{2\pi} \ln\left(\frac{2h_i}{r_{ii}} \right) \tag{46}$$

- $[C'_{ij}]$ is the per-unit-length line capacitance matrix. It can be evaluated directly from the inductance matrix using the following expression [1]

$$[C'_{ij}] = \varepsilon_0 \mu_0 [L'_{ij}]^{-1} \tag{47}$$

- $[G'_{ij}]$ is the per-unit-length transverse conductance matrix. The transverse conductance matrix elements can be evaluated starting either from the capacitance matrix or the inductance matrix using the following relations:

$$[G'_{ij}] = \frac{\sigma_{\text{air}}}{\varepsilon_0} [C'_{ij}] = \sigma_{\text{air}} \mu_0 [L'_{ij}]^{-1} \tag{48}$$

  In most practical cases, the transverse conductance matrix elements G'_{ij} are negligible in comparison with $j\omega C'_{ij}$ [3] and can therefore be neglected in the computation.
- Finally, $[Z'_{g_{ij}}]$ is the ground impedance matrix. The general expression for the mutual ground impedance between two conductors *i* and *j* derived by Sunde is given by [14]

$$Z'_{g_{ij}} = \frac{j\omega\mu_0}{\pi} \int_0^\infty \frac{e^{-(h_i + h_j)x}}{\sqrt{x^2 + \gamma_g^2} + x} \cos(r_{ij} x)\, dx \tag{49}$$

In a similar way as for the case of a single-wire line, an accurate logarithmic approximation is proposed by Rachidi *et al.* [15] which is given by

$$Z'_{g_{ij}} \cong \frac{j\omega\mu_0}{4\pi} \ln\left[\frac{\left(1 + \gamma_g \left(\frac{h_i + h_j}{2}\right)\right)^2 + \left(\gamma_g \frac{r_{ij}}{2}\right)^2}{\left(\gamma_g \frac{h_i + h_j}{2}\right)^2 + \left(\gamma_g \frac{r_{ij}}{2}\right)^2} \right] \tag{50}$$

Note that in eqns (43) and (44), the terms corresponding to the wire impedance and the so-called ground admittance have been neglected. This approximation is valid for typical overhead power lines [9].

The boundary conditions for the two line terminations are given by

$$[V_i^{\mathrm{s}}(0)] = -[Z_{\mathrm{A}}][I_i(0)] + \left[\int_0^{h_i} E_z^{\mathrm{e}}(0,z)\,\mathrm{d}z\right] \tag{51}$$

$$[V_i^{\mathrm{s}}(L)] = [Z_{\mathrm{B}}][I_i(L)] + \left[\int_0^{h_i} E_z^{\mathrm{e}}(L,z)\,\mathrm{d}z\right] \tag{52}$$

in which $[Z_{\mathrm{A}}]$ and $[Z_{\mathrm{B}}]$ are the impedance matrices at the two line terminations.

6 Time-domain representation of the coupling equations

A time domain representation of the field-to-transmission line coupling equations is sometimes preferable because it allows the straightforward treatment of non-linear phenomena as well as the variation in the line topology [4]. On the other hand, frequency-dependent parameters, such as the ground impedance, need to be represented using convolution integrals.

The field-to-transmission line coupling eqns (43) and (44) can be converted into the time domain to obtain the following expressions:

$$\frac{\partial}{\partial x}[v_i^{\mathrm{s}}(x,t)] + [L'_{ij}]\frac{\partial}{\partial t}[i_i(x,t)] + \left[\xi'_{\mathrm{g}_{ij}}\right] \otimes \frac{\partial}{\partial t}[i_i(x,t)] = [E_x^{\mathrm{e}}(x,h_i,t)] \tag{53}$$

$$\frac{\partial}{\partial x}[i_i(x,t)] + [G'_{ij}][v_i^{\mathrm{s}}(x,t)] + [C'_{ij}]\frac{\partial}{\partial t}[v_i^{\mathrm{s}}(x,t)] = 0 \tag{54}$$

in which $\otimes$ denotes convolution product and the matrix $\left[\xi'_{\mathrm{g}_{ij}}\right]$ is called the transient ground resistance matrix; its elements are defined as

$$\left[\xi'_{\mathrm{g}_{ij}}\right] = \mathrm{F}^{-1}\left\{\frac{\left[\mathrm{Z}'_{\mathrm{g}_{ij}}\right]}{j\omega}\right\} \tag{55}$$

The inverse Fourier transforms of the boundary conditions written, for simplicity, for resistive terminal loads read

$$[v_i(0,t)] = -[R_{\mathrm{A}}][i_i(0,t)] + \left[\int_0^{h_i} E_z^{\mathrm{e}}(0,z,t)\,\mathrm{d}z\right] \tag{56}$$

$$[v_i(L)] = [R_B][i_i(0)] + \left[\int_0^{h_i} E_z^e(L,z,t)\,dz\right] \tag{57}$$

where $[R_A]$ and $[R_B]$ are the matrices of the resistive loads at the two line terminals.

The general expression for the ground impedance matrix terms in the frequency domain (49) does not have an analytical inverse Fourier transform. Thus, the elements of the transient ground resistance matrix in the time domain are to be, in general, determined using a numerical inverse Fourier transform algorithm. However, analytical expressions have been derived which have been shown to be reasonable approximations to the numerical values obtained using an inverse FFT (see Chapter 2).

7 Frequency-domain solutions

Different approaches can be employed to find solutions to the presented coupling equations. Sections 7 and 8 present some commonly used solution methods in the frequency domain and in the time domain, respectively.

To solve the coupling equations in the frequency domain, it is convenient to use Green's functions that relate, as a function of frequency, the individual coupling sources to the scattered or the total voltages and currents at any point along the line. Green's functions solutions require integration over the length of the line, where the distributed sources are located. This approach is the subject of Section 7.1.

Under special conditions, it is possible to obtain more compact solutions or even analytical expressions. In particular, if solutions are required at the loads only, it is possible to write the load voltages and currents in a compact manner, with the complexity essentially hidden in the source. This formulation, termed the BLT equations, will be presented in Section 7.2.

7.1 Green's functions

The field-to-transmission line coupling equations, together with the boundary conditions, can be solved using Green's functions, which represent the solutions for line current and voltage due to a point voltage and/or current source [1]. In this section, we will present the solutions, using the Agrawal *et al.* model (Section 2.2) for the case of a single-conductor line. Similar solutions can be found for the case of a multiconductor line (see e.g. [1, 3]).

Considering a voltage source of unit amplitude at a location x_s along the line (since only distributed series voltage sources are present in the model of Agrawal *et al.*, it is not necessary to consider a parallel unitary current source), the Green's functions for the current and the voltage along the line read, respectively [1],

$$G_I(x;x_s) = \frac{e^{-\gamma L}}{2Z_c(1-\rho_1\rho_2 e^{-2\gamma L})}(e^{-\gamma(x_> - L)} - \rho_2 e^{\gamma(x_> - L)})(e^{\gamma x_<} - \rho_1 e^{-\gamma x_<}) \tag{58}$$

$$G_V(x;x_s)=\frac{\delta\,\mathrm{e}^{-\gamma L}}{2(1-\rho_1\rho_2\mathrm{e}^{-2\gamma L})}(\mathrm{e}^{-\gamma(x_>-L)}+\delta\rho_2\mathrm{e}^{\gamma(x_>-L)})(\mathrm{e}^{\gamma x_<}-\delta\rho_1\mathrm{e}^{-\gamma x_<}) \quad (59)$$

where

- $x_<$ represents the smaller of x or x_s, and $x_>$ represents the larger of x or x_s.
- $\delta = 1$ for $x > x_s$ and $\delta = -1$ for $x < x_s$.
- $\gamma = \sqrt{Z'Y'}$ is the complex propagation constant along the transmission line,
- $Z_c = \sqrt{Z'/Y'}$ is the line's characteristic impedance.
- r_1 and r_2 are the voltage reflection coefficients at the loads of the transmission line given by

$$\rho_1=\frac{Z_A-Z_c}{Z_A+Z_c},\qquad \rho_2=\frac{Z_B-Z_c}{Z_B+Z_c} \quad (60)$$

Z_A and Z_B are the termination impedances as illustrated in Fig. 1. The solutions in terms of the total line current and *scattered* voltage can be written as the following integrals of the Green's functions [1]

$$I(x)=\int_0^L G_I(x;x_s)V_s'\,\mathrm{d}x_s+G_I(x;0)\int_0^h E_z^e(0,z)\,\mathrm{d}z-G_I(x;L)\int_0^h E_z^e(L,z)\,\mathrm{d}z \quad (61)$$

$$V^s(x)=\int_0^L G_V(x;x_s)V_s'\,\mathrm{d}x_s+G_V(x;0)\int_0^h E_z^e(0,z)\,dz-G_V(x;L)\int_0^h E_z^e(0,z)\,\mathrm{d}z \quad (62)$$

Note that the second and the third terms on the right-hand side of eqns (61) and (62) are due to the contribution of equivalent lumped sources at the line ends (see Fig. 3).

The total voltage can be determined from the scattered voltage by adding the contribution from the exciting field as

$$V(x)=V^s(x)-\int_0^h E_z^e(x,z)\mathrm{d}z \quad (63)$$

7.2 BLT equations

If we are interested in the transmission line response at its terminal loads, the solutions can be expressed in a compact way by using the so-called BLT (Baum, Liu, Tesche) equations [1]

$$\begin{bmatrix}I(0)\\I(L)\end{bmatrix}=1/Z_c\begin{bmatrix}1-\rho_1 & 0\\0 & 1-\rho_2\end{bmatrix}\begin{bmatrix}-\rho_1 & \mathrm{e}^{\gamma L}\\\mathrm{e}^{\gamma L} & -\rho_2\end{bmatrix}^{-1}\begin{bmatrix}S_1\\S_2\end{bmatrix} \quad (64)$$

$$\begin{bmatrix} V(0) \\ V(L) \end{bmatrix} = \begin{bmatrix} 1+\rho_1 & 0 \\ 0 & 1+\rho_2 \end{bmatrix} \begin{bmatrix} -\rho_1 & \mathrm{e}^{\gamma L} \\ \mathrm{e}^{\gamma L} & -\rho_2 \end{bmatrix}^{-1} \begin{bmatrix} S_1 \\ S_2 \end{bmatrix} \tag{65}$$

where the source vector is given by

$$\begin{pmatrix} S_1 \\ S_2 \end{pmatrix} = \begin{pmatrix} \dfrac{1}{2}\displaystyle\int_0^L \mathrm{e}^{\gamma x_s} E_x^{\mathrm{e}}(x_s, h)\,\mathrm{d}x_s + \dfrac{1}{2}\int_0^h E_z^{\mathrm{e}}(0,z)\,\mathrm{d}z - \dfrac{\mathrm{e}^{\gamma L}}{2}\displaystyle\int_0^h E_z^{\mathrm{e}}(L,z)\,\mathrm{d}z \\ \dfrac{-1}{2}\displaystyle\int_0^L \mathrm{e}^{\gamma(L-x_s)} E_x^{\mathrm{e}}(x_s, h)\,\mathrm{d}x_s - \dfrac{\mathrm{e}^{\gamma L}}{2}\displaystyle\int_0^h E_z^{\mathrm{e}}(0,z)\,\mathrm{d}z + \dfrac{1}{2}\displaystyle\int_0^h E_z^{\mathrm{e}}(L,z)\,\mathrm{d}z \end{pmatrix} \tag{66}$$

Note that in the BLT equations, the solutions are directly given for the total voltage and not for the scattered voltage.

For an arbitrary excitation field, the integrals in eqn (66) cannot be carried out analytically. However, for the special case of a plane wave excitation field, the integrations can be performed analytically and closed-form expressions can be obtained for the load responses. General solutions for vertical and horizontal field polarizations are given in [1].

8 Time-domain solutions

Several approaches can be used to solve the coupling equations in the time domain [1, 3]. We will present here simple analytical expressions that can be obtained for the case of a lossless line involving infinite summations. In Chapter 2, the Finite Difference Time Domain (FDTD) technique is applied to obtain general solutions of field-to-transmission line coupling equations including frequency-dependent losses.

Under the assumption of a lossless line, it is possible to obtain analytical solutions for the transient response of a transmission line to an external field excitation [1]. In this case, the propagation constant becomes purely imaginary $\gamma = j\omega/c$ and the characteristic impedance is purely real $Z_c = \sqrt{L'/C'}$. If we assume further that the termination impedances are purely resistive, the reflection coefficients ρ_1 and ρ_2, too, become real. For $|\rho_1\rho_2\mathrm{e}^{-2\gamma L}| < 1$, the denominator in Green's functions (58) and (59) can be expanded to

$$\frac{1}{(1-\rho_1\rho_2\mathrm{e}^{-2\gamma L})} = \sum_{n=0}^{\infty} (\rho_1\rho_2\mathrm{e}^{-j\omega 2L/c})^n \tag{67}$$

This equation is not valid for the case of a lossless line with reflection coefficients of magnitude 1, in which the condition $|\rho_1\rho_2\mathrm{e}^{-2\gamma L}| = 1$ will be met at a number of resonance frequencies causing the solutions to be unbounded.

With the above transformation, it is easy to show that all the frequency dependences in eqns (64) and (65) will be in the form $e^{-j\omega\tau}$, τ being a constant. Therefore, it is possible to convert the frequency domain solutions to the time domain analytically to obtain the following transient responses for the load voltages (for details, see [1])

$$v(0,t) = (1+\rho_1)\sum_{n=0}^{\infty}(\rho_1\rho_2)^n \frac{1}{2}\left(\rho_2 v_s\left(t - \frac{2(n+1)L - x_s}{c}\right) - v_s\left(t - \frac{2nL + x_s}{c}\right)\right) \tag{68}$$

$$v(L,t) = (1+\rho_2)\sum_{n=0}^{\infty}(\rho_1\rho_2)^n \frac{1}{2}\left(v_s\left(t - \frac{2(n+1)L - x_s}{c}\right) - \rho_1 v_s\left(t - \frac{2(L+1) + x_s}{c}\right)\right) \tag{69}$$

where

$$v_s(t) = \int_0^L E_x^e(x_s,h,t)\,dx_s + \int_0^h E_z^e(0,z,t)\,dz - \int_0^h E_z^e(L,z,t)\,dz \tag{70}$$

Note that $E_x^e(x_s,h,t)$, $E_z^e(0,z,t)$ and $E_z^e(L,z,t)$ are the time-domain components of the exciting field.

9 Conclusions

We discussed the transmission line theory and its application to the problem of external electromagnetic field coupling to transmission lines. After a short discussion on the underlying assumptions of the transmission line theory, the field-to-transmission line coupling equations were derived for the case of a single wire line above a perfectly conducting ground. Three different but completely equivalent approaches that have been proposed to describe the electromagnetic field coupling to transmission lines were also presented and discussed. The derived equations were extended to deal with the presence of losses and multiple conductors. The time-domain representation of field-to-transmission line coupling equations which allows a straightforward treatment of non-linear phenomena as well as the variation in the line topology was also described. Finally, solution methods in the frequency domain and the time domain were presented.

References

[1] Tesche, F.M., Ianoz, M. & Karlsson, T., *EMC Analysis Methods and Computational Models*, Wiley Interscience: New York, 1997.
[2] Cooray, V., *The Lightning Flash*, IEE: London, UK, 2003.
[3] Paul, C.R., *Analysis of Multiconductor Transmission Lines,* John Wiley & Sons: New York, 1994.

[4] Nucci, C.A. & Rachidi, F., Interaction of electromagnetic fields generated by lightning with overhead electrical networks. *The Lightning Flash*, IEE: London, UK, pp. 425–478, 2003.

[5] Taylor, C.D., Satterwhite, R.S. & Harrison, C.W., The response of a terminated two-wire transmission line excited by a nonuniform electromagnetic field, *IEEE Transactions on Antennas and Propagation*, **AP-13**, pp. 987–989, 1965.

[6] Agrawal, A.K., Price, H.J. & Gurbaxani, S.H., Transient response of multiconductor transmission lines excited by a nonuniform electromagnetic field, *IEEE Transactions on Electromagnetic Compatibility*, **EMC-22**, pp. 119–129, 1980.

[7] Rachidi, F., Formulation of the field-to-transmission line coupling equations in terms of magnetic excitation fields, *IEEE Transactions on Electromagnetic Compatibility*, **35**, pp. 404–407, 1993.

[8] Nucci, C.A. & Rachidi, F., On the contribution of the electromagnetic field components in field-to-transmission lines interaction, *IEEE Transactions on Electromagnetic Compatibility*, **37**, pp. 505–508, 1995.

[9] Rachidi, F., Nucci, C.A., Ianoz, M. & Mazzetti, C., Influence of a lossy ground on lightning-induced voltages on overhead lines, *IEEE Transactions on Electromagnetic Compatibility*, **38**, pp. 250–263, 1996.

[10] Ramo, S., Whinnery, J.R. & van Duzer, T., *Fields and Waves in Communication Electronics*, 3rd edn., Wiley: New York, 1994.

[11] Rachidi, F., Nucci, C.A., Ianoz, M. & Mazzetti, C., Importance of losses in the determination of lightning-induced voltages on overhead lines. *EMC '96 ROMA. International Symposium on Electromagnetic Compatibility*, Univ. Rome 'La Sapienza', Rome, Italy, Vol. 2, 1996.

[12] Tesche, F.M., Comparison of the transmission line and scattering models for computing the HEMP response of overhead cables, *IEEE Transactions on Electromagnetic Compatibility*, **34**, pp. 93–99, 1992.

[13] Nucci, C. & Rachidi, F., Interaction of electromagnetic fields generated by lightning with overhead electrical networks. in *The Lightning Flash*, ed. V. Cooray, IEE: London, pp. 425–478, 2003.

[14] Sunde, E.D., *Earth Conduction Effects in Transmission Systems,* Dover Publication: New York, 1968.

[15] Rachidi, F., Nucci, C.A. & Ianoz, M., Transient analysis of multiconductor lines above a lossy ground, *IEEE Transactions on Power Delivery*, **14**, pp. 294–302, 1999.

CHAPTER 2

Surge propagation and crosstalk in multiconductor transmission lines above ground

Nelson Theethayi & Rajeev Thottappillil
Division for Electricity, Uppsala University, Uppsala, Sweden.

Abstract

Surges/transients due to direct or indirect lightning strikes or switching faults are common phenomena in multiconductor transmission line (MTL) systems above ground, whether it is power systems, railway systems, communication systems or electronic systems with printed circuit board lands. In a given MTL system, transient surge in any one of the conductors (emitter) causes crosstalk in other adjacent conductors (receptors). It's a common electromagnetic interference (EMI) phenomenon due to electromagnetic coupling between the conductors. In this chapter, we discuss the methods to study the crosstalk mechanisms in above ground MTL systems and also by examples show various parameters that could influence the crosstalk mechanisms. Analysis in time and frequency domain will be also made wherever necessary.

1 Introduction

In the two-conductor transmission line theory [1–3], as discussed in the earlier chapter, one of the wires carries the currents in the opposite direction with respect to the other, because of which a sign convention is adopted for the voltages of the conductor, i.e. the conductor carrying current in the positive direction of the wire has a positive voltage with respect to a remote reference and the conductor carrying the current in the negative (opposite) direction has a negative voltage with respect to a remote reference. The wire that was carrying current in the negative direction is referred to as return conductor. In case of multiconductor transmission line (MTL) systems to be discussed here, for the above ground conductors the reference conductor is the ground that carries or returns currents in the

negative direction. Thus the theories discussed in the previous chapter apply here as well. One of the difficulties with MTL systems with ground return could be the effects of imperfect ground (i.e. real conducting earth having some dielectric constant) on the voltages and currents propagating in the wires. It is also referred to as frequency dependant loss in the MTL system due to electromagnetic field penetration in the ground [3–16]. More emphasis is given for direct numerical time domain solutions of the telegrapher's or transmission line equations. Time domain solutions are preferred because in practical systems, like power, railway, etc., whenever transients propagate there are protection equipment connected to the system to divert the transients for providing safety to important equipments and personnel [17, 18]. All the protection systems contain devices like insulators, surge protective devices, grounding systems undergoing soil ionization, circuit breakers and fuses, etc. [19–21]. These being non-linear devices, hence continuous monitoring of the voltages and currents on the MTL systems is needed, for modelling the non-linear phenomena like flashover, arcing, soil ionization, etc.

2 Telegrapher's or transmission line equations for MTL systems

Voltage and current wave propagation in MTL systems is represented by the two sets of equations given by eqn (1) in frequency domain, for perfectly conducting ground and non-dissipative line (lossless/ideal).

$$\frac{\mathrm{d}V(x,j\omega)}{\mathrm{d}x} + L_{\mathrm{e}}\, j\omega I(x,j\omega) = 0 \tag{1a}$$

$$\frac{\mathrm{d}I(x,j\omega)}{\mathrm{d}x} + C_{\mathrm{e}}\, j\omega V(x,j\omega) = 0 \tag{1b}$$

Similarly, for a perfectly conducting ground with constant or frequency-independent internal losses the transmission line equations are given by eqn (2) in frequency domain.

$$\frac{\mathrm{d}V(x,j\omega)}{\mathrm{d}x} + RI(x,j\omega) + (L_{\mathrm{i}} + L_{\mathrm{e}})\, j\omega I(x,j\omega) = 0 \tag{2a}$$

$$\frac{\mathrm{d}I(x,j\omega)}{\mathrm{d}x} + G_{\mathrm{e}} V(x,j\omega) + C_{\mathrm{e}}\, j\omega V(x,j\omega) = 0 \tag{2b}$$

Note that in conventional form, the Laplace or Fourier domain, the frequency is represented by $S \Leftrightarrow j\omega$ [22]. Equations (1) and (2) are popularly known as telegrapher's equations. Kelvin (William Thomson) was studying the pulse propagation in the transatlantic cable (1855), a landline connecting North America and Europe via Alaska and Siberia. The cable failed, as Kelvin's theory neglected the magnetic effects and only the effects due to the capacitance and resistance per unit length

of the cable were accounted, which when used in the actual telegrapher's eqns (2) yields the diffusion equation. In 1857, Kirchoff proposed the long line theory to include self-induction effects. Heaviside later formulated all the parameters required for complete transmission line theory [23]. Equations (1a) and (2a) are the voltage wave equations and eqns (1b) and (2b) are the current wave equations. For a system of n conductors as shown in Fig. 1 and corresponding to eqns (1) and (2), the terms $V(x, j\omega)$ and $I(x, j\omega)$, are the voltage and current vectors having size n. Further, L_i, L_e, C_e, R and G_e are per unit length series inductance (internal and external), shunt capacitance, series resistance and shunt conductance matrices of size n, respectively. Note that for convenience, discussions below are for no external field illuminations, i.e. there are no illuminating field forcing terms in eqns (1) and (2), but the field to wire coupling theories discussed in the previous chapter apply here as well.

The R and L_i matrices are diagonal due to the constant internal loss of the conductor and have meaning only when the skin effect phenomenon is not prominent, i.e. under the conditions when the radius of the circular wire satisfies $r_i < 2\delta$, where δ is the skin depth [24, 25]. Usually, under low frequency or DC conditions the current is uniformly distributed over the wire cross-section, but at high frequencies the current crowds to the surface and distributes itself uniformly in thickness given by the skin depth applicable for good conductors $\delta_i = \sqrt{2/\omega\mu\sigma}$. At high frequencies the internal loss has to be represented as internal impedance which will be discussed later. The elements corresponding to R and L_i are given by eqns (3) and (4).

$$R_{kk} = \frac{1}{\sigma\pi r_k^2} \quad \text{and} \quad R_{kj} = 0 \tag{3}$$

$$L_{ikk} = \frac{\mu_0}{8\pi} \quad \text{and} \quad L_{ikj} = 0 \tag{4}$$

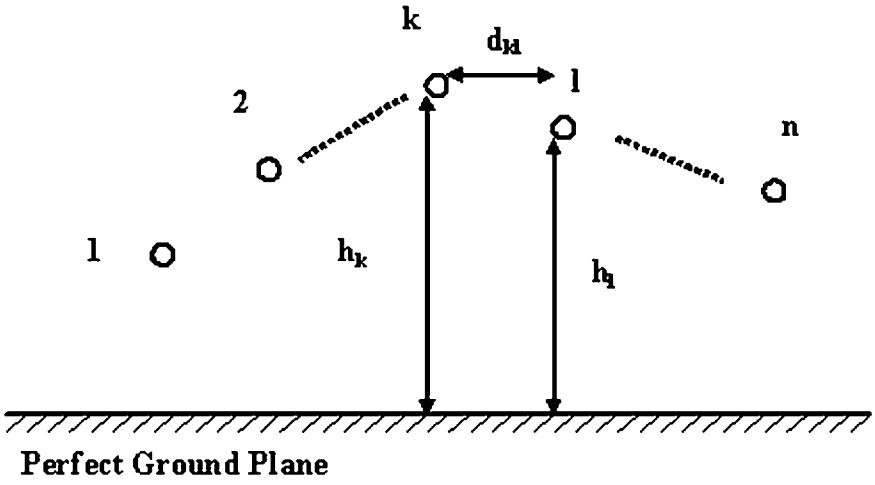

Figure 1: System of MTL above a perfectly conducting ground.

The external transmission line parameters, L_e, C_e and G_e corresponding to Fig. 1, are calculated using the image theory [1–3] and is due to the external magnetic and electric fields, respectively. The external self-inductance of kth conductor and lth mutual inductance between wires k and l are given by

$$L_{ekk} = \frac{\mu_0}{2\pi} \ln\left(\frac{2h_k}{r_k}\right) \tag{5a}$$

$$L_{ekl} = \frac{\mu_0}{2\pi} \ln\left(\frac{\sqrt{(h_k + h_l)^2 + d_{kl}^2}}{\sqrt{(h_k - h_l)^2 + d_{kl}^2}}\right) \tag{5b}$$

To get the external capacitance matrix one has to first obtain the potential coefficient matrix in the same way as the inductance coefficient matrix (5). The potential coefficient matrix is given by eqn (6) for the self and mutual values.

$$P_{ekk} = \frac{1}{2\pi\varepsilon_0} \ln\left(\frac{2h_k}{r_k}\right) \tag{6a}$$

$$P_{ekl} = \frac{1}{2\pi\varepsilon_0} \ln\left(\frac{\sqrt{(h_k + h_l)^2 + d_{kl}^2}}{\sqrt{(h_k - h_l)^2 + d_{kl}^2}}\right) \tag{6b}$$

Inverting the potential coefficient matrix, we have the capacitance coefficient matrix (7).

$$C_e = P_e^{-1} \tag{7}$$

The conductance coefficient matrix can be obtained from capacitance matrix directly (8). Since the conductivity of air is negligible, this matrix can be neglected for the above ground wires.

$$G_e = \frac{\sigma}{\varepsilon_0} C_e \tag{8}$$

Since the internal losses are not completely represented by just the resistance and internal inductance of the wire, we now rewrite the transmission line equations in terms of series impedances (internal impedance Z_i and external impedance Z_e) and the external shunt admittance Y_e as shown in eqn (9).

$$\frac{dV(x, j\omega)}{dx} + (Z_i + Z_e) I(x, j\omega) = 0 \tag{9a}$$

$$\frac{dI(x, j\omega)}{dx} + Y_e V(x, j\omega) = 0 \tag{9b}$$

2.1 Expressions for internal impedance of wires

An expression for the internal impedance of the wire that can properly represent the frequency dependence is needed. Schelkunoff [24, 25] gave the exact expression for internal impedance for round wires of radius r_w as shown in eqn (10), which was in terms of modified Bessel's functions and internal wire propagation constant $\gamma_i = \sqrt{j\omega\mu\sigma}$.

$$Z_i(j\omega) = \frac{\gamma_i}{2\pi\sigma r_w} \frac{I_0(\gamma_i r_w)}{I_1(\gamma_i r_w)} \tag{10}$$

Wedepohl and Wilcox [26] gave another approximate formula as given by eqn (11) which is an approximation of eqn (10).

$$Z_i(j\omega) = \frac{\gamma_i}{2\pi\sigma r_w} \coth(0.777 r_w \gamma_i) + \frac{0.356}{\pi\sigma r_w^2} \tag{11}$$

There is another approximation to eqn (10) proposed by Nahman and Holt [27] and is given by eqn (12).

$$Z_i(j\omega) = \frac{1}{\pi\sigma r_w^2} + \frac{1}{2\pi r_w}\sqrt{\frac{\mu}{\sigma}}\sqrt{j\omega} = A + B\sqrt{S} \tag{12}$$

A comparison of all the above expressions for wide frequency range is shown in Fig. 2 for an aluminium circular wire of radius 5.6 mm. It is seen that the internal impedance expressions (10) and (11) are identical and also the expression (12) is in good agreement. Interestingly eqn (12) can be used in the time domain calculations easily [2, 27], which will be discussed later.

2.2 External impedance and admittance of wires above finitely conducting ground

An imperfect (lossy) ground has finite value of ground conductivity σ_g and is characterized further by the ground permittivity ε_g and ground permeability $\mu = \mu_0$. All these material properties are also referred to as ground return parameters. Ground conductivity is of infinite value when the ground is assumed to be perfect. When a current pulse is propagating along an overhead wire the electromagnetic fields from the wire source impinges the ground surface. If the ground was perfectly conducting, then those impinging electromagnetic fields get completely reflected from the ground surface and nothing penetrates into the ground, since the reflection coefficient for a perfect ground is unity. This allows us to use the well-known image theory (image of the wires' is fixed irrespective of the frequency of the propagating pulse) for perfectly conducting ground and the external impedance can be obtained using expressions (5). But one has to be careful with the limits of transmission line approximation (see also Chapter 1). This limiting condition is

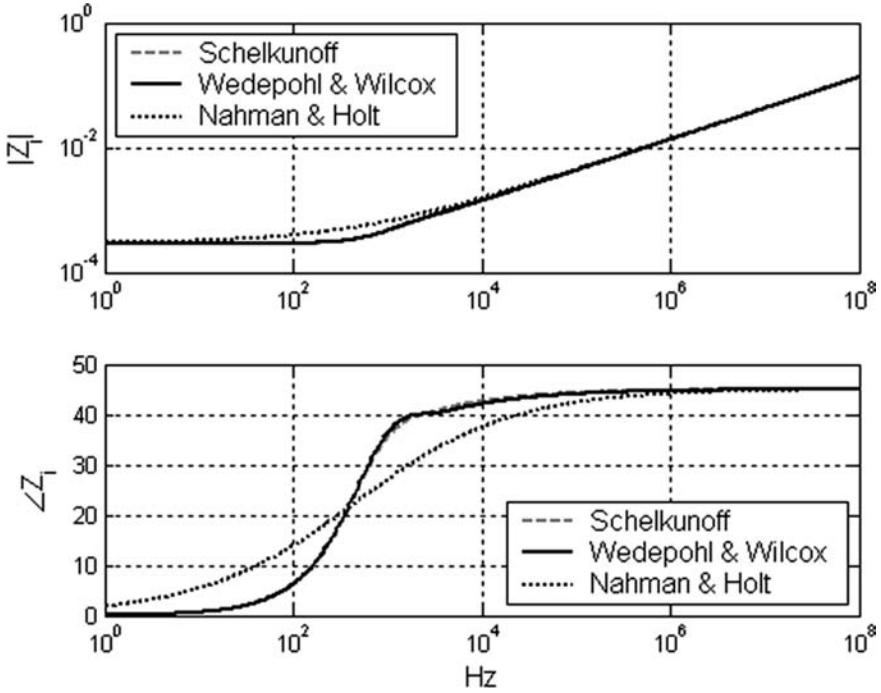

Figure 2: Comparison of internal impedance expressions (10)–(12) for an aluminium circular wire of radius 5.6 mm.

such that the wavelength λ_{pulse} of the pulse propagating on the wire under perfect ground conditions should be much larger than the conductor's height h, i.e. $\lambda_{pulse} >> 2\pi h$ [2, 3]. As the pulse frequency increases, the wavelength decreases and above some critical frequency, the wavelength would become comparable to the heights of the conductor. Therefore, the discussions in this chapter are valid only under the limits of transmission line approximations [3]. For transients having frequencies of the order of a few megahertz, the transmission line approximation is still valid for typical overhead power lines. We shall discuss the limits of transmission line approximation for finitely conducting ground conditions later.

For an imperfect ground, the reflection coefficients are complex valued functions [3, 5] leading to finite frequency-dependant penetration of fields into the ground as shown in Fig. 3. In the earlier discussion of skin effect phenomena, it was seen that magnitude of the current flowing in a conductor tend to crowd towards the surface of the conductor depending upon the frequency or skin depth. A somewhat similar phenomenon, rather more complex, happens (see penetration depth shown in Fig. 3) if, instead of a perfectly conducting ground plane, a real soil or ground medium is present. The complexity is in identifying the proper meaning to the line voltage. In principle the line voltage is defined as the line integral of electric field from the reference conductor to the location of the other conductor. Thus, for wires' above perfect ground, the voltage is the line integral from the ground surface (referenced

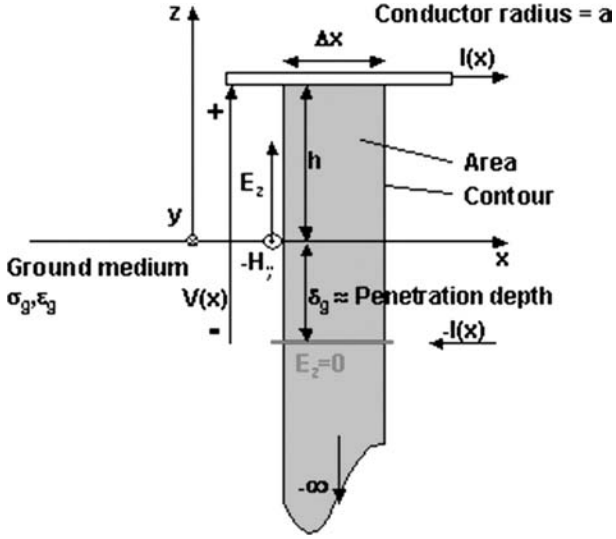

Figure 3: Single conductor above a dissipative semi-infinite earth (adapted from [3] and modified).

at zero potential) to the height of the conductor (note the reference wire based on image theory [3, 6, 13, 14] is located at a distance twice the conductor height). For real ground or soil, the electric field in the earth is non-zero and the zero/reference level is only at a certain depth due to fields penetrating the ground. Well, the question is at what depth one can find this?

Tesche *et al*. [3] mention that in order to get the total wire voltage, the line integral is to be split into two parts. One integral is between the surface of the ground to the wire location in air and the other integral is from the –∞ in the earth to the surface of the earth. For discussions below, let us drop the incident fields (for brevity) and consider only the wire above the ground and assume that some incident field caused the induced current in the wire (see details in Chapter 1 on field to wire coupling). For a transverse electric and magnetic (TEM) field structure and referring to Fig. 3, taking the integration from –∞ (assuming the zero reference point) to h (conductor height), we have eqns (13)–(15).

The first integral on the left-hand side of eqn (13) is the required voltage at two points on the line and the second integral corresponds to the internal loss or the contribution due to internal impedance, as discussed in earlier section, which, for a perfect conductor is zero.

$$\int_{-\infty}^{h} [E_z(x+\Delta x,z) - E_z(x,z)]\mathrm{d}z - \int_{x}^{x+\Delta x} [E_x(x,h) - E_x(x,-\infty)]\mathrm{d}x$$
$$= -j\omega\mu_0 \int_{-\infty}^{h}\int_{x}^{x+\Delta x} -H_y \,\mathrm{d}x\,\mathrm{d}z \qquad (13)$$

Under the limits $\Delta x \to 0$, the left-hand side of eqn (13) gives the derivative of the voltage drop and also the drop due to skin effect (internal impedance) of the conductor as shown in eqn (14).

$$\int_{-\infty}^{h} [E_z(x+\Delta x, z)E_z(x,z)]\mathrm{d}z - \int_{x}^{x+\Delta x} [E_x(x,h) - E_x(x,-\infty)]\mathrm{d}x = \frac{\mathrm{d}V(x,j\omega)}{\mathrm{d}x} + Z_i(j\omega)I(x,j\omega) \tag{14}$$

Similarly, the right-hand side of eqn (13), for no incident or transmitted fields and with only scattered field or field due to current on the wire, gives eqn (15). Equation (15) is the flux due to the wire current and the return current in the ground.

$$-j\omega\mu_0 \int_{-\infty}^{h} \int_{x}^{x+\Delta x} -H_y \mathrm{d}x\,\mathrm{d}z = -[j\omega L_\mathrm{e} + Z_\mathrm{g}(j\omega)]I(x,j\omega) \tag{15}$$

Note that there exists only external inductance term for wire above a perfect ground. From eqn (15), it is seen that the total external impedance is a series combination of external impedance due to inductance of wire with perfect ground and the ground impedance Z_g. Similar to external mutual inductances (5b) for wires above ground, one has mutual ground impedance too. Many researchers have contributed to deriving the ground impedance expressions. Only the most important ones applicable to transmission line type problems will be discussed here.

The critical frequency for the soil is the instant when the displacement currents become equal to the conduction currents. For a given soil if the critical frequency is $\omega_\mathrm{c} = \sigma_\mathrm{g}/\varepsilon_\mathrm{g}$ and if the propagating pulse on the wire or the associated electromagnetic fields have a frequency ω, then the behaviour of the earth to those incident fields are the following (various types of electromagnetic pulses that are encountered in practical electromagnetic compatibility problems are also given [3, 8, 28–31]),

- If $\omega < 0.1\omega_\mathrm{c}$, then it is low-frequency approximation and the earth behaves as a conductor (Carson region). All the pulses like power, switching and typical first lightning return strokes belong to this category.
- If $0.1\omega_\mathrm{c} < \omega < 2\omega_\mathrm{c}$, then it is high-frequency approximation and the earth behaves as both conductor and insulator (transition region). Most of the first and lightning subsequent return stroke pulses belong to this category.
- If $\omega > 2\omega_\mathrm{c}$, then it is very high-frequency approximation and the earth behaves as an insulator (asymptotic region). Most of the high-altitude electromagnetic and nuclear electromagnetic [31] pulses belong to this category. Care has to be exercised that the transmission line approximation may be strictly questionable at these frequencies.

2.2.1 Carson's ground impedance expression for low-frequency pulse propagation studies

Carson [16] was the first to investigate the concept of ground impedance (also called earth return impedance). He first derived the general solution of axial electric field in the ground and related this axial electric field to the magnetic field components using the Maxwell's curl equation. He then split the magnetic field components into two parts, i.e. one part of the field coming from the current in the wire and the other from the current in the ground. The axial displacement currents in the ground were neglected (low-frequency approximation), i.e. the ground propagation constant is $\gamma'_{\mathrm{g}} = \sqrt{j\omega\mu_0\sigma_{\mathrm{g}}}$ and it is assumed that the wire is of sufficiently small radius so that the distribution of current over its cross-section is symmetrical for the electric field. The axial electric field was further related to the scalar and vector potentials and he derived the final ground impedance expressions as an improper integral shown in eqns (16a) and (16b) for self and mutual values respectively (refer Fig. 1 for geometry).

$$Z_{gkk}^{\mathrm{Carson}}(j\omega) = \frac{j\omega\mu_0}{\pi}\int_0^{\infty} \frac{\mathrm{e}^{-2h_k u}}{\sqrt{u^2 + j\omega\mu_0\sigma_{\mathrm{g}}} + u}\,\mathrm{d}u \tag{16a}$$

$$Z_{gkl}^{\mathrm{Carson}}(j\omega) = \frac{j\omega\mu_0}{\pi}\int_0^{\infty} \frac{\mathrm{e}^{-2(h_k+h_l)\cdot u}\cos(d_{kl}u)}{\sqrt{u^2 + j\omega\mu_0\sigma_{\mathrm{g}}} + u}\,\mathrm{d}u \tag{16b}$$

The infinite integral terms in eqn (16) have certain solutions in terms of Bessel's functions of first and second kind. Those functions can be expanded in terms of infinite series. For simpler computations, Carson further expanded the integrals to infinite series [16], which is widely used by power engineers. Carson's infinite series converge very quickly at low frequencies. The convergence decreases as frequencies increase and could lead to truncation errors. The low-frequency approximation is used (see the denominator terms, wherein ε_{g} is missing in eqn (16)). Further, under the limits frequency tending to infinity, Carson's expression poses singularity, i.e. ground impedance tends to infinity. In reality, as frequency tends to infinity the ground impedance tends to be finite, which will be discussed later.

To overcome the difficulty of convergences of Carson's equations and perhaps to study some of the power system faults, Gary proposed the complex depth earth return method in 1976 but without any analytical proof of his proposition [6]. In 1981, Deri *et al*. [6] theoretically proved the relationship between the Carson's method and the complex depth ground return method, thereby proving Gary's proposition of complex depth ground return method.

This method is somewhat a closed-form approximation to Carson's integral equation (16). Deri *et al*. [6] method assumes that the current in conductor say, k returns through an imagined earth path located directly under the original conductor at a depth of $(h_k + 2p)$ as shown in Fig. 4, in which k'' refers to the imagined earth return conductor of conductor k and p to the low-frequency approximation of the skin depth of the ground. In other words, earth can be replaced by a set of earth

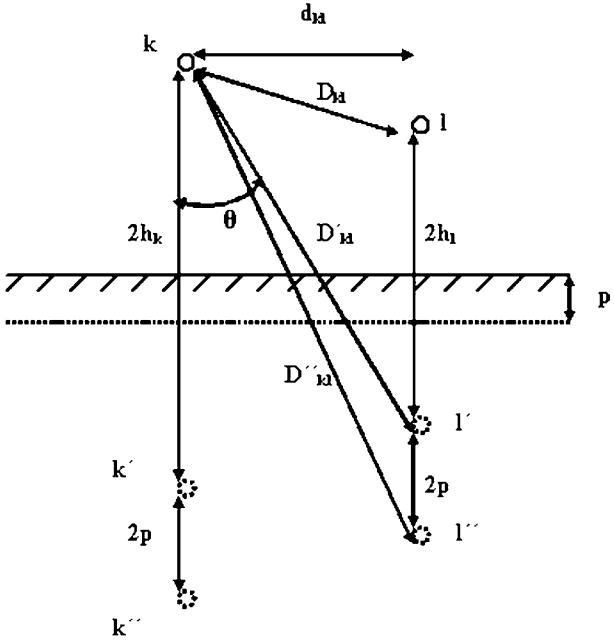

Figure 4: Allocation of conductors k and l and their images k' and l' with a low-frequency approximation of skin depth p [6].

return conductors. The distance between a conductor and its imagined earth return conductor equals twice its height above ground plus the skin depth of the ground (i.e. $2(h_k + p)$). It must be emphasized that the skin depth $p = (j\omega\mu_0\sigma_g)^{-1/2}$ is a complex number. The relevant ground impedance equations are shown in eqn (17) which have symbols as defined in Fig. 4.

$$Z_{gkk}^{\text{Deri et al.}}(j\omega) = \frac{j\omega\mu_0}{2\pi}\ln\left(\frac{h_k + p}{h_k}\right) \tag{17a}$$

$$Z_{gkl}^{\text{Deri et al.}}(\mathrm{j}\omega) = \frac{j\omega\mu_0}{2\pi}\ln\left(\frac{D_{kl}^{''}}{D_{kl}^{'}}\right) \tag{17b}$$

The drawbacks of Carson's integral equations with regard to high frequency also apply to Deri *et al*. expressions as well. Further, it is observed that $p = 0$ as $\omega \to \infty$. This is not true because as the frequency tends to infinity the penetration depth tends to an asymptote decided by the ground material properties. This will be discussed after the high-frequency expression for ground impedance. Note that the low-frequency approximation is strictly valid only if the conduction currents are much larger compared with the displacement currents in the soil, i.e. $\sigma_g >> \omega\varepsilon_g$.

2.2.2 Sunde's ground impedance expression for high-frequency pulse propagation studies

After Carson, the next important person to contribute to the development of ground impedance was Sunde [4]. In his classic text on Earth conduction effects on transmission systems, Sunde analysed several other cases with regard to the location of wire, above and below ground, for wide frequency range and with specific attention to propagation characteristics. In authors' opinion, he was the first to bring the concept of transmission line modelling with earth conduction effects, judged from all his interesting works and publications during the 1940s. During his time, the lightning-induced transients and other power system fault estimations was of utmost significance. This may have led him to investigate the wave propagation in buried cables, overhead wires, grounding rods and wires, etc. Sunde [4] derived his expression by assuming a dipole in air above the earth surface, with earth assumed to consist of two layers. He then used the wave functions or the Hertz potentials [32] in the three media and derived the result by satisfying the boundary conditions corresponding to the continuity of the tangential components of the electric and magnetic fields at interfaces. His ground impedance expressions (18) include the displacement currents in the soil, i.e. ground propagation constant $\gamma_g = \sqrt{j\omega\mu_0 (\sigma_g + j\omega\varepsilon_g)}$ was used (refer Fig. 1 for geometry).

$$Z_{gkk}^{\text{Sunde}}(j\omega) = \frac{j\omega\mu_0}{\pi} \int_0^{\infty} \frac{e^{-2h_k \cdot u}}{\sqrt{u^2 + \gamma_g^2} + u} du \tag{18a}$$

$$Z_{gkl}^{\text{Sunde}}(j\omega) = \frac{j\omega\mu_0}{\pi} \int_0^{\infty} \frac{e^{-2(h_k + h_l) \cdot u} \cos(d_{kl} u)}{\sqrt{u^2 + \gamma_g^2} + u} du \tag{18b}$$

The only difference between Carson's (16) and Sunde's (18) expressions is that full propagation constant in the ground was used by Sunde, the justification being that at higher frequencies the displacement currents in the soil could not be neglected. For the self-ground impedance eqn (18a), Sunde gave a logarithmic approximation as shown in eqn (19a).

$$Z_{gkk}^{\text{Sunde-log}}(j\omega) = \frac{j\omega\mu_0}{2\pi} \ln\left(\frac{1 + h_k\gamma_g}{h_k\gamma_g}\right) \tag{19a}$$

In the recent studies on the field wire coupling problems in overhead power lines for a wide range of frequencies the Sunde's logarithmic approximation is used [28, 31]. There is yet another ground impedance expression by Vance in terms of Hankel functions and it is mathematically equivalent to Sunde's expressions (19a) [5]. However, according to Chen and Damrau [7], Sunde's logarithmic approximation is more valid. It is further said in [3, 7] that for overhead power lines eqn (19a) is a very good approximation of eqn (18a) and the logarithmic formula are valid for a wide frequency range [28, 29]. Now, having known the

drawback of low-frequency approximations of Carson, the immediate question is, does Sunde's logarithmic or integral expression suffer the same drawbacks? No! As the frequency tends to infinity Sunde's expression, specifically logarithmic expression is finite and never poses any singularity. The integral expression (18a) have convergence problems, hence the authors have not investigated its behaviour for higher frequency. Rachidi *et al*. [28, 29] have mentioned that the integral expression (19a) does not pose any singularity. Let us discuss this finite value in a little while. Sunde's expression has greater validity compared with other low-frequency approximations.

Equation (19a) has been extended by Rachidi *et al*. [28] for the mutual impedance as given below in eqn (19b) and it is also claimed that (19b) is a very good approximation of eqn (18b). It can be shown that eqns (19b) and (17b) are similar, excepting that the low-frequency approximation of ground propagation constant was used in eqn (17b).

$$Z_{gkl}^{\text{Sunde-log}}(j\omega) = \frac{j\omega\mu_0}{2\pi} \ln\left(\frac{\left[1+\left(\frac{\gamma_g(h_k+h_l)}{2}\right)\right]^2 + \left(\frac{\gamma_g d_{kl}}{2}\right)^2}{\left(\frac{\gamma_g(h_k+h_l)}{2}\right)^2 + \left(\frac{\gamma_g d_{kl}}{2}\right)^2} \right) \tag{19b}$$

As mentioned earlier, we next discuss the asymptotic nature of the ground impedance as the frequency tends to infinity based on the field penetration depth. A comparison of various ground impedance expressions is shown in Fig. 5 for a conductor of height 8 m and for different ground conductivities as a function of frequency.

2.2.3 Asymptotic nature of ground impedance and the concept of penetration depth of fields in the ground

From Fig. 5, it is seen that the ground impedance magnitude is tending to a constant value as frequency tends to infinity. To understand this, we need to see what happens to the ground penetration depth as the frequency tends to infinity. The penetration depth of the fields in the soil is given by eqn (20) [5].

$$\delta_g = \frac{1}{\omega\sqrt{\frac{\mu_0\varepsilon_g}{2}\left[\sqrt{1+\left(\frac{\sigma_g}{\omega\varepsilon_g}\right)^2}-1\right]}} \tag{20}$$

It can be shown that eqn (20) tends to eqn (21) as the frequency tends to infinity [5, 8].

$$\lim_{\omega\to\infty} \delta_g = \frac{2}{\sigma_g}\sqrt{\frac{\varepsilon_g}{\mu_0}} \tag{21}$$

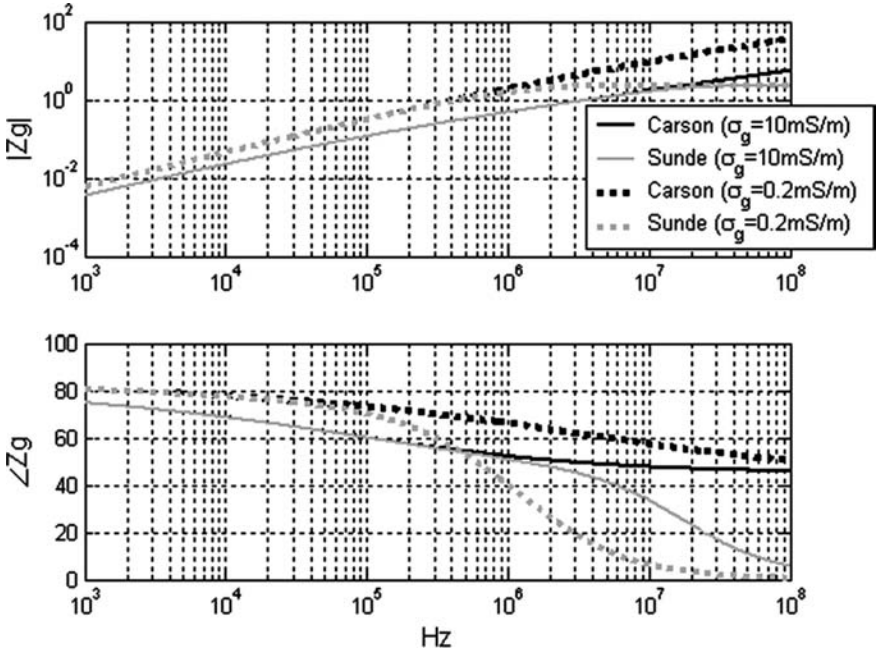

Figure 5: Ground impedance amplitude and argument plots for conductor height 8 m and ground conductivity σ_g = 10 mS/m and σ_g = 0.2 mS/m, ground relative permittivity ε_{rg} = 10.

Figure 6 shows the variation of ground penetration depth as a function of frequency for various ground conductivities. Note that the low-frequency approximation of the ground penetration depth will lead to zero penetration depth as frequency tends to infinity, which is incorrect, due to which the low-frequency approximation of the ground impedance, rather than approaching a constant asymptotic value, approaches infinity. Thus, Sunde's ground impedance is valid as it approaches finite value under the limits frequency approaching infinity.

The value of the ground impedance, as frequency tends to infinity, is given by eqns (22a) and (22b) for self and mutual values respectively [8], which is necessary for time domain calculations.

$$\lim_{\omega\to\infty} Z_{gkk} = \frac{1}{2\pi h_k}\sqrt{\frac{\mu_0}{\varepsilon_g}} \tag{22a}$$

$$\lim_{\omega\to\infty} Z_{gkl} = \frac{h_k + h_l}{\pi\left[(h_k + h_l)^2 + d_{kl}^2\right]}\sqrt{\frac{\mu_0}{\varepsilon_g}} \tag{22b}$$

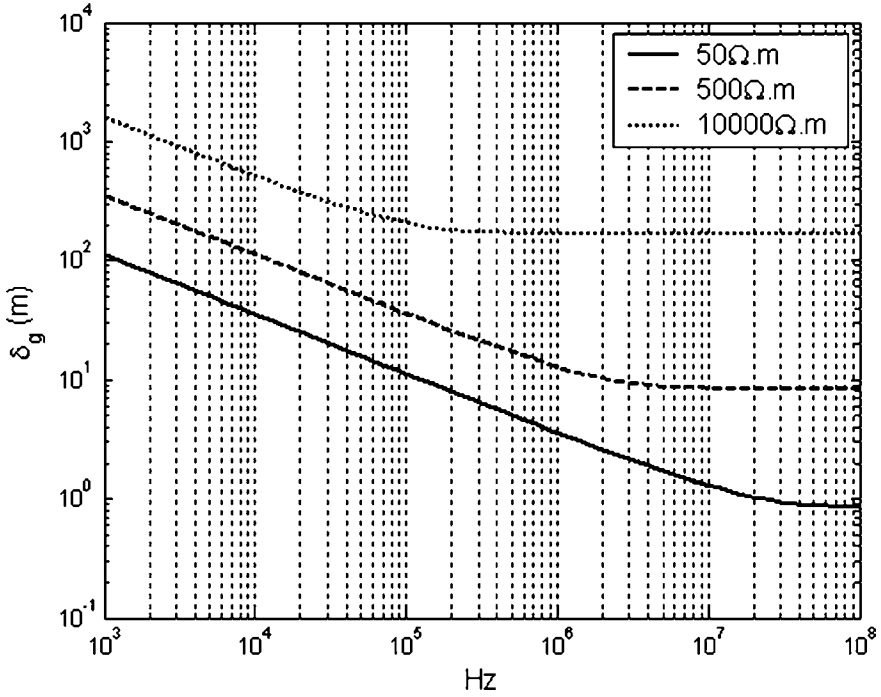

Figure 6: Penetration depth of electromagnetic fields in the ground for various ground conductivities $\varepsilon_{rg} = 10$.

If one observes the manner in which the ground impedance curves of Sunde in Fig. 5 varies as a function of frequency for different ground conductivity, it can be seen that the poorer the ground conductivity, the earlier the frequency at which the asymptotic value is attained. This is also observed in the case of Fig. 6 for ground penetration depth. Thus, using the concept of ground penetration depth, Theethayi *et al*. [33] discussed somewhat philosophically/intuitively, the limits of transmission line approximation for wires above finitely conducting ground.

It should be emphasized that we are discussing a case where ground has uniform conductivity, but in practical situations there are several layers in the soil having different conductivity and permittivity. Sunde in his book [4] has proposed the ways to calculate the ground impedance under such circumstances. But there are always assoicated uncertainties, i.e. lack of information regarding thickness of layers, proper ground conductivity, etc. Sunde [4] and Vance [5] mention that uncertainties in the soil conditions could cause around 20% errors in the analysis. Some works to this direction under low-frequency approximations have been proposed in [6, 34]. However, analysis and accuracy with regard to transmission line solution for the

kind of problem we are dealing with is only dependant on the accuracy of ground impedance expression.

2.2.4 Limits of transmission line approximation for overhead wires

In the above discussions, we have mentioned the upper frequency limits if transmission line approximations are to be valid. For all the above ground wires with earth return it was shown that currents return in the soil at various depths depending on the penetration depth which is further dependant on the frequency.

Along the length of a normal transmission line, both electric and magnetic fields are perpendicular (transverse) to the direction of wave travel [1–3], which is known as the principal mode, or TEM mode, thereby allowing us to use the quasi-static analysis. This type of analysis has been carried out earlier by Bannister [13–15]. Now the condition for the TEM propagation to be dominant at any given frequency is, that the distance between the actual wire location and the return wire (return path in the ground) is less than or equal to the wavelengths of the pulse propagating in the air. Thus, under limiting conditions, for any given frequency the pulse of the wavelength should be such that $\lambda_{\text{pulse}} \geq 2(h + \delta_g)$. It is clear that if at all the wavelength violates the above condition, then there would possibly be other modes of propagation that should be considered and that the definition of voltage will no longer be valid as the wire might be radiating or return may not be through earth. A solution based on exact Maxwell or Hertz dipole theory as carried out by Wait [9], Olsen *et al*. [10], etc. could answer such doubts. Thus in the present study assuming that only a TEM or a quasi-static field structure exists (dominant), with all the other modes suppressed the minimum frequency beyond which the transmission line approximation might be questionable is given by $f_{\text{TL}} = 3 \times 10^8/2(\text{h} + \delta_\infty)$, where $\delta_\infty = 2/\sigma_g \sqrt{\varepsilon_g/\mu_0}$.

Figure 7 shows the actual frequency-dependant distance between wire location in air and its corresponding image wire or return plane for a conductor height of 10 m. The distance between the wire and its actual image is an extension of the analysis based on Bannister [13–15], which is twice the sum of height and the skin/penetration depth in the soil. Note that the whole medium under consideration now is air. Therefore, in Fig. 7 the wavelength in air is also shown as a function of frequency. It is seen that when the ground conductivity decreases, the limiting frequency for the transmission line analysis to be valid also decreases based on the arguments presented earlier and is similar to conclusions made in [28, 29].

Thus, we have determined all the parameters corresponding to the frequency-dependant series impedance terms in the first transmission line equations. We now move on to the calculation of shunt admittance parameters of the line in the presence of finitely conducting ground.

2.2.5 Ground admittance for above ground wires

If ground impedance is obtained, then one can obtain the ground admittance too. The ground impedance is due to the contribution of magnetic field in the ground.

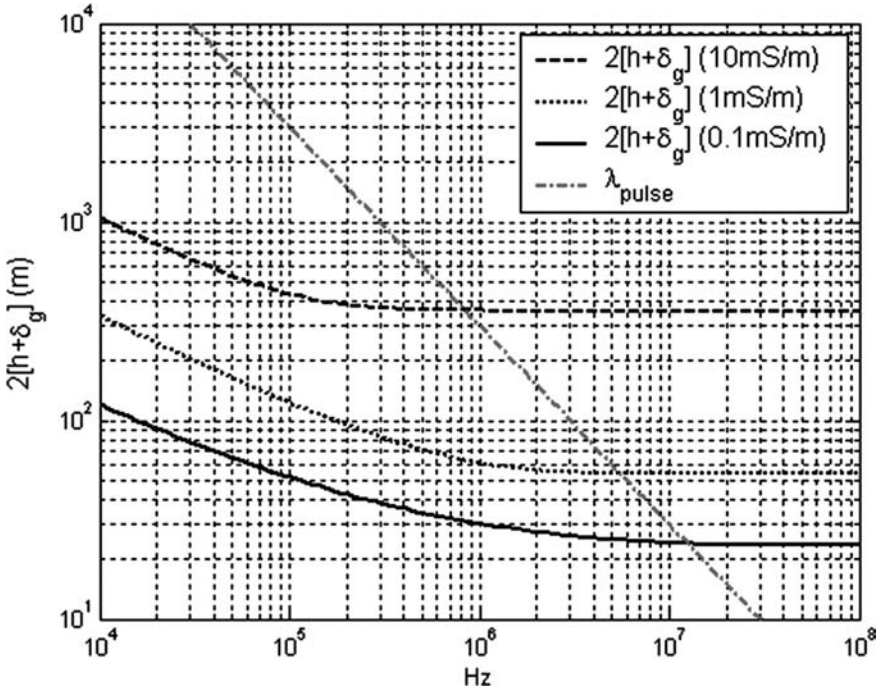

Figure 7: Frequency-dependant distance between the source wire and fictitious return path for conductor height 10 m, σ_g = 10, 1 and 0.1 mS/m and ε_{rg} = 10.

Similarly the ground admittance is due to the contribution of electric field in the ground. The linear charge density along the conductor and admittance of the line is related to the electric field as shown in eqn (23) and based on Fig. 3 [3].

$$\frac{j\omega q\int(x,j\omega)}{Y_e(j\omega)} = \int_0^h E_z\,\mathrm{d}z + \int_{-\infty}^0 E_z\,\mathrm{d}z \tag{23}$$

$$\frac{1}{Y_e(j\omega)} = \frac{1}{j\omega C_e} + \frac{1}{Y_g(j\omega)} \tag{24}$$

The overall shunt admittance of the line is thus given by eqn (25), which implies that the total line admittance is a series combination of external admittance due to capacitance of the wire to ground with perfect ground conditions and the ground admittance.

$$Y_e(j\omega) = \frac{j\omega C_e Y_g(j\omega)}{\mathrm{j}\omega C_e + Y_g(j\omega)} \tag{25}$$

Again, there are some expressions in the literature for the ground admittance of the line [5]. However, as an approximation, the ground admittance and ground impedance are related through ground propagation constant as in eqn (26).

$$Y_g(j\omega) = \gamma_g^2 [Z_g(j\omega)]^{-1} \tag{26}$$

2.3 Complete per unit transmission line representation and the sensitivity of each transmission line parameters

We have seen in the previous sections all the relevant parameters to represent a distributed transmission line segment of an overhead wire with ground as return. Using those parameters the per unit length representation of the above ground wire is shown in Fig. 8. In the MTL systems, there will be mutual couplings external impedance and admittance parameters. The analysis, however, remains the same but with matrices as explained earlier. These parameters are part of the transmission line eqns (9). Let us next see which parameter among the previously mentioned list of transmission line parameters is dominant in various analyses.

Let us begin with series impedance parameters, i.e. we shall compare the magnitudes of internal impedance, external impedance under lossless ground conditions and external self-impedance under lossy conditions. For comparisons, we shall use the internal impedance expression (10), the external inductance expression (5a) and the ground impedance expression (19a) for a typical overhead copper wire, 8 m height, 1 cm radius and with a ground conductivity 10 mS/m. The comparisons are shown in Fig. 9.

From Fig. 9, it is clearly seen that the external impedance parameters dominate largely over the internal impedance only at extremely low frequencies and typically

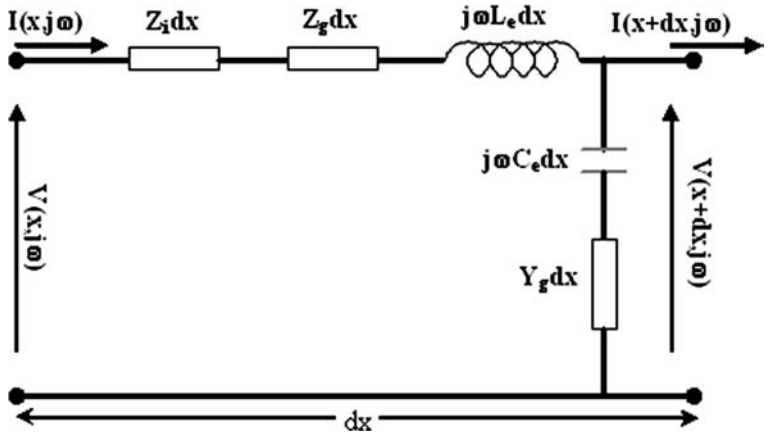

Figure 8: Transmission line segment with all the transmission line parameters for an above ground wire.

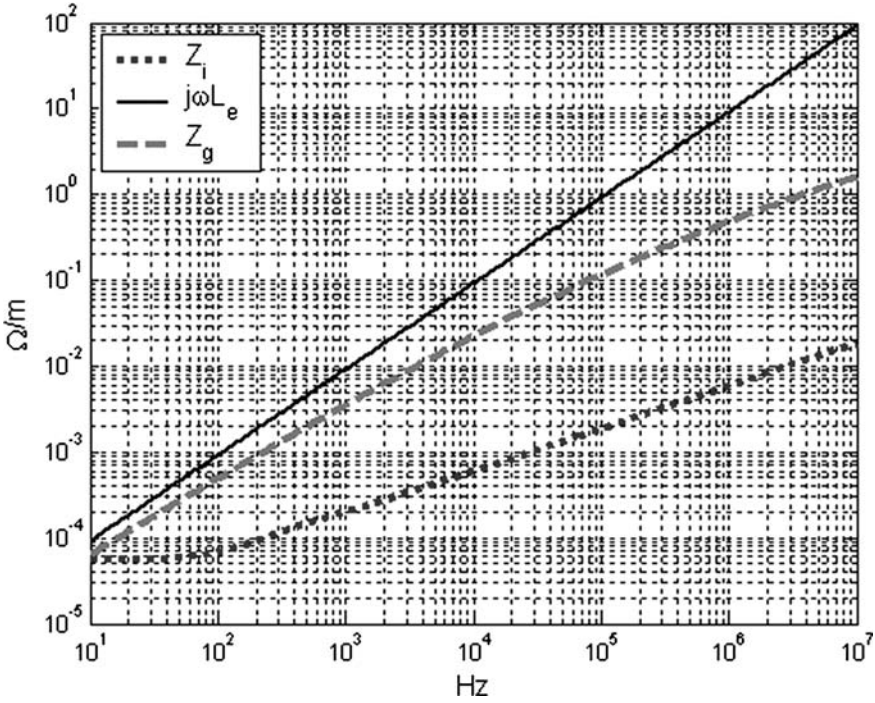

Figure 9: Transmission line impedance parameters comparisons as a function of frequency for copper wire 1 cm radius, 8 m height above ground of conductivity 10 mS/m and ground relative permittivity of 10.

when the conductor heights are close to the ground the internal impedance effects should also be considered. Similar conclusion has been made in [28, 29] for typical overhead wires. In [35] it is shown that even for conductors close to the lossy ground the internal impedance effects are negligible. Hence, in the analysis with ground losses internal impedance could be neglected to reduce computational difficulties. We shall however see how to include internal impedance in later time domain simulations. Paul in [1, 2] has shown that skin effect phenomenon could be important in simulations of crosstalk phenomenon with printed circuit board lands, etc. with high-frequency pulses.

Next, let us look at the shunt admittance parameters under lossy and lossless conditions. We take the same example as above and calculate the external capacitance using eqn (7); and the ground admittance using eqn (26). The comparison is shown in Fig. 10, where it can be seen that ground impedance can be simply neglected for above ground wires since its contribution to the overall shunt admittance of the line is negligible. Similar comparison/conclusion was made in [28]. It is shown that influence of ground admittance is negligible when the wire is close to the ground. In [7, 35] it is mentioned that the ground admittance is important only when the wires are on the ground or below the ground which will be

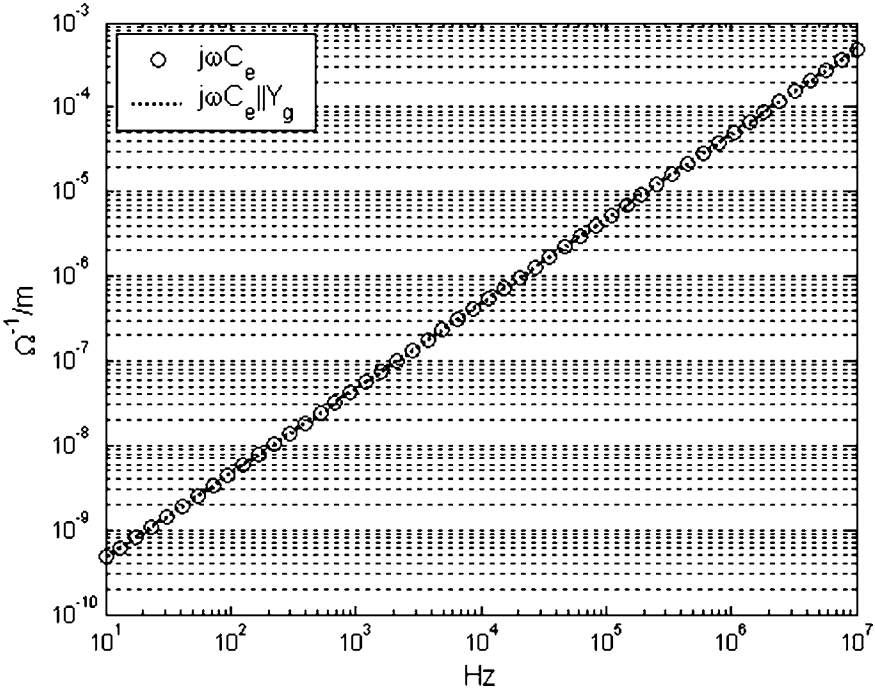

Figure 10: Transmission line admittance parameters comparisons as a function of frequency for copper wire 1 cm radius, 8 m height above ground of conductivity 10 mS/m and ground relative permittivity of 10.

discussed in Chapter 3. Note that we shall from now on neglect the ground admittance for further analysis in this chapter.

The authors would like to mention that pioneering works of Wait [9] and other interesting works by researchers like [10, 36–38], etc., on the subject of wave propagation on wires above ground will give broader insight into the electromagnetism and mathematical principles underlying the problem under study. Those works could motivate researchers and engineers to develop more accurate and simple expressions for ground impedance and admittance for direct application to various practical problems.

2.4 Transmission line equations time domain for wires above ground

Any frequency-dependant loss in time domain will lead to convolutions in time domain. Thus with ground losses and skin effect losses included for wires above ground the relevant transmission line equations, i.e. the voltage and current wave equations are given by eqns (27a) and (27b), respectively, for a system of MTL under the zero external field illumination. Note that for the skin effect loss the impedance corresponding to eqn (12) is used in eqn (27a). Thus the problem remains in solving the two convolutions in eqn (27a). We shall adopt the most widely used method in solving the transmission line equations, i.e. the finite difference time domain

(FDTD) method. This method has been applied by various researchers for different external field excitation problems (electromagnetic pulse, lightning, switching, etc.), grounding systems, electronic printed circuit boards, etc. This method also allows us to include other non-linear devices as terminal loads, making it very suitable to simulate practical systems for transient protection.

$$\frac{\partial V(x,t)}{\partial x} + AI(x,t) + \frac{B}{\sqrt{\pi}}\left(\int_0^t \frac{1}{\sqrt{\tau}} \frac{\partial I(x,t-\tau)}{\partial (t-\tau)} \mathrm{d}\tau\right) + L_\mathrm{e} \frac{\partial I(x,t)}{\partial t} + \int_0^t \zeta(t-\tau) \frac{\partial I(x,\tau)}{\partial \tau} \mathrm{d}\tau = 0 \tag{27a}$$

$$\frac{\partial I(x,t)}{\partial x} + C_\mathrm{e} \frac{\partial V(x,t)}{\partial t} = 0 \tag{27b}$$

2.4.1 Time domain transient ground impedance

Before going further, it is important that we discuss the concept of transient ground impedance, i.e. the last term on the left-hand side of eqn (27a). In principle, the transient ground impedance is defined as either Laplace or Fourier inverse of ground impedance as eqn (28).

$$\zeta(t) = L^{-1}\left(\frac{Z_\mathrm{g}(j\omega)}{j\omega}\right) = F^{-1}\left(\frac{Z_\mathrm{g}(j\omega)}{j\omega}\right) \tag{28}$$

Using the initial value theorem, it is easier to find the transient ground impedance value at $t = 0$, which is necessary for FDTD calculations (to be discussed later).

$$\lim_{t\to 0} \zeta(t) = \lim_{S\to\infty} S \frac{Z_\mathrm{g}(S)}{S} \tag{29}$$

It is clear that based on eqn (29) the value of transient ground impedance at zero time is eqn (22) for self or mutual impedance as the case may be. It is important to mention that in the literature there are no time domain expressions for transient ground impedance (28). But there are some expressions that are based on approximations. We shall take them one by one as transient ground impedance for complete time including $t = 0$ is needed for the FDTD calculations [33, 39, 40].

Timotin [41] first developed the time domain transient ground impedance expression by performing inverse Fourier transforms of Carson's expression. Later, Orzan [42] extended Timotin's expressions for the mutual transient ground impedance, as shown in eqn (30), which is applicable only when $\sigma_\mathrm{g} >> \omega\varepsilon_\mathrm{g}$. This approximation is also called the late time (LT) approximation as it is applicable to the complete low-frequency spectrum.

It is not certain as to how the transient ground impedance behaves in the transition region and in the very high-frequency region as there could be some doubts on the limits of transmission line approximation itself. Still to facilitate the calculations by FDTD method, it is essential that some time domain expression covering both early and the late time regions should be known.

$$\zeta_{kl}^{\mathrm{LT}}(t) = \frac{1}{2}\left\{\frac{\mu_0}{\pi\tau_{kl}^*}\left[\frac{1}{2\sqrt{\pi}}\sqrt{\frac{\tau_{kl}^*}{t}}+\frac{1}{4}\exp\left(\frac{\tau_{kl}^*}{t}\right)\mathrm{erfc}\left(\sqrt{\frac{\tau_{kl}^*}{t}}\right)-\frac{1}{4}\right]\right.$$
$$\left.+\frac{\mu_0}{\pi\tau_{kl}}\left[\frac{1}{2\sqrt{\pi}}\sqrt{\frac{\tau_{kl}}{t}}+\frac{1}{4}\exp\left(\frac{\tau_{kl}}{t}\right)\mathrm{erfc}\left(\sqrt{\frac{\tau_{kl}}{t}}\right)-\frac{1}{4}\right]\right\} \tag{30a}$$

$$\tau_{kl} = \left(\frac{h_k+h_l}{2}+j\frac{d_{kl}}{2}\right)^2 \mu_0\sigma_{\mathrm{g}} \tag{30b}$$
$$\tau_{kl}^* = \mathrm{Conj}(\tau_{kl})$$

Two expressions that are available in the literature are due to Araneo and Cellozi [39] (eqn (31a)) and Rachidi *et al*. [40] (eqn (32)).

$$\zeta_{kl}^{\mathrm{AC}}(t) = \mathrm{e}^{-\left(\frac{5t}{\tau_L}\right)}(\zeta_{kl}^{\mathrm{ET}}-\zeta_{kl}^{\mathrm{LT}})+\zeta_{kl}^{\mathrm{LT}} \tag{31a}$$

$$\tau_{\mathrm{L}} = \frac{1}{\min\left\{\frac{0.1\sigma_{\mathrm{g}}}{2\pi\varepsilon_{\mathrm{g}}};\frac{0.1(h_k+h_l)3\times10^8}{\pi(d_{kl}^2+[h_k+h_l]^2)}\right\}} \tag{31b}$$

$$\zeta_{kl}^{\mathrm{RE}}(t) = \min\left\{\sqrt{\frac{\mu_0}{\varepsilon_{\mathrm{g}}}}\frac{h_k+h_l}{\pi(d_{kl}^2+[h_k+h_l]^2)};\zeta_{kl}^{\mathrm{LT}}(t)\right\} \tag{32}$$

In eqn (31a) the early time (ET) ground impedance expression (33) is used, which was obtained by Araneo and Cellozi [39] by Laplace transforming the very high-frequency approximation of ground expression proposed by Semlyen [8].

$$\zeta^{\mathrm{ET}}(t) = \frac{h_k+h_l}{\pi(d_{kl}^2+[h_k+h_l]^2)}\sqrt{\frac{\mu_0}{\varepsilon_{\mathrm{g}}}}\,\mathrm{e}^{-\sigma_{\mathrm{g}}t/2\varepsilon_{\mathrm{g}}}I_0\left(\frac{\sigma_{\mathrm{g}}t}{2\varepsilon_{\mathrm{g}}}\right) \tag{33}$$

In eqn (33), $I_0(\cdot)$ is the modified Bessel function of the first kind. A comparison of various ground impedance expressions has been made in [33, 35]. According to [39], the maximum frequency at which Carson's equation is valid is evaluated

as the minimum criterion $f_{cr}^{LF} = \min(0.1\sigma_g/2\pi\varepsilon_g, 0.1c/2\pi h)$ [8, 39]. Hence in time domain the corresponding late time approximation (30a) can be used at a time greater than $1/f_{cr}^{LF}$ [39]. The Semlyen's very high-frequency ground impedance expression proposed in [8] can be used when the frequency is higher than $f_{cr}^{LF} = \sigma_g/\pi\varepsilon_g$ [39]. Therefore, in time domain the early time transient ground impedance (33) can be used for times less than $1/f_{cr}^{HF}$ [39]. In the expression (31), the filter concept was used [39] to arrive at the transient ground impedance approximation. The other approximation, proposed by Rachidi *et al*. [40] (eqn (32)) uses the minimum of asymptotic value of the transient impedance and the late time approximation. A comparison of these two transient ground impedance expressions (31) and (32) with the inverse Fourier transform of Sunde's ground impedance expression using eqns (19) and (28) is shown in Fig. 11 for a conductor of 10 m height and ground conditions of σ_g = 2 mS/m and ε_{rg} = 10.

It is seen that both the transient ground impedance expressions (31) and (32) are reasonably good approximations. However, the deviation between two transient ground impedance expressions will be higher when the ground conductivity is poor or conductor heights are smaller [33, 35]. Let us next discuss the method of solving the transmission line equations (27) using the FDTD method.

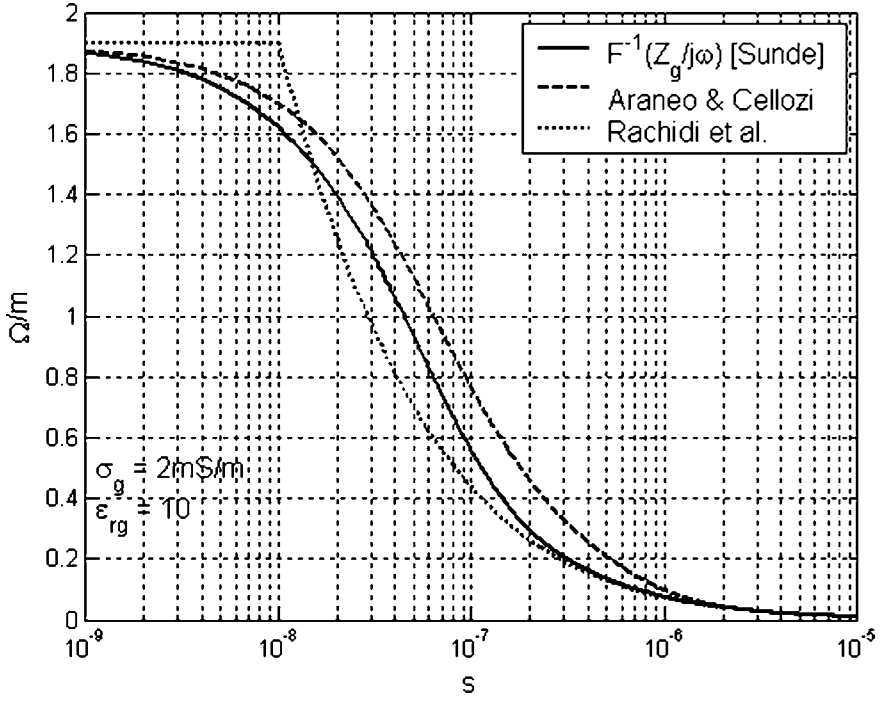

Figure 11: Transient ground impedance comparisons between Araneo and Cellozi, Rachidi *et al*. and actual inverse Fourier transforms of Sunde ground impedance expressions for 10 m conductor height and σ_g = 2 mS/m and ε_{rg} = 10.

3 Time domain numerical solutions for transmission line equations

3.1 Finite difference time domain method

The best available and simple method to solve the telegrapher's equations is to use the FDTD technique. It was first used to solve the Maxwell equations in differential form using the Yee cell approach [43]. Note that excellent discussions to the subject of FDTD methods for transmission lines problems and full wave field solutions can be found in the books by Taflove [44] and specifically for transmission lines in Paul [2]. To discuss the FDTD method let us assume a system of MTLs that are terminated in some resistive loads. We refer one of the ends as the source end and the other as the load end. The diagonal matrix of loads at the source end will be referred to as R_S and similarly for the far-end as R_L. Let the voltage source vector at the source end be V_S and similarly for the far-end be V_L. The representation is shown in Fig. 12.

For transmission line type problems, the simplicity of FDTD method is such that the problem is one-dimensional propagation and all the main parameters with regard to field coupling between wires is inherent in the inductance, capacitance and ground impedance and admittance matrix. Thus, space and time variables are connected to voltages and currents (dual to electromagnetic fields) along the line in differential equations (27). The FDTD method uses central difference approximations to discretize (27) in terms of time and space steps.

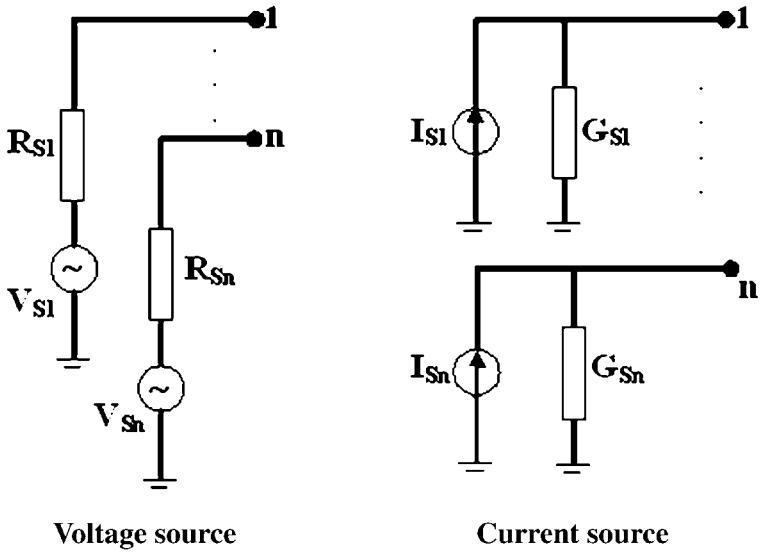

Figure 12: The possible types of injection at the terminations on a system of n conductor MTLs (shown only at the source end here).

The solution to the problem is achieved by means of leap-frog scheme [2, 44], i.e. for a given time step, first the voltages are calculated and then the currents; again the voltages and then the currents; and so on. In the FDTD method there are NDX+1 voltage nodes and NDX current nodes on the line separated by a length of dx [2]. The ends of the line are essentially voltage nodes and every current node is at the mid-point between two voltage nodes. The voltage nodes are solved first and then the current nodes, the recursive equations for the voltage nodes are given below and are obtained by discretization of the current wave equation and then satisfying the boundary condition at the two end nodes. Note that the stability of FDTD method depends on the time and space discretization and it must satisfy the Courant condition, i.e. $\Delta x/\Delta t \geq \upsilon$, where υ is the maximum phase velocity of the currents or voltages propagating on the line. Paul [2] suggests that stability of the system is assured when the total number of time steps NDT and space steps NDX satisfy (34).

$$\text{NDT} \geq \text{NDX} \times \frac{\upsilon}{\text{Line length}} \times \text{Final solution time} \tag{34}$$

The voltage nodes are solved first and then the current nodes, the recursive equations for the voltage nodes are given below.

For the first node the recursive relation is eqn (35).

$$V_1^{n'+1} = \left(\frac{R_S^{-1}}{2} + \frac{C_e\,\Delta x}{2\,\Delta t}\right)^{-1}\left[\left(-\frac{R_S^{-1}}{2} + \frac{C_e\,\Delta x}{2\,\Delta t}\right)V_1^{n'} + \frac{R_S^{-1}}{2}(V_S^{n'+1} + V_S^{n'}) - I_1^{n'+\frac{1}{2}}\right] \tag{35}$$

For the last node the recursive relation is eqn (36).

$$V_{\text{NDX}+1}^{n'+1} = \left(\frac{R_L^{-1}}{2} + \frac{C_e\,\Delta x}{2\,\Delta t}\right)^{-1}\left[\left(-\frac{R_L^{-1}}{2} + \frac{C_e\,\Delta x}{2\,\Delta t}\right)V_{\text{NDX}+1}^{n'} + \frac{R_L^{-1}}{2}(V_L^{n'+1} + V_L^{n'}) + I_{\text{NDX}}^{n'+\frac{1}{2}}\right] \tag{36}$$

For any node in between the line the recursive relation is eqn (37).

$$V_k^{n'+1} = \left(\frac{C_e}{2\,\Delta t}\right)^{-1}\left[\left(\frac{C_e}{2\,\Delta t}\right)V_k^{n'} + \frac{I_k^{n'+\frac{1}{2}} + I_{k-1}^{n'+\frac{1}{2}}}{\Delta x}\right] \tag{37}$$

Before going to the current wave equations, it is necessary to understand that we need to use the recursive convolutions [45], which are computationally more

efficient than the convolution by numerical integration as carried out in [28, 29]. This is now explained by an example. Consider we need to convolute two time functions $f(t)$ and $g(t)$ as in eqn (38) at any given time using trapezoidal rule of integration (39).

$$cv(t) = f(t) \otimes g(t) = \int_0^t f(\tau)\, g(t-\tau)\, \mathrm{d}\tau \tag{38}$$

$$\begin{aligned} cv(n'\Delta t) &= \int_0^{n'\Delta t} f(\tau) g(t-\tau)\, \mathrm{d}\tau \\ &= \frac{\Delta t}{2}\left(f(0) g(n'\Delta t) + 2\sum_{i=1}^{n'} [f(i\,\Delta t)\, g((n'-i)\Delta t)] + f(n'\Delta t)\, g(0) \right) \end{aligned} \tag{39}$$

As mentioned earlier, it is seen that the product terms in the trapezoidal integration changes at every time step and therefore the summation has to be made using all the previous current terms, which certainly will put a heavy computational burden and memory requirements if we have many conductors in the MTL system. At this juncture, we can use the concept of recursive convolution as proposed in [39]. This demands only the saving of a couple of old current values. One of the requirements to use recursive convolution is to find an exponential approximation for $g(t)$. For our case we need to find an exponential approximation for the transient ground impedance $\zeta(t)$. Let us assume that we have an exponential approximation for $g(t)$ with p exponential terms as in eqn (40). Note that the transient ground impedance could be fitted using Prony approximation [46].

$$g(t) = \sum_{i=1}^{p} a_i \mathrm{e}^{-\alpha_i t} a \tag{40}$$

Note that eqn (40) in frequency domain is eqn (41), which requires the determination of poles and residues for this well-known frequency domain fitting called the vector fitting [47] could be used. The authors have adopted this method for fitting Sunde's ground impedance expression.

$$G(S) = \sum_{i=1}^{p} \frac{a_i}{S + a_i} \tag{41}$$

Assuming, for simplicity, that there is just one exponential, we have recursive convolutions technique as explained below. This interesting trick was introduced by Semlyen and Dabuleanu, see appendix in [45].

$$cv(t) = \int_0^t f(t-\tau) a_1 \mathrm{e}^{-\alpha_1 \tau}\, \mathrm{d}\tau \tag{42}$$

$$cv(t-\Delta t)=\int_{0}^{t-\Delta t} f(t-\Delta t-\tau)\,a_1 e^{-a_1\tau}\,d\tau \tag{43}$$

Equation (43) can be split as eqn (44)

$$cv(t)=\int_{\Delta t}^{t} f(t-\tau)a_1 e^{-a_1\tau}\,d\tau+\int_{0}^{\Delta t} f(t-\tau)a_1 e^{-a_1\tau}\,d\tau \tag{44}$$

Making a change of variables as $\tau=\tau'+\Delta t$, in the first term on the right-hand side of eqn (44) and after simplification and change of limits we have

$$\int_{\Delta t}^{t} f(t-\tau)a_1 e^{-a_1\tau}\,d\tau = e^{-a_1\Delta t}\int_{0}^{t-\Delta t} f(t-\Delta t-\tau)a_1 e^{-a_1\tau'}\,d\tau' \tag{45}$$

Comparing eqns (45) and (43) and substituting in eqn (44), we have eqn (46).

$$cv(t)=e^{-a_1\Delta t}cv(t-\Delta t)+\int_{0}^{\Delta t} f(t-\tau)a_1 e^{-a_1\tau}\,d\tau \tag{46}$$

As can be seen from eqn (46) any new value of the convolution is dependant on the old value of the convolution.

This technique has been adopted by Araneo and Celozzi [39] for the solution of the FDTD method involving ground loss to discretize the first transmission line equation and the recursive relation is shown below. Note that the internal impedance loss is also included as recursive convolution which is adopted from Paul [2]. The recursive relation for the current is given by eqn (47) for any node.

$$I_k^{n'+\frac{1}{2}}=\left(\frac{L_e}{\Delta t}+\frac{A}{2}+\frac{2s\rho(0)}{\sqrt{\pi\Delta t}}+\frac{\zeta(0)}{2}\right)^{-1}\left[\left(\frac{L_e}{\Delta t}-\frac{A}{2}+\frac{2B\rho(0)}{\sqrt{\pi\Delta t}}+\frac{\zeta(0)}{2}-\frac{\zeta(\Delta t)}{2}\right)I_k^{n'-\frac{1}{2}}\right.$$
$$\left.-\frac{B}{\sqrt{\pi\Delta t}}\sum_{i=1}^{10}\Psi_i^{n'}+\frac{\zeta(\Delta t)}{2}I_k^{n'-\frac{3}{2}}-\frac{V_{k+1}^{n'}-V_k^{n'}}{\Delta x}-CI_k^{n'}\right] \tag{47}$$

There are various terms in eqn (48) that need to be calculated before evaluating eqn (47). Let the transient ground impedances be fitted as sums of exponentials as in eqn (48).

$$\zeta(t)\approx AA_1 e^{-\chi_1 t}+AA_2 e^{-\chi_2 t}+\cdots+AA_N e^{-\chi_N t} \tag{48}$$

For the skin effect mechanisms, the table in Fig. 13 shows the constants and exponential terms as taken from Paul [2]. Note that based on the conductor geometry and material properties, A and B in eqn (12) have to be calculated a priory. Using constants from Fig. 13, terms $\rho(0)$ and Ψ in eqn (47) can be calculated as below.

$$\rho(0) = \sum_{i=1}^{10} a_i \tag{49}$$

$$\Psi_i^n = a_i \mathrm{e}^{\alpha_i} \left(I_k^{n'+\frac{1}{2}} - I_k^{n'-\frac{1}{2}} \right) + \mathrm{e}^{\alpha_i} \Psi_i^{n'-1} \tag{50}$$

The terms $\zeta(0)$ and $\zeta(\Delta t)$ are the value of transient ground impedance and zero time and first time steps. The convolution term *CI* is calculated as below and the method is same as explained in [39]. For an *n* conductor MTL system *CI* is a summation as in eqn (51) for a given node and time instant.

$$CI_m = \sum_{j=1}^{n} CI_{mj} \tag{51}$$

Each convolution term in eqn (51) is given by eqn (52) for *N* number of exponential or constant terms in the fitting of transient ground impedance.

$$CI_{mj} = \sum_{r=1}^{N} CI_{mj,r} \tag{52}$$

i	a_i	α_i
1	0.790 981 80E − 1	−0.114 844 27E − 2
2	0.115 434 23E0	−0.138 183 29E − 1
3	0.134 353 80E0	−0.540 375 96E − 1
4	0.218 704 22E0	−0.142 164 94E0
5	0.982 296 67E − 1	−0.301 284 37E0
6	0.513 604 84E0	−0.561 421 85E0
7	−0.209 628 98E0	−0.971 171 26E0
8	0.119 744 47E1	−0.163 384 33E1
9	0.112 254 91E − 1	−0.289 513 29E1
10	−0.744 252 55E0	−0.504 109 69E1

Figure 13: Table of constants and exponential terms for the skin effect phenomena (adapted from [2]).

The recursive relation for each term in eqn (52) at a given node and time instant is given by eqn (53).

$$CI_{mj,r_k^{n'+1}} = \mathrm{e}^{\chi_{mj,r}\Delta t}\left(CI_{mj,r_k^{n'}} + \frac{1}{2}AA_{mj,r}\left[I_k^{n'+\frac{1}{2}} - I_k^{n'-\frac{1}{2}}\right] + \frac{1}{2}AA_{mj,r}\mathrm{e}^{\chi_{mj,r}\Delta t}\left[I_k^{n'-\frac{1}{2}} - I_k^{n'-\frac{3}{2}}\right]\right) \tag{53}$$

It is worth discussing the errors associated with recursive convolution. It is largely dependant on the accuracy of fitting. Based on [39], care has to be taken to have minimum error at the time $t = 0$ and at first time step. The decaying nature of the transient impedance decides the peaks and rise times of the final wave shapes. When the number of conductors is more, it is not computationally efficient to use more exponential terms for the highest possible accuracy. Hence, an exponential approximation that fits the transient ground impedance to a reasonable accuracy is needed.

Note that in all the discussions above the sources at ends of the line were assumed to be voltage sources and that it is also possible to extend all the above equations to current source feeding at the ends of the line by using the conventional circuit theory, i.e. source transformations, Thevinin and Norton equivalents, etc. Next we shall discuss the frequency domain solution for completeness.

3.2 Frequency domain solutions for MTL systems

In frequency domain the MTL system has to be uncoupled and then the system of uncoupled equations have to be solved. There are numerical complexities involved in frequency domain, while solving for eigenvalue problem [2]. The Matlab [48] functions for eigenvalue calculations can be used. Some errors could propagate at this stage. Some errors could occur while performing the inverse Fourier transforms to the frequency response of voltages or currents. This, however, could be minimized by playing around with sampling frequency and a number of points in the 2^f values. The frequency domain analysis is also referred to as modal analysis. A discussion on the transmission line solutions have been presented in various texts, e.g. [2, 3].

Let us begin with coupled second-order MTL equations. Note that the impedance matrix has inductance, internal impedance and ground impedance matrix and the admittance matrix has the external capacitance matrix.

$$\frac{\mathrm{d}V^2(x, j\omega)}{\mathrm{d}x^2} = ZYV(x, j\omega) \tag{54a}$$

$$\frac{\mathrm{d}I^2(x, j\omega)}{\mathrm{d}x^2} = ZYI(x, j\omega) \tag{54b}$$

Paul in [2] mentions that if we can find two $n \times n$ matrices T_V and T_I which can diagonalize simultaneously both the per-unit length impedance and admittance matrices, then the solution reduces to the solution of n uncoupled first-order differential equations [2]. Thus when the matrices are diagonalized, the system of equations is known as modal telegrapher's equations, which can be easily solved since they are in uncoupled form. Let in modal form the transmission line equations be represented as eqn (55)

$$\frac{\mathrm{d}V_{\mathrm{m}}\left(x, j\omega\right)}{\mathrm{d}x} = -zI_{\mathrm{m}}\left(x, j\omega\right) \tag{55a}$$

$$\frac{\mathrm{d}I_{\mathrm{m}}(x, j\omega)}{\mathrm{d}x} = -yV_{\mathrm{m}}(x, j\omega) \tag{55b}$$

In eqn (55) z and y are the modal impedance matrices (diagonal) and they are connected to the actual line impedance and admittance matrix through the transformation matrix, obtained as

$$z = T_V^{-1} Z T_I \tag{56a}$$

$$y = T_I^{-1} Y T_V \tag{56b}$$

The second-order modal MTL equations in uncoupled form is given by

$$\frac{\mathrm{d}V_{\mathrm{m}}^2(x, j\omega)}{\mathrm{d}x^2} = zyV_{\mathrm{m}}(x, j\omega) \tag{57a}$$

$$\frac{\mathrm{d}I_{\mathrm{m}}^2(x, j\omega)}{\mathrm{d}x^2} = zyI_{\mathrm{m}}(x, j\omega) \tag{57b}$$

It is important to mention that that the product of diagonal modal impedance and admittance matrix is commutative because of which it can be shown by conventional matrix methods that $T_I^{\mathrm{t}} = T_V^{-1}$ [2].

Consider the second-order modal MTL equation corresponding to the current

$$\frac{\mathrm{d}^2 I_{\mathrm{m}}(x, j\omega)}{\mathrm{d}x} = T_I^{-1} Y Z T_I I_{\mathrm{m}}(x, j\omega) = \gamma^2 I_{\mathrm{m}}(x, j\omega) \tag{58}$$

In eqn (58) γ^2 is a diagonal matrix. The solution to the modal currents are given by

$$I_{\mathrm{m}}(x, j\omega) = \mathrm{e}^{-\gamma x} I_{\mathrm{m}}^{+} - \mathrm{e}^{\gamma x} I_{\mathrm{m}}^{-} \tag{59}$$

The exponential terms in eqn (59) are diagonal matrices and the other terms are vectors. The final solution for the current and voltage are given by eqn (60).

$$I(x, j\omega) = T_I I_{\mathrm{m}}(x, j\omega) \tag{60}$$

Similar analysis can be made for the determination of voltage starting form eqn (61).

$$V(x, j\omega) = (T_I^{-1})^{\mathrm{t}} V_{\mathrm{m}}(x, j\omega) \tag{61}$$

$$V(x, j\omega) = (T_I^{-1})^{\mathrm{t}} V_{\mathrm{m}}(x, j\omega) \tag{62}$$

$$V(x, j\omega) = Z_0 T_I \left[\mathrm{e}^{-\gamma x} I_{\mathrm{m}}^{+} + \mathrm{e}^{\gamma x} I_{\mathrm{m}}^{-} \right] \tag{63}$$

The characteristic impedance Z_0 can be calculated from eqn (64).

$$Z_0 = Z T_I \gamma^{-1} T_I^{-1} = Y^{-1} T_I \gamma T_I^{-1} \tag{64}$$

Note that in all the above analyses, the matrix multiplication order must be maintained. The unknown parameters that could be encountered while solving above equations can be obtained by proper treatment of boundary condition at the near- and far-end of the lines. Note that Thevenin and Norton theorems shall be applied appropriately at the line ends. For a voltage feeding at the line ends, we have the following corresponding to Fig. 12 and assuming that L is the length of the line or line location.

$$V(0, j\omega) = V_{\mathrm{S}}(j\omega) - R_{\mathrm{S}} I(0, j\omega) \tag{65a}$$

$$V(L, j\omega) = V_{\mathrm{L}}(j\omega) - R_{\mathrm{L}} I(L, j\omega) \tag{65b}$$

Using eqn (65) the parameters I_{m}^{+} and I_{m}^{-} can be obtained as eqn (66) [2]

$$\begin{pmatrix} (Z_0 + R_{\mathrm{S}}) \cdot T_I & (Z_0 - R_{\mathrm{S}}) T_I \\ (Z_0 - R_{\mathrm{L}}) T_I \mathrm{e}^{-\gamma L} & (Z_0 + R_{\mathrm{L}}) T_I \mathrm{e}^{\gamma L} \end{pmatrix} \begin{pmatrix} I_{\mathrm{m}}^{+} \\ I_{\mathrm{m}}^{-} \end{pmatrix} = \begin{pmatrix} V_{\mathrm{S}} \\ V_L \end{pmatrix} \tag{66}$$

Similarly for a current source feeding at the ends of the line can be derived as eqn (67) [2].

$$\begin{pmatrix} (G_{\mathrm{S}} Z_0 + 1^n) T_I & (G_{\mathrm{S}} Z_0 - 1^n) T_I \\ (G_{\mathrm{L}} Z_0 - 1^n) T_I \mathrm{e}^{-\gamma L} & (G_L Z_0 + 1^n) T_I \mathrm{e}^{\gamma L} \end{pmatrix} \begin{pmatrix} I_{\mathrm{m}}^{+} \\ I_{\mathrm{m}}^{-} \end{pmatrix} = \begin{pmatrix} I_{\mathrm{S}} \\ I_{\mathrm{L}} \end{pmatrix} \tag{67}$$

Thus, we have the expressions for voltage and current distribution along the line which can be calculated for any source injection or illumination. An example of comparison between frequency domain and time domain FDTD method by a typical lossy problem will be demonstrated next.

3.3 Comparison between direct frequency domain solutions and FDTD method

It is to be mentioned that majority of the transients have double exponential wave shape as given by eqn (68).

$$I_{\mathrm{s}}(t) = I_{\mathrm{p}}(\mathrm{e}^{-t/t_1} - \mathrm{e}^{-t/t_2}) \tag{68}$$

Let us first take an example of perfectly conducting ground and ideal case. The case being simulated is the following. Two conductors are parallel to each other and located at 10 m height and have radii of 5.6 mm. The conductors have a horizontal separation of 1 m and lines are 3 km long. A current source having shape given by eqn (68) with $I_p = 1.13$, $t_1 = 100$ μs, $t_2 = 2.5$ μs is directly fed into the source line and at the far-end of the source line a resistance of 490 Ω is terminated.

This current source has a peak of 1 A and about 10 μs rise time and 50% tail time of 60–70 μs. On the other line (receptor line, which is a crosstalk nomenclature discussed in Section 4) both at the near- and far-ends the termination resistances are 490 Ω. Simulations are carried out by the FDTD method and frequency domain solutions (see Section 3.2). Note that the frequency responses are inverse Fourier transformed to compare with time domain solutions. The time responses of currents at the near- and far-end loads of the receptor wire are shown in Fig. 14. It is seen that more or less the two solutions by different methods are identical.

Next let us take up the same example as above but now by using the finitely conducting ground. The ground conductivity chosen was 1 mS/m with ground relative permittivity of 10. The Sunde ground impedance was vector fitted [47] to obtain the constants and exponential parameters for the recursive convolution in the FDTD method. This was made to eliminate any approximations associated

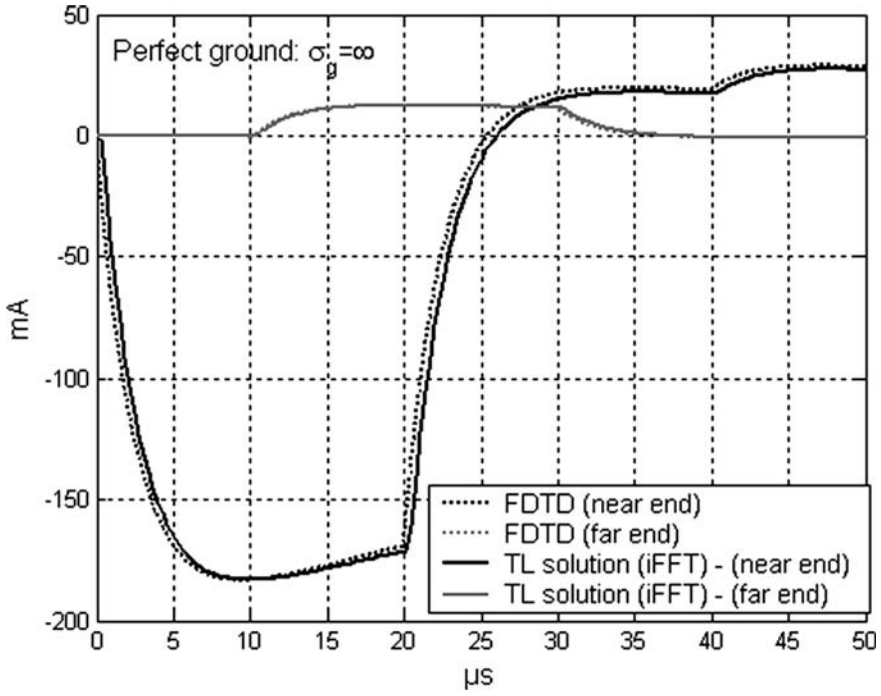

Figure 14: Frequency and time domain solution comparison for a typical crosstalk problem for perfect ground conditions.

with transient ground impedance calculations in time domain. The simulations for this lossy case with all the other simulation parameters remaining unaltered compared to the previous case are shown in Fig. 15 for the near- and far-end currents of the receptor.

As can be seen from Fig. 15 that just by the introduction of ground losses the shapes and magnitudes of currents at near- and far-ends of the wire have changed considerably. For this reason in Section 4, we deal with the interesting subject of crosstalk in MTL system. Note that only parameters that will influence the crosstalk mechanisms will be discussed using typical examples and simple circuit analysis. The subject of crosstalk is wide area of research in electromagnetic compatibility.

4 Crosstalk in MTL systems

When the distance between source of disturbance and the system suffering interference is very small, the victim system is in the near-field region of the source system. Then the coupling path process between the source and victim is referred to as crosstalk. Crosstalk from one system to other can occur when the systems share a common-impedance (or shared conductor). It also happens through electromagnetic coupling in the near-field. Sometimes electromagnetic

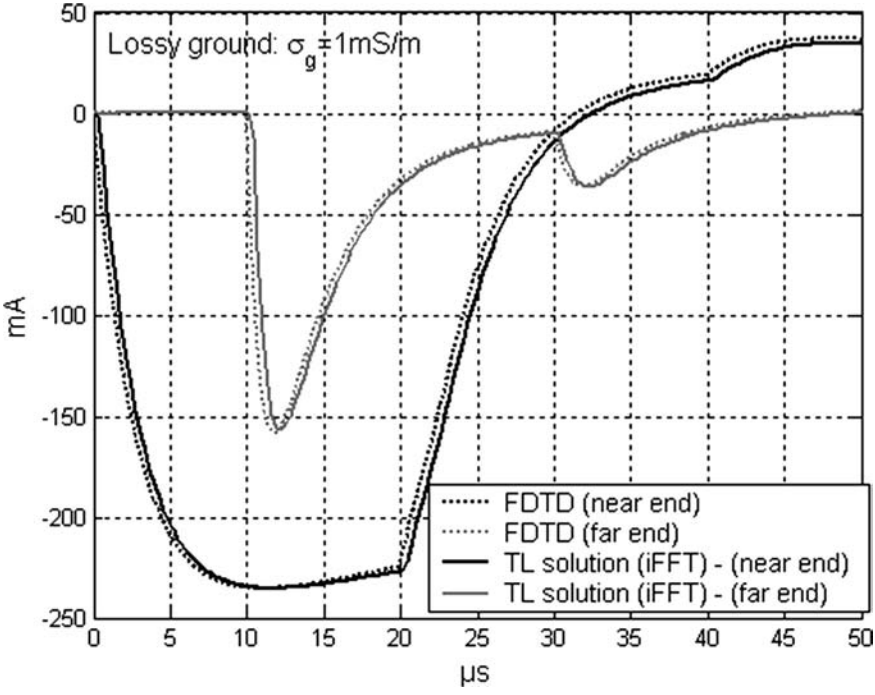

Figure 15: Frequency and time domain solution comparison for a typical crosstalk problem for lossy ground conditions σ_g = 1 mS/m and ε_{rg} = 10.

field coupling can be decomposed into that primarily due to magnetic field (inductive crosstalk) or primarily due to electric field (capacitive crosstalk). In many situations, crosstalk happens as a mixture of common-impedance and electromagnetic field coupling. Various researchers have contributed to studying the mechanism of crosstalk. The authors' at this juncture would like to acknowledge that it was Paul [1, 2] through his interesting works has given a new dimension and better understanding of the phenomena of crosstalk. In order to have crosstalk, we need to have at least three conductors, one source wire and the other receptor wire (one could have many receptor wires in MTL systems) and the third wire or plane is the return path. Crosstalk in general increases with increasing frequency, unless the skin effect acts to screen it off as in a homogeneous shield of a cable. In the following sections we will analyse different types of crosstalk and find out the various factors influencing them under weak coupling assumptions and for lossless case, i.e. for the case of MTL systems above perfectly conducting ground.

4.1 Crosstalk under weak coupling conditions and for electrically short lines

In a system of MTLs one can on priory determine whether the system has weak or strong coupling mechanism from the source frequency, geometry, etc., i.e. system has weak coupling when the coupling coefficients between the source and the receptor as given by eqn (69) satisfies $\kappa << 1$. If in an MTL system the external self and mutual inductance/capacitance per meter is known for perfectly conducting wires above ground then,

$$\kappa_{kl} = \frac{L_{ekl}}{\sqrt{L_{ek}L_{el}}} = \frac{C_{ekl}}{\sqrt{C_{ek}C_{el}}} \tag{69}$$

It should also be mentioned that under weak coupling conditions, the source or emitter voltage and currents are not affected by the receptor or adjacent conductors. In the following analysis, besides weak coupling, electrically small MTL is assumed, i.e. when line length satisfies $L << \lambda$, where λ is the wavelength. Also it is assumed that self-inductive impedance of the conductors are small compared to the terminal loads, i.e. $\omega L_e << R_L$ *or* $R_g$and that capacitive impedance to ground is far greater than the terminal loads, i.e. $1/\omega C_e >> R_L$ *or* R_g.

4.1.1 Crosstalk due to common impedance coupling

Often, two or more current loops share a common conductor, usually the reference conductor or plane as shown in Fig. 16. Let the desired signal be the voltage drop V_{L1} across the resistor R_{L1}. This signal is affected by the current I_2 in circuit 2 (source circuit). In the following analysis we will see how the impedance Z_c of the common connection between circuit 1 (receptor) and circuit 2 (emitter) is the reason for the interference in signal voltage V_{L1}. Remember that at high frequencies, conductors have finite impedance that should not be neglected.

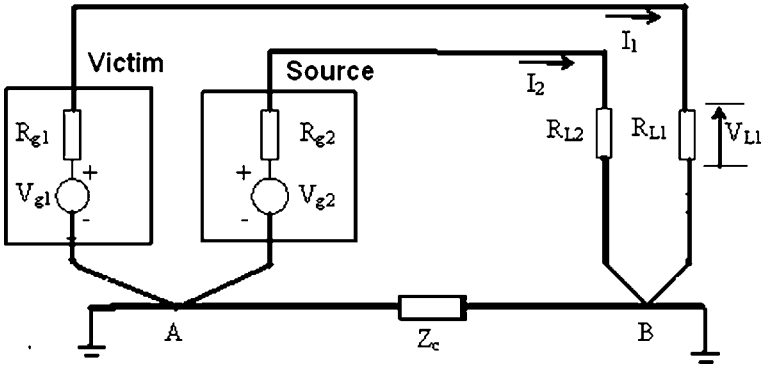

Figure 16: Common impedance coupling representation.

From mesh analysis of loops 1 and 2,

$$V_{g1} = R_{g1}I_1 + R_{L1}I_1 + Z_c(I_1 + I_2) \tag{70a}$$

$$V_{g2} = R_{g2}I_2 + R_{L2}I_2 + Z_c(I_1 + I_2) \tag{70b}$$

If the loop resistances are represented as $R_{loop1} = R_{g1} + R_{L1} + Z_c$ and $R_{loop2} = R_{g2} + R_{L2} + Z_c$ then the voltage drop at can be obtained as eqn (71).

$$I_1 R_{L1} = \frac{V_{g1}R_{L1}}{R_{loop1}} - \frac{Z_c R_{L1}(V_{g2} - Z_c I_1)}{R_{loop1}R_{loop2}} \tag{71}$$

The common impedance Z_c compared with the sum of loop resistances is very small, hence assuming $Z_c^2 << R_{loop1}\, R_{loop2}$, eqn (71) can be simplified to eqn (72).

$$V_{L1} = I_1 R_{L1} = \frac{V_{g1}R_{L1}}{R_{loop1}} - \frac{V_{g2}Z_c R_{L1}}{R_{loop1}R_{loop2}} \tag{72}$$

The second term of eqn (72) represents the noise introduced due to the common impedance Z_c. Interference due to common impedance increases (1) if the common impedance Z_c is increased and (2) if the current through the common impedance due to the disturbing circuit ($I_2 \approx V_{g2}/R_{loop2}$) is increased. Crosstalk due to common impedance can be reduced by keeping Z_c as low as possible or avoiding Z_c altogether. This can be achieved by assigning separate conductors to each loop and connecting each loop to the reference at a single point. Note that common impedance Z_c contains a resistive part and a reactive part. In the case of a shared conductor, the inductive part is dominant at high frequencies ($Z_c \approx j\omega L_c$). Also, in the foregoing analysis, the dimensions of the circuits are assumed to be much less than the wavelengths of interest (electrically small).

If the victim circuit (circuit 1) does not contain any sources ($V_{g1} = 0$), we can rewrite eqn (72) as eqn (73).

$$\frac{V_{L1}}{V_{g2}} = -\frac{Z_c R_{L1}}{R_{loop1} R_{loop2}} \tag{73}$$

Equation (73) can be regarded as a crosstalk transfer function due to common impedance. It is the voltage produced in the victim circuit per unit source voltage in the disturbing circuit.

4.1.2 Crosstalk due to capacitive coupling

Consider two current loops over a conducting plate forming an MTL as shown in Fig. 17, and the loops are electrically small.

Current loops have electromagnetic fields associated with it. First, consider only the electric fields. That is, consider only the capacitive coupling, neglecting the inductive and common impedance couplings. The capacitive coupling between the two loops can be represented by the circuit diagram in Fig. 18. Note C_{12} is the mutual external capacitance and C_r is the external capacitance of the receptor.

Writing equation for currents at node 1 we have,

$$\frac{V_{L1}}{R_{L1}} + \frac{V_{L1}}{R_{g1}} + j\omega C_r V_{L1} + j\omega C_{12}(V_{L1} - V_{L2}) = 0 \tag{74a}$$

Simplifying eqn (74a), we have eqn (74b).

$$V_{L2} = \frac{V_{L1}}{j\omega C_{12}}\left(\frac{1}{R_{g1}} + \frac{1}{R_{L1}} + j\omega C_r + j\omega C_{12}\right) \tag{74b}$$

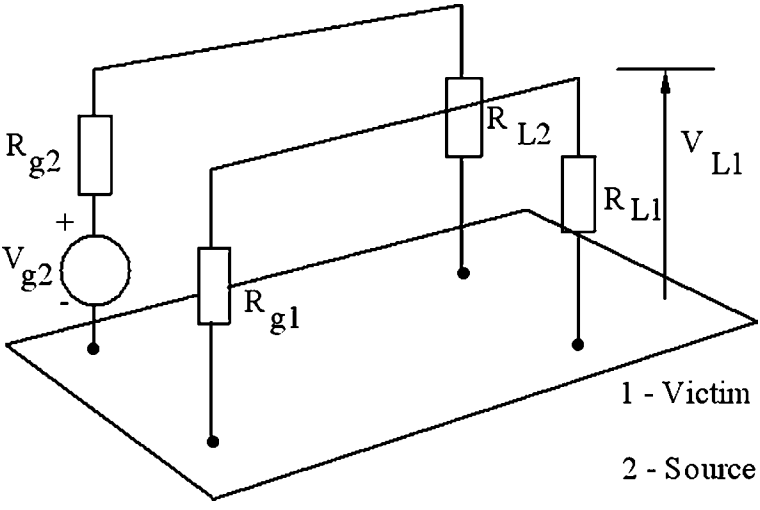

Figure 17: Two conducting wires above a conducting plate forming current loops.

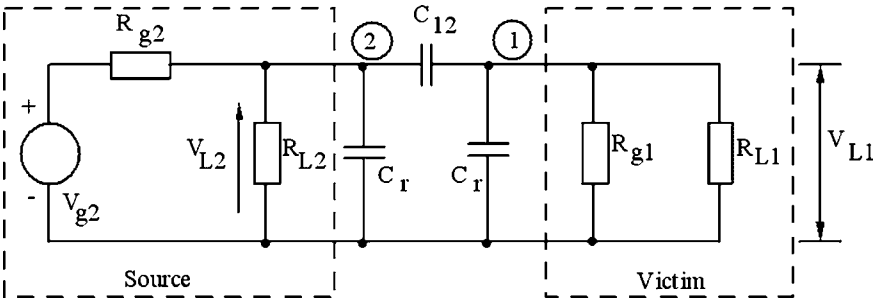

Figure 18: Equivalent circuit showing the capacitive coupling between two loops.

Writing equation for currents at node 2, we have

$$\frac{V_{L2}-V_{g2}}{R_{g2}}+\frac{V_{L2}}{R_{L2}}+j\omega C_r V_{L2}+j\omega C_{12}(V_{L2}-V_{L1})=0 \tag{75a}$$

Simplifying eqn (75a), we have eqn (75b).

$$V_{L2}=\frac{V_{L1}[j\omega C_{12}]+\dfrac{V_{g2}}{R_{g2}}}{\dfrac{1}{R_{g2}}+\dfrac{1}{R_{L1}}+j\omega C_r+j\omega C_{12}} \tag{75b}$$

Equating (74b) and (75b) it is possible to get an expression for transfer function for capacitive crosstalk, V_{L1}/V_{g2} in terms of impedance and capacitance. In a simple case in which all resistance are matched and equal to R we obtain eqn (76).

$$\frac{V_{L1}}{V_{g2}}=\frac{j\omega RC_{12}}{4+j4\omega R(C_{12}+C_r)-\omega^2R^2C_r{}^2\left(1+\dfrac{2C_{12}}{C_r}\right)} \tag{76}$$

Note that eqn (76) is valid only for electrically small circuits and it can be approximated as eqn (77).

$$\frac{V_{L1}}{V_{g2}}\approx\frac{j\omega RC_{12}}{4} \tag{77}$$

From (77), it is observed that: (1) Capacitive crosstalk increases in proportion to the frequency. In time domain, the fast variations in the signal could be responsible for the capacitive crosstalk. (2) For a given mutual capacitance C_{12} and disturbing source V_{g2}, the crosstalk increases with increasing circuit impedance R.

Capacitive crosstalk is present in transformers, switch contacts and in components. The general circuit presented here can be used to analyse these various situations.

In those cases the conductors represent the carriers of common mode signals and the metal plate represent the reference (metal casing, metal cable trunk, reinforcement meshing in concrete floor and walls). It is possible to model the capacitive crosstalk as a current injection into the victim circuit as shown in Fig. 19.

Equation (78) can be obtained from the circuit in Fig. 18.

$$\frac{V_{L1}}{R_{L1}} + \frac{V_{L1}}{R_{g2}} + j\omega C_r V_{L1} - I_c = 0 \tag{78}$$

Substituting eqn (78) in eqn (74a), we get I_c as eqn (79) in frequency and time, with V_{L1} - V_{L2} = V, as the voltage difference between the two circuits.

$$\left.\begin{aligned} I_c &= j\omega(V_{L1} - V_{L2}) \\ I_c &= C_{12}\frac{dV}{dt} \end{aligned}\right\} \tag{79}$$

To avoid/reduce capacitive crosstalk some measures are:

(1) Reduce mutual coupling capacitance C_{12}. This can be achieved by decreasing the surface area of conductors and increasing the distance between them. As a rule-of-thumb, keep the wire separation distance ten times the wire diameter. Introducing a ground plane can significantly reduce C_{12}. In printed circuit boards conductive planes are used to reduce capacitive crosstalk between tracks. In equipment with metal cabinets, the cables may be routed close to the metal panels, so that the crosstalk between the common mode signals of two different cables can be reduced. In metal cable trunks, the cables can be arranged closely against the trunk walls. Caution! If the ground is noisy, the capacitance C_r between the ground and the circuit will introduce noise signals into the circuit.

(2) Capacitive crosstalk increases with frequency, hence do not use frequencies more than that is absolutely necessary. For example, in a digital circuit, do not use pulse rise times (or fall times) more than necessary.

(3) Reduce capacitive coupling using metallic screen (shielding), e.g. screen transformers to reduce crosstalk. Screening breaks up the coupling capacitance

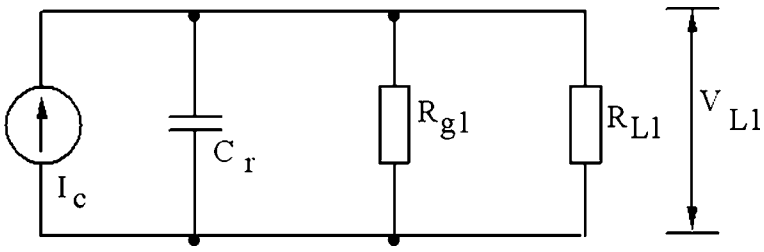

Figure 19: Modelling capacitive coupling as a current injection into the victim or receptor circuit.

C_{12} into two capacitances connected in series. Screening is most effective if it is connected to the reference by low impedance. Then the injected disturbance current has a low-impedance path to the ground.

4.1.3 Crosstalk due to inductive coupling

Consider the two parallel current loops of Fig. 16. Now consider only the magnetic field coupling between the wires. The circuit can be redrawn as shown in Fig. 20.

The mutual inductance M (external inductance L_{12}) accounts for the coupling through the magnetic fields.

The loop equations for loop 1 can be written as eqn (80a).

$$R_{g1}I_1 + j\omega L_1 I_1 + j\omega M I_2 + R_{L1}I_1 = 0 \tag{80a}$$

Equation (80a) can be simplified to eqn (80b).

$$I_2 = \frac{-I_1(R_{g1} + R_{L1} + j\omega L_1)}{j\omega M} \tag{80b}$$

The loop equations for loop 2 can be written as eqn (81a).

$$R_{g2}I_2 + j\omega L_2 I_2 + j\omega M I_1 + R_{L2}I_2 = V_{g2} \tag{81a}$$

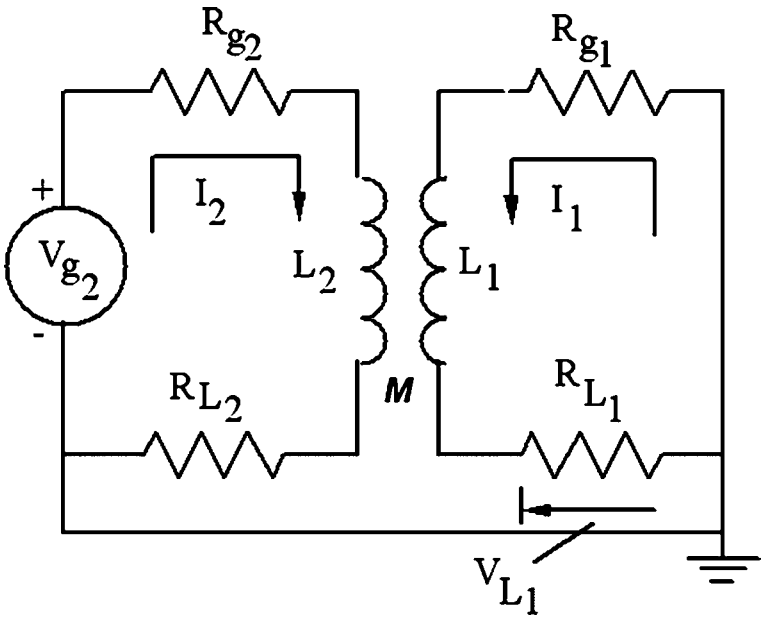

Figure 20: Inductive coupling between two electrically small circuits.

Equation (81a) can be simplified to eqn (81b).

$$I_2 = \frac{V_{g2} - j\omega M I_1}{R_{g2} + R_{L1} + j\omega L_2} \tag{81b}$$

From eqns (80b) and (81b), we can get the transfer function for inductive crosstalk V_{L1}/V_{g2}, for a simplified case in which all resistances are matched and equal to R, and $L_1 = L_2 = L$ is given by eqns (82). Equation (82) can be approximated as eqns (83) when $R > \omega L$.

$$\frac{V_{L1}}{V_{g2}} = \frac{-j\omega RM}{4R^2 + j4\omega RL - \omega^2(L^2 - M^2)} \tag{82}$$

$$\frac{V_{L1}}{V_{g2}} \approx \frac{-j\omega M}{4R} \tag{83}$$

From eqn (83), it is observed that: (1) inductive crosstalk increases in proportion to frequency and (2) for a given mutual inductance M and disturbing source V_{g2}, the inductive crosstalk increases with decreasing circuit impedance R.

It is possible to model inductive crosstalk by a voltage source in series with the victim circuit as shown in Fig. 21.

From Fig. 21, we can write the loop equation (84)

$$R_{g1} I_1 + j\omega L_1 I_1 + R_{L1} I_1 - V_i = 0 \tag{84}$$

Substituting eqn (84) in eqn (80a), we get V_i as eqn (85) in frequency and time.

$$\begin{aligned} V_i &= -j\omega M I_2 \\ V_i &= -M \frac{dI_2}{dt} \end{aligned} \tag{85}$$

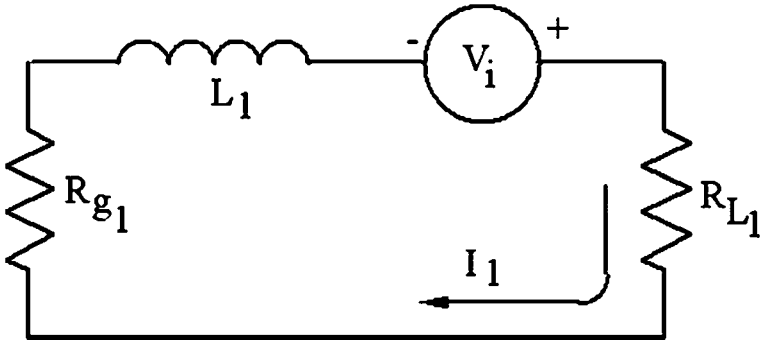

Figure 21: Modelling inductive coupling as a series voltage source.

There are various methods to reduce inductive crosstalk. Make the mutual inductance (M) as low as possible. The value of M decreases as the areas of the loops are reduced and the distances between them are increased.

As far as possible, orient the loops perpendicular to each other so that there is very little coupling between them. Keep the magnetic field H produced by the 'transmitting' loop, as shown in Fig. 22 as small as possible. The value of H can be reduced by running the two conductors of the loop very close to each other. Referring to Fig. 22, the magnetic field strength at a position P is given by eqn (86) which is valid when the radius $r_P >> D_2$.

$$H = \frac{I_2}{2\pi}\left[\left(r_P - \frac{D_2}{2}\right)^{-1} - \left(r_P + \frac{D_2}{2}\right)^{-1}\right] \approx \frac{I_2}{2\pi}\frac{D_2}{r_P{}^2} \tag{86}$$

From eqn (86), it can be clearly seen that reducing the separation, D_2, of conductors in the transmitting loop (equivalent to reducing loop area) reduces the magnetic field at the position of the receiving conductors. The induced voltage per unit length in the receiving loop is eqn (87).

$$V_{\text{ind}} \approx D_1\mu_0\frac{\mathrm{d}H}{\mathrm{d}t} \approx j\omega D_1\mu_0 H \tag{87}$$

From eqn (87), we see that the voltage pickup by the receiving loop is reduced if the distance, D_1, between the conductor pair is small.

Another method is to use twisted pair type conductors. Twisting the conductor pairs or using twisted cables can reduce the crosstalk due to magnetic field coupling. Twisting the transmitting conductor pair reduces the H-field. Twisting the receiving conductor pair further reduces the induced voltage. This is illustrated by an example. Consider an emitter carrying a current I_G that varies with time as shown in Fig. 23.

In Fig. 23, consider the area formed by the one twisted-wire pair with the ground conductor (reference). The unbalanced common mode currents produced in the two wires of the twist effectively produce a net magnetic field opposing the original magnetic flux produced by the generator wire circuit. This is equivalent to a circulating current as shown in Fig. 23. The direction of this induced current in

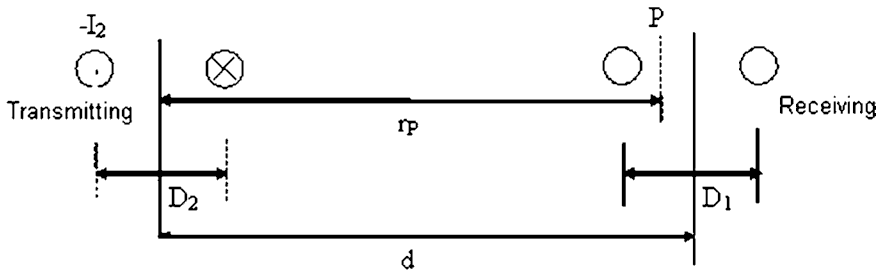

Figure 22: Inductive crosstalk between loops.

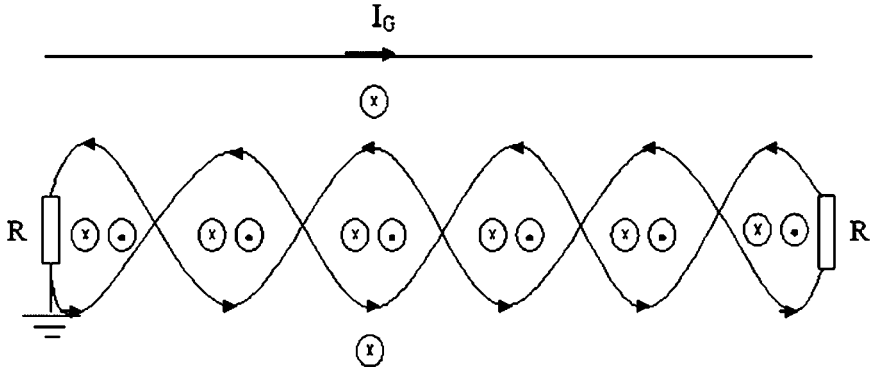

Figure 23: Diagram illustrating the reduction of induced voltage due to magnetic field coupling in a twisted-wire pair.

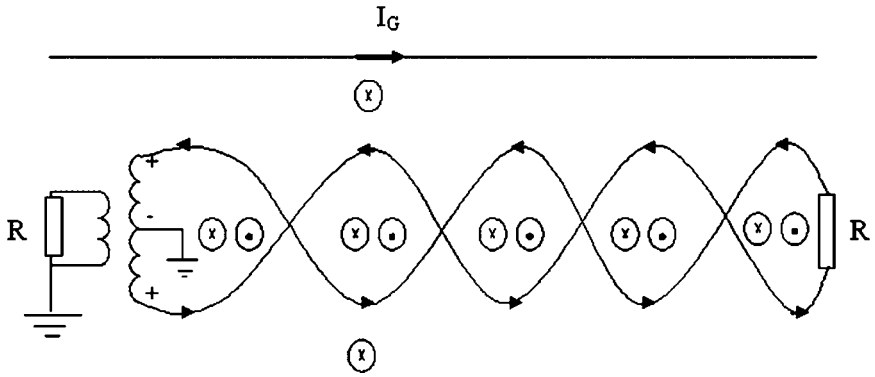

Figure 24: Balanced twisted-wire pair that minimises both the inductive and the capacitive coupling.

each of the twist is such that it produces a magnetic flux that is opposite to the original flux. Therefore, there are only extremely small currents due to induction at the terminal loads. However, there is no reduction in induced currents due to capacitive coupling. The arrangement in Fig. 23 is called unbalanced twisted-wire. To eliminate both inductive and capacitive coupling, a balanced twisted-wire arrangement, as in Fig. 24, can be used [1]. If possible, avoid fast changing currents. Induced voltage is proportional to rate of change of current, or in frequency domain proportional to frequency.

4.1.4 Capacitive and inductive crosstalk combinations

In a practical circuit, different types of crosstalk may be present simultaneously. We will consider the case of simultaneous capacitive and inductive crosstalk and for simplicity we neglect the common impedance coupling part. Consider the two

current loops over a conducting plane as shown in Fig. 17. Assume that crosstalk due to both electric and magnetic fields are present. Modelling the capacitive crosstalk as a current injection into circuit 1 (victim) and modelling the inductive crosstalk as a voltage source in series with circuit 1, we can represent the crosstalk combination as shown in Fig. 25, representative of fictitious source feeding the receptor line.

In Fig. 25, all the symbols $I_c = C_{12}(\mathrm{d}V/\mathrm{d}t)$, where V is the voltage difference between the two circuits and $V_i = M(\mathrm{d}I/\mathrm{d}t)$, where I_2 is the current in the disturbing circuit. C_{12} and M are the coupling capacitance and mutual inductance between the two circuits. For convenience R_{g1} and R_{L1} are renamed as R_N and R_F, respectively. Terminal N stands for the 'near end' (near to the disturbing source voltage V_{g2}) and F stands for the 'far end'. Also note that the Lenz's law requires that the polarity of the voltage source V_i, representing the inductive mutual coupling, should be as shown in Fig. 25, driving a current from the far-end to the near-end. It is assumed that the line is electrically small and the frequencies involved are sufficiently small so that the effects of L and C_r (self-inductance and capacitance to the ground) can be neglected.

Solving the circuit of Fig. 25, we can easily get the expressions for voltage at the near- and far-ends V_N and V_F and they are given by eqns (88) and (89), respectively.

$$V_N = \frac{R_N}{R_N + R_F} j\omega M I_2 + \frac{R_N R_F}{R_N + R_F} j\omega C_{12} V \tag{88}$$

$$V_F = -\frac{R_F}{R_N + R_F} j\omega M I_2 + \frac{R_N R_F}{R_N + R_F} j\omega C_{12} V \tag{89}$$

A photograph of typical crosstalk setup used for laboratory demonstrations is shown in Fig. 26. For details of the set up, see the figure caption. The source having a frequency of 500 kHz, connected to the emitter has a sinusoidal shape as shown by the oscillogram in Fig. 27. This demonstration will be used for the discussions later in describing inductive and capacitive crosstalk.

To demonstrate the near-end and far-end crosstalk voltages under the dominance of capacitive coupling consider the following case with regard to the crosstalk set up

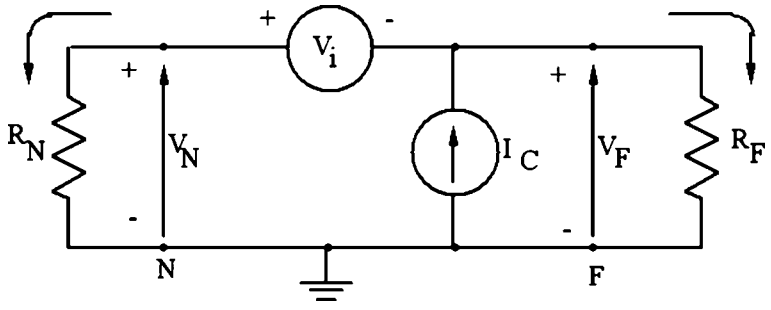

Figure 25: Model for capacitive and inductive crosstalk combination.

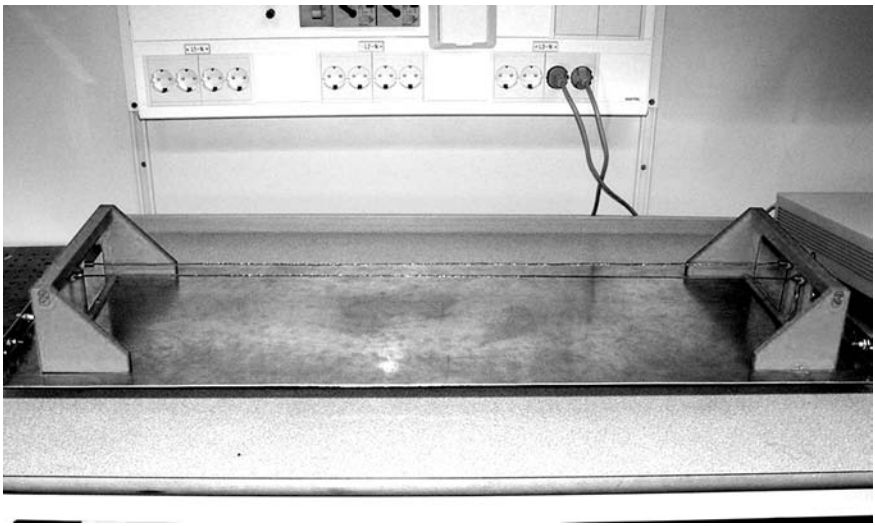

Figure 26: Photograph of a typical crosstalk arrangement. Two copper wires above a perfectly conducting ground plane; one of them is the emitter (to which the source is connected at one of the ends called near-end with respect to the ground plane) and the other is the receptor separated by a certain horizontal distance from the emitter. The length of the wires is 1 m.

shown in Fig. 26. Let the sinusoidal source shown in Fig. 27 be connected to the emitter. The far-end of the emitter is open circuit. Let the corresponding near- and far-ends of the receptor be under open circuit (large resistance). This clearly indicates the dominance of capacitive crosstalk, and the responses at the near-end and far-end for the sinusoidal source shown in Fig. 27 are shown in Fig. 28. As expected based on the equivalent circuit corresponding to Fig. 25 assuming V_i to be negligible (short circuited) and with first terms neglected on the right-hand side of eqns (88) and (89), we have similar near-end and far-end responses and the responses are in phase as shown in Fig. 28.

To demonstrate the near-end and far-end cross talk voltages under the dominance of inductive coupling, consider the following case with regard to the crosstalk set up shown in Fig. 26. Let the sinusoidal source shown in Fig. 27 be connected to the emitter. The far-end of the emitter is terminated with 50 Ω load to ground plane. Let the corresponding near- and far-ends of the receptor be terminated with 50 Ω load to ground plane. This clearly indicates the dominance of inductive crosstalk and the responses at the near-end and far-ends for the sinusoidal source shown in Fig. 27 are shown in Fig. 29. As expected based on the equivalent circuit corresponding to Fig. 25, assuming I_C to be negligible (open circuited) and with second terms neglected on the right-hand side of eqns (88) and (89), we have similar near- end and far-end responses and the responses are out of phase by 180° as shown in Fig. 29.

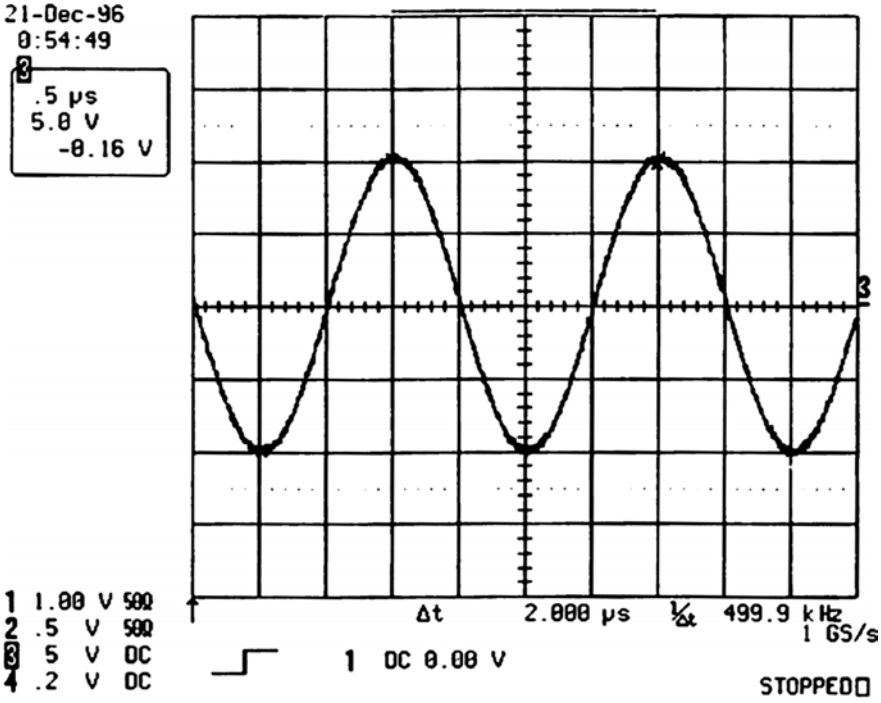

Figure 27: Oscillogram of the sinusoidal source connected to the emitter having a voltage of 20 V peak to peak and frequency of 500 kHz.

Inspecting eqns (88) and (89), we can make the following observations:

1. In general, the voltages due to crosstalk at the near-end and far-end are different. It is the inductive component of the crosstalk that is responsible for the difference.
2. The inductive component of the crosstalk produces opposite polarity voltages at the near-end and at the far-end. Their magnitudes are also different unless the impedance are matched ($R_N = R_F$).
3. The capacitive component of the crosstalk produces voltages of same polarity and magnitude at both ends, even if the impedances are not matched!
4. For deriving eqns (88) and (89), we have neglected any series inductance in the receptor circuit and any shunt capacitance to the reference. However, series self-inductance and shunt self-capacitance can be neglected only if magnitude of ωL is far less than the terminal loads and if $(\omega C)^{-1}$ is far greater than the terminal loads.

The reasons for (2) and (3) above can be found from the equivalent circuit of Fig. 25. In general, we can consider the capacitive-crosstalk currents of different magnitudes and same polarity flowing from the centre of the loop to the ends and

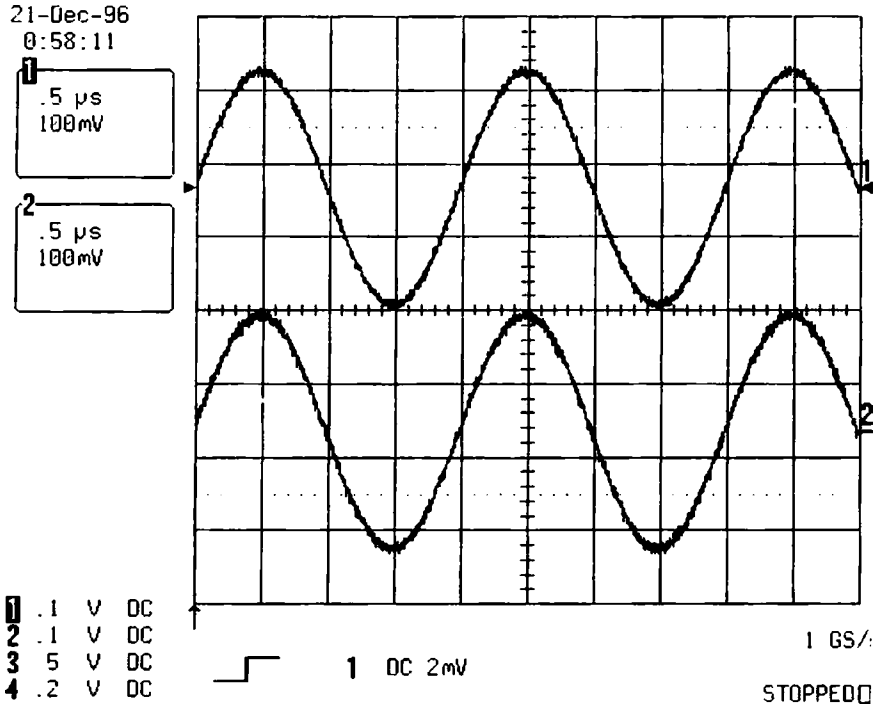

Figure 28: Capacitive crosstalk voltages at the near-end and far-end of the receptor for the setup shown in Fig. 26 with emitter source voltage given by Fig. 27.

inductive-crosstalk currents of the same magnitude and opposite polarity flowing from the centre to the ends as indicated in Fig. 30.

If the disturbing circuit has high impedance, the current I_2 is small and the capacitive crosstalk becomes dominant. If the disturbing circuit has low impedance, the current I_2 is large and the inductive crosstalk becomes dominant. The near-end crosstalk can be a nuisance in the transmission of digital signals, when the driver and receiver circuits are at the same end of a ribbon cable.

We next discuss the situation when the coupling is not weak but strong. Unfortunately in that case, we cannot perform any simplified mathematical analysis as before because all the simplifying assumptions made above are not valid anymore in the strong coupling case and only through simulations or examples we make some of our observations and conclusions.

4.2 Crosstalk under strong coupling conditions

Usually most of the outdoor practical systems fall into this category, e.g. power railway, telecommunication systems. We take examples and demonstrate some influential parameters that are to affect the crosstalk mechanisms. There could be other mechanisms too but it is indeed a subject of research. The system under

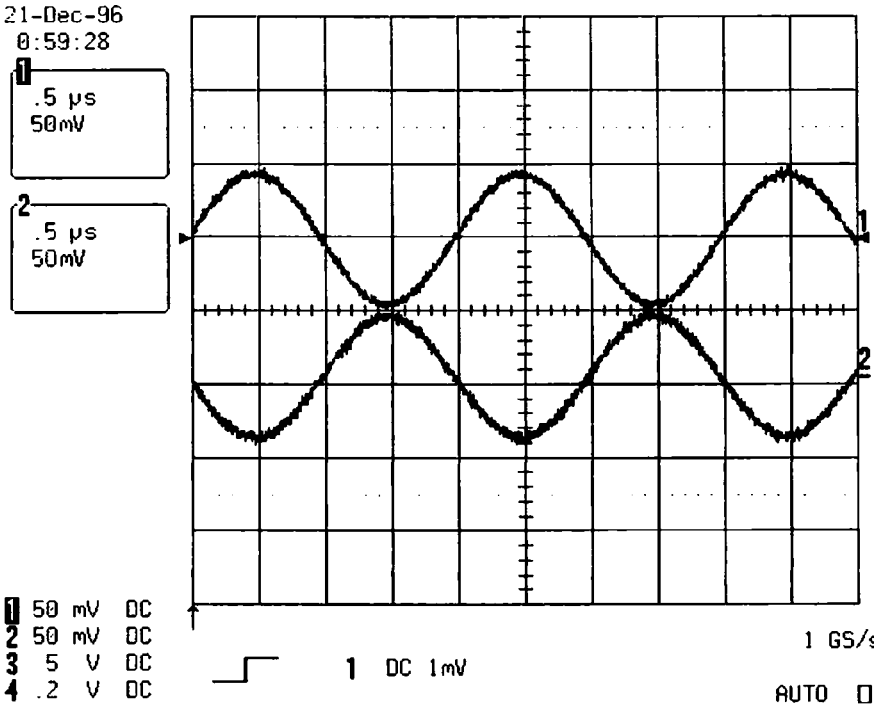

Figure 29: Inductive crosstalk voltages at the near-end and far-end of the receptor for the setup shown in Fig. 26 with emitter source voltage given by Fig. 27.

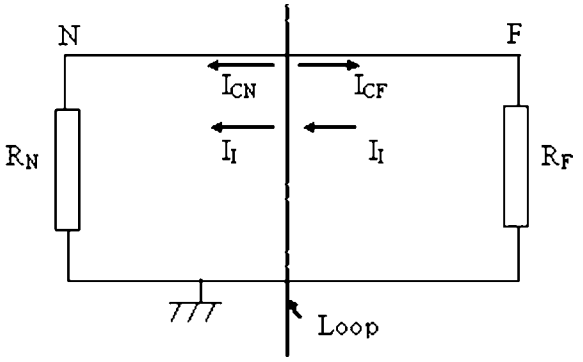

Figure 30: Directions of capacitive and inductive current components.

study is shown in Fig. 31 [33]. In the previous sections, we have seen that the increase in source pulse frequency increases the crosstalk magnitude. For a given pulse input (double exponential), we shall see the influence of conductor heights (Case 1), ground conductivity (Case 2) and loads on the receptor (Case 3) on the crosstalk phenomena.

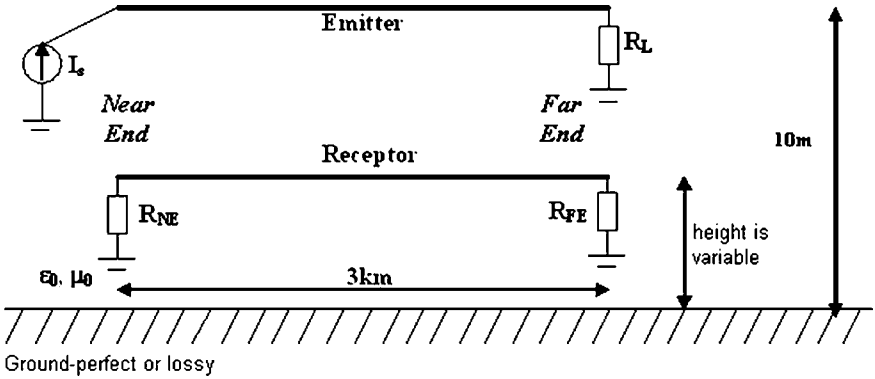

Figure 31: Simulation configuration for crosstalk studies under typical strong coupling conditions (adapted from [33]).

The receptor line was at a horizontal distance of 1 m from the emitter line, but the height of the receptor line was either 10 m or 0.5 m as the case may be. The radius of the conductors was 5.6 mm. The line length is 3 km long, which is about three times longer compared to the injected pulse wavelength. One of the ends of the emitter is injected with an double exponential impulse source having 0.1 μs rise time and 50% tail time of the waveform is 50–60 μs. The current source for the sake of demonstration of crosstalk phenomenon was a double exponential wave, with a peak current of about 1 A. The pulse has a maximum frequency of about 3 MHz calculated from the product $1/\pi T_{\text{rise time}}$. Assuming linearity, the results can be extrapolated to only peak current with similar wave shape by simple multiplication. The far-end of the emitter for any of the cases treated here is terminated in its self-characteristic impedance R_L = 490 Ω under perfect ground conditions. The loads at the ends of the receptor line are based on the following situations.

Case 1 (influence of receptor height): simulations are under perfect ground conditions with: $R_{NE} = R_{FE}$ = 490 Ω for receptor at 10 m height case and $R_{NE} = R_{FE}$ = 310 Ω for receptor at 0.5 m height case.

Case 2 (influence of finitely conducting ground): simulations with ground loss with: $R_{NE} = R_{FE}$ = 490 Ω for receptor at 10 m height case and the ground conductivity was varied 20, 5 and 0.4 mS/m. The relative permittivity of the earth was chosen to be 10, which is a reasonable value for most of the types of soil. Note the simulations are largely dependant on the ground impedance expression chosen for calculations.

Case 3 (influence of receptor terminal loads): simulations are under perfect ground conditions for receptor at 10 m height: short circuit loads $R_{NE} = R_{FE}$ = 1 Ω and then open circuit loads $R_{NE} = R_{FE}$ = 1 MΩ.

The current distributions are shown at the following points on the receptor: 0 m (near-end load), 750, 1500, 2250 and 3000 m (far-end load). The injected current has a shape given by eqn (68) with I_p = 1.0, t_1 = 100 μs, t_2 = 0.02 μs.

Some of the simulations above are taken from [33], which were carried out by the authors. The height of the receptor, ground conductivity and the receptor load influence the crosstalk currents. It is often difficult to isolate one influence from another. As a first approximation, the source is considered to be vertical current/voltage source connected between the emitter and ground. The Poynting vector is directed along the emitter conductor and points away from the source. Since the distance between the receptor and the emitter is very small compared with the length of the line (3 km), the Poynting vector is almost along the receptor too.

As discussed in the previous chapter, the interaction of electromagnetic fields with two lines can be viewed in terms of (a) vertical electric field and the horizontal magnetic field [49] or (b) vertical and horizontal electric fields [50], or (c) completely in terms of horizontal magnetic fields [51]. The equivalency between the three approaches has been proven before [52]. When ground is perfectly conducting, there is no horizontal electric field component at ground level. At ground level, there is a horizontal magnetic field, perpendicular to the plane of the circuit, and a vertical electric field. At height different from zero, there is also a horizontal electric field component, which increases in value with the increase in height. This horizontal field is directed away from the source, in the same direction as the Poynting vector, and is approximately along the receptor conductor. As the energy flows away from the source, the influence of horizontal electric field can be modelled as distributed series voltage sources on the receptor [2, 3, 49–52], turned on in succession as the wave moves along the line from the source end. Alternatively, one can imagine distributed series voltage sources on the receptor due to changing magnetic field with the receptor circuit, which are being turned on as the wave moves along the line from the source end. Decreasing the ground conductivity can be seen as an increase in the loop area of the receptor because of increased magnetic field penetration with decreasing ground conductivity [3]. The influence of vertical electric field between the receptor conductor and ground can be modelled as parallel distributed current sources. Decreasing ground conductivity does not have much influence on these current sources because the penetration of electric field into finitely conducting ground is small. The use of a fictitious line with distributed sources for modelling the electromagnetic field interaction was also carried out in [2, 3].

Transmission lines terminated in its surge impedance do not have reflections from the ends. However, in the case of crosstalk there is reflection from the far-end of the receptor even though it is terminated in the surge impedance. This is due to the presence of equivalent series voltage sources. Once turned on these sources produce currents that travel along with the wave front towards the far-end and currents that travel opposite to the wave front towards the near-end. The time varying voltage drop across the far-end load drives a current wave towards the near-end and this current appears at the near-end as a kind of ‘reflection’ from the far-end, the direction of this reflection current being opposite to that of the near-end current.

4.2.1 Case 1: influence of receptor height

The simulations for current distribution on the receptor at two different heights are shown in Fig. 32. It is seen that when the receptor is close to the emitter, i.e. 10 m height the induced currents are comparatively larger than when the receptor is close to the ground at 0.5 m. The magnitudes of induced currents are somewhat proportional to the conductor height. For this case, the ratio of conductor heights is 20 (10 ÷ 0.5) and the same ratio is seen for the induced currents (≈200 mA ÷ 10 mA). The shape of the currents at the far-end loads, in either case, is different from the current distribution at other points on the receptor line clearly due to the mismatch of the far-end load. It also appears that the shape of the current is somewhat like the derivative of the injected pulse. The ratio of the far-end currents do not follow any ratio corresponding to the conductor heights. Note that we cannot talk in general about matching the line ends by surge impedances to avoid reflections because we are not terminating the lines' mutual impedance. It is also seen that the induced currents shown here are within 12 μs windows. There could be reflections from the far-end loads at the later times which may not follow the above said

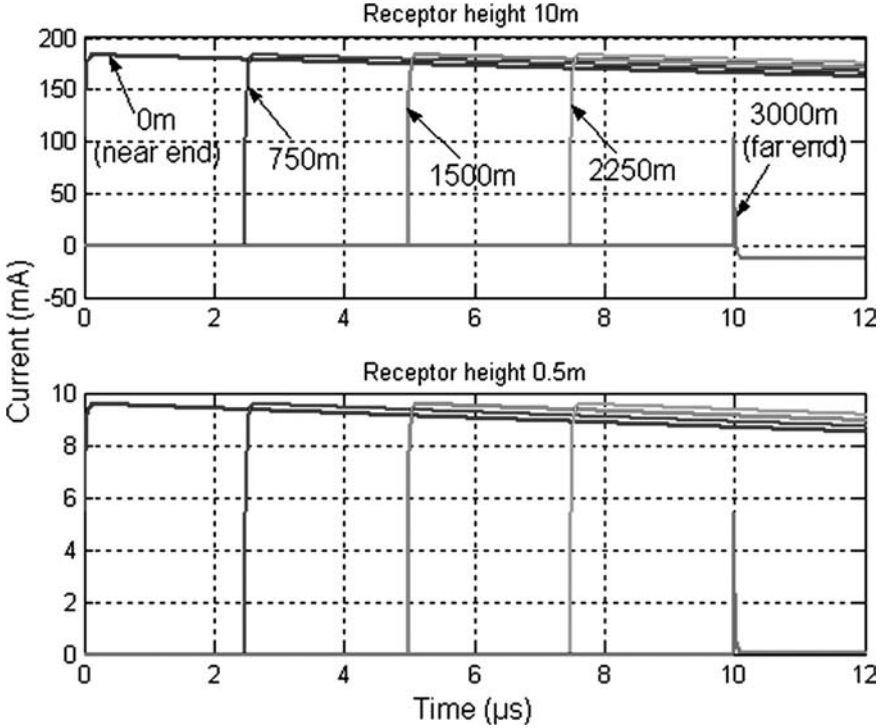

Figure 32: Crosstalk currents for receptor at 10 m (top window) and 0.5 m (bottom window), with perfect ground conditions.

height ratio. Also note that if the line lengths are increased, the crosstalk currents would increase owing to the fact that the number of distributed voltage and current sources corresponding to the inductive and capacitive crosstalk would increase. Next, let us study the influence of finitely conducting ground on the induced currents on the receptor.

4.2.2 Case 2: influence of finitely conducting ground

The simulations for this case are shown in Fig. 33. In general the finitely conducting ground increases the crosstalk currents. When ground conductivity is infinite, there is no magnetic field penetration into the ground and the return current is along the surface of the ground. When the ground conductivity is reduced, there will be field penetration into ground and the penetration depth is more for low frequency than high-frequency components. With decreasing ground conductivity there is stronger magnetic field coupling between the emitter and receptor circuit because the per unit length area of the circuit is now larger. The frequency-dependent penetration of magnetic field into ground and the resultant losses in the ground causes distortion (rise time change) and attenuation (amplitude change) of the travelling current waves between the far-end and near-end. Distortion and

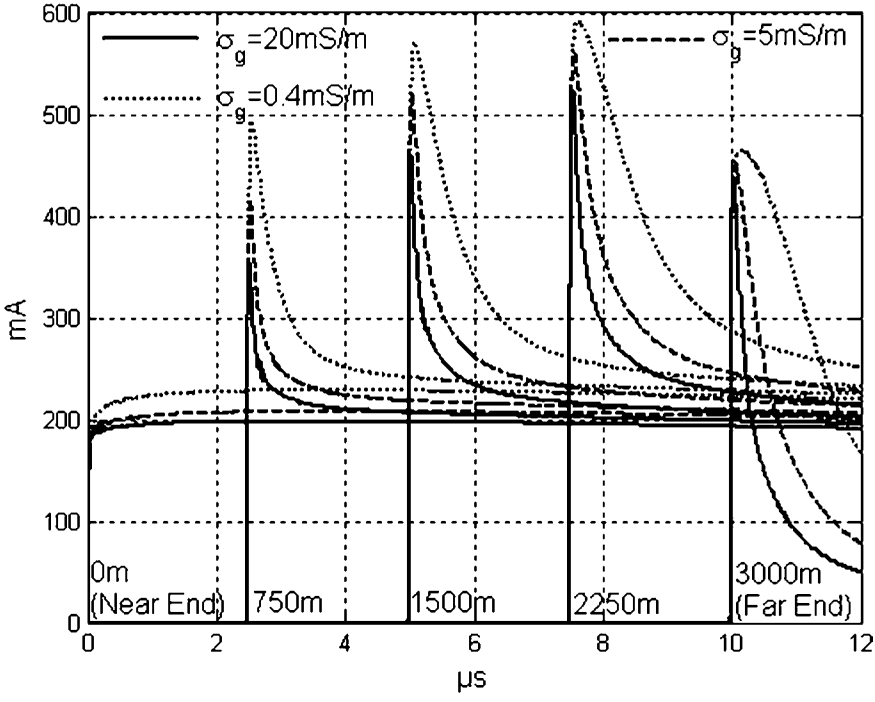

Figure 33: Crosstalk currents for receptor height 10 m, with ground conductivities 20, 5 and 0.4 mS/m and ground relative permittivity of 10.

attenuation increases with the number of times the wave travels back and forth between far- and near-ends. The phase velocities of the wave under the ground surface and in the air above ground are different. Generally waves below ground travel slower than speed of light.

4.2.3 Case 3: influence of receptor terminal loads

The simulations for this case are shown in Fig. 34. It is common, that in various systems when the loads are not line surge impedance. There could be also faults that could lead to situations of open circuit or short circuit loads. For this reason, we shall see some examples here with these two load conditions. Some general conclusions are that if the loads are short circuited, there is dominance of inductive crosstalk. Similarly under open circuit conditions capacitive crosstalk dominates. As can be seen from Fig. 34, the induced currents have increased under short circuit conditions compared with the case of surge impedance terminations (see top window of Fig. 34 and top window of Fig. 32). Under open circuit conditions currents have decreased considerably compared with the case of surge impedance termination (see bottom window of Fig. 34 and top window of Fig. 32). The crosstalk currents at the receptor loads can be viewed as the sum of currents produced by the distributed series voltage sources and distributed parallel current

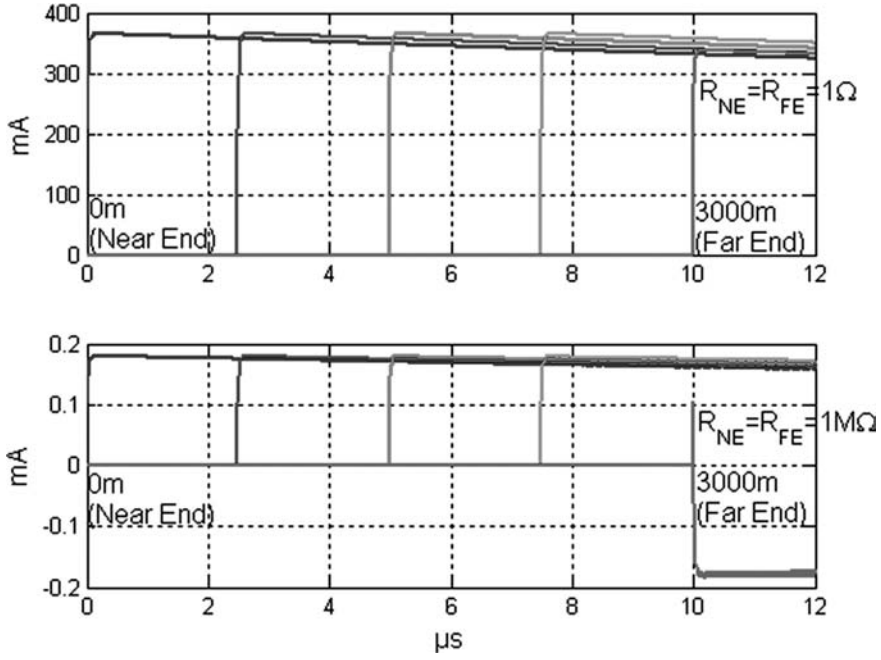

Figure 34: Comparison of crosstalk currents on the receptor when receptor is terminated in short circuit loads of 1 Ω (top window) and open circuit loads 1 MΩ (bottom window) for perfect ground conditions.

sources on the receptor. With short circuit at the ends, the series voltage sources can drive large currents through the ends. This is the reason why we have larger current distribution on the receptor line under short circuit conditions. When the receptor is terminated in high impedance (open circuit), the series voltage source cannot drive much of a current, while there is no substantial difference in the current driven through the loads by the vertical electric field coupling. This is the reason why we see lesser currents at the near- and far-end loads. For other loads between open circuit and short circuit, the currents produced by the magnetic field add up with the current produced by the vertical electric field in the near-end load and subtract in the far-end load. As mentioned earlier, the concept of impedance matching to avoid reflections is not valid for circuit containing distributed time varying sources, as in the case of receptor circuit.

5 Concluding remarks

In this chapter, we have seen various factors that could influence the pulse propagation in above ground wires. We have discussed in some detail the internal impedance, external impedance and external admittance parameters necessary for the analysis of wave propagation on above ground wires based on transmission line solutions. Simple and valid expressions for impedance and admittance parameters are also discussed for computationally efficient solutions. It is found that the ground impedance (ground loss) is more dominant than the internal impedance (skin effect loss) and also the ground admittance for the typical above ground wires could be neglected in the wave propagation studies. Two methods for numerical solutions of transmission line equations based on time and frequency domain are presented. The FDTD method for solving transmission line equations with frequency dependant internal (skin effect) and external (ground) losses with recursive convolutions is presented. This is computationally efficient for solving wave propagation problems in large distributed systems like power or railway systems. The factors influencing the crosstalk mechanisms with above ground wires under various coupling conditions are also presented.

Acknowledgements

The authors wish to thank F. Rachidi, C.A. Nucci, M. Paolone, V. Cooray, S. Celozzi and V.A. Rakov for various technical discussions applicable to the present topic. U. Ring is thanked for the construction of the crosstalk setup. Z. Mazloom is thanked for the crosstalk measurements presented in this chapter. V. Gopinathan is thanked for the editorial assistance for the language.

References

[1] Paul, C.R., *Introduction to Electromagnetic Compatibility*, John Wiley and Sons Inc.: New York, 1992.

[2] Paul, C.R., *Analysis of Multiconductor Transmission Lines*, John Wiley and Sons: New York, 1994.
[3] Tesche, F.M., Ianoz, M.V. & Karlsson, T., *EMC Analysis Methods and Computational Models*, John Wiley and Sons Inc.: New York, 1997.
[4] Sunde, E.D., *Earth Conduction Effects in the Transmission Systems*, Van Nostrand: New York, 1949.
[5] Vance, E.F., *Coupling to Cable Shields*, Wiley Interscience: New York, 1978.
[6] Deri, A., Tevan, G., Semlyen, A. & Castanheira, A., The complex ground return plane a simplified model for homogenous and multilayer earth return. *IEEE Trans. on Power Apparatus & Systems*, **100(8)**, pp. 3686–3693, 1981.
[7] Chen, K.C. & Damrau, K.M., Accuracy of approximate transmission line formulas for overhead wires. *IEEE Trans. on Electromagnetic Compatibility*, **31(4)**, pp. 396–397, 1989.
[8] Semlyen, A., Ground return parameters of transmission lines an asymptotic analysis for very high frequencies. *IEEE Trans. on Power Apparatus & Systems*, **PAS-100(3)**, pp. 1031–1038, 1981.
[9] Wait, J.R., Theory of wave propagation along a thin wire parallel to an interface. *Radio Science*, **7(6)**, pp. 675–679, 1972.
[10] Olsen, R.G., Young, J.L. & Chang, D.C., Electromagnetic wave propagation on a thin wire above earth. *IEEE Trans. on Antennas and Propagation*, **48(9)**, pp. 1413–1418, 2000.
[11] D'Amore, M. & Sarto, M.S., Simulation models of a dissipative transmission line above a lossy ground for a wide-frequency range. I. Single conductor configuration. *IEEE Trans. on Electromagnetic Compatibility*, **38(2)**, pp. 127–138, 1996.
[12] D'Amore, M. & Sarto, M.S., Simulation models of a dissipative transmission line above a lossy ground for a wide-frequency range. II. Multiconductor configuration. *IEEE Trans. on Electromagnetic Compatibility*, **38(2)**, pp. 139–149, 1996.
[13] Bannister, P.R., Electric and magnetic fields near a long horizontal line source above the ground. *Radio Science*, **3(2)**, pp. 203–204, 1968.
[14] Bannister, P.R., The image theory electromagnetic fields of a horizontal electric dipole in the presence of a conducting half space. *Radio Science*, **17(5)**, pp. 1095–1102, 1982.
[15] Bannister, P.R., Utilization of image theory techniques in determining the mutual coupling between elevated long horizontal line sources. *Radio Science*, **5(11)**, pp. 1375–1381, 1970.
[16] Carson, J.R., Wave propagation in overhead wires with ground return. *Bell Systems Technical Journal*, **5**, pp. 539–556, 1926.
[17] *EMMA Hand Book* (Elektromagnetisk miljö anvädarhandbok), Försvarets MaterielVerk (FMV), 2002.
[18] Lee, C.H. & Meliopoulos, A.P.S., Comparison of touch and step voltages between IEEE Std 80 and IEC 479 – 1. *IEEE Proc. on Generation, Transmission and Distribution*, **146(5)**, pp. 593–601, 1999.

[19] Crane, P.H.G., *Switchgear Principles*, Cleaver-Hume Press Ltd.: New York, 1957.

[20] Chowdhuri, P., *Electromagnetic Transients in Power Systems*, Research Studies Press Ltd.: Taunton, John Wiley & Sons Inc.: New York, 1996.

[21] Standler, R.B., *Protection of Electronic Circuits from Overvotlages*, A Wiley-Interscience Publication, John Wiley & Sons Inc.: New York, 1989.

[22] Starkey, B.J., *Lapalce Transforms for Electrical Engineers*, Published for 'Wireless Engineers', Iliffe & Sons, Ltd.: London, 1954.

[23] Unz, H., Oliver Heaviside (1850–1925). *IEEE Trans. on Education*, **E-6**, pp. 30–33, 1963.

[24] Schelkunoff, S.A., The electromagnetic theory of coaxial transmission lines and cylindrical shields. *Bell Systems Technical Journal*, **13**, pp. 532–579, 1934.

[25] Schelkunoff, S.A., *Electromagnetic Waves*, D. Van Nostrand Company Inc.: New York, 1943.

[26] Wedepohl, L.M. & Wilcox, D.J., Transient analysis of underground power transmission systems: system-model and wave propagation characteristics. *IEE Proc. on Generation, Transmission and Distribution*, **20(2)**, pp. 253–260, 1973.

[27] Nahman, N.S. & Holt, D.R., Transient analysis of coaxial cables using the skin effect approximation. *IEEE Trans. on Circuit Theory*, **19(5)**, pp. 443–451, 1972.

[28] Rachidi, F., Nucci, C.A. & Ianoz, M., Transient analysis of multiconductor lines above lossy ground. *IEEE Trans. on Power Delivery*, **14(1)**, pp. 294–302, 1999.

[29] Rachidi, F., Nucci, C.A., Ianoz, M. & Mazzetti, C., Influence of a lossy ground on lightning induced voltages on overhead lines. *IEEE Trans. on Electromagnetic Compatibility*, **38(3)**, pp. 250–264, 1996.

[30] Theethayi, N., Liu, Y., Montano, R. & Thottappillil, R., On the influence of conductor heights and lossy ground in multiconductor transmission lines for lightning interaction studies in railway overhead traction systems. *Electric Power Systems Research*, **71(2)**, pp. 186–193, 2004.

[31] Tesche, F.M., Comparison of the transmission line and scattering models for computing the HEMP response of overhead cables. *IEEE Trans. on Electromagnetic Compatibility*, **34(2)**, pp. 93–99, 1992.

[32] Essex, E.A., Hertz vector potentials of electromagnetic theory. *American Journal of Physics*, **45(11)**, pp. 1099–1101, 1977.

[33] Theethayi, N., Thottappillil, R., Liu, Y. & Montano, R., Important parameters that influence crosstalk in multiconductor transmission lines. *Electric Power Systems Research*, **77(8)**, pp. 896–909, 2007.

[34] Papagiannis, G.K., Tsiamitros, D.A., Labridis, D.P. & Dokopoulos, P.S., A systematic approach to the evaluation of the influence of multilayered earth on overhead power transmission lines. *IEEE Trans. on Power Delivery*, **20(4)**, pp. 2594–2601, 2005.

[35] Theethayi, N., *Electromagnetic Interference in Distributed Outdoor Electrical Systems, with an Emphasis on Lightning Interaction with Electrified Railway Network*, PhD Thesis, ISBN 91–554–6301–0, Uppsala University, September 2005.
[36] Bridges, G.E.J. & Shafai, L., Plane wave coupling to multiple conductor transmission lines above lossy ground. *IEEE Trans. on Electromagnetic Compatibility*, **31(1)**, pp. 21–33, 1989.
[37] Olsen, R.G. & Chang, D.C., Current induced by a plane wave on a thin infinite wire near the earth. *IEEE Trans. on Antennas and Propagation*, **22(4)**, pp. 586–589, 1974.
[38] Kikuchi, H., Propagation characteristics of a dielectric coated cylindrical conductor above ground. *Proc. of IEEE*, **66(3)**, pp. 351–352, 1978.
[39] Araneo, R. & Celozzi, S., Direct time domain analysis of transmission lines above a lossy ground. *IEE Proc. on Science and Measurement Technology*, **148(2)**, pp. 73–79, 2001.
[40] Rachidi, F., Loyka, S.L., Nucci, C.A. & Ianoz, M., A new expression for ground transient resistance matrix elements of multiconductor overhead transmission lines. *Electric Power Systems Research*, **65(1)**, pp. 41–46, 2003.
[41] Timotin, A.L., Longitudinal transient parameters of a unifilar line with ground return. *Rev. Rumanian Science Technical – Electrotechn. et Energ*, **12(4)**, pp. 523–535, 1967.
[42] Orzan, D., Time domain low frequency approximation for the off-diagonal terms of the ground impedance matrix. *IEEE Trans. on Electromagnetic Compatibility*, **39(1)**, pp. 64, 1997.
[43] Yee, K.S., Numerical solution of initial boundary value problems involving Maxwell's equations in isotropic media. *IEEE Trans. on Antennas and Propagation*, **14**, pp. 302–307, 1966.
[44] Taflove, A. (ed.), *Computational Electrodynamics: the Finite Difference Time Domain Method*, Artech House: Boston, 1995.
[45] Semlyen, A. & Dabulenau, A., Fast and accurate switching transient calculations on transmission lines with ground return recursive convolution. *IEEE Trans. Power Apparatus and Systems*, **94**, pp. 561–571, 1975.
[46] Hildebrand, F.B., *Introduction to Numerical Analysis*, McGraw-Hill: New York, 1956.
[47] Gustavsen, B. & Semlyen, A., Rational approximation of frequency domain responses by vector fitting. *IEEE Trans. on Power Delivery*, **14(3)**, pp. 1052–1061, 1999.
[48] The Math Works Inc., USA.
[49] Taylor, C.D., Satterwhite, R.S. & Harrison, C.W., The response of a terminated two-wire transmission line excited by a nonuniform electromagnetic field. *IEEE Trans. on Antennas and Propagation*, **13**, pp. 987–989, 1965.
[50] Agrawal, A.K., Price, H.J. & Gurbaxani, S.H., Transient response of multiconductor transmission lines excited by a nonuniform electromagnetic field. *IEEE Trans. on Electromagnetic Compatibility*, **22(2)**, pp. 119–129, 1980.

[51] Rachidi, F., Formulation of the field-to-transmission line coupling equations in terms of magnetic excitation fields. *IEEE Trans. on Electromagnetic Compatibility*, **35**, pp. 404–407, 1993.

[52] Nucci, C.A. & Rachidi, F., On the contribution of the electromagnetic field components in field-to-transmission lines interaction. *IEEE Trans. on Electromagnetic Compatibility*, **37**, pp. 505–508, 1995.

CHAPTER 3

Surge propagation in multiconductor transmission lines below ground

Nelson Theethayi & Rajeev Thottappillil
Division for Electricity, Uppsala University, Uppsala, Sweden.

Abstract

Surge propagation in underground systems has been a subject of interest for many power and telecommunication engineers. Any typical buried electrical installation involves cables (power or telecommunication) and grounding systems. The cables could have multiple shields and multiconductor configuration for the core with either twisted or non-twisted conductors. The grounding conductor system could have counterpoise, rods, grids, etc. Interestingly, all these conductor systems could be modelled as multiconductor transmission line (MTL) systems for the wave propagation studies. In this chapter, we shall see how they can be modelled for transmission line analysis using the Telegrapher's equations as discussed in Chapters 1 and 2. A brief discussion on crosstalk mechanisms will also be given, even though the analysis for crosstalk in MTL systems is similar to that in Chapter 2.

1 Introduction

Before we begin this chapter, it is good to visualize some practical problems that constitute a buried conductor system. In power and railway systems, we have cables used for bulk power transmission and signalling/telecommunication purposes. Every high-voltage power transmission tower has a long running counterpoise wire [1, 2] in the ground connected to the foot of the tower. The main purpose is to divert the lightning stroke current directly to the counterpoise wire. This is particularly important when the potential at the tower top or at the footing is of interest. Moreover, in the substation, there are complex grounding systems, which include counterpoise wires, buried rods and buried grids/meshes. To get a broader insight into the problem, let us take an example

of a communication system. Lightning strike to communication towers is a usual phenomenon [3]. A schematic diagram showing most of buried conductor systems connected to a communication tower in a communication tower complex is shown in Fig. 1 [3].

In Fig. 1, the tower foundation and building foundation are connected to their respective ring conductors. The ring conductors are provided primarily to minimize the danger of step voltage [4]. Besides, the ring conductor relieves the electrical stress at the tower foundation reducing chances of damage to the foundation. The earth conductor between the tower and building ring conductors prevents ground surface arcs between tower and building, and reduces lightning currents carried by cable shields by sharing a part of it. The follow-on earth conductor takes a part of the lightning current away from the service cables. The radial conductors around the tower are for reducing the percentage of lightning current dispatched to the building via the tower cables and earth conductors. The radial conductors are beneficial only if it can substantially reduce the lightning currents dispatched to the building, especially if the distance between the tower and building is long. The length and design of the radial conductors are to be governed by economy and its efficiency in dissipating lightning currents into the bulk earth. How do we analyse those buried conductor or grounding systems in the event when lightning or switching fault currents are diverted to them? This could benefit in the design of protection and grounding systems. This chapter will discuss as to how to use transmission line concepts to such problems but, of course, under the limits of transmission line approximations as discussed in Chapter 2.

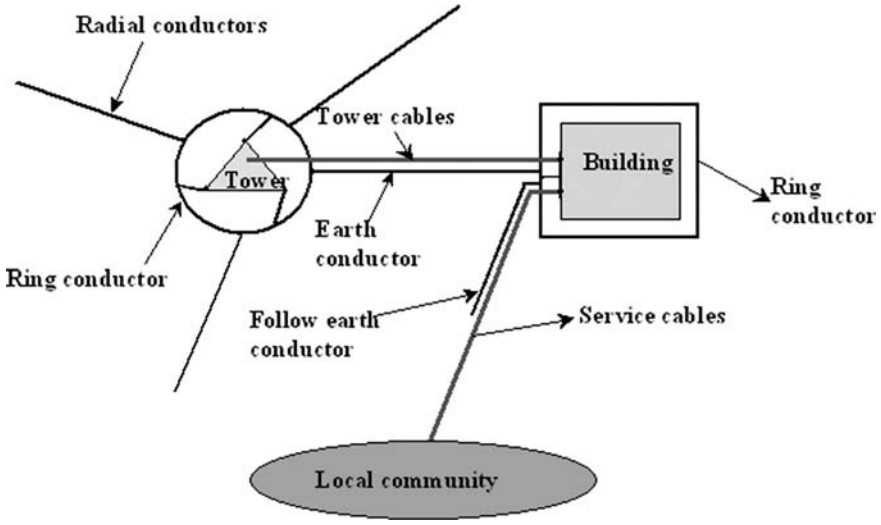

Figure 1: Schematic diagram of grounding conductors considering the tower and building as separate units (not to scale), adapted from [3].

2 Telegrapher's or transmission line equations for the buried wires

Underground wires can be either bare (counterpoise – representative of grounding conductors) or insulated (representative of cable shields or unshielded cables). We shall come to the analysis of coupling through shields later. Hence, one has two different systems for study as shown in Fig. 2.

In addition to ground conductivity and ground permittivity, there is also insulation permittivity for the insulated cables. The soil is characterized by its conductivity and permittivity. For insulated wires, we have insulation permittivity additionally. The corresponding per unit length transmission line representation of the above system is shown in Fig. 3 [5–9] and the relevant equations are shown below. For bare conductor,

$$\frac{\mathrm{d}V(x,j\omega)}{\mathrm{d}x} = -Z_{\mathrm{gb}} I(x,j\omega) \tag{1a}$$

$$\frac{\mathrm{d}I(x,j\omega)}{\mathrm{d}x} = -Y_{\mathrm{gb}} V(x,j\omega) \tag{1b}$$

For insulated conductors,

$$\frac{\mathrm{d}V(x,j\omega)}{\mathrm{d}x} = -(j\omega L + Z_{\mathrm{gi}}) I(x,j\omega) \tag{2a}$$

$$\frac{\mathrm{d}I(x,j\omega)}{\mathrm{d}x} = -j\omega \left(\frac{CY_{\mathrm{gi}}}{j\omega C + Y_{\mathrm{gi}}} \right) V(x,j\omega) \tag{2b}$$

$$L = \frac{\mu_0}{2\pi} \ln\left(\frac{b}{a}\right) \tag{3a}$$

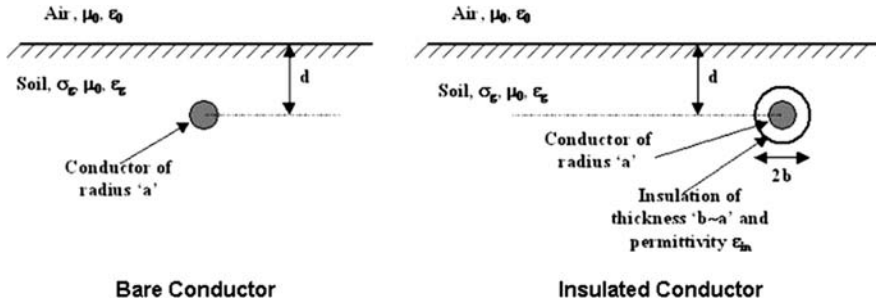

Figure 2: Bare and insulated conductor systems in the soil under study.

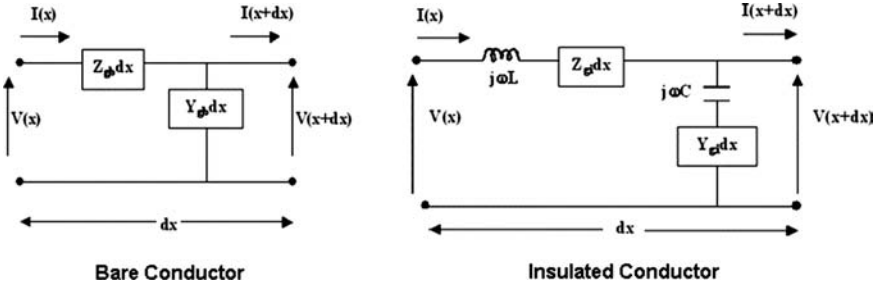

Figure 3: Per unit length transmission line representation for bare and insulated conductor systems in the soil under study.

$$C = \frac{2\pi\varepsilon_{\text{in}}}{\ln(b/a)} \tag{3b}$$

The transmission line equations presented here can be extended to the multiconductor transmission line (MTL) system of several buried cables or grounding wires similar to the discussions in Chapter 2. In eqns (1) and (2), V and I are the voltage and currents, respectively. In eqn (1), Z_{gb} and Y_{gb} are the ground impedance and ground admittance of the bare conductor(s). In eqn (2), Z_{gi} and Y_{gi} are the ground impedance and admittance of the insulated conductor(s). Hence, in discussions to follow for ground impedance and ground admittance for buried wires, we define Z_{gu} and Y_{gu}, for ground impedance and admittance, respectively, and the subscript 'u' is either 'b' or 'i', as the case may be, for bare or insulated wires. In eqn (2), L and C are the insulation inductance and capacitance, respectively [5], calculated using eqn (3). Lightning first return stroke or switching transients have frequency components ranging from a few tens to a few hundreds of kilohertz and subsequent lightning return strokes could have frequencies up to a few megahertz [10, 11]. For this reason, we shall investigate the ground impedance behaviour up to 10 MHz, beyond which the validity of transmission line approximation for buried wires could be questionable and will be discussed later.

The current wave equation for insulated wires can be written in a convenient form as in eqn (4) so that the total shunt element, i.e. series combination of insulation capacitance $j\omega C$ and Y_{gi} in Fig. 3 can be transformed to a parallel combination of insulation capacitance and modified ground admittance, i.e. $j\omega C \,||\, Y_{\text{gi}}^{\text{P}}$, which is comparable with above-ground wires' transmission line equations as discussed in Chapter 2, and researchers like [12] have adopted this.

$$\frac{\mathrm{d}I(x, j\omega)}{\mathrm{d}x} = -(j\omega C + Y_{\text{gi}}^{\text{P}})V(x, j\omega \tag{4a}$$

$$Y_{\text{gi}}^{\text{P}} = \frac{-(j\omega C)^2}{j\omega C + Y_{\text{gi}}} \tag{4b}$$

2.1 Ground impedance for buried wires

In the analysis below, let us assume the radius of the wire as R_{ab}. If the bare wire is in the analysis, then $R_{ab} = a$ else $R_{ab} = b$, the outer radius of the insulated wire, and the depth of the wire is d. Several researchers have contributed to the development of ground impedance expression for buried wires. The ground impedance expression for buried wires was developed first by Pollaczek [13] in 1926, as shown in eqn (5), which is a low-frequency approximation (similar to that in Chapter 2) in the sense that it can only be used when frequency of incident pulse satisfies $\omega << \sigma_g/\varepsilon_g$.

$$Z_g^{\text{Pollaczek}} = \frac{j\omega\mu_0}{2\pi}\left(\begin{array}{l} K_0\left(R_{ab}\sqrt{j\omega\mu_0\sigma_g}\right) \\ -K_0\left(\sqrt{R_{ab}^2+4d^2}\cdot\sqrt{j\omega\mu_0\sigma_g}\right) \\ +\displaystyle\int_{-\infty}^{+\infty}\frac{e^{-2d\sqrt{u^2+j\omega\mu_0\sigma_g}}}{|u|+\sqrt{u^2+j\omega\mu_0\sigma_g}}\cdot e^{ju\cdot R_{ab}}\cdot du \end{array}\right) \tag{5}$$

Because of the low-frequency approximation one can see that eqn (5) does not include the permittivity of the ground. All limitations associated with Carson's ground impedance as explained in Chapter 2 for above-ground wires are applicable to Pollaczek's ground impedance expression for buried wires as well. Saad *et al*. [14] have analytically showed that an excellent approximation for eqn (5) is given by eqn (6).

$$Z_g^{\text{Saad et al.}} = \frac{j\omega\mu_0}{2\pi}\left(\begin{array}{l} K_0\left(R_{ab}\sqrt{j\omega\mu_0\sigma_g}\right)+ \\ \dfrac{2}{4+R_{ab}^2(j\omega\mu_0\sigma_g)}\cdot e^{-2\cdot d\sqrt{j\omega\mu_0\sigma_g}} \end{array}\right) \tag{6}$$

Observe that if the infinite integral, e.g. in eqn (5), is eliminated, then those expressions without infinite integrals we shall here refer to as closed form approximations. Wedepohl and Wilcox [15] and Dommel [16, 17] (who presents expressions of A. Semlyen and A. Ametani) have proposed their own closed form ground impedance expressions, and Saad *et al.* [14] have shown that those expressions are more or less identical to eqn (6) when numerical calculations were compared.

For a wide range of frequencies, as long as the transmission line approximation is valid, Sunde [6] has derived the ground impedance expression as given by eqn (7). It is similar to eqn (5), but the only difference is that full propagation constant of the soil was used in eqn (7).

$$Z_g^{\text{Sunde}} = \frac{j\omega\mu_0}{2\pi}\left[\begin{array}{l} K_0(R_{ab}\gamma_g)-K_0\left(\gamma_g\sqrt{R_{ab}^2+4d^2}\right) \\ +2\displaystyle\int_0^{\infty}\frac{e^{-2d\sqrt{u^2+\gamma_g^2}}}{u+\sqrt{u^2+\gamma_g^2}}\cdot\cos(uR_{ab})\cdot du \end{array}\right] \tag{7}$$

The integral term in eqn (7) converges slowly leading to longer computation times and possible truncation errors as the frequency is increased. Further, it was found that the first two Bessel terms in eqn (7) are oscillatory, when frequency is high. However, one can say Sunde's expression for ground impedance is more valid than Pollaczek's ground impedance expression in the sense that it uses the full expressions for propagation constant. Recently, Bridges [8], Wait [9] and Chen [18] have independently proposed more complex ground impedance expressions derived from rigorous electromagnetic theory, and in [8, 18] closed form logarithmic approximations for transmission line solution have been proposed. The authors found that even those expressions in appearance, though simple, are oscillatory (perhaps numerical convergence problems) at high frequency, hence not discussed here as it needs further investigation.

Bridges [8] mentions that his complete expression for ground impedance has two modes, namely transmission line modes and radiation/and surface wave modes. Moreover, the solution of his ground impedance expressions is based on complex integration theory and adds that pole term in his expression corresponds to transmission line mode and the branch cut corresponds to radiation/and surface wave modes [8]. Thus, under the transmission line modes, it can be shown that Bridges's expression is identical to Sunde's expression. Further, Wait [9] proposed a quasi-static approximation (under transmission line modes) and is given by eqn (8).

$$Z_{\mathrm{g}}^{\mathrm{Wait}} = \frac{j\omega\mu_0}{2\pi}(1+\Theta)\ln\left(\frac{-j1.12}{\kappa R_{\mathrm{ab}}}\right) \tag{8a}$$

$$\kappa = \sqrt{\varepsilon_{\mathrm{g}}\mu_0\omega^2 - j\omega\mu_0\sigma_{\mathrm{g}}} \tag{8b}$$

$$\varsigma = 2j\kappa d \tag{8c}$$

$$\Theta = \frac{1}{K_0(j\kappa R_{\mathrm{ab}})}\left[K_0(\varsigma) + \frac{2}{\varsigma}K_1(\varsigma) - \frac{2}{\varsigma^2}(1+\varsigma)\mathrm{e}^{-\varsigma}\right] \tag{8d}$$

Vance [7] proposed one of the simplest closed form approximations for eqn (7) given by eqn (9), where Henkel functions are used instead of Bessel's functions.

$$Z_{\mathrm{g}}^{\mathrm{Vance}} = \frac{\mu_0\omega}{2\pi R_{\mathrm{ab}}\gamma_{\mathrm{g}}}\frac{H_0^1(jR_{\mathrm{ab}}\gamma_{\mathrm{g}})}{H_1^1(jR_{\mathrm{ab}}\gamma_{\mathrm{g}})} \tag{9}$$

Petrache *et al.* [12] have proposed a logarithmic approximation as shown in eqn (10) for the ground impedance and also claim that it's the simplest expressions for the ground impedance.

$$Z_{\mathrm{g}}^{\mathrm{Log}} = \frac{j\omega\mu_0}{2\pi}\ln\left(\frac{1+\gamma_{\mathrm{g}}R_{\mathrm{ab}}}{\gamma_{\mathrm{g}}R_{\mathrm{ab}}}\right) \tag{10}$$

It can be seen in eqns (9) and (10) the depth of the wire is missing. Models that neglect air–earth interface [7] are known as infinite earth models. Wait [9] has

shown that this condition exists if $|2jd\sqrt{\varepsilon_g\mu_0\omega^2 - j\omega\mu_0\sigma_g}| >> 1$. From this condition, it was found that neglecting the wire depth might not be a good approximation for higher frequencies typical for lightning. Moreover, it was found that for any combination of ground material property, the logarithmic approximation (10) and Vance's approximation (9) for the ground impedance are identical.

Theethayi *et al.* [19] proposed a modified empirical logarithmic-exponential approximation (11), which is similar to eqn (9) but with an extra term accounting for wire depth taken from Saad *et al.* expression (6).

$$Z_g^{\text{Log-Exp}} = \frac{j\omega\mu_0}{2\pi}\left(\ln\left(\frac{1+\gamma_g R_{ab}}{\gamma_g R_{ab}}\right) + \frac{2}{4+R_{ab}^2\gamma_g^2}e^{-2d|\gamma_g|}\right) \tag{11}$$

Note that, in all the expressions above for the mutual impedance between the wires R_{ab} needs to be replaced by horizontal distance between the buried wires and d by average depth [15].

Figures 4 and 5 show the comparison of various ground impedance expressions and the deviations between expressions can be seen clearly both in amplitude and argument responses. The example is a wire of radius 2 cm and a depth of 0.5 m.

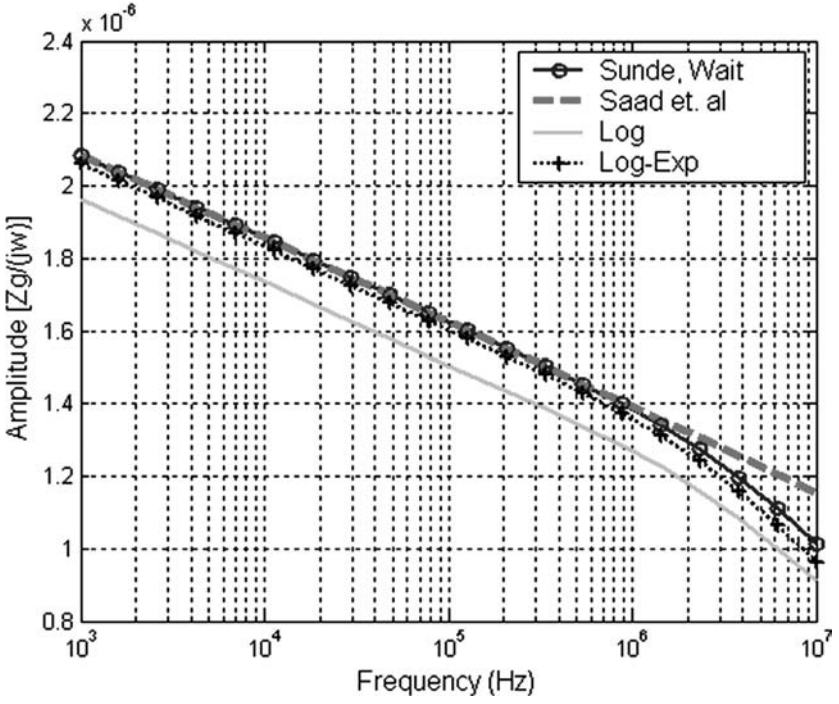

Figure 4: Amplitude, $|Z_g/j\omega|$ for comparing eqns (6)–(11): ground conductivity is σ_g = 1 mS/m and ε_{rg} = 10.

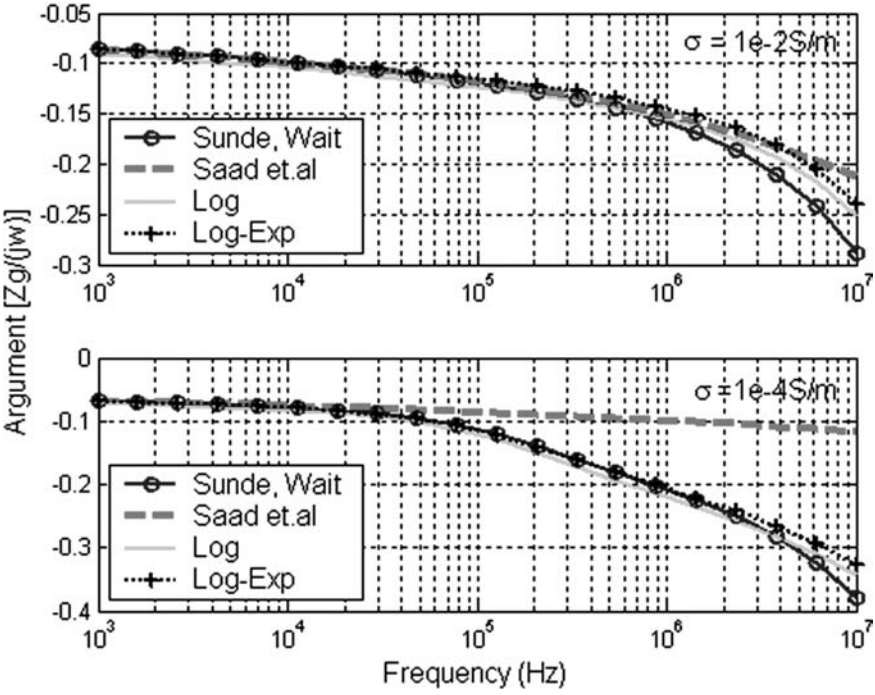

Figure 5: Argument (radians), $\angle(Z_g/j\omega)$ for comparing eqns (6)–(10): ground conductivity is σ_g = 10 and 0.1 mS/m and ε_{rg} = 10.

The consequence of missing depth term in logarithmic expression can be seen in the amplitude, and the consequence of low-frequency approximation in argument response. It can be seen that empirical logarithmic-exponential approximation has some agreement with either Sunde's or Wait's expression.

2.1.1 Asymptotic analysis

Now let us see the asymptotic behaviour of the ground impedance for buried wires as frequency tends to infinity (even though such an approach is questionable under transmission line limits). For using the time domain analysis, it is necessary to know the value of the ground impedance at $t = 0$. It is thus necessary to confirm if at all the ground impedance pose any singularity as the frequency tends to infinity. Similar to overhead wires, as discussed in Chapter 2, the ground impedance in time domain is referred to as transient ground impedance [5, 10], given by inverse Fourier or Laplace transform as, $\zeta(t) = F^{-1}[Z_g/j\omega]$. The value at $t = 0$ can be obtained by initial value theorem as $\lim_{t\to 0}\zeta(t) = \lim_{\omega\to\infty} Z_g$. Vance's expression (9) can be rewritten as eqn (12).

$$Z_g^{\text{Vance}} = \frac{\mu_0 j\omega}{2\pi j R_{ab}\gamma_g}\left[\frac{J_0(jR_{ab}\gamma_g) + jY_0(jR_{ab}\gamma_g)}{J_1(jR_{ab}\gamma_g) + jY_1(jR_{ab}\gamma_g)}\right] = \frac{\mu_0 j\omega}{2\pi j R_{ab}\gamma_g}\Gamma \tag{12}$$

Simplifying eqn (12), we obtain eqn (13) and using the asymptotic expansions given in [20] it can be shown that $\lim_{\omega\to\infty} \Gamma \to j$.

$$Z_{\mathrm{g}}^{\mathrm{Vance}} = \frac{\mu_0 j\omega}{2\pi j R_{\mathrm{ab}} \gamma_{\mathrm{g}}} \Gamma = \frac{\mu_0}{2\pi j} \sqrt{\frac{j\omega}{\mu_0(\sigma_{\mathrm{g}} + j\omega\varepsilon_{\mathrm{g}})}}\, \Gamma \tag{13}$$

Thus, under the asymptotic conditions, it can be shown that eqn (13) tends to eqn (14) as frequency approaches infinity. The same is applicable with the logarithmic expression (10). Further, in the empirical expression, as frequency tends to infinity the exponential part approaches zero.

$$\lim_{\omega\to\infty} Z_{\mathrm{g}}^{\mathrm{Vance}} = \left(\frac{1}{2\pi R_{\mathrm{ab}}}\right) \sqrt{\frac{\mu_0}{\varepsilon_{\mathrm{g}}}} \tag{14}$$

A similar expression to eqn (14) has been obtained in Chapter 2 for the overhead wires, the only difference was that in eqn (14) the radius of the conductor R_{ab} is to be replaced by the height of the conductor above ground. For wire of radius 2 cm at a depth of 0.5 m, the asymptotic value of ground impedance is 948 Ω/m. The important dimension here is the outer diameter of the conductor. Equation (14) is also applicable for a tubular conductor or for the shield of a cable in contact with the ground. Clearly, a singularity would appear if ground impedance expression corresponding to the low-frequency approximation was used.

2.2 Ground admittance for buried wires

Once we have the ground impedance, it is simple to get the ground admittance term. Vance [7] suggests that ground impedance and ground admittance are related to each other approximately by the propagation constant as in eqn (15). This approximation is valid in the sense that most of the currents return with in the soil because of which the ratio of electric to magnetic fields in the ground should be associated with intrinsic impedance of the soil as discussed in Chapter 2.

$$Y_{\mathrm{g}} = \frac{\gamma_{\mathrm{g}}^2}{Z_{\mathrm{g}}} \tag{15}$$

For a wire of radius 2 cm at a depth of 0.5 m, Figs 6 and 7 show both ground impedance and admittance amplitudes and arguments, respectively. The ground admittance appears to be more sensitive to ground conductivity than ground impedance. This is unlike overhead wires where the ground impedance is very sensitive to ground conductivity, as discussed in Chapter 2. The interesting feature is that even though the ground impedance has asymptotic value at a very high frequency, the ground admittance monotonically increases and tends to infinity as the

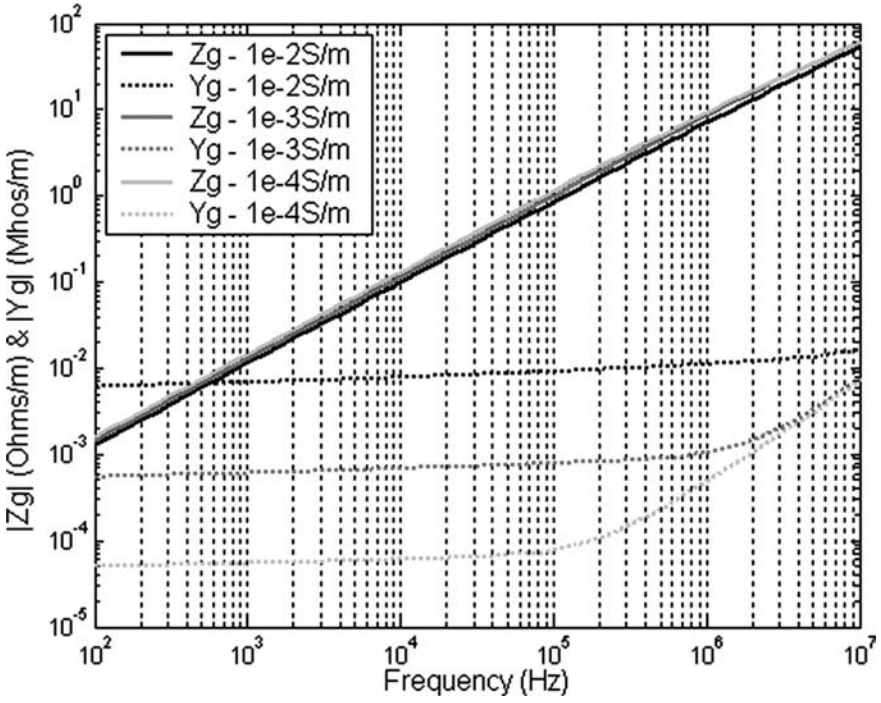

Figure 6: Ground impedance and admittance magnitude response for various ground conductivities for a bare wire of radius 2 cm, buried at 0.5 m depth and $\varepsilon_{rg} = 10$.

frequency is increased, i.e. $\lim_{\omega\to\infty} Y_g \to \infty$. Thus it is clear that surge or characteristic impedance $\sqrt{Z/Y}$ of the buried bare wire will tend to zero at a very high frequency, unlike overhead wires where it tends to a constant value. For buried insulated cables, the insulation permittivity additionally modifies the behaviour of total series impedance and shunt admittance of the wire. The modified ground admittance for insulated cables in eqn (4b) has an asymptotic value given by eqn (17) as the frequency tends to infinity even though the ground admittance of bare wire tends to infinity. The following arguments support this statement. Petrache *et al.* [12] have also obtained similar expression as eqn (17). A reason why the total shunt admittance in the current wave equation (2b) tends to infinity as the frequency tends to infinity is that because the ground admittance term Y_{gi} tends to infinity as frequency tends to infinity.

$$Y_{gi}^{P} = -\frac{C^2 Z_{gi}}{\frac{CZ_{gi}}{j\omega} + \frac{\mu_0\sigma_g}{j\omega} + \mu_0\varepsilon_g} \tag{16}$$

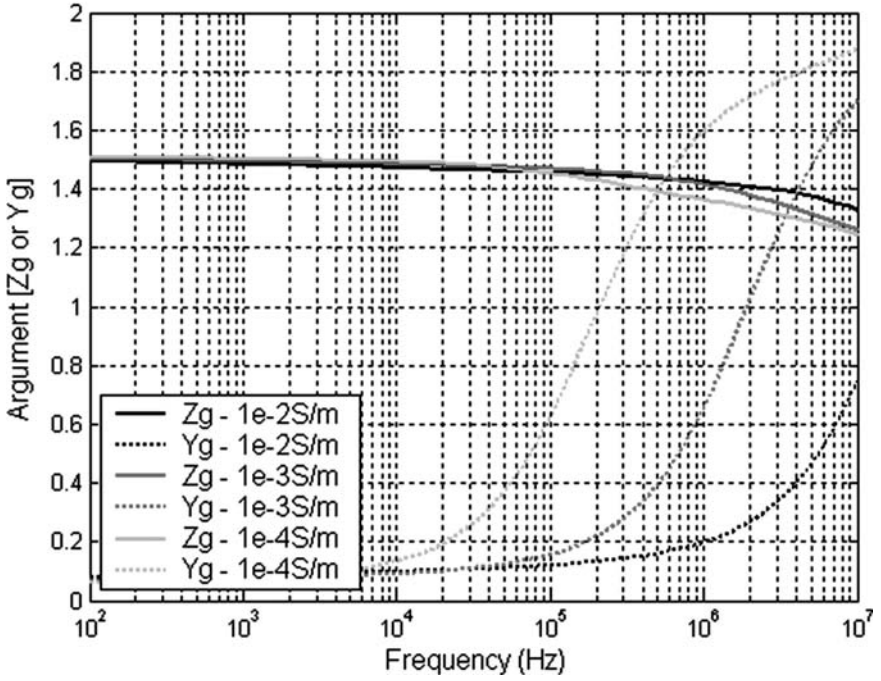

Figure 7: Ground impedance and admittance argument response for various ground conductivities for a bare wire of radius 2 cm, buried at 0.5 m depth and $\varepsilon_{rg} = 10$.

$$\lim_{\omega\to\infty} Y_{gi}^{P} \to \left[\frac{2\pi\varepsilon_{in}}{\ln(b/a)}\right]^2 \frac{1}{2\pi b\mu_0\varepsilon_g}\sqrt{\frac{\mu_0}{\varepsilon_g}} \tag{17}$$

Transient simulation packages like Electromagnetic Transients Program (EMTP) [16, 21] ignores ground admittance and uses low-frequency approximation of ground impedance, i.e. neglects ground permittivity for underground cables. For bare wires, one cannot ignore ground admittance at all that is the reason why there are not any models for counterpoises etc., unlike line and cable models in EMTP [16, 21]. The inadequacies of low-frequency approximations for ground impedance have been discussed in the earlier section and also in Chapter 2. To illustrate the importance of ground admittance, let us consider two cases for an insulated wire corresponding to cable transmission line representation shown in Fig. 3. Case 1 is with ground admittance and Case 2 without ground admittance, i.e. $Y_{gi} \to \infty$. The line propagation constant for Cases 1 and 2 are given by eqns (18) and (19), respectively in Laplace domain $s \Leftrightarrow j\omega$.

$$\gamma_1 = \left[(sL + Z_{gi})\left(\frac{sCY_{gi}}{sC + Y_{gi}}\right)\right]^{1/2} \tag{18}$$

$$\gamma_2 = \left[(sL + Z_{gi})sC\right]^{1/2} \tag{19}$$

Observe that when $Y_{gi} \to \infty$, then $\gamma_1 \to \gamma_2$. The system that is being considered is an insulated cable buried at a depth of 0.5 m and having a radius of 2 cm and an insulation thickness of 2 mm. The ground conductivity is 1 mS/m, and the ground relative permittivity is 10, and the insulation relative permittivity is either 2 or 5. The ratio of attenuation factors for Cases 1 and 2, a_1/a_2, and the velocity ratio of propagation v_1/v_2 (note velocity is obtained by the ratio ω/β, where ω is the angular frequency and β is the phase constant calculated independently, which further is the imaginary part of γ) are shown in Figs 8 and 9, respectively.

It can be seen from Fig. 8 that the attenuation per meter for Cases 1 and 2 is same only at 100 Hz, and beyond that frequency, attenuation for Case 1 is a few times higher than Case 2. Situation is worse when the insulation permittivity is higher. Incorrect attenuation of currents at various points would predict incorrect rise times for propagating pulses.

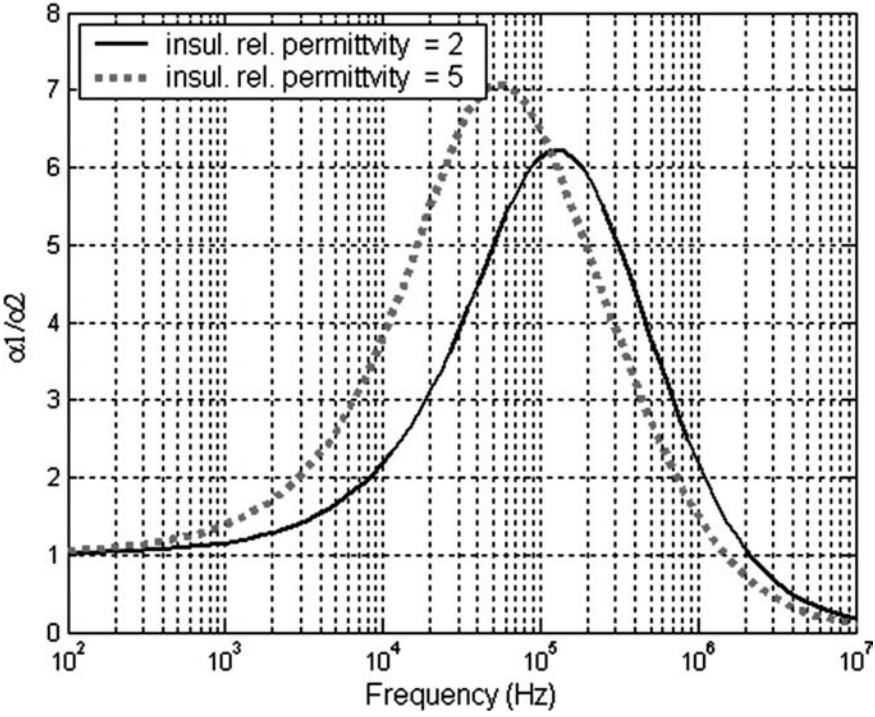

Figure 8: Attenuation ratio for Case 1 (Y_g included) and Case 2 (Y_g neglected) for a wire of radius 2 cm, insulation thickness of 2 mm and buried at 0.5 m depth, $\varepsilon_{rin} = 2$ or 5, $\sigma_g = 1$ mS/m and $\varepsilon_{rg} = 10$.

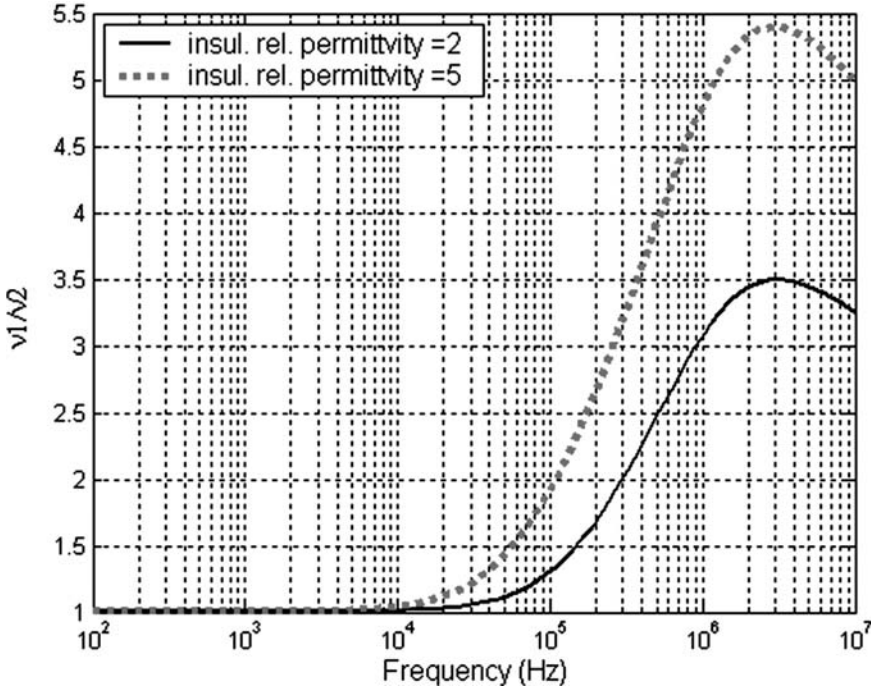

Figure 9: Velocity ratio for Case 1 (Y_g included) and Case 2 (Y_g neglected) for a wire of radius 2 cm, insulation thickness of 2 mm and buried at 0.5 m depth, $\varepsilon_{rin} = 2$ or 5, $\sigma_g = 1$ mS/m and $\varepsilon_{rg} = 10$.

Now consider the velocity ratio as shown in Fig. 9. The velocity of propagating waves is same for Cases 1 and 2 only until 10 kHz. Beyond this point, again, the velocity ratio is increasing, that is underestimation of velocity when ground admittance is neglected. Situation is worse when the insulation permittivity is higher. Velocity of waves propagating in Case 2 is much slower than Case 1. The consequence of different velocities between Cases 1 and 2 will result different time delays. Case 2 is certain to predict incorrect velocities. Changing velocity with frequency will cause dispersion in the propagating waves. For the above problem, Theethayi *et al.* [19] have shown the difference in the attenuations and velocities clearly with time domain simulations as well for a typical pulse propagation problem.

3 Possible limits of transmission line approximation for buried wires

The discussions until now are the analysis based on the transmission line theory. Some discussion on the limits of transmission line approximation was made in Chapter 2. A critical reader may wonder as to what the limit of transmission line approximation is for the buried system as well. For this, we shall use the same

philosophies that were used for overhead wires, i.e. using the concept of penetration depth. Assume the wire is buried at a depth of d meters. The penetration depth at which the currents return in the soil can be calculated using the expression given in Chapter 2 and are shown in Fig. 10 (solid lines) for ground relative permittivity of 10. It should be remembered that the discussion here is applicable for infinite earth model. So if one considers the infinite depth models, the penetration depth is defined not from the surface of the ground but from the surface of the wire because of the axis-symmetric nature of the problem, unlike overhead wires where the depth was measured from the surface of the ground.

For a wire located at a certain depth in the soil, the currents have a return path only in the soil but at various depths depending upon the frequency of the pulse propagating in the wire. Generally, underground wire type systems in the soil will not be at a depth more than 1 or 2 m. As shown in Chapter 2, the penetration depth attains asymptotic value when the frequency is sufficiently high, which then becomes independent of frequency and is only dependant on the material properties of the soil. Further, the maximum velocity of the waves propagating in the soil is determined by its permittivity [7], i.e. $\upsilon_{gmax} = 3 \times 10^8/\sqrt{\varepsilon_{rg}}$. The velocity of the

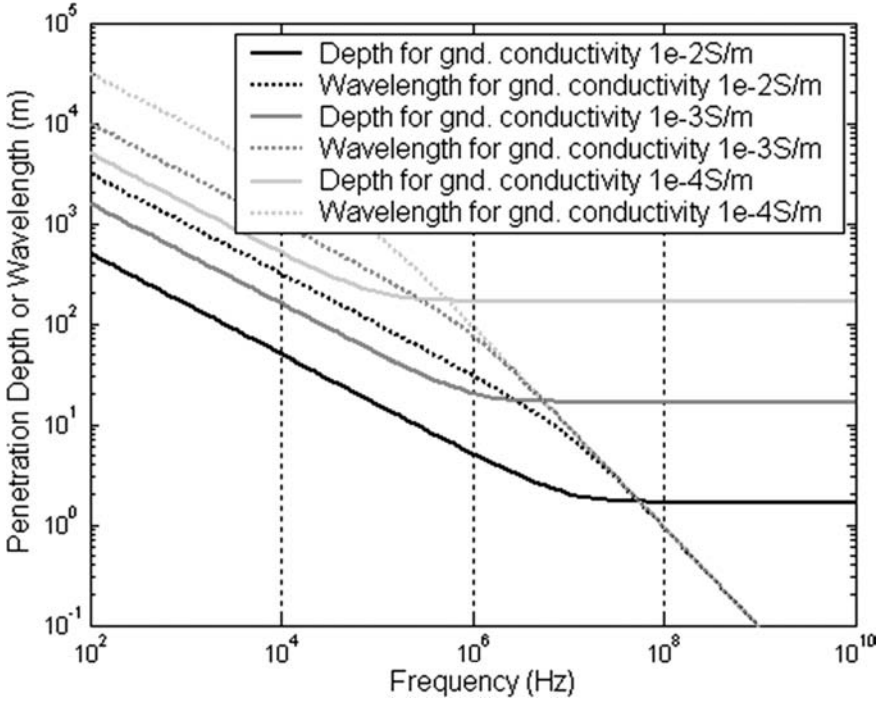

Figure 10: Penetration depth at which the currents return in the soil for buried wires and wavelength in the soil for $\varepsilon_{rg} = 10$ and for various ground conductivities.

wave propagating in the soil is a function of frequency as given by eqn (20) and the wavelength in the soil at any frequency is given by $\lambda_{\text{gpulse}} = 2\pi\upsilon_{\text{g}}/\omega$.

$$\upsilon_{\text{g}} = \frac{1}{\sqrt{\frac{\varepsilon_{\text{g}}\mu_0}{2}\left(\sqrt{1+(\sigma_{\text{g}}/\omega\varepsilon_{\text{g}})^2}+1\right)}} \tag{20}$$

Similar to overhead wires, for underground wires, one can impose a condition that the currents should return at a plane measured from the surface of the wire in the soil at depths smaller than the wavelength in soil, i.e. $\lambda_{\text{gpulse}} \geq \delta_{\text{g}}$. The condition $\geq$ is used instead of >>, because most of the return current is in the soil and the air-earth interface is neglected due to the infinite earth model. Figure 10 shows the crossover points where the penetration depth (solid lines) equals the wavelength (dashed lines) in the soil for ground relative permittivity of 10. Mathematically, this limit occurs at a frequency approximately given by eqn (21). This limit is possibly the limit for transmission line approximation, because if the incident pulse has frequencies beyond this limiting frequency, clearly, the transmission line approximation is questionable as discussed in Chapter 2 for overhead wires.

$$f_{\text{TLlimit}} = \frac{\mu_0\sigma_{\text{g}}\pi(3\times10^8)^2}{\sqrt{\varepsilon_{\text{rg}}(\varepsilon_{\text{rg}}+\mu_0\varepsilon_{\text{g}}[2\pi(3\times10^8)]^2)}} \tag{21}$$

4 Coupling to cable core through cable shields

Having seen how the external impedance and admittance for the buried insulated and bare wires influence the externally induced voltages and currents, we now move on to yet another interesting area of how induced voltages are developed in the inner core conductors within the cable, particularly the shielded cables. This is mainly attributed to the fact that fields due to currents in cable shields not only couples the external environment of the cable, i.e. shield–soil insulation medium and insulation–soil medium, but also to the internal conductors of the cable (core) due to shield imperfections. The word imperfections mean that the shield is not a perfect conductor and it could be leaky due to cavities/apertures as in braided shields [5, 7]. To understand the phenomenon of coupling to cable core, one needs to know which parameter of the shield contributes to the coupling phenomenon between the shield and internal conductors. One could have multiple cable shields. Sometimes the outermost one facing the soil is known as armour.

To describe the various parts of multiple shield cables and the twisted pair inner core conductors, we take the example of a typical telecommunication cable used by the Swedish Railways (Banverket) for its telecommunication and signalling applications, as shown in Fig. 11. The outermost metallic tubular/cylindrical conductor is called the armour and the inner metallic tubular/cylindrical conductor is called the shield. Electromagnetic compatibility and power engineers interchange

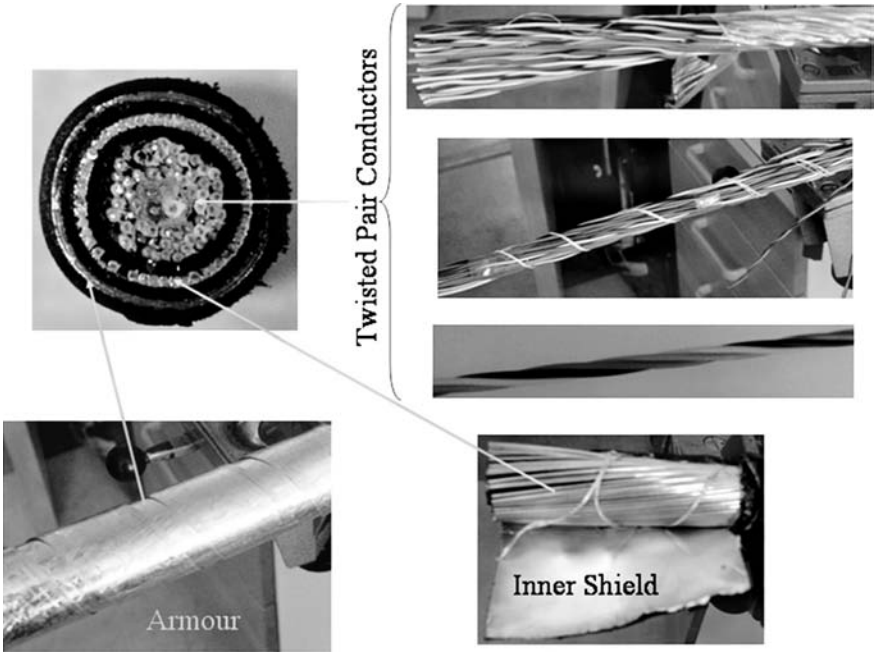

Figure 11: A typical telecommunication cable used by the Swedish railways for signalling and telecommunication applications.

the words between armour and outermost shield. Perhaps, for them, armour serves as a mechanical protection for the cable as such. In the coming sections, let us investigate whether an MTL can be derived for multiple shield and multiple core conductors for the transient analysis based on transmission line analysis.

To understand the coupling phenomenon between the tubular/cylindrical conductors and the internal conductors, let us start with the concept of transfer impedance [5, 7, 22] and later develop expressions for those phenomena in terms of what are known as tube impedances, first introduced by Schelkunoff [22] and later applied by Wedepohl and Wilcox [15]. We extended the analysis of single core cables proposed in [15] to multicore cables, with a view to applying transient analysis of cables with complex internal conductor system. The analysis is based on tubular shields, because it is reasonable to represent the armour and shield of the telecommunication or power cables for frequencies up to several hundreds of kHz as a solid tube. The leakage effects, in authors' opinion, due to tube apertures and imperfections are predominant only at high frequencies beyond 1 MHz. Under such circumstances, no generalized expressions exist for tube impedances with imperfections and they have to be determined either through experiments or extensive theory. A simple/approximate method for determining the capacitance matrix by bridge method is shown and is particularly useful for twisted pair cables applicable to most of the telecommunication cables.

4.1 Generalized double shield three-core cable

The discussion presented here is a generalization for a multiconductor arrangement of the cable. By using the analogy presented here, one can apply the same to any practical arrangement of the cables. Let us take the following examples: (a) an RG-58 cable that has single core and braided shield – a discussion on the concept of transfer impedance [5, 7] and its experimental determination are presented; (b) three conductor power cables that have a similar shield as that of RG-58 cable. In the authors' opinion, the analysis of coupling mechanism between the shield and inner conductor as proposed by Vance [7] is valid only for a particular terminal condition. In Vance's method, when the inner conductor circuit does not carry any appreciable current, the coupling mechanism between the shield and the inner circuit, due to current in the shield, is represented by distributed series voltage sources in the transmission line formed by the inner circuit. This allows us to eliminate the shield circuit and simplify the problem only to a transmission line due to inner circuit. This, in general, is not true for any arbitrary terminal conditions at the near and far ends of the shield and inner conductor/circuit. On the other hand, the analysis presented in the discussions to follow is valid for any arbitrary terminal conditions on either the shield or inner core conductors of the cable.

4.1.1 Telegrapher's equations for shielded cables

Consider a cable cut away view as shown in Fig. 12, which shows a three-core cable arrangement. It has two shields, solid tubular/cylindrical with annular cross-section. Let the core conductors carry currents I_1, I_2 and I_3. The currents through

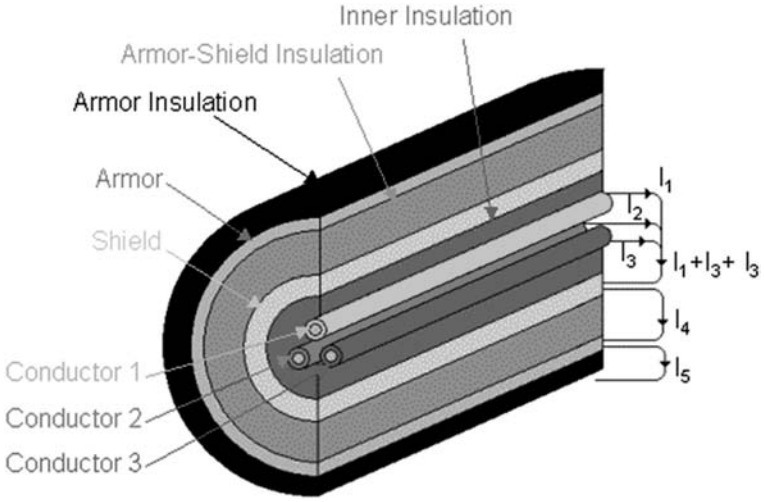

Figure 12: Generalized three-conductor cable arrangement for studying the coupling between the shields and internal conductors.

the shield and the armour are marked as I_4 and I_5. In all the cases, let us assume that the external inductance and capacitance matrices are known with the shield as the reference for Fig. 12.

In eqn (22), the voltages V_1, V_2, V_3, V_4 and V_5 are written in differential form between inner conductors (cores) and the shield, between the shield and the armour and the armour to remote reference, respectively. These voltages are also referred to as loop voltages [15, 16]. The voltages like $V_{1\text{core}}$, $V_{2\text{core}}$, $V_{3\text{core}}$, V_{shield} and V_{armour} are that of the conductors with respect to remote reference [15, 16]. These voltages are later useful for a transformation by which one can find voltages on any conductor with respect to any given/specified reference.

$$V_1 = V_{1\text{core}} - V_{\text{shield}} \tag{22a}$$

$$V_2 = V_{2\text{core}} - V_{\text{shield}} \tag{22b}$$

$$V_3 = V_{3\text{core}} - V_{\text{shield}} \tag{22c}$$

$$V_4 = V_{\text{shield}} - V_{\text{armour}} \tag{22d}$$

$$V_5 = V_{\text{armour}} \tag{22e}$$

The voltage wave equations based on the loop voltages are given by eqn (23).

$$-\frac{\mathrm{d}V_1}{\mathrm{d}x} = Z'_{11}I_1 + Z'_{12}I_2 + Z'_{13}I_3 + Z'_{14}I_4 + Z'_{15}I_5 \tag{23a}$$

$$-\frac{\mathrm{d}V_2}{\mathrm{d}x} = Z'_{21}I_1 + Z'_{22}I_2 + Z'_{23}I_3 + Z'_{24}I_4 + Z'_{25}I_5 \tag{23b}$$

$$-\frac{\mathrm{d}V_3}{\mathrm{d}x} = Z'_{31}I_1 + Z'_{32}I_2 + Z'_{33}I_3 + Z'_{34}I_4 + Z'_{35}I_5 \tag{23c}$$

$$-\frac{\mathrm{d}V_4}{\mathrm{d}x} = Z'_{41}I_1 + Z'_{42}I_2 + Z'_{43}I_3 + Z'_{44}I_4 + Z'_{45}I_5 \tag{23d}$$

$$-\frac{\mathrm{d}V_5}{\mathrm{d}x} = Z'_{51}I_1 + Z'_{52}I_2 + Z'_{53}I_3 + Z'_{54}I_4 + Z'_{55}I_5 \tag{23e}$$

Since loop voltages are adopted, the currents in eqn (23) are referred to as loop currents I_1, I_2, I_3, I_4 and I_5. These loop currents are related to the core currents $I_{1\text{core}}$, $I_{2\text{core}}$, $I_{3\text{core}}$, shield current I_{shield} and armour current I_{armour} as shown in eqn (24).

$$I_1 = I_{1\text{core}} \tag{24a}$$

$$I_2 = I_{2\text{core}} \tag{24b}$$

$$I_3 = I_{3\text{core}} \tag{24c}$$

$$I_4 = I_{\text{shield}} + I_{1\text{core}} + I_{2\text{core}} + I_{3\text{core}} \tag{24d}$$

$$I_5 = I_{\text{armour}} + I_{\text{shield}} + I_{1\text{core}} + I_{2\text{core}} + I_{3\text{core}} \tag{24e}$$

$$-\frac{\mathrm{d}I_1}{\mathrm{d}x} = Y'_{11}V_1 + Y'_{12}V_2 + Y'_{13}V_3 + Y'_{14}V_4 + Y'_{15}V_5 \tag{25a}$$

$$-\frac{\mathrm{d}I_2}{\mathrm{d}x} = Y'_{21}V_1 + Y'_{22}V_2 + Y'_{23}V_3 + Y'_{24}V_4 + Y'_{25}V_5 \tag{25b}$$

$$-\frac{\mathrm{d}I_3}{\mathrm{d}x} = Y'_{31}V_1 + Y'_{32}V_2 + Y'_{33}V_3 + Y'_{34}V_4 + Y'_{35}V_5 \tag{25c}$$

$$-\frac{\mathrm{d}I_4}{\mathrm{d}x} = Y'_{41}V_1 + Y'_{42}V_2 + Y'_{43}V_3 + Y'_{44}V_4 + Y'_{45}V_5 \tag{25d}$$

$$-\frac{\mathrm{d}I_5}{\mathrm{d}x} = Y'_{51}V_1 + Y'_{52}V_2 + Y'_{53}V_3 + Y'_{54}V_4 + Y'_{55}V_5 \tag{25e}$$

The relationship between the conductor currents and loop currents also helps in the transformation by which telegrapher's equations become in the form similar to MTL systems, as discussed earlier. Now each parameter in the impedance matrix Z' in eqn (23) is a combination of series loop impedances in terms of internal and external impedances. Similarly, each admittance term in Y' in eqn (25) is a combination of external and mutual admittance terms forming the loop admittances. These are discussed in Section 4.1.2.

4.1.2 Transmission line impedance and admittance parameters for shielded cables

Our aim is to arrive at the MTL equations of the form eqn (26) after simplifying eqns (22) and (24) using eqns (25) and (23).

$$-\frac{\mathrm{d}}{\mathrm{d}x}\begin{bmatrix} V_{1\text{core}} \\ V_{2\text{core}} \\ V_{3\text{core}} \\ V_{\text{shield}} \\ V_{\text{armour}} \end{bmatrix} = [Z]\begin{bmatrix} I_{1\text{core}} \\ I_{2\text{core}} \\ I_{3\text{core}} \\ I_{\text{shield}} \\ I_{\text{armour}} \end{bmatrix} \quad X \tag{26a}$$

$$-\frac{\mathrm{d}}{\mathrm{d}x}\begin{bmatrix} I_{1\text{core}} \\ I_{2\text{core}} \\ I_{3\text{core}} \\ I_{\text{shield}} \\ I_{\text{armour}} \end{bmatrix} = [Y]\begin{bmatrix} V_{1\text{core}} \\ V_{2\text{core}} \\ V_{3\text{core}} \\ V_{\text{shield}} \\ V_{\text{armour}} \end{bmatrix} \tag{26b}$$

The impedance parameters of eqn (23) are defined in eqn (27).

$$Z'_{11} = Z_{\mathrm{i}} + j\omega L_{11} + Z_{\text{Shield-in}} \tag{27a}$$

$$Z'_{12} = Z'_{21} = j\omega L_{12} + Z_{\text{Shield-in}} \tag{27b}$$

$$Z'_{22} = Z_{\mathrm{i}} + j\omega L_{22} + Z_{\text{Shield-in}} \tag{27c}$$

$$Z'_{13} = Z'_{31} = j\omega L_{13} + Z_{\text{Shield-in}} \tag{27d}$$

$$Z'_{23} = Z'_{32} = j\omega L_{23} + Z_{\text{Shield-in}} \tag{27e}$$

$$Z'_{33} = Z_{i} + j\omega L_{33} + Z_{\text{Shield-in}} \tag{27f}$$

$$Z'_{14} = Z'_{24} = Z'_{34} = Z'_{41} = Z'_{42} = Z'_{43} = -Z_{\text{Shield-mutual}} \tag{27g}$$

$$Z'_{44} = Z_{\text{Shield-out}} + Z_{\text{Shield-Armour-insulation}} + Z_{\text{Armour-in}} \tag{27h}$$

$$Z'_{15} = Z'_{25} = Z'_{35} = Z'_{51} = Z'_{52} = Z'_{53} = 0 \tag{27i}$$

$$Z'_{45} = Z'_{54} = -Z_{\text{Armour-mutual}} \tag{27j}$$

$$Z'_{55} = Z_{\text{Armour-out}} + Z_{\text{Armour-Earth-insulation}} + Z_{\mathrm{g}} \tag{27k}$$

The admittance parameters of eqn (25) are given by eqn (28). Many of the mutual admittance terms are null as shown in eqn (28b), this assumption may not be valid at very high frequencies.

$$\begin{bmatrix} Y'_{11} & Y'_{12} & Y'_{13} \\ Y'_{21} & Y'_{22} & Y'_{23} \\ Y'_{31} & Y'_{32} & Y'_{33} \end{bmatrix} = j\omega \begin{bmatrix} C_{11} & C_{12} & C_{13} \\ C_{21} & C_{22} & C_{23} \\ C_{31} & C_{32} & C_{33} \end{bmatrix} \tag{28a}$$

$$\left.\begin{aligned} &Y'_{14} = Y'_{15} = Y'_{24} = Y'_{25} = Y'_{34} = Y'_{35} = 0 \\ &Y'_{41} = Y'_{51} = Y'_{42} = Y'_{52} = Y'_{43} = Y'_{53} = 0 \\ &Y'_{45} = Y'_{54} = 0 \end{aligned}\right\} \tag{28b}$$

$$Y'_{44} = j\omega C_{\text{Sheath-Armour-insulation-capacitance}} \tag{28c}$$

$$Y'_{55} = j\omega C_{\text{Armour-Earth-insulation-capacitance}} \parallel Y_{\mathrm{g}} \tag{28d}$$

In eqn (27), Z_{i} is the internal impedance of the conductors, which is a consequence of skin effect phenomena of the core conductors as discussed in Chapter 2. There are some impedance terms in addition to external inductance (discussed later) of the internal conductors in eqn (27). Those impedances, excluding the internal impedances, are the ones that contribute to the coupling between the shield and

inner conductors and the shield and the armour. Let us discuss them in some detail in a while. Insulation capacitance and inductance calculations were explained earlier, i.e. using eqn (3). The ground impedance and ground admittance terms appear in eqns (27k) and (28d), which has been discussed in the earlier sections.

If $[L]_{3\times3}$ and $[C]_{3\times3}$ are the inductance and the capacitance matrix of the core conductors with respect to the shield, then for arbitrarily located untwisted conductors inside the shield as shown in Fig. 13 (adapted from Paul's book [23]), those parameters for the core conductors are given by eqns (29) and (30), respectively, in the same notations as discussed by Paul [23].

$$L_{\mathrm{GG,\,RR}} = \frac{\mu_0}{2\pi}\ln\left(\frac{r_{\mathrm{SH}}^2 - d_{\mathrm{G,R}}^2}{r_{\mathrm{SH}} r_{\mathrm{wG,R}}}\right) \tag{29a}$$

$$L_{\mathrm{GR}} = \frac{\mu_0}{2\pi}\ln\left(\frac{d_{\mathrm{R}}}{r_{\mathrm{SH}}}\sqrt{\frac{\left(d_{\mathrm{G}}d_{\mathrm{R}}\right)^2 + r_{\mathrm{SH}}^4 - 2d_{\mathrm{G}}d_{\mathrm{R}}r_{\mathrm{SH}}^2\cos\left(\theta_{\mathrm{GR}}\right)}{\left(d_{\mathrm{G}}d_{\mathrm{R}}\right)^2 + d_{\mathrm{R}}^4 - 2d_{\mathrm{G}}d_{\mathrm{R}}^3\cos\left(\theta_{\mathrm{GR}}\right)}}\right) \tag{29b}$$

For the capacitance matrix as explained in Chapter 2, we first estimate the potential coefficient matrix, then invert the potential coefficient matrix similar to the above-ground wires. Note that in eqns (30a) and (30b) the permittivity of the insulation medium is used.

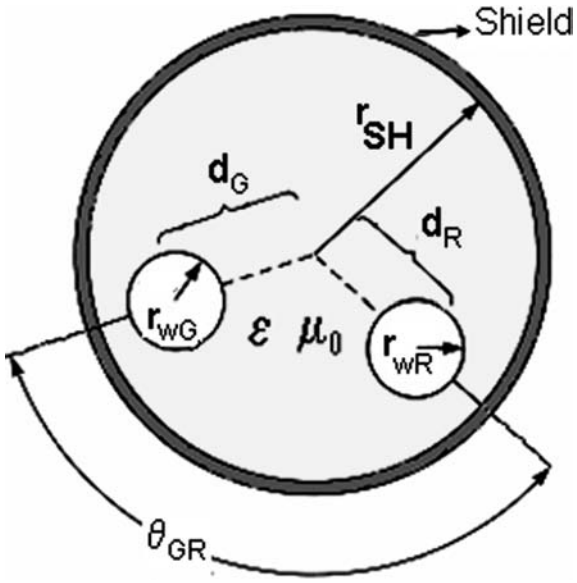

Figure 13: Untwisted parallel conductor arrangement in the shield for MTL parameter estimation for multiconductor cables, adapted from [23].

$$P_{\mathrm{GG,RR}} = \frac{1}{2\pi\varepsilon_0\varepsilon_{\mathrm{r}}} \ln\left(\frac{r_{\mathrm{SH}}^2 - d_{\mathrm{G,R}}^2}{r_{\mathrm{SH}} r_{\mathrm{wG,R}}}\right) \tag{30a}$$

$$P_{\mathrm{GR}} = \frac{1}{2\pi\varepsilon_0\varepsilon_{\mathrm{r}}} \ln\left(\frac{d_{\mathrm{R}}}{r_{\mathrm{SH}}} \sqrt{\frac{(d_{\mathrm{G}} d_{\mathrm{R}})^2 + r_{\mathrm{SH}}^4 - 2 d_{\mathrm{G}} d_{\mathrm{R}} r_{\mathrm{SH}}^2 \cos(\theta_{\mathrm{GR}})}{(d_{\mathrm{G}} d_{\mathrm{R}})^2 + d_{\mathrm{R}}^4 - 2 d_{\mathrm{G}} d_{\mathrm{R}}^3 \cos(\theta_{\mathrm{GR}})}}\right) \tag{30b}$$

$$C = [P]^{-1} \tag{30c}$$

Schelkunoff [22] gives a very good discussion on the surface impedances of hollow solid cylindrical shells. Discussions in this section are applicable only for imperfect conductors. Consider a hollow conductor whose inner and outer radii are a and b, respectively. The return of the coaxial path for the current may be provided either outside the given conductor or inside it or partly inside and partly outside. Let Z_{aa} be the surface impedance with internal return and Z_{bb}, with that of external return. This situation has appears to have in effect, two transmission lines with distributed mutual impedance Z_{ab}.

According to Schelkunoff, Z_{ab} is due to the mingling of two currents in the hollow conductor common to both lines; and since Z_{ab} is not the total mutual impedance between the two lines, Z_{ab} is called the transfer impedance from one surface of the conductor to the other [22]. Using magnetomotive intensities associated with the two currents, he derived the surface impedances as given by eqns (31) and (32). The analysis presented here are applicable only to tubular shields.

$$Z_{\mathrm{aa}} = \frac{\sqrt{j\omega\mu\sigma}}{2\pi\sigma a\Lambda} \begin{bmatrix} I_0(a\sqrt{j\omega\mu\sigma}) K_1(b\sqrt{j\omega\mu\sigma}) + \\ I_1(b\sqrt{j\omega\mu\sigma}) K_0(a\sqrt{j\omega\mu\sigma}) \end{bmatrix} \tag{31a}$$

$$Z_{\mathrm{bb}} = \frac{\sqrt{j\omega\mu\sigma}}{2\pi\sigma b\Lambda} \begin{bmatrix} I_0(b\sqrt{j\omega\mu\sigma}) K_1(a\sqrt{j\omega\mu\sigma}) + \\ I_1(a\sqrt{j\omega\mu\sigma}) K_0(b\sqrt{j\omega\mu\sigma}) \end{bmatrix} \tag{31b}$$

$$\Lambda = \begin{bmatrix} I_1(b\sqrt{j\omega\mu\sigma}) K_1(a\sqrt{j\omega\mu\sigma}) - \\ I_1(a\sqrt{j\omega\mu\sigma}) K_1(b\sqrt{j\omega\mu\sigma}) \end{bmatrix} \tag{31c}$$

$$Z_{\mathrm{ab}} = Z_{\mathrm{ba}} = \frac{1}{2\pi\sigma ab\Lambda} \tag{32}$$

Two theorems proposed by Schelkunoff [22] with regard to tube impedances are the following.

Theorem 1: If the return path is wholly external ($I_{\mathrm{a}} = 0$) or wholly internal ($I_{\mathrm{b}} = 0$), the longitudinal electromotive force (voltage) on that surface which is the nearest to the return path equals the corresponding surface impedance (self) multiplied by

the total current flowing in the conductor and the longitudinal electromotive force (voltage) on the other surface equals the transfer impedance (mutual) multiplied by the total current.

Theorem 2: If the return path is partly external and partly internal then the total longitudinal electromotive force (voltage) on either side of the surface can be obtained by applying Theorem 1 with the principle of superposition.

Equations (31) and (32) give the tube impedances. In comparison with eqn (27), one can define eqn (31a) as the tube-in impedance of either shield or the armour (31b), as the tube-out impedance of either the shield or the armour, and eqn (32) as the tube-mutual impedance of either the shield or the armour.

Wedepohl and Wilcox [15] have given a very simple approximation as shown in eqns (33) and (34) for the tube impedances without any Bessel functions, and they are valid only if $[(b - a)/(b + a)] < 1/8$. This has been validated for various practical tubular cable shields by the authors and it was seen that approximations (33) and (34) are excellent ones to exact Schelkunoff equations (31) and (32), respectively.

$$Z_{aa} \approx \frac{\sqrt{j\omega\mu\sigma}}{2\pi\sigma a}\coth\left(\sqrt{j\omega\mu\sigma}(b-a)\right) - \frac{1}{2\pi\sigma a(a+b)} \tag{33a}$$

$$Z_{bb} \approx \frac{\sqrt{j\omega\mu\sigma}}{2\pi\sigma b}\coth\left(\sqrt{j\omega\mu\sigma}(b-a)\right) - \frac{1}{2\pi\sigma b(a+b)} \tag{33b}$$

$$Z_{ab} = Z_{ba} \approx \frac{\sqrt{j\omega\mu\sigma}}{\pi\sigma(a+b)}\frac{1}{\sinh\left((b-a)\sqrt{j\omega\mu\sigma}\right)} \tag{34}$$

It is now shown how to obtain all the important impedance and admittance parameters that are needed to create the voltage and current wave equations (26a) and (26b).

4.2 An example of RG-58 cable

This cable, based on standard catalogues, has a single core and a braided copper shield. The capacitance of the core conductor with respect to the shield for the RG-58 cable is about 101 pF/m. This can be obtained using the formula (30) if the geometry of the cable is known. The inductance of this cable using the characteristic impedance of 50 Ω will be 0.255 μH/m. The shield is braided because of which the tube mutual impedance or the transfer impedance will not be the same as discussed in Section 4.1. Vance [7] mentions that there will be two components that contribute to the net transfer impedance. One is due to the diffusion of electromagnetic energy across the thickness of the shield and the other, due to

the penetration of the magnetic field through apertures of the braid. The diffusion part is identical to the case as if the shield were like a solid tube, similar to the tube mutual impedance as shown in Section 4.1. The penetration or the leakage part is usually represented as a leakage inductance term as in eqn (35).

$$Z_{\text{Shield-mutual}} = Z_T = Z_d + j\omega M_{12} \tag{35a}$$

$$Z_d = r_{\text{dc}} \frac{2r_{\text{bw}}\sqrt{j\omega\mu\sigma}}{\sinh\left(2r_{\text{bw}}\sqrt{j\omega\mu\sigma}\right)} \tag{35b}$$

The values of Z_d and M_{12} are calculated from the shield geometries and the number of carrier wires on the braid and on the weave angles. The terms r_{dc} and r_{bw} are the dc resistance of the shield and radius of the carrier wire with which the shield is formed. Associated formulas can be found in [7].

Can transfer impedance be measured experimentally? Under the assumption of weak coupling between the inner circuit and the external circuit, it is possible to determine the transfer impedance exactly. Let us get back to our differential equation (23). For the RG-58, the equations reduce to eqns (36) and (37).

$$-\frac{\mathrm{d}}{\mathrm{d}x}\begin{bmatrix} V_{\text{core}} \\ V_{\text{shield}} \end{bmatrix} = \begin{bmatrix} Z_{11} & Z_{12} \\ Z_{21} & Z_{22} \end{bmatrix}\begin{bmatrix} I_{\text{core}} \\ I_{\text{shield}} \end{bmatrix} \tag{36}$$

$$\begin{aligned} Z_{11} &= Z'_{11} + Z'_{12} + Z'_{21} + Z'_{22} \\ Z_{12} &= Z_{21} = Z'_{12} + Z'_{22} = Z'_{21} + Z'_{22} \\ Z_{22} &= Z'_{22} \end{aligned} \tag{37}$$

Assume a 1 m length of the RG-58 cable, which is electrically small. At one end (near end marked as suffix N) let us short the inner conductor and shield, and inject a current source with respect to reference plane. At the other end (far end marked as suffix F), let us open circuit the inner conductor and short the shield to the reference plane. Thus the voltage at the near and far ends with respect to core and shield currents can be written as

$$-(V_{\text{coreF}} - V_{\text{coreN}}) = Z_{11}I_{\text{core}} + Z_{12}I_{\text{shield}} \tag{38a}$$

$$-(V_{\text{shieldF}} - V_{\text{shieldN}}) = Z_{21}I_{\text{core}} + Z_{22}I_{\text{shield}} \tag{38b}$$

The core current is zero, because of which we have,

$$-(V_{\text{coreF}} - V_{\text{coreN}}) = Z_{12}I_{\text{shield}} \tag{39a}$$

$$-(V_{\text{shieldF}} - V_{\text{shieldN}}) = Z_{22}I_{\text{shield}} \tag{39b}$$

Also V_{coreN} and V_{shieldN} are the same as they are shorted at the injection point, hence by subtracting the two equations from each other in eqn (39) we have

$$(V_{\text{coreF}} - V_{\text{shieldF}}) = (-Z_{12} + Z_{22})I_{\text{shield}} \tag{40a}$$

$$(-Z_{12} + Z_{22}) = Z'_{12} = Z'_{21} \approx Z_T = \frac{V_{\text{coreF}} - V_{\text{shieldF}}}{I_{\text{shield}}} \approx \frac{V_{\text{coreF}}}{I_{\text{shield}}} \tag{40b}$$

This is the concept used in various transfer impedance measurement methods. Similar to transfer impedance, one can also define the transfer admittance. Experimentally the Triax set up as shown in Fig. 14 is used for the transfer impedance measurement [24]. There could be other more accurate or simple methods as discussed in [5]. To illustrate the Triax measurements, consider an RG-58 cable of 1 m length and make a simple Triax arrangement [24] as shown in Fig. 14. Note that one can make the radius of the tube smaller so as to be in contact with the outer insulation (not shown in Fig. 14) in order to get rid of the external inductance and capacitance between the tube wall and insulation. Now inject a step pulse current at the near end with the connection as shown in Fig. 14 and measure the open circuit voltage at the far end between the inner core and the shield. The ratio of the open circuit voltage and the shield current should give us the required tube mutual impedance or the transfer impedance.

Assume that for using eqn (35) for the RG-58 cable, the values needed (taken from [7]) are M_{12} = 1 nH/m, r_{dc} = 14 mΩ/m, r_{bw} = 63.5 μm and the copper conductivity and permeability is chosen. The transfer impedance as a function of frequency using eqn (35a) for the above values are shown in Fig. 15.

Note that one could also reproduce the curve using the equations corresponding to eqns (32) or (34), if the shield thickness or inner and outer radii are known. It is seen that if the shield was tubular of certain thickness, then the transfer

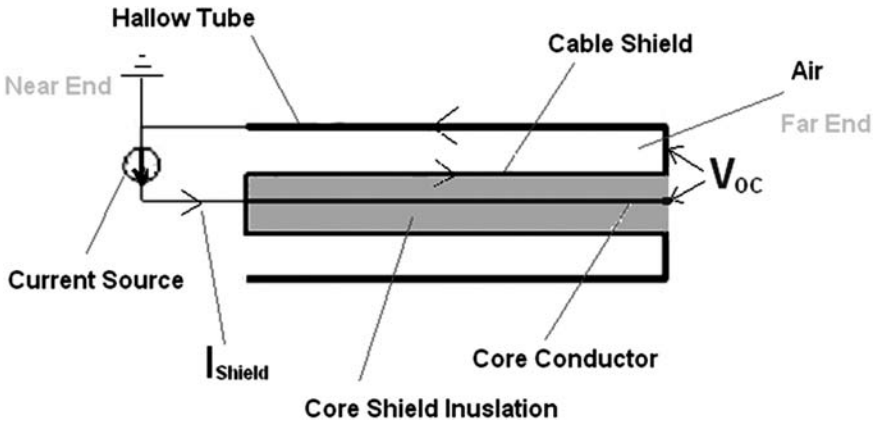

Figure 14: Triax setup for measuring the transfer impedance.

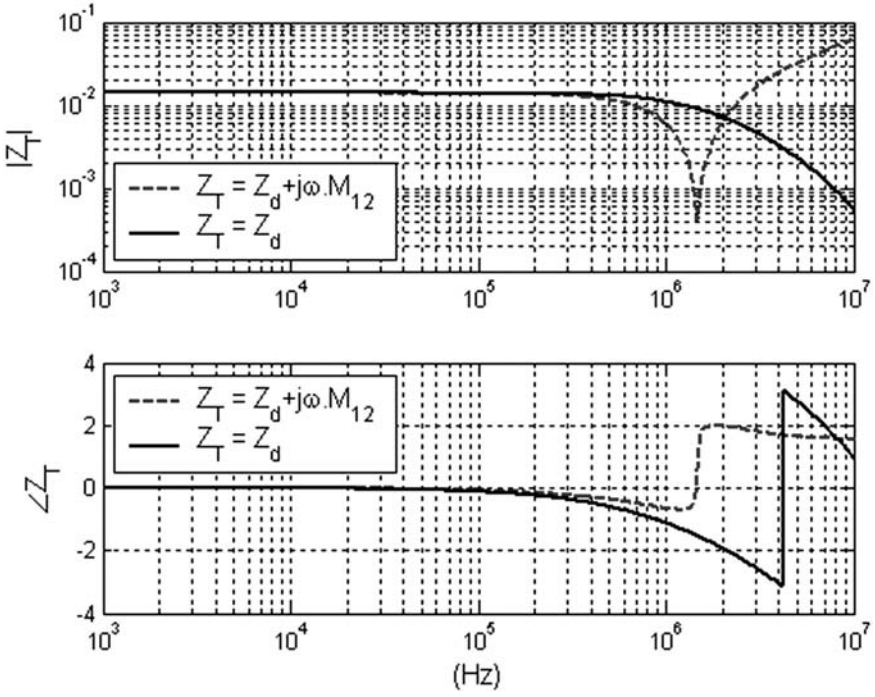

Figure 15: Transfer impedance for an RG-58 cable with braided shield, showing the influences of leakage and diffusion part.

impedance magnitude decays at high frequencies as shown in Fig. 15, when only the diffusion part is considered. However, if the shield was leaky or braided, then the transfer impedance first decreases at high frequency and then increases as shown in Fig. 15 with both diffusion and the leakage part considered. Tesche *et al.* [5] mention that the transfer impedance increases at high frequency either as $\propto f$ or $\propto \sqrt{f}$, perhaps dependant on the type of the shield. Usually the leakage part is difficult to calculate as it depends on number of carrier wires, their optical coverage, weave angle and, more importantly, they are functions of complete elliptic integrals of first and second kinds. There could be other types of shields that are not braided but similar to the ones shown in Fig. 11, for which no formula exists and controlled measurements can only give the transfer impedance. At low frequencies, the transfer impedance is dominated by only DC resistance of the shield. Similar to transfer impedance one could have transfer admittance, but it exists only if the shield is leaky and at high frequency. The transfer admittance is approximately given by eqn (41). In eqn (41), C_1 is the capacitance per unit length between the internal conductors and the shield, C_2 is the capacitance per unit length between shield and the external current return path and K is a function with complete elliptic integrals and carriers and weave angle, etc. More details can be

found in [5, 7]. As a reasonable approximation, transfer admittance is usually neglected.

$$\begin{aligned} Y_T &\approx j\omega C_{12} \\ C_{12} &\approx C_1 C_2 K \end{aligned} \tag{41}$$

4.3 Influence of shield thickness in the coupling phenomena

Let us now consider as to what would be the influence of shield thickness on the transfer impedance characteristics. For simplicity, we shall consider the example of tubular shields with two thicknesses, namely, 127 and 254 μm, made of copper with an arbitrary outer radius of the shield as 1.65 mm. The expressions (32) or (34) can be used for transfer impedance. One would also get the same if the Traix experiments as explained earlier were made and the ratio of open circuit voltage and shield current were determined. The transfer impedances for the two shield thickness are shown in Fig. 16.

The higher the thickness, the less the transfer impedance, as can be clearly seen in Fig. 16. The transfer impedance in frequency domain shown in Fig. 16 is

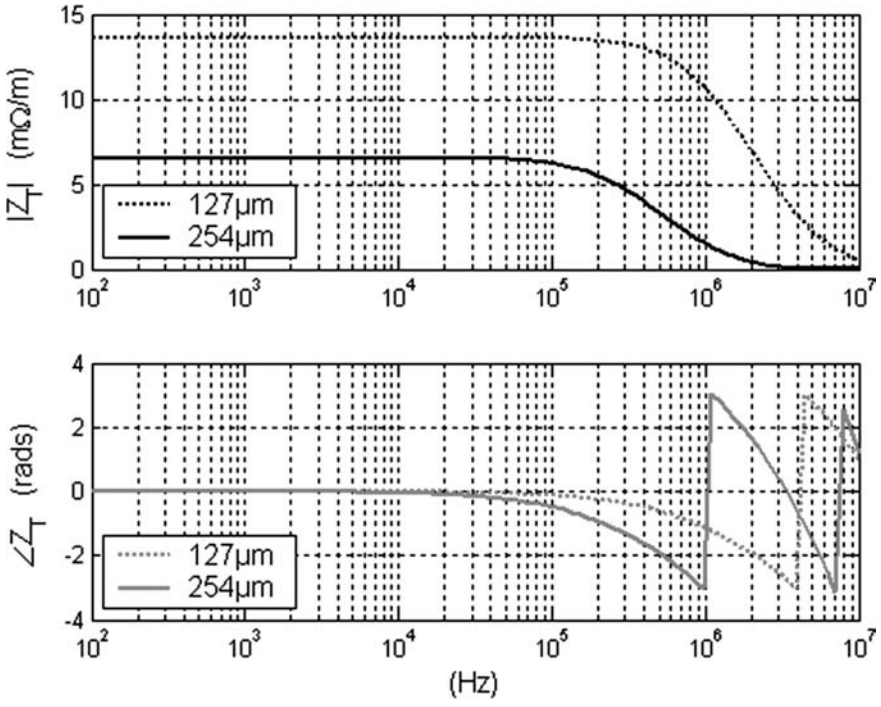

Figure 16: Transfer impedance for two shield thicknesses assuming a shield to be solid tubular.

vector fitted [25] using ten poles and the time domain response is shown in Fig. 17. The value of transfer impedance in time domain is large, which is a result of convolution.

An interpretation can be provided to time domain 'transfer impedance' presented in Fig. 17. It takes some time for the shield current (magnetic field) to penetrate inside. The time, when the steady low value of transfer impedance is achieved in Fig. 17, is nearly the same as the time at which the steady value of the open circuit voltage is achieved in Fig. 18. Stern [26] has provided a time domain formula as a series expansion for expression (35b). The convergence of such a time domain formula depends on shield properties and shield dimensions. Another interesting feature of the transfer impedance is that it predicts the diffusion time [7] required for the development of the internal voltage. The diffusion time constant can be obtained from the shield thickness and shield material properties and is given by eqn (42).

$$\tau_s = \mu\sigma(\text{shield thickness})^2 \tag{42}$$

To demonstrate this, let us take the same example of transfer impedance as above. The internal open circuit voltages, which corresponding to the Triax setup, would have been the product of transfer impedance and shield current for two shield thicknesses

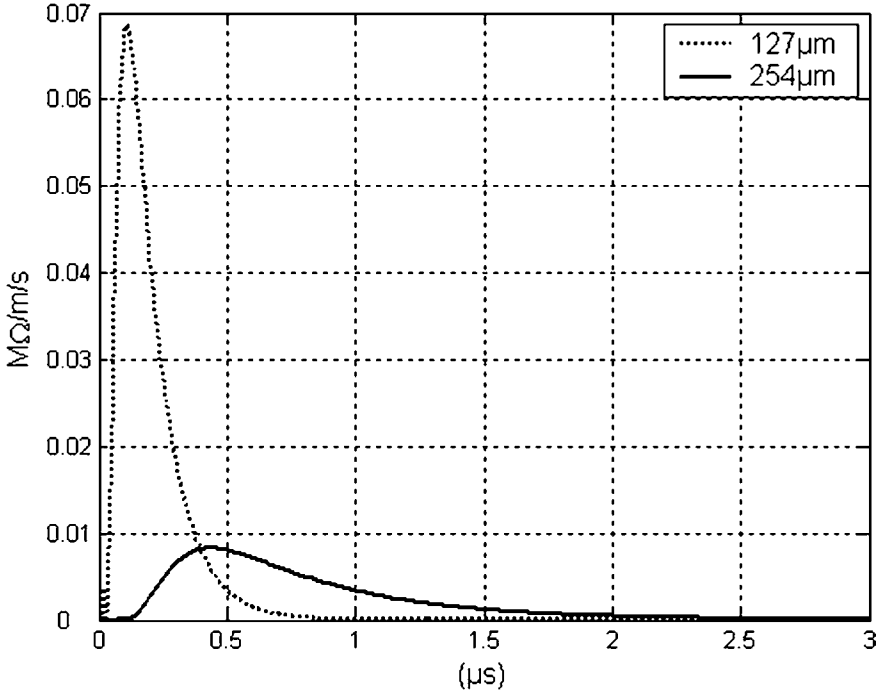

Figure 17: Transfer impedance in time domain for two shield thicknesses assuming a shield to be solid tubular.

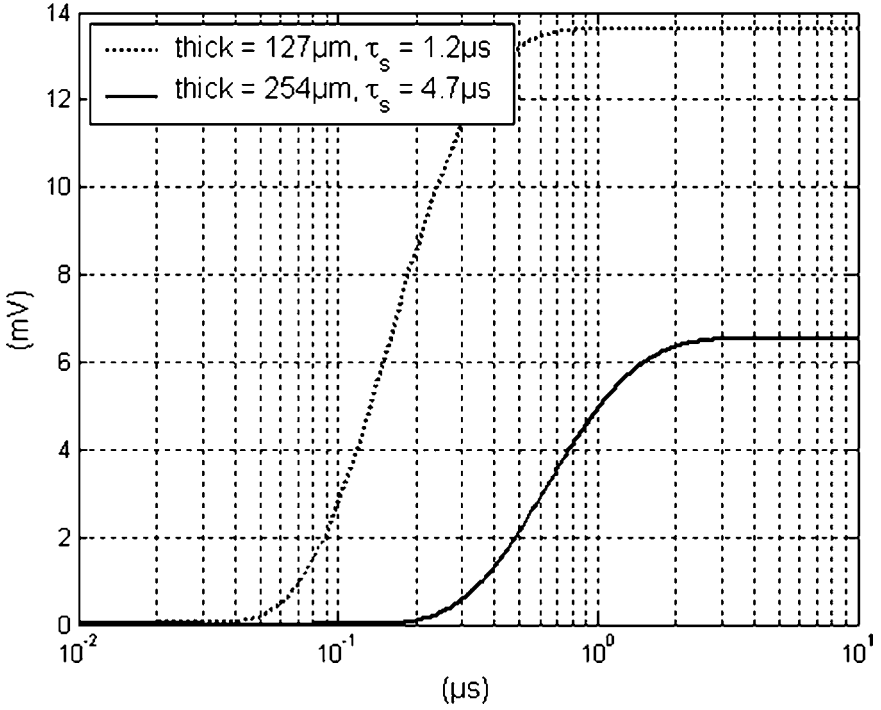

Figure 18: Time domain response of the internal open circuit voltages for two shield thicknesses assuming the shield to be solid tubular.

are shown in Fig. 18. Let us assume a step function for injected shield current. It can then be seen that the constant voltage is attained at about times corresponding to diffusion time of the shield and those times are marked in Fig. 18. Note that in generating the curves corresponding to Fig. 18, the frequency domain voltage obtained from the product of transfer impedance and step current in frequency domain were Vector fitted using ten poles. It is readily see that, higher the thickness, the larger the diffusion time and the less the internal voltages due to low value of transfer impedance.

4.4 A simple measurement for estimating inductance and capacitance matrix elements for internal conductors of cables

Today, very sensitive, high precision and accurate measurement systems like AC bridges are commercially available for measurement of smaller values of capacitance and inductances. Further, there are voltage and current sensors or instruments for measuring small currents and voltages. In this section, we discuss some of the methods to evaluate through experiments, the inductance and capacitance matrix elements for the MTL arrangement of conductors in the cable with respect to the shield based on the method proposed in [5]. This is necessary because there

could be situations where the medium between the core conductors and the shield is not homogenous and, at the same time, one could have twisted pair arrangement. Under such circumstances practical formulae as discussed earlier, i.e. using eqns (29) and (30), no longer applies.

4.4.1 MTL capacitance matrix estimation

Let there be a system of n conductors forming an MTL system inside the shield and let the length of the cable be L. Let one of the ends of the cable be referred to as the near end and the other, as the far end. From the transmission line equations, the relationship between the current in the ith conductor and the voltages on the other conductors are related through admittances as follows.

$$\frac{\mathrm{d}I_i}{\mathrm{d}x} = Y_{i1}V_1 + Y_{i1}V_2 + \cdots + Y_{1n}V_n \tag{43}$$

For a source with line length much less than the wavelength, i.e. under weak coupling assumptions we can rewrite eqn (43) as

$$I_i(0) - I_i(L) \approx [Y_{i1}V_1 + Y_{i1}V_2 + \cdots + Y_{1n}V_n]L \tag{44}$$

In eqn (43), $I_i(0)$ and $I_i(L)$ represent the current at the near and far ends, respectively. Let all the lines at the far end be left open circuited. Then, for any conductor, the current $I_i(L) = 0$.

Now at the near end, say if we are interested in calculating the self-capacitance of kth conductor, C_{kk}, then we do the following. Short all the conductors to the shield in the near end except for the kth conductor where a voltage source V_k is connected to the shield. This voltage source injects a current I_k on the kth, conductor which can also be measured. Then based on eqn (44), since all the voltages are zero at the near end excepting on the kth conductor, we will have

$$I_k(0) \approx Y_{kk}V_kL = j\omega C_{kk}V_kL \tag{45}$$

If the voltage source frequency, measured current and applied voltage at the near end is known, then the self capacitance C_{kk} can be calculated.

Similarly, if we measure the short-circuit current in the jth conductor with the same voltage source V_k with respect to the shield at the near end then we will have eqn (46), from which the mutual capacitance C_{jk} or C_{kj} can be obtained.

$$I_j(0) \approx Y_{jk}V_kL = j\omega C_{jk}V_kL \tag{46}$$

4.4.2 MTL inductance matrix estimation

Similar to eqn (43), we can have the voltage and the currents in the conductor related through the impedance parameters as follows:

$$\frac{\mathrm{d}V_i}{\mathrm{d}x} = Z_{i1}I_1 + Z_{i1}I_2 + \cdots + Z_{1n}I_n \tag{47}$$

For a source with line length much less than the wavelength, i.e. under weak coupling assumptions, we can rewrite eqn (47) as

$$V_i(0) - V_i(L) \approx [Z_{i1}I_1 + Z_{i1}I_2 + \cdots + Z_{1n}I_n]L \tag{48}$$

In eqn (43), $V_i(0)$ and $V_i(L)$ represent the voltage at the near and far ends, respectively. Let all the lines at the far end be short-circuited to shield. Then, for any conductor, the current $V_i(L) = 0$.

Now at the near end, say if we are interested in calculating the self-inductance of kth conductor, L_{kk}, then we do the following. Open-circuit all the conductors in the near end except on the kth conductor, connect a voltage source V_k with respect to the shield, which injects a current I_k on the kth conductor and that is measured. Then based on eqn (48), since all the currents are zero at the near end excepting on the kth conductor, we will have

$$V_k(0) \approx Z_{kk}I_kL = j\omega L_{kk}I_kL \tag{49}$$

If the voltage source frequency, measured current and applied voltage at the near end is known, then the self-inductance L_{kk} can be calculated.

Similarly, if we measure the open circuit voltage in the jth conductor with the same voltage source V_k with respect to the shield injecting current I_k on the kth conductor at the near end, then we will have eqn (50), from which the mutual inductance either L_{jk} or L_{kj} can be obtained.

$$V_j(0) \approx Z_{jk}I_kL = j\omega L_{jk}I_kL \tag{50}$$

5 Some additional cases of ground impedance based on wire geometry

5.1 Impedance with wires on the ground

Having known the expressions for ground impedance and admittance for wires above and below ground, it would be interesting to see what would be the expressions for the ground impedance for wires on the surface of the ground. This is needed because there are railway systems where cables are sometimes laid beside the tracks either on the ground or in cable trenches. This can be seen in some typical power and communication systems too. Therefore, it is necessary to know the ground impedance expressions for wires on the ground. Sunde [6] has given the expression for ground impedance for the wires on the ground as eqn (51).

$$Z_{\text{gsbi}}^{\text{Sunde}} = \frac{j\omega\mu_0}{\pi\gamma_g^2 R_{\text{ab}}^2}[1 - \gamma_g R_{\text{ab}} K_1(\gamma_g R_{\text{ab}})] \tag{51}$$

In the above expressions, the Bessel's function is used. An expression for ground impedance for wires on the ground can be obtained by using the ground impedance expressions for wires below ground, i.e. using eqn (11) with depth d approaching zero.

$$Z_{\text{gsbi}}^{\text{Log}} = \frac{j\omega\mu_0}{2\pi}\left(\ln\left(\frac{1+\gamma_g R_{ab}}{\gamma_g R_{ab}}\right)+\frac{2}{4+R_{ab}^2\gamma_g^2}\right) \tag{52}$$

What is interesting to note is that there is not any exponential term in eqn (52). It was seen that the logarithmic term corresponds to ground impedance of wires buried at infinite depth in the soil [7]. The second term in eqn (52) modifies or corrects the infinite depth ground impedance model to obtain the ground impedance expression for the wires on the surface of the earth. Therefore, the authors refer eqn (52) as modified logarithmic formula. A comparison between the Sunde's formula (using Bessel function) and the modified logarithmic formula is shown in Fig. 19. The example is a wire of radius 2 cm, ground conductivity is varied from 10 to 0.1 mS/m, and the ground relative permittivity is 10. It is seen

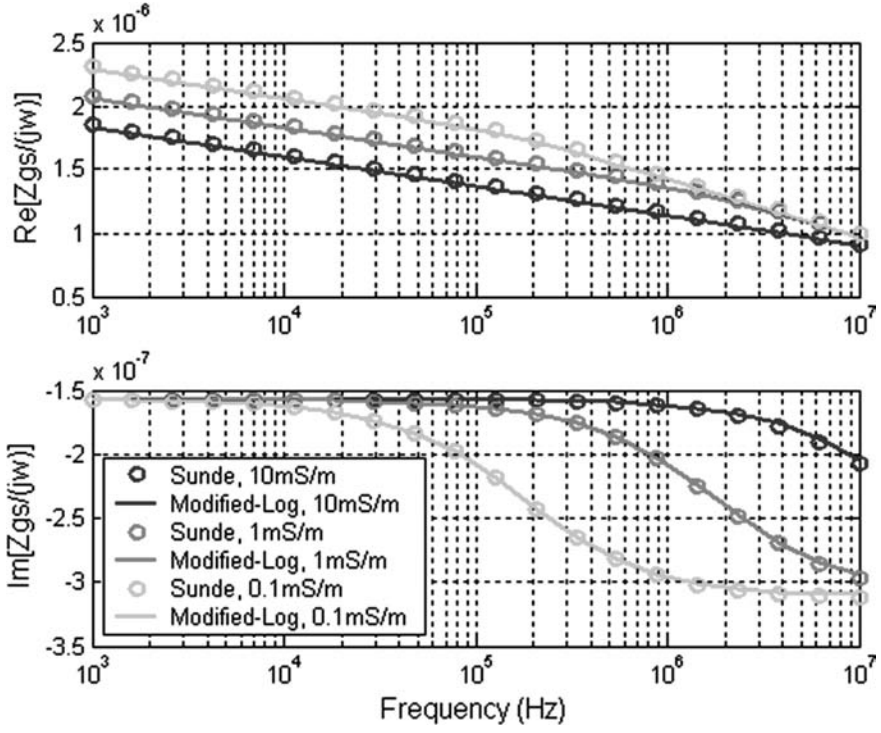

Figure 19: Comparison between Sunde and modified-logarithmic formula for the ground impedance of wires on the surface of the earth.

that eqn (52) is a good approximation for eqn (51) and does not involve Bessel function. It should be remembered that if there are many parallel wires on the ground surface, the mutual ground impedance expressions could be obtained by substituting in eqn (52) the radius of the wire with horizontal distance between the wires, the same analogy as was applicable for the wires below ground. The ground admittance can be obtained using the propagation constant and the relation (15).

5.2 Mutual impedance with one wire above ground and the other below the ground

The mutual ground impedance expressions between an overhead wire and buried wire can be derived from Sunde's method [6] but it involves infinite integrals as shown in eqn (53). In eqn (53), d_{kl} is the horizontal distance between above ground and buried conductors. The height of the overhead wire is h and the wire depth is d. The authors feel that simplified expression for eqn (53) in terms of logarithms or exponentials should be derived to avoid infinite integrals. It is a subject for future study.

$$Z_{\text{gabbi}} = \frac{j\omega\mu_0}{\pi}\int_0^\infty \frac{\mathrm{e}^{-\left(hu - d\sqrt{u^2+\gamma_{\text{g}}^2}\right)}}{u+\sqrt{u^2+\gamma_{\text{g}}^2}}\cos(d_{kl}u)\mathrm{d}u \tag{53}$$

6 Some examples

We have seen various expressions for impedance and admittances for the bare and insulated wires. We have also seen how to model the coupling through cable shields. In this section, we take some examples, which will describe the solutions in time or frequency domain and also a practical example of how crosstalk phenomena can be minimized using shielded cables.

6.1 Time domain simulation of pulse propagation in bare and insulated wires

When large transient currents or voltages propagate in bare wires or insulated cables there will be non-linear arcing or breakdown mechanisms occurring within the soil or insulation medium. The mechanisms of soil ionization in grounding systems and insulation breakdown in cables are common during power system transients/faults. To include such non-linear effects only time domain solution of transmission line equations helps. An efficient way of solving numerically lossy transmission line equations in time domain is by using the finite difference time domain (FDTD) method with recursive convolutions as discussed in Chapter 2. The only difference is that a vector fitting [25] of ground admittance in addition to ground impedance is to be made. The discussions presented here can be found in

Theethayi *et al.* [19] as well. Further, we will have constant term in addition to the exponential terms while fitting the ground impedance and admittance terms which has to be used in the FDTD equations as discussed in Chapter 2.

As discussed in the beginning of this chapter, the transmission line equations, either eqns (1) or (2), when transformed to time domain will appear as eqn (54).

$$\frac{\partial V(x,t)}{\partial x}+\int_0^t \zeta(t-\tau)\frac{\partial I(x,\tau)}{\partial \tau}\mathrm{d}\tau = 0 \tag{54a}$$

$$\frac{\partial I(x,t)}{\partial x}+\int_0^t \eta(t-\tau)\frac{\partial V(x,\tau)}{\partial \tau}\mathrm{d}\tau = 0 \tag{54b}$$

Note that in eqn (54), the terms $\zeta(t)$ and $\eta(t)$ are given by eqns (55a) and (55b), respectively.

$$\zeta(t) = F^{-1}\left(\frac{Z(j\omega)}{j\omega}\right) \tag{55a}$$

$$\eta(t) = F^{-1}\left(\frac{Y(j\omega)}{j\omega}\right) \tag{55b}$$

Let us assume that eqns (55) or (56), when fitted with Vector fitting, say, up to 10 MHz, will give eqns (57) and (58).

$$\zeta(t) \approx Cz_0\delta(t)+\sum_{i=1}^{n} Cz_i \mathrm{e}^{-\alpha_i t} \tag{56a}$$

$$\eta(t) \approx Cy_0\delta(t)+\sum_{i=1}^{n} Cy_i \mathrm{e}^{-\beta_i t} \tag{56b}$$

To demonstrate the final time domain expression, let us discuss considering only eqns (54a) and (56a). Substituting eqns (56a) into (54a), we have

$$\frac{\partial V(x,t)}{\partial x}+\int_0^t \left[Cz_0\delta(t-\tau)+\sum_{i=1}^{n} Cz_i \mathrm{e}^{-\alpha_i (t-\tau)}\right]\frac{\partial I(x,\tau)}{\partial \tau}\mathrm{d}\tau = 0 \tag{57}$$

Let us split eqn (57) as

$$\frac{\partial V(x,t)}{\partial x}+\int_0^t \left[Cz_0\delta(t-\tau)\right]\frac{\partial I(x,\tau)}{\partial \tau}\mathrm{d}\tau+\int_0^t \left[\sum_{i=1}^{n} Cz_i \mathrm{e}^{-\alpha_i (t-\tau)}\right]\frac{\partial I(x,\tau)}{\partial \tau}\mathrm{d}\tau = 0 \tag{58}$$

In eqn (58), the second term with a delta function can be written as a convolution given by eqn (59).

$$\int_0^t \left[Cz_0\delta(t-\tau)\right]\frac{\partial I(x,\tau)}{\partial \tau}\mathrm{d}\tau = \left[Cz_0\delta(t-\tau)\right]\otimes\frac{\partial I(x,\tau)}{\partial \tau} \tag{59}$$

$$\left[Cz_0\delta(t-\tau)\right]\otimes\frac{\partial I(x,\tau)}{\partial \tau} = F^{-1}\left[Cz_0 j\omega I(x,j\omega)\right] \tag{60}$$

$$F^{-1}\left[Cz_0 j\omega I(x,j\omega)\right] = Cz_0\frac{\partial I(x,t)}{\partial t} \tag{61}$$

From eqn (61), it is clear that Cz_0 has dimensions similar to line series inductance and term Cy_0 to shunt capacitance. Thus, the final set of transmission line equations in time domain for pulse propagation that needs to be solved is given by eqn (62).

$$\frac{\partial V(x,t)}{\partial x} + Cz_0\frac{\partial I(x,t)}{\partial t} + \int_0^t\left[\sum_{i=1}^{n} Cz_i \mathrm{e}^{-a_i(t-\tau)}\right]\frac{\partial I(x,\tau)}{\partial \tau}\mathrm{d}\tau = 0 \tag{62a}$$

$$\frac{\partial I(x,t)}{\partial x} + Cy_0\frac{\partial V(x,t)}{\partial t} + \int_0^t\left[\sum_{i=1}^{n} Cz_i \mathrm{e}^{-\beta_i(t-\tau)}\right]\frac{\partial V(x,\tau)}{\partial \tau}\mathrm{d}\tau = 0 \tag{62b}$$

It is interesting to see that eqn (62) appears similar to the expressions for overhead wires and the solutions to these equations using the FDTD method are straight forward, as discussed in Chapter 2, using the recursive convolution.

To demonstrate the differences one would obtain between the application of the FDTD method to eqn (62) and solutions using direct frequency domain solutions, as discussed in Chapter 2, we take an example of a bare wire 1 km long and buried at a depth of 0.5 m and having a radius of 7.5 mm. A current source having a peak of 1 A with the shape given by $I_0(t) = 1.1274\left(\mathrm{e}^{(1\times10^4)t} - \mathrm{e}^{(4\times10^5)t}\right)$ is injected one end, and the voltage at the injection point, 100, 200, 300, 400 and 500 m from the injection point by two different methods are shown in Fig. 20 for a ground with σ_g = 1 mS/m and ε_{rg} = 10. The differences between the two methods are nominal, which could be due to the numerical errors inherent in both the methods.

6.2 A practical crosstalk problem

In Chapter 2, we have seen the crosstalk mechanisms with the MTL conductor system in the presence of finitely conducting ground. Here, we shall consider crosstalk to shielded wires based on weak coupling analysis, i.e. the generator wire circuit currents (source) is not influenced by the current in the shielded cable.

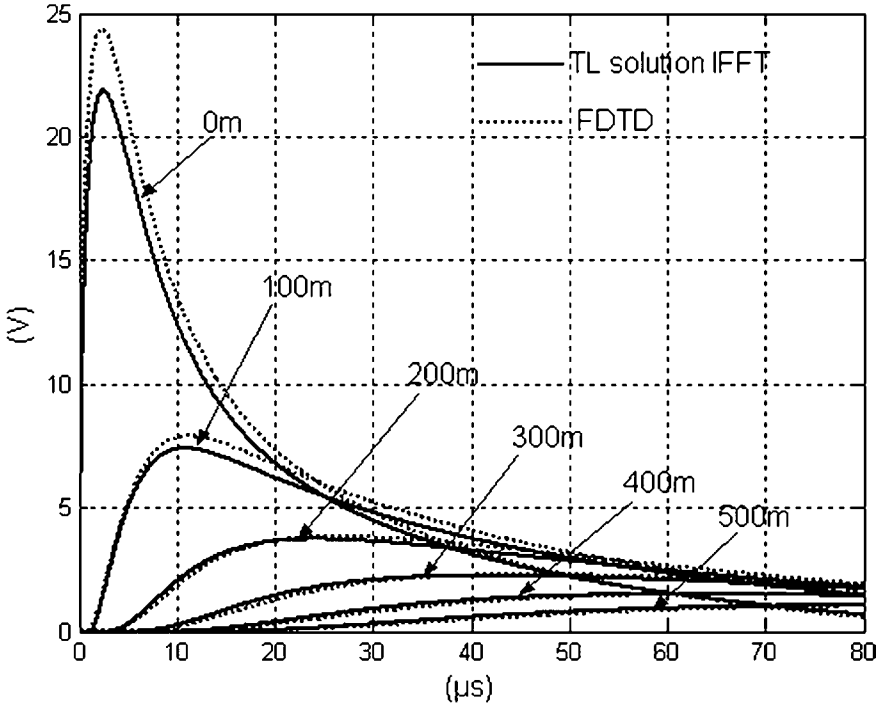

Figure 20: Calculated voltages using the transmission line solution and the FDTD method for a bare wire buried at a depth of 0.5 m, 1 km long and radius of 7.5 mm. The ground medium has σ_g = 1 mS/m and ε_{rg} = 10.

Note that the analysis to be presented is applicable to electrically short lines as discussed in Chapter 2. Shielded cables are used to protect the signal wires from external interference and also to provide a return path or reference (e.g. the common coaxial cable type RG-58). First, we consider a perfect shield without any direct field penetration inside, and then find out how connecting the shield ends to the ground influence the crosstalk (Fig. 21). For simplicity, the ground is assumed to be perfectly conducting. The cable length is assumed to be electrically small so that the circuit analysis is valid. Let us now consider crosstalk to the shielded wire in the set up shown below. This situation is treated in detail by Paul [23].

First consider the capacitive coupling as discussed in Chapter 2. The shield is assumed to be perfect. Therefore, there is no 'direct' coupling between the generator wire and the receptor wire. The coupling capacitance between them is a series combination of C_{GS} and C_{RS} (Fig. 22)

$$C_{12} = \frac{C_{RS}C_{GS}}{C_{RS} + C_{GS}} \tag{63}$$

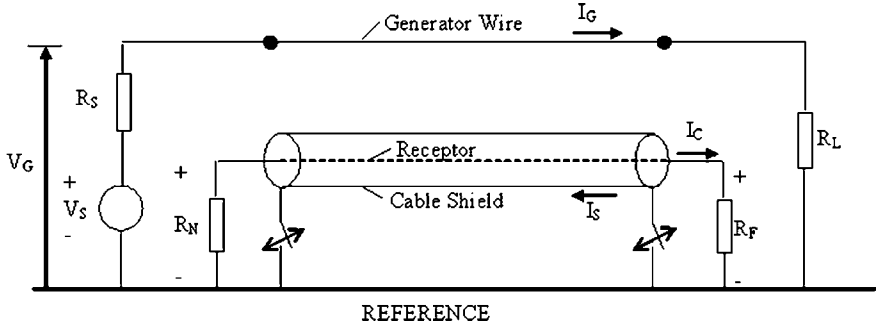

Figure 21: Basic model for crosstalk to shielded cable.

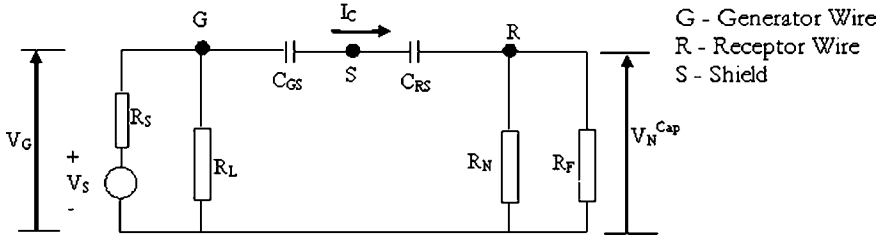

Figure 22: Equivalent circuit for capacitive crosstalk to shielded cable.

The near end and far end crosstalk due to capacitive coupling is given by eqn (64).

$$V_{\mathrm{F}}^{\mathrm{Cap}} = V_{\mathrm{N}}^{\mathrm{Cap}} = \frac{R_{\mathrm{N}} R_{\mathrm{F}}}{R_{\mathrm{N}} + R_{\mathrm{F}}} j\omega C_{12} I_2 \tag{64}$$

Where I_2 is approximately given by eqn (65) (assuming currents and voltages in the receptor and shield circuit do not influence the currents and voltages of the generator circuit, that is, weak coupling with the generator circuit).

$$I_2 \approx \frac{V_{\mathrm{g}}}{R_{\mathrm{g}} + R_{\mathrm{L}}} \tag{65}$$

If the screen is connected to the ground at either end, the screen voltage becomes zero everywhere (low-frequency approximation) and the capacitor C_{RS} is shorted out. There is no capacitive crosstalk in this case, $V_{\mathrm{F}}^{\mathrm{Cap}} = V_{\mathrm{N}}^{\mathrm{Cap}} = 0$ when screen is connected to ground at one end or both ends.

Next, we will consider the inductive coupling. The disturbing current in the generator circuit produces a flux in the circuit formed by the shield and the ground plane. This flux induces a current in the shield which produces a flux opposing the original flux in the space between the shield and ground plane. That is, the flux linking with the circuit formed by the receptor wire and the ground plane is also reduced.

In electrically small cables, there can be a shield current flow only if both ends of the shield are connected to the ground. Therefore, to reduce inductive coupling, both ends of the shield are to be connected to the ground. The equivalent circuit for the inductive coupling of the shielded wire is given in Fig. 23. In Fig. 23,

- M_{GR} – Mutual inductance between the generator circuit and the receptor circuit.
- M_{RS} – Mutual inductance between the receptor circuit and the shield circuit.
- M_{GR} – Mutual inductance between the generator circuit and the shield circuit.
- R_S, L_S – Resistance and self inductance of the shield.

The direction of the disturbing current is from near end to the far end. It produces a voltage $j\omega M_{GS} I_2$ in the shield and drives a current I_S in the direction shown. In the absence of the shield, the voltage induced by I_2 in the inner wire (receptor wire) would have been $j\omega M_{GR} I_2$. The shield current I_S produces a flux that opposes the flux produced by I_2. Therefore, the induced voltage in the receptor wire would be reduced by an amount equal to $j\omega M_{RS} I_2$. Note that the two voltage sources in the receptor wire oppose each other. In the absence of shield current, I_S, the voltage $j\omega M_{GS} I_2 = 0$. Shield current is given by eqn (66).

$$I_S = \frac{j\omega M_{GS} I_2}{R_S + j\omega L_S} \tag{66}$$

The near end inductive crosstalk voltage is given by eqn (67).

$$V_N^{IN} = \frac{R_N}{R_N + R_F} j\omega (M_{GR} I_2 - M_{RS} I_S) \tag{67}$$

Substituting eqn (66) in eqn (67), we have

$$\left.\begin{aligned} V_N^{IN} &= \frac{R_N}{R_N + R_F}\left(j\omega M_{GR} - \frac{\omega^2 M_{GS} M_{RS}}{R_S + j\omega L_S} \right) I_2 \\ &= \frac{R_N}{R_N + R_F} \frac{j\omega R_S M_{GR} + \omega^2 (M_{GS} M_{RS} - M_{GR} L_S)}{R_S + j\omega L_S} I_2 \end{aligned}\right\} \tag{68}$$

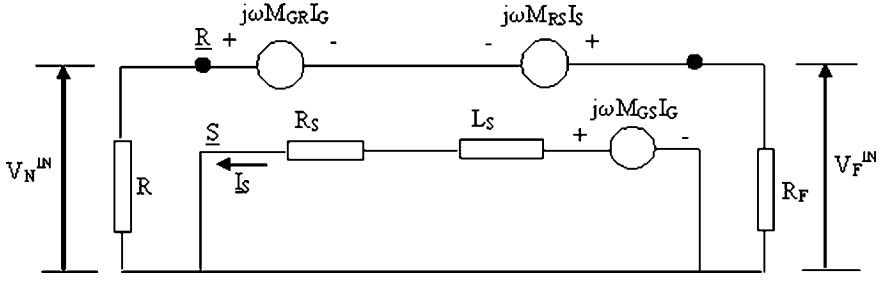

Figure 23: Equivalent circuit for inductive crosstalk to shielded cable.

Under weak coupling assumptions, the mutual flux linking the receptor circuit and the shield circuit is about the same as the mutual flux linking the generator circuit and the receptor wire circuit, leading to $M_{GR} \approx M_{GS}$. Similarly, the magnetic flux in the shield-ground circuit due to shield current is the same as that magnetic flux produced by an equal current in the receptor wire leading to $L_s \approx M_{RS}$. Applying these two conditions in eqn (68), we get

$$V_N^{IN} = \underbrace{\frac{R_N}{R_N + R_F} j\omega M_{GR} I_2}_{\substack{\text{Crosstalk with} \\ \text{shield removed}}} \underbrace{\frac{R_S}{R_S + j\omega L_S}}_{\substack{\text{Effect of} \\ \text{the shield}}} \tag{69}$$

In a similar manner, we can find the crosstalk at the far end, as

$$V_F^{IN} = \underbrace{-\frac{R_F}{R_N + R_F} j\omega M_{GR} I_2}_{\substack{\text{Crosstalk with} \\ \text{shield removed}}} \underbrace{\frac{R_S}{R_S + j\omega L_S}}_{\substack{\text{Effect of} \\ \text{the shield}}} \tag{70}$$

The effect of the shield appears as a multiplying factor (71) on the crosstalk without shield, where $\tau_s = L_s/R_s$ is the shield time constant.

$$SF = \frac{R_S}{R_S + j\omega L_S} = \frac{1}{1 + j\omega\tau_S} \tag{71}$$

Shielding Factor (SF) can be approximated as

$$SF = \begin{cases} 1 & \text{for} \quad \omega < 1/\tau_S \\ \dfrac{R_S}{j\omega L_S} & \text{for} \quad \omega > 1/\tau_S \end{cases} \tag{72}$$

For $\omega < 1/\tau_s$,

$$\left.\begin{aligned} |V_N^{IN}| &= \frac{R_N}{R_N + R_F} j\omega M_{GR} I_2 \\ |V_F^{IN}| &= \frac{-R_F}{R_N + R_F} j\omega M_{GR} I_2 \end{aligned}\right\} \tag{73}$$

That is, inductive crosstalk increases by 20 dB/decade increase in frequency up to about $f = 1/2\ \pi\tau_s$, or $R_s = \omega L_s$.

For $\omega > 1/\tau_s$,

$$\left.\begin{aligned} |V_N^{IN}| &= \frac{R_N}{R_N + R_F} \frac{M_{GR} R_S}{L_S} I_2 \\ |V_F^{IN}| &= \frac{R_F}{R_N + R_F} \frac{M_{GR} R_S}{L_S} I_2 \end{aligned}\right\} \tag{74}$$

Equation (74) is independent of frequency. That is, inductive crosstalk remains constant for $f > 1/2\ \pi\tau_s$.

Total crosstalk is the sum of capacitive and inductive crosstalk. If the shield is grounded, at least one end, the capacitive coupling contribution is zero, and the inductive coupling is reduced by the shield only if the shield is grounded at both ends and the frequency of the interfering signal is greater than the shield cut-off frequency.

7 Concluding remarks

In this chapter, we have seen how the transmission line theory can be extended to solve pulse propagation problems in buried conductors, bare as well as insulated. Two of the key concepts for including the effect of finitely conducting ground are the ground impedance and ground admittance. After a review of different expressions for these two quantities, we have presented a set of new simple expressions that can represent them. These two new expressions do not involve any complicated infinite integrals and hence computationally very efficient, at the same time retaining the accuracy. It was pointed out that ground admittance is very sensitive to ground conductivity, whereas for overhead conductors (chapter 2) it was ground impedance that was sensitive to ground conductivity. The popularly used transient simulation packages like EMTP/ATP ignores ground admittance and the pitfalls of using these programs for the analysis of underground systems have been pointed out. For the given conductivity and permittivity of ground, the frequency up to which transmission line methods could be used for buried systems without significant errors is derived. An MTL method for buried shielded cables is presented. This model is capable of calculating the voltages and current developed internal to the cable due to induced external currents in the shield under all possible terminal conditions (short circuit to open circuit). Numerical examples of pulse propagation in buried bare wires and cables have been presented in time domain and discussed.

Acknowledgements

The authors wish to thank F. Rachidi, C.A. Nucci, M. Paolone, V. Cooray and V.A. Rakov for various technical discussions applicable to the present topic. V. Gopinathan is thanked for the editorial assistance for the language.

References

[1] Bewley, L.V., *Travelling Waves on Transmission Systems*, John Wiley & Sons, Inc., Chapman & Hall, Ltd.: London, 1933.

[2] *Transmission Line Reference Book 345 kV and Above*, Electric Power Research Institute, Fred Weidner and Son Printers Inc., 1975.

[3] *EMMA Handbook (Elektromagnetisk miljö anvädarhandbok)*, Electromagnetic Environment Handbook, Försvarets MaterielVerk (FMV), 2002.

[4] Lee, C.H. & Meliopoulos, A.P.S., Comparison of touch and step voltages between IEEE Std 80 and IEC 479 – 1. *IEE Proc. on Generation, Transmission and Distribution*, **146(5)**, pp. 593–601, 1999.

[5] Tesche, F.M., Ianoz, M.V. & Karlsson, T., *EMC Analysis Methods and Computational Models*, John Wiley and Sons Inc.: New York, 1997.

[6] Sunde, E.D., *Earth Conduction Effects in the Transmission Systems*, Van Nostrand, New York, 1949.

[7] Vance, E.F., *Coupling to Cable Shields*, Wiley Interscience: New York, 1978.

[8] Bridges, G.E., Fields generated by bare and insulated cables buried in a lossy half-space. *IEEE Trans. on Geoscience and Remote Sensing*, **30(1)**, pp. 140–146, 1992.

[9] Wait, J.R., Electromagnetic wave propagation along a buried insulated wire. *Canadian Journal of Physics*, **50**, pp. 2402–2409, 1972.

[10] Cooray, V. (ed.), *The Lightning Flash*, IEE power series, IEE: London, 2003.

[11] Rakov, V.A. & Uman, M.A., *Lightning Physics and Effects*, Cambridge University Press: Cambridge, 2003.

[12] Petrache, E., Rachidi, F., Paolone, M., Nucci, C.A., Rakov, V.A. & Uman, M.A., Lightning induced disturbances in buried cables – part I: theory. *IEEE Trans. on Electromagnetic Compatibility*, **47(3)**, pp. 498–508, 2005.

[13] Pollaczek, F., Sur le champ produit par un conducteur simple infiniment long parcouru par un courant alternatif. *Revue Gen. Elec.*, **29,** pp. 851–867, 1931.

[14] Saad, O., Gaba, G. & Giroux, M., A closed-form approximation for ground return impedance of underground cables. *IEEE Trans. on Power Delivery*, **11(3)**, pp. 1536–1545, 1996.

[15] Wedepohl, L.M. & Wilcox, D.J., Transient analysis of underground power transmission systems. *Proc. IEE*, **120**, pp. 253–260, 1973.

[16] Dommel, H.W., *Electromagnetic Transients Program (EMTP Theory Book)*, Bonneville Power Administration, 1986.

[17] Dommel, H.W., Overhead line parameters from handbook formulas and computer programs. *IEEE Trans. on Power Apparatus & Systems*, **PAS-104**, pp. 366–372, 1985.

[18] Chen, K.C., Transient response of an infinite wire in a dissipative medium. *Interaction Notes on EMP and Related Subjects*, ed. C.E. Baum, IN453, 2001.

[19] Theethayi, N., Thottappillil, R., Paolone, M., Nucci, C.A. & Rachidi, F., External impedance and admittance of buried horizontal wires for transient studies using transmission line analysis. *IEEE Transactions on Dielectric and Electrical Insulation,* **14(3)**, pp. 751-761, 2007.

[20] Spiegel, M.R., *Mathematical Handbook of Formulas and Tables*, Schaum's outline series, McGraw-Hill Book Company: New York, 1968.

[21] Meyer, W.S. & Liu, T., *Alternative Transient Program (ATP) Rule Book*, ©1987–1992 by Canadian/American EMTP User Group.

[22] Schelkunoff, S.A., The Electromagnetic theory of coaxial transmission lines and cylindrical shields. *Bell Systems Technical Journal*, **13**, pp. 532–579, 1934.

[23] Paul, C.R., *Introduction to Electromagnetic Compatibility*, John Wiley and Sons Inc.: New York, 1992.

[24] Tang, H. & Scuka, V., Time-domain study of a shielding cable system with a nonlinear load. *IEEE Trans. on Electromagnetic Compatibility*, **41(3)**, pp. 214–220, 1999.

[25] Gustavsen, B. & Semlyen, A., Rational approximation of frequency domain responses by vector fitting. *IEEE Trans. on Power Delivery*, **14(3)**, 1999, pp. 1052–1061.

[26] Stern, R.B., Time domain calculation of electric field penetration through metallic shields. *IEEE Trans. on Electromagnetic Compatibility*, **30(3)**, pp. 307–311, 1988.

PART II

Enhanced Transmission Line Thoery

This page intentionally left blank

CHAPTER 4

High-frequency electromagnetic coupling to transmission lines: electrodynamics correction to the TL approximation

S.V. Tkachenko[1], F. Rachidi[2] & J.B. Nitsch[1]
[1]*Otto-von-Guericke-University Magdeburg, Magdeburg, Germany.*
[2]*Ecole Polytechnique Federale de Lausanne, Lausanne, Switzerland.*

Abstract

A system of integral-differential equations for evaluating currents and potentials induced by external electromagnetic field on a wire of different geometric form above a perfectly conducting ground is derived under the thin-wire approximation. Based on the perturbation theory, an iterative procedure is proposed to solve the derived coupling equations, where the zero-iteration term is determined by using the transmission line approximation. The method can be applied both in the frequency domain and in the time domain. The proposed iterative procedure converges rapidly to exact analytical solutions for the case of infinite and semi-infinite straight wires, and to the Numerical Electromagnetics Code (NEC) solution for straight and bent wires of infinite length. Moreover, with only one iteration, an excellent approximation to the exact solution can be obtained.

1 Introduction

The use of transmission line (TL) approximation for the calculation of the response of long lines to an external exciting electromagnetic field has permitted to solve a large range of problems related mainly to lightning and electromagnetic pulse (EMP) effects. The accuracy of the TL approximation has been investigated in different papers (e.g. [1–3]). The TL approximation is mainly limited by the condition that the transverse dimensions of the line and its return path (essentially the line height) should be much smaller than the minimum significant wavelength of the exciting electromagnetic field $\lambda_{\min}$. Therefore, for cases when this condition is

not met, one generally resorts to the use of scattering theory. However, a systematic use of the scattering theory for long lines becomes cumbersome due to computer time and storage requirements.

Exact analytical expressions for the calculation of the response of infinite overhead lines excited by an incident electromagnetic field have been developed [1, 3]. Using those expressions, it has been shown [2] that corrections to the TL approximation can be considerable under certain circumstances. However, the method does not give the possibility to take into account boundary conditions at the line ends.

In this chapter, we derive the general field-to-TL coupling equations for an overhead wire of different geometric forms: a straight horizontal line of finite length and an infinite horizontal wire with bend. The coupling equations will be expressed as in the classical telegrapher's equations with some additional source terms representing the correction to the TL approximation.

We also present a simple iterative approach to correct the results obtained using TL approximation both in frequency and in time domains.

2 High-frequency electromagnetic field coupling with a straight wire above a perfectly conducting ground

2.1 Derivation of an electric field integral equation in a TL-like form for a straight thin wire of finite length

Consider a lossless current filament of finite length above a perfectly conducting ground (see Fig. 1). The line is in presence of an external electromagnetic field.

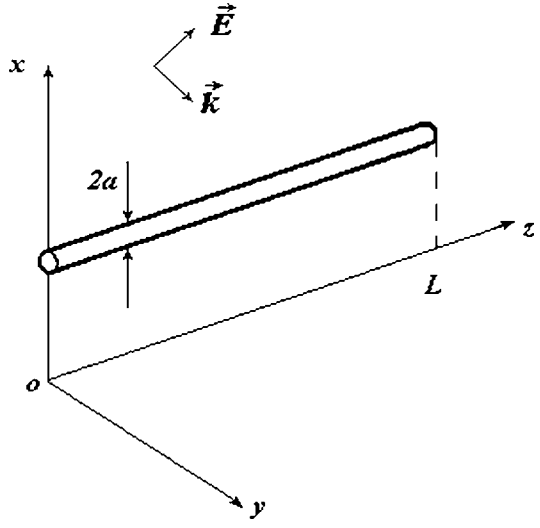

Figure 1: Geometry of the problem.

The boundary conditions on the wire surface imply that the total electric field tangential to the wire should be equal to zero

$$\vec{e}_z \cdot \vec{E}^{\text{tot}} = \vec{e}_z \cdot (\vec{E}^{\text{e}} + \vec{E}^{\text{s}}) = 0 \tag{1}$$

In eqn (1), $\vec{E}^{\text{e}}$ is the exciting electric field obtained by the sum of the incident field $\vec{E}^{\text{i}}$ and the ground reflected field $\vec{E}^{\text{r}}$, both determined in the absence of the wire; $\vec{E}^{\text{s}}$ is the scattered electric field which represents the reaction of the wire to the excitation field.

The following development will be based on the thin-wire approximation, that is, the current and change densities are assumed to be distributed along the wire axis and the condition (1) is satisfied on the surface of the wire. The scattered electric field, produced by the charge and current densities ρ and $\vec{J}$, can be expressed in terms of the retarded scalar and vector potentials:

$$\vec{E}^{\text{s}} = -j\omega\vec{A} - \nabla\Phi \tag{2}$$

with

$$\vec{A}(\vec{r}) = \frac{\mu_0}{4\pi}\int_0^L \vec{e}_z I(z')\, g(\vec{r},\vec{r}')\,\mathrm{d}z' \tag{3a}$$

and

$$\vec{A}(h,z) = \frac{\mu_0 \vec{e}_z}{4\pi}\int_0^L I(z')\, g(z-z')\,\mathrm{d}z' \tag{3b}$$

where z' is the length variable along the wire axis; $\vec{r} = x\vec{e}_x + y\vec{e}_y + z\vec{e}_z$ is measured from the observation point to the origin, $\vec{r}'$ from the source point to the origin, and $I(z')$ and $\rho(z')$ are the current and change density along the wire. $g(\vec{r},\vec{r}')$ is the scalar Green's function defined as

$$g(\vec{r},\vec{r}') = \frac{\mathrm{e}^{-jk|\vec{r}-\vec{r}'|}}{|\vec{r}-\vec{r}'|} - \frac{\mathrm{e}^{-jk|\vec{r}-(\vec{r}'-2x'\vec{e}_x)|}}{|\vec{r}-(\vec{r}'-2x'\vec{e}_x)|} \tag{4}$$

For the considered case of Fig. 1, the Green's function becomes

$$g(\vec{r},\vec{r}') = \frac{\mathrm{e}^{-jk\sqrt{(z-z')^2+(y-y')^2+(x-h)^2}}}{\sqrt{(z-z')^2+(y-y')^2+(x-h)^2}} - \frac{\mathrm{e}^{-jk\sqrt{(z-z')^2+(y-y')^2+(x+h)^2}}}{\sqrt{(z-z')^2+(y-y')^2+(x+h)^2}} \tag{5}$$

where the wave number k is related to the angular frequency ω by $k = \omega/c$.

When the field point is on the wire surface, the expression for the retarded scalar and vector potential read:

$$\vec{A}(h,z) = \frac{\mu_0 \vec{e}_z}{4\pi}\int_0^L I(z')\, g(z-z')\,\mathrm{d}z' \tag{6a}$$

and

$$\Phi(h,z)=\frac{1}{4\pi\varepsilon_0}\int_0^L \rho(z')\,g(z-z')\,\mathrm{d}z' \tag{6b}$$

in which the scalar Green's function (Fig. 2) $g(z)$ is given by

$$g(z)=\frac{\mathrm{e}^{-jk\sqrt{z^2+a^2}}}{\sqrt{z^2+a^2}}-\frac{\mathrm{e}^{-jk\sqrt{z^2+4h^2}}}{\sqrt{z^2+4h^2}} \tag{7}$$

The current and the charge density along the wire are related by the continuity equation:

$$\rho=-\frac{1}{j\omega}\frac{\mathrm{d}I}{\mathrm{d}z} \tag{8}$$

Introducing eqns (2), (6)–(8) into eqn (1), we get

$$E_z^{\mathrm{e}}(h,z)-j\omega\frac{\mu_0}{4\pi}\int_0^L g(z-z')I(z')\,\mathrm{d}z'-\frac{\partial}{\partial z}\Phi(h,z)=0 \tag{9}$$

where

$$\begin{aligned}\Phi(h,z)&=-\frac{1}{j\omega}\frac{1}{4\pi\varepsilon_0}\int_0^L g(z-z')\frac{\partial I(z')}{\partial z'}\mathrm{d}z'\\&=-\frac{1}{j\omega}\frac{1}{4\pi\varepsilon_0}\left[g(z-L)I(L)-g(z-0)I(0)-\int_0^L I(z')\frac{\partial}{\partial z'}g(z-z')\,\mathrm{d}z'\right]\end{aligned} \tag{10}$$

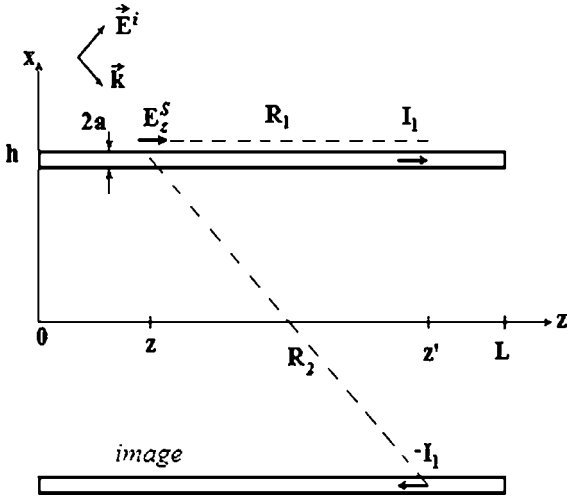

Figure 2: Geometry for the determination of the scalar Green's function.

Since the line is open-circuit at both extremities, we have

$$I(0) = I(L) = 0 \tag{11}$$

Additionally, it can be shown from eqn (7) that

$$\frac{\partial}{\partial z'} g(z - z') = -\frac{\partial}{\partial z} g(z - z') \tag{12}$$

Using eqns (11) and (12), the retarded scalar potential expression (10) becomes

$$\Phi(h, z) = -\frac{1}{j\omega} \frac{1}{4\pi\varepsilon_0} \frac{\partial}{\partial z'} \int_0^L g(z - z') I(z') \, \mathrm{d}z' \tag{13}$$

Let us consider the scattered voltage as defined in the standard TL theory [4]

$$V^{\mathrm{S}}(z) = -\int_0^h E_x^{\mathrm{s}}(x, z) \, \mathrm{d}x \tag{14}$$

Equation (2), written in terms of the x-component, yields

$$E_x^{\mathrm{s}}(x, z) = -\frac{\partial}{\partial x} \Phi(x, z) \tag{15}$$

Using eqn (14), the scattered voltage becomes

$$V^{\mathrm{s}}(z) = \Phi(h, z) - \Phi(0, z) \tag{16}$$

From eqns (6b) and (5), it follows that

$$\Phi(0, z) = 0 \tag{17}$$

which means

$$V^{\mathrm{s}}(z) = \Phi(h, z) \tag{18}$$

Inserting eqn (18) into eqns (9) and (13) yields

$$\frac{\mathrm{d}V^{\mathrm{s}}(z)}{\mathrm{d}z} + j\omega \frac{\mu_0}{4\pi} \int_0^L g(z - z') I(z') \, \mathrm{d}z' = E_z^{\mathrm{e}}(h, z) \tag{19}$$

$$\frac{\mathrm{d}}{\mathrm{d}z} \int_0^L g(z - z') I(z') \, \mathrm{d}z' + j\omega \, 4\pi \, \varepsilon_0 \, V^{\mathrm{s}}(z) = 0 \tag{20}$$

Equations (19) and (20) are the final field-to-transmission line coupling equations. In what follows, we will express these equations in a form similar to the classical TL coupling equations. To do that, let us consider the integral term, in eqns (19) and (20)

$$C(z) = \int_0^L g(z - z') I(z') \, \mathrm{d}z' \tag{21}$$

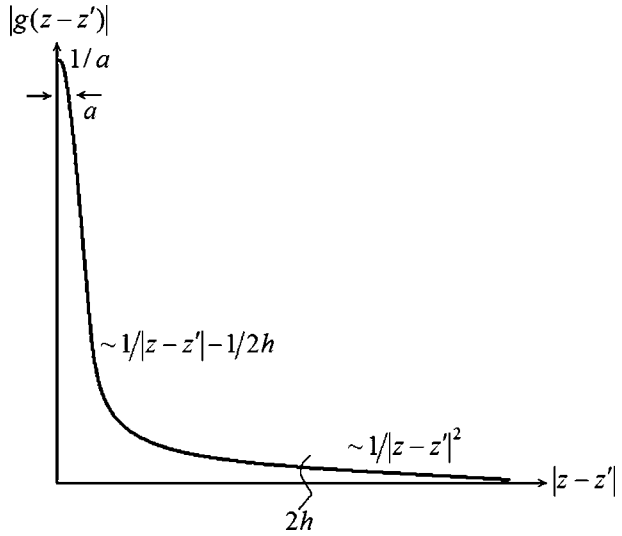

Figure 3: Approximate representation of $|g(z-z')|$.

The approximate wave shape of the scalar Green's function $|g(z - z')|$ is shown in Fig. 3. From this figure, one can deduce that the effective length for the integration along the line is about $2h$.

On the other hand, the effective length of the current variation is obviously equal to its wavelength λ. Now, let the following conditions be satisfied

$$kh << 1 \tag{22a}$$

$$L >> 2h \tag{22b}$$

In this case, eqn (21) can be written as

$$C(z) \approx I(z) \int_0^L \left(\frac{1}{\sqrt{(z-z')^2 + a^2}} - \frac{1}{\sqrt{(z-z')^2 + 4h^2}} \right) \mathrm{d}z' \tag{23}$$

Further, if the observation point z is sufficiently far from the wire ends, that is, if

$$2h << z << L - 2h \tag{24}$$

then the integration limits of eqn (23) can be taken from $-\infty$ to $+\infty$ (since the integrals from $-\infty$ to L and from L to $+\infty$ are negligible) and the integral reduces to

$$C(z) \approx I(z)\, 2\ln(2h/a) \tag{25}$$

Introducing eqn (25) in eqns (19) and (20) results in the well-known TL coupling equations – the generalized telegrapher's equations.

In the general case when the simplifying conditions (22) and (24) are not satisfied, the function $C(z)$ in the exact system of eqns (19) and (20) may be written as the sum of the term (25) and an additional corrective term as follows:

$$\frac{\mathrm{d}V^{\mathrm{s}}(z)}{\mathrm{d}z} + j\omega L_0' I(z') = E_z^{\mathrm{e}}(h,z) + j\omega \frac{\mu}{4\pi} \widehat{D}\{I(z)\} \tag{26}$$

$$\frac{\mathrm{d}I(z)}{\mathrm{d}z} + j\omega C_0' V^{\mathrm{s}}(z) = \frac{1}{2\ln(2h/a)} \frac{\mathrm{d}}{\mathrm{d}z} \widehat{D}\{I(z)\} \tag{27}$$

where the operator $\widehat{D}$ is defined as

$$\widehat{D}\{I(z)\} = 2\ln(2h/a) I(z) - \int_0^L \left[\frac{\mathrm{e}^{-jk\sqrt{(z-z')^2+a^2}}}{\sqrt{(z-z')^2+a^2}} - \frac{\mathrm{e}^{-jk\sqrt{(z-z')^2+4h^2}}}{\sqrt{(z-z')^2+4h^2}} \right] I(z')\,\mathrm{d}z' \tag{28}$$

and L_0' and C_0' are the per-unit-length inductance and capacitance of the horizontal infinite wire above a perfect ground, as defined in the classical TL theory [1]. They are given by

$$L_0' = \frac{\mu_0}{2\pi} \ln(2h/a) \tag{29a}$$

$$C_0' = \frac{2\pi\varepsilon_0}{\ln(2h/a)} \tag{29b}$$

The above pair of eqns (26) and (27) is absolutely equivalent to the general field-to-TL coupling equations (19) and (20) derived earlier. This system of eqns (26) and (27) has a form similar to that of classical field-to-TL coupling equations in the Agrawal *et al.* formulation [4] (see also Chapter 1). However, additional distributed voltage and current source which depend on the unknown current are also present. These terms represent electrodynamics corrections (including radiation) to the TL theory. The use of the system of eqns (26) and (27) is more suitable than (19) and (20) because it can be solved using a simple iteration technique (see Section 2.2). Moreover, the factor $\ln(2h/a)$ in (28) being frequency independent, makes it possible to transform the iterative solution in the time domain.

2.2 Iterative solution of the coupling equations in frequency-domain

A frequency-domain iterative approach based on the perturbation theory has been proposed in [5, 6] and applied to the case of a wire in the free space. In this section, we will present a similar approach to solve the coupling equations (26) and (27) in which the induced currents and voltages along the line are calculated using a series expansion in terms of the parameter $1/2\ln(2h/a)$, which is a small parameter for thin horizontal wires (e.g. for $h = 0.5$ m and $a = 1$ mm, its value is about 0.072).

$$V^{\mathrm{s}}(z) = V_0^{\mathrm{s}}(z) + V_1^{\mathrm{s}}(z) + V_2^{\mathrm{s}}(z) + \cdots \tag{30}$$

$$I(z) = I_0(z) + I_1(z) + I_2(z) + \cdots \tag{31}$$

The initial iterations V_0^s and $I_0(z)$ are determined from the classical TL equations:

$$\frac{\mathrm{d}V_0^s(z)}{\mathrm{d}z} + j\omega L_0' \, I_0(z') = E_z^e(h,z) \tag{32}$$

$$\frac{\mathrm{d}I_0(z)}{\mathrm{d}z} + j\omega C_0' \, V_0^s(z) = 0 \tag{33}$$

The following terms ($n \geq 1$) are solutions of the following system of equations:

$$\frac{\mathrm{d}V_n^s(z)}{\mathrm{d}z} + j\omega L_0' \, I_n(z') = j\omega \frac{\mu}{4\pi} \widehat{D}\{I_{n-1}(z)\} \tag{34}$$

$$\frac{\mathrm{d}I_n(z)}{\mathrm{d}z} + j\omega C_0' \, V_n^s(z) = \frac{1}{2\ln(2h/a)} \frac{\mathrm{d}}{\mathrm{d}z} \widehat{D}\{I_{n-1}(z)\} \tag{35}$$

For each iteration $n \geq 0$, the open-circuit boundary condition is valid

$$I_n(0) = I_n(L) = 0 \tag{36}$$

To obtain a general solution for eqns (34)–(36), we substitute the expression for $V_n^s(z)$ obtained from eqn (35) into eqn (34), and after making some simple mathematical manipulations, we get

$$\frac{\mathrm{d}^2}{\mathrm{d}z^2}\left[-I_n(z) + \frac{1}{2\ln(2h/a)} \widehat{D}\{I_{n-1}(z)\}\right] = \frac{\omega^2}{c^2} I_n(z) - \frac{\omega^2}{c^2} \frac{1}{2\ln(2h/a)} \widehat{D}\{I_{n-1}(z)\} \tag{37}$$

which is equivalent to

$$\left(\frac{\mathrm{d}^2}{\mathrm{d}z^2} + k^2\right)[I_n(z) - F_{n-1}(z)] = 0 \tag{38a}$$

where

$$F_{n-1}(z) = \frac{1}{2\ln(2h/a)} \widehat{D}\{I_{n-1}(z)\} \tag{38b}$$

The general solution of the homogeneous differential equation (38a) is given by

$$I_n(z) = F_{n-1}(z) + C_1 \mathrm{e}^{-jkz} + C_2 \mathrm{e}^{jkz} \tag{39}$$

The constants C_1 and C_2 can be determined provided that all the iteration terms satisfy the boundary conditions (36) at the line extremities. The final solution of eqn (38a) can be therefore obtained as

$$I_n(z) = \frac{F_{n-1}(0)\mathrm{e}^{-2jkL} - F_{n-1}(L)\mathrm{e}^{-jkL}}{1 - \mathrm{e}^{-2jkL}} \mathrm{e}^{jkz} + \frac{F_{n-1}(L)\mathrm{e}^{-jkL} - F_{n-1}(0)}{1 - \mathrm{e}^{-2jkL}} \mathrm{e}^{-jkz} + F_{n-1}(z) \tag{40}$$

where

$$F_n(z) = I_n(z) - \frac{1}{2\ln(2h/a)} \int_0^L \left[\frac{\mathrm{e}^{-jk\sqrt{(z-z')^2+a^2}}}{\sqrt{(z-z')^2+a^2}} - \frac{\mathrm{e}^{-jk\sqrt{(z-z')^2+4h^2}}}{\sqrt{(z-z')^2+4h^2}} \right] I_n(z')\,\mathrm{d}z' \quad (41)$$

The above equation can be rewritten in a more convenient form for numerical integration in which the dependence to the small parameter $1/2\ln(2h/a)$ appears more explicitly

$$F_n(z) = \frac{1}{2\ln(2h/a)} \left\{ I_n(z) \ln \left[\frac{\left(L - z + \sqrt{(L-z)^2+4h^2}\right)\left(z + \sqrt{z^2+4h^2}\right)}{\left(L - z + \sqrt{(L-z)^2+a^2}\right)\left(z + \sqrt{z^2+a^2}\right)} \right] \right.$$
$$\left. + \int_0^L \left[\frac{I_n(z) - I_n(z')\mathrm{e}^{-jk\sqrt{(z-z')^2+a^2}}}{\sqrt{(z-z')^2+a^2}} - \frac{I_n(z) - I_n(z')\mathrm{e}^{-jk\sqrt{(z-z')^2+4h^2}}}{\sqrt{(z-z')^2+4h^2}} \right] \mathrm{d}z' \right\} \quad (42)$$

Equations (40)–(42) permit to calculate the term I_n as a function of the previous term I_{n-1}. As stated before, the zeroth iteration term I_0 is determined from the classical TL theory equations (32), (33) and (36).

2.3 Coupling of a plane wave to an infinite wire: exact and iterative solutions

In this section, we present the first test of the proposed iterative procedure and investigate how the solution converges to the exact solution. The considered case is an infinite horizontal wire above a perfectly conducting ground excited by a plane wave (see Fig. 4). (The solution of this problem is well known, see, e.g. [1, 7]. However, we derive it here for the sake of consistency.) The general system for the finite horizontal line (eqns (19) and (20)) can be written for the case of an infinite line:

$$\frac{\mathrm{d}V^{\mathrm{s}}(z)}{\mathrm{d}z} + j\omega\frac{\mu}{4\pi}\int_{-\infty}^{\infty} g(z-z')I(z')\,\mathrm{d}z' = E_z^{\mathrm{e}}(h,z) \quad (43)$$

$$\frac{\mathrm{d}}{\mathrm{d}z}\int_{-\infty}^{\infty} g(z-z')\ I(z')\,\mathrm{d}z' + j\omega 4\pi\varepsilon_0 V^{\mathrm{s}}(z) = 0 \quad (44)$$

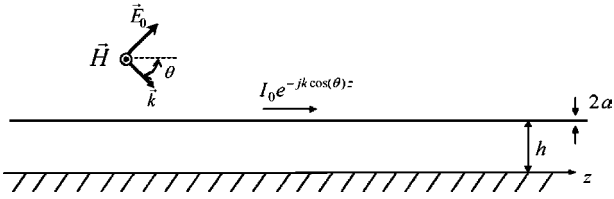

Figure 4: Plane wave coupling with infinite horizontal wire.

The term $E_z^e(z)$ is the tangential exciting (incident + ground-reflected) electric field at the line height. This latter is defined as the sum of the incident electric field $E_z^i(h, z)$ and the ground reflected one $E_z^r(h, z)$, both determined in absence of the wire. For the case of vertically – polarized plane wave $E_z^e(z)$ is given by

$$E_z^e(h,z) = E^i e^{-jkz\cos\theta}(1 - e^{-2jkh\sin\theta})\sin\theta = E_z^e(h, j\omega)e^{-jk_1 z} \tag{45}$$

in which

$$E_z^e(h, j\omega) = E^i(1 - e^{-2jkh\sin\theta})\sin\theta \tag{46}$$

where E^i is the amplitude of the incident electric field, and $k_1 = k\cos\theta$, where θ is the elevation angle of the incident field (the azimuth angle $\Phi = 0$).

Expressing the scattered voltage from eqn (44) and substituting it in eqn (43) yields a Pocklington integral–differential equation for the induced current in the infinite horizontal wire:

$$\left(\frac{d^2}{dz^2} + k^2\right)\int_{-\infty}^{\infty} g(z - z')\ I(z')\,dz' = -j\omega 4\pi\varepsilon_0 E_0^e(h, j\omega)e^{-jk_1 z} \tag{47}$$

Note that the interval of integration in the above integral-differential equation extends from $-\infty$ to $+\infty$. Moreover, the kernel of the equation, the function $g(z - z')$, depends on the difference of arguments. Under these circumstances, it is possible that the solution be in the form

$$I(z) = I_0(j\omega)\exp(-jk_1 z) \tag{48}$$

The integral in eqn (47) can be written as

$$\begin{aligned}\int_{-\infty}^{\infty} g(z - z')\ I(z')\,dz' &= I_0(j\omega)\int_{-\infty}^{\infty} g(z' - z)\exp(-jk_1 z')\,dz' \\ &\underset{\xi = z' - z}{=} I_0(j\omega)\exp(-jk_1 z)\int_{-\infty}^{\infty} g(\xi)\exp(-jk_1\xi)\,d\xi \\ &= I_0(j\omega)\exp(-jk_1 z)G(j\omega)\end{aligned} \tag{49}$$

with

$$G(j\omega) = -j\pi\{H_0^{(2)}(ka\sin\theta) - H_0^{(2)}(2kh\sin\theta)\} \tag{50}$$

where, we have used the following identity [8, 9]:

$$\int_{-\infty}^{\infty} \frac{e^{-jk_1 z - jk\sqrt{z^2 + a^2}}}{\sqrt{z^2 + a^2}} = -j\pi H_0^{(2)}\left(a\sqrt{k^2 - k_1^2}\right), \quad |k_1| < k \tag{51}$$

and $H_0^{(2)}(x) = J_0(x) - jY_0(x)$ denotes the Hankel function of the zeroth order and second kind [10].

After substituting eqns (48) and (49) in eqn (47), we obtain an algebraic equation for the unknown current amplitude $I_0(jw)$ instead of the integral equation:

$$(-k_1^2 + k_2^2) I_0 G(j\omega) \mathrm{e}^{-jk_1 z} = -j\omega 4\pi\varepsilon_0 E_0^{\mathrm{e}}(j\omega) \mathrm{e}^{-jk_1 z} \tag{52}$$

The solution of eqn (52) is the well-known expression for the induced current

$$I_0(j\omega) = \frac{4\omega\varepsilon_0 E_0^{\mathrm{e}}(j\omega)}{(k^2 - k_1^2)(H_0^{(2)}(ka\sin\theta) - H_0^{(2)}(2kh\sin\theta))} \tag{53}$$

Now, let us apply the general iteration formulas (40) and (41) to solve the system of eqns (43) and (44). We assume that the value k in eqn (40) has a small imaginary part (which corresponds, for example, to small ohmic losses) $k \to k - j\delta$. For very long wire $L \to \infty$ and for observation points quite far from the end of the wire $z \sim L - z \sim L$, only the last term of eqn (40) 'survives' and we will have

$$I_n(z) \underset{\substack{L\to\infty \\ k\to k-j\delta}}{\to} F_{n-1}(z) = I_{n-1}(z) - \frac{1}{2\ln(2h/a)} \int_{-\infty}^{\infty} g(z'-z) I_{n-1}(z')\,\mathrm{d}z' \tag{54}$$

Again, the nth current iteration should have a form with the same coordinate dependence as the exciting electric field (eqn (45)), but with unknown amplitude $I_{0,n}(j\omega)$

$$I_n(z) = I_{0,n}(j\omega)\exp(-jk_1 z) \tag{55}$$

The function $F_n(z)$ can be found after integration

$$F_n(z) = \exp(-jk_1 z)\left\{1 - \frac{G(j\omega)}{2\ln(2h/a)}\right\} I_{0,n}(j\omega) \tag{56}$$

Substituting eqn (56) into eqn (54), we can obtain the solution for the current amplitude at any iteration (57)

$$I_{0,n}(j\omega) = \left\{1 - \frac{G(j\omega)}{2\ln(2h/a)}\right\} I_{0,n-1}(j\omega) = \cdots = \left\{1 - \frac{G(j\omega)}{2\ln(2h/a)}\right\}^n I_{0,0}(j\omega) \tag{57}$$

which is function of the zero-order iteration current amplitude $I_{0,0}(j\omega)$, obtained by the solution of the telegrapher's equations (32) and (33) with exciting source (eqn (45))

$$I_{0,0}(j\omega) = -\frac{j\omega C_0' E_0^{\mathrm{e}}(j\omega)}{k^2 - k_1^2} = -j\omega \frac{2\pi\varepsilon_0}{\ln(2h/a)} \frac{E_0^{\mathrm{e}}(j\omega)}{k^2 - k_1^2} \tag{58}$$

The total amplitude of the induced current $I_0(j\omega)$ can be obtained by summation of all iterations (31). As expected, the summation coincides with the exact solution (53):

$$\begin{aligned} I_0(j\omega) &= \sum_{n=0}^{\infty} \left\{1 - \frac{G(j\omega)}{2\ln(2h/a)}\right\}^n I_{0,0}(j\omega) = \frac{I_{0,0}(j\omega)}{G(j\omega)/2\ln(2h/a)} \\ &= \frac{4\omega\varepsilon_0}{H_0^{(2)}(ka\sin\theta) - H_0^{(2)}(2kh\sin\theta)} \frac{E_0^{\mathrm{e}}(j\omega)}{(k^2 - k_1^2)} \end{aligned} \tag{59}$$

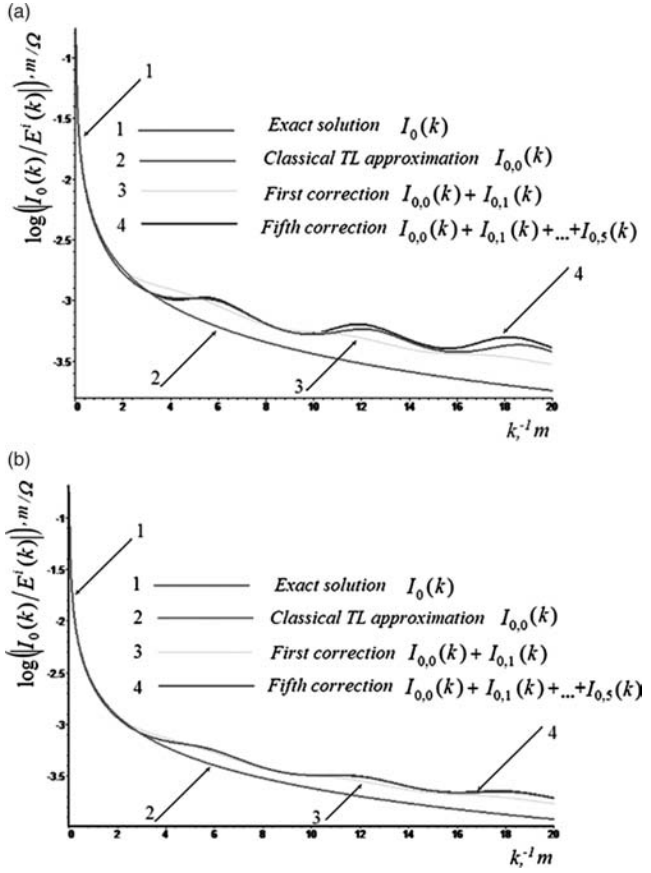

Figure 5: Frequency dependence of the current induced by the normal incident wave in the infinite wire above a perfectly conducting ground (h = 1 m) for the exact solution (curve 1), classical TL approximation (curve 2), and the first (curve 3) and the fifth (curve 4) iterations of the perturbation theory for different radiuses of the wire. (a) Radius of the wire a = 1 cm. (b) Radius of the wire a = 1 mm.

The numerical example – comparison of the exact current amplitude with those of perturbation theory is shown in Fig. 5a and b. One can see from these examples that the perturbation series converges quickly to the exact solution. It is worth observing that even after one iteration, we obtain satisfactory results in comparison with the TL approximation. Note also that the series convergence is faster for thinner wires.

2.4 Correction to the reflection coefficient for a semi-infinite open-circuit line

In this section, we consider a good conducting semi-infinite wire above a perfectly conducting ground, without external exciting electromagnetic field (see Fig. 6).

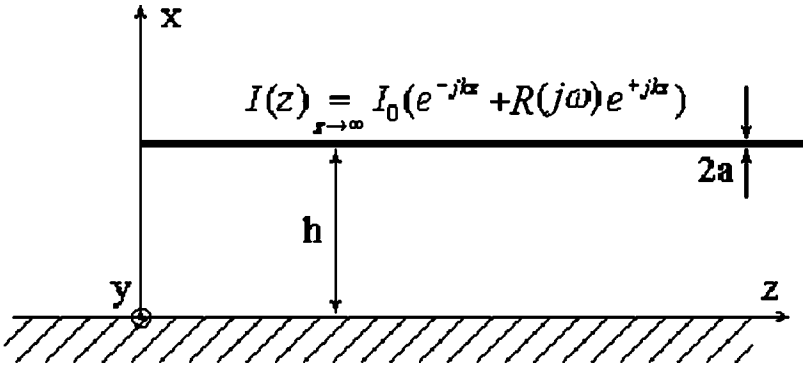

Figure 6: Geometry of the homogeneous current wave scattering problem for a semi-infinite wire.

An incident current wave, $I_0 \exp(jkz)$, travels from ∞ and returns after reflection and scattering at the open-circuit left end of the line.

Sufficiently far from the termination, the current is defined by the solution of the homogeneous system equations (43) and (44) (which is equivalent to the homogeneous Pocklington's equation) for the infinite line [7]. It represents a transverse electromagnetic (TEM) wave and does not radiate ([11], chapter 4). At a distant location from the termination the current is given by

$$I(z) \underset{z\to\infty}{=} \tilde{I}(\mathrm{e}^{jkz} + R(j\omega)\mathrm{e}^{-jkz}) \tag{60}$$

where $\tilde{I}$ is the amplitude of the incident current wave, $R(j\omega)$ is the complex reflection coefficient at the open-circuit end of the line. This coefficient defines the radiation of the scattering current (see end of this section).

The exact solution for the complex amplitude of the reflection coefficient in a system of two parallel wires in free space has been derived by Weinstein, using the Wiener–Hopf technique [8]. This expression reduces in our case to the following form:

$$R(j\omega) = -\exp\left\{\frac{4kh}{\pi}\left[-\int_0^{2kh}\frac{W(x)\,\mathrm{d}x}{x\sqrt{(2kh)^2 - x^2}} - j\int_{2kh}^{\infty}\frac{W(x)\,\mathrm{d}x}{x\sqrt{x^2 - (2kh)^2}}\right]\right\} \tag{61a}$$

and

$$W(x) = \arctan\left[-\frac{J_0(ax/2h) - J_0(x)}{Y_0(ax/2h) - Y_0(x)}\right] \tag{61b}$$

in which $J_0(x)$ and $Y_0(x)$ are the zero-order Bessel function of the first and second kind, respectively [10].

In what follows, we will derive an expression for the reflection coefficient using the iterative approach developed in Section 2.2. The solution for the current $I(z)$

should satisfy the asymptotic condition (60) and the open-circuit boundary condition for $z = 0$ (eqn (36)).

The zero iteration term, determined by the TL approximation, reads

$$I_0(z) = \tilde{I}\,(\mathrm{e}^{jkz} - \mathrm{e}^{-jkz}) = 2j\tilde{I}\sin(kz) \tag{62a}$$

$$R_0(j\omega) = -1 \tag{62b}$$

To find the first iteration term, $I_1(z)$, we will use the general expressions (39)–(41) with $n = 1$ and a semi-infinite integration domain

$$I_1(z) = \frac{1}{2\ln(2h/a)}\hat{D}\{I_0(z)\} + C_1\,\mathrm{e}^{-jkz} + C_2\mathrm{e}^{jkz} \tag{63a}$$

where

$$\hat{D}\left(I_0(z)\right) = 2\ln\left(\frac{2h}{a}\right)I_0(z) - \int_0^{\infty}\left[\frac{\mathrm{e}^{-jk\sqrt{(z-z')^2+a^2}}}{\sqrt{(z-z')^2+a^2}} - \frac{\mathrm{e}^{-jk\sqrt{(z-z')^2+4h^2}}}{\sqrt{(z-z')^2+4h^2}}\right]I_0(z')\,\mathrm{d}z' \tag{63b}$$

Since the asymptotic amplitude of the incident current wave is considered to be specified, it is necessary to set $C_2 = 0$ in eqn (63a). Physically, this means that the scattering and radiation processes near the termination affect only the reflected current wave. Using the open-end boundary condition (36), the final expression for the first iteration term follows:

$$I_1(z) = \frac{1}{2\ln(2h/a)}\hat{D}\{I_0(z)\} - \frac{\mathrm{e}^{-jkz}}{2\ln(2h/a)}\hat{D}\{I_0(z)\}\Big|_{z=0} \tag{64}$$

Having

$$\lim_{z\to\infty}\hat{D}\{I_0(z)\} \to 0 \tag{65}$$

the asymptotic expression for the first iteration is given by

$$\lim_{z\to\infty} I_1(z) \to \tilde{I}\,R_1(j\omega)\mathrm{e}^{-jkz} \tag{66a}$$

where

$$R_1(j\omega) = -\frac{\mathrm{e}^{-jkz}}{2\ln(2h/a)}\hat{D}\{I_0(z)\}\Big|_{z=0} \tag{66b}$$

Finally, the expression for the reflection coefficient $R^1(j\omega)$ (including the zero and first iterative approximations) reads

$$R^{(1)} = R_0 + R_1 \tag{67}$$

Using eqns (62b), (63b) and (66b), we obtain the following expression:

$$R(j\omega) \cong R^{(1)}(j\omega) = -1 + \frac{j}{\ln(2h/a)} \int_0^{\infty} \sin(\xi) \left[\frac{e^{-j\xi}}{\xi} - \frac{e^{-j\sqrt{\xi^2+(2kh)^2}}}{\sqrt{\xi^2+(2kh)^2}} \right] d\xi \qquad (68)$$

After straightforward mathematical manipulations (carrying out a change of variable $\zeta = \sqrt{\xi^2+(2kh)^2}$ in the second term into the brackets), it is possible to obtain

$$R^{(1)}(j\omega) = -1 + \frac{j}{\ln(2h/a)} \int_0^{\infty} \frac{1-e^{-jx}}{x} dx = -1 + j\frac{Si(2kh)}{\ln(2h/a)} + \frac{C + \ln(2kh) - Ci(2kh)}{\ln(2h/a)} \qquad (69)$$

where $Si(x)$ and $Ci(x)$ are sine and cosine integral functions, $C = 0.577\ldots$ is the Euler's constant [10].

For thin wires, when $1/2\ln(2h/a) << 1$, the perturbation theory (only after the first iteration) yields a good agreement with exact results, when the wavelength λ is less than, or about several h, i.e. when the diffraction effects predominant (see numerical example in Fig. 7). Analytically, the approximate equation (69) can be directly obtained from the exact result (eqn (61)): assuming $a << h$, using small

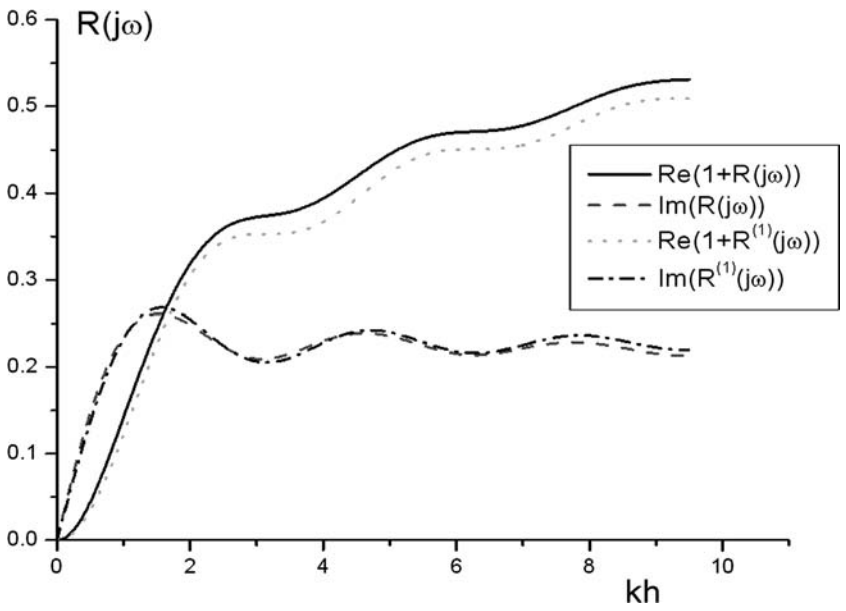

Figure 7: Reflection coefficient of a semi-infinite wire above a perfectly conducting ground. Comparison between the proposed approach after only one iteration and the exact solution ($a/2h = 0.001$).

argument asymptotic approximations for the function $J_0(x)$ and $Y_0(x)$, and calculating after that the lowest term in the expansion (61b) in terms of $1/2\ln(2h/a)$.

Let us establish now a connection between reflection coefficient and radiation. As mentioned earlier, the current for $z \to \infty$ has a form given by eqn (60), indicating that the electromagnetic field has a TEM structure and does not radiate [11]. Near the end, however, the field of the current wave deviates from the TEM structure, and the wave can radiate. The amount of the radiation power can be expressed in terms of the reflection coefficient as it will be shown in what follows.

The average power of TEM mode, propagating along the ideal TL can be written as

$$P(\omega) = \frac{1}{2}\mathrm{Re}(V^{s*}(z)I(z)) \tag{70}$$

where $V^s(z)$ is the scattered voltage of the line. Using the asymptotic expression (60) for the current at distant locations from the line end, and calculating the scalar potential and scattered voltage of the infinite wire by usual way (see [7]; [11], chapter 4), it is possible to obtain the following equation for the time-averaged power propagating along the line at far distances from the termination:

$$P(\omega) = -\frac{|\tilde{I}|^2 Z_c}{2}\ (1-|R(j\omega)|^2) \tag{71a}$$

$$Z_c = \frac{\eta_0}{2\pi}\ln\left(\frac{2h}{a}\right) \tag{71b}$$

As far as we neglect the ohmic losses in the wire, the power has to convert itself into radiation $P_{\mathrm{Rad}}(\omega) = -P(\omega)$. Therefore, eqn (71) expresses the radiation losses. The radiation, of course, is absent in the TL approximation (62). It is convenient to introduce a 'lumped radiation resistance', which is responsible for the radiation losses

$$R_{\mathrm{Rad}}(\omega) = P_{\mathrm{Rad}}(\omega)/|\tilde{I}|^2 = Z_c(1-|R(j\omega)|^2) \tag{72}$$

In Fig. 8, we have plotted the radiation resistance computed by eqn (72) calculated using exact equations for the reflection coefficients (61) and the approximate formula (69). It can be seen that the proposed approximation yields results which are in a very good agreement with the exact solution.

2.5 Iterative solution of the coupling equations for a finite-length straight line in time-domain

In this section, we apply the developed method to calculate the electrodynamical correction to the induced current in a straight wire of finite length, directly in time domain. The series expansion parameter in the corresponding coupling equations (40) and (41) in frequency domain being frequency independent makes is

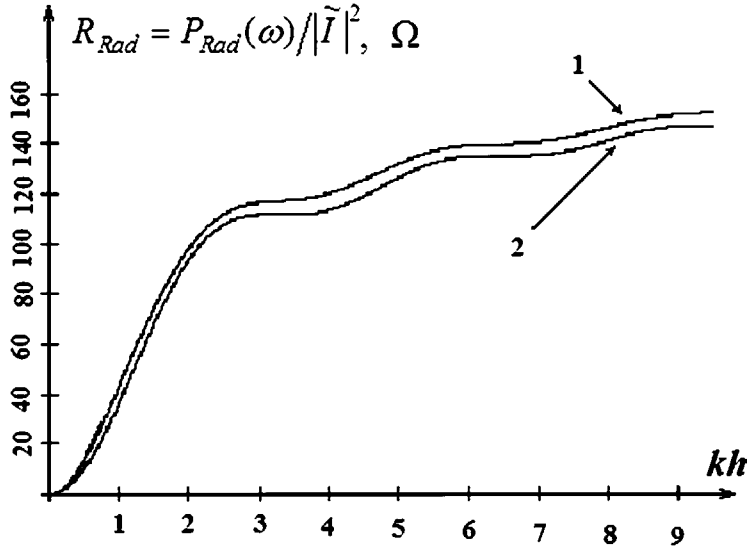

Figure 8: Radiation resistance for the semi-infinite open-circuit line: 1 – exact theory; 2 – the first iteration for the perturbation theory.

possible to convert the iterative equation (40) in time domain. To do that, let us write eqn (40) in the following form:

$$\begin{aligned} I_n(z) &= F_{n-1}(z) + \Big[F_{n-1}(0)(\mathrm{e}^{-jk(2L-z)} - \mathrm{e}^{-jkz}) \\ &\quad + F_{n-1}(L)(-\mathrm{e}^{jk(z-L)} + \mathrm{e}^{-jk(L+z)}) \Big] \sum_{m=0}^{\infty} \mathrm{e}^{-2jmkL} \\ &= F_{n-1}(z) + F_{n-1}(0) \left[\sum_{m=0}^{\infty} \mathrm{e}^{-jk[2(m+1)L-z]} - \sum_{m=0}^{\infty} \mathrm{e}^{-jk(2mL+z)} \right] \\ &\quad + F_{n-1}(L) \left[\sum_{m=0}^{\infty} \mathrm{e}^{-jk[2(m+1)L+z]} - \sum_{m=0}^{\infty} \mathrm{e}^{-jk[2(m+1)L-z]} \right] \end{aligned} \tag{73}$$

Introducing the expression for $F_{n-1}(z)$, eqn (38b) and rearranging, we get

$$\begin{aligned} I_n(z) = \frac{1}{2\ln(2h/a)} \Bigg[& \hat{D}\{I_{(n-1)}(z)\} - \hat{D}\{I_{(n-1)}(z)\}\big|_{z=L} \\ & \sum_{m=0}^{\infty} (\mathrm{e}^{-jk[(2m+1)L-z]} - \mathrm{e}^{-jk[(2m+1)L+z]}) \\ & - \hat{D}\{I_{(n-1)}(z)\}\Big|_{z=0} \sum_{m=0}^{\infty} (\mathrm{e}^{-jk(2mL+z)} - \mathrm{e}^{-jk[(2m+1)L-z]}) \Bigg] \end{aligned} \tag{74}$$

It is now straightforward to convert eqn (74) in time domain

$$i_n(z,t) = \frac{1}{2\ln(2h/a)}\left[\hat{D}\left\{i_{(n-1)}(z,t)\right\}_{z,t} - \sum_{m=0}^{\infty}\left(\hat{D}\left\{i_{(n-1)}(z,t)\right\}_{z=L,t=t-\frac{(2m+1)L-z}{c}}\right.\right.$$
$$- \hat{D}\left\{i_{(n-1)}(z,t)\right\}_{z=L,t=t-\frac{(2m+1)L+z}{c}} + \hat{D}\left\{i_{(n-1)}(z,t)\right\}_{z=0,t=t-\frac{2mL+z}{c}}$$
$$\left.\left. - \hat{D}\left\{i_{(n-1)}(z,t)\right\}_{z=0,t=t-\frac{(2m+1)L-z}{c}}\right)\right] \tag{75}$$

where the time-domain integral operator $\hat{D}\{i_n(z,t)\}$ is given by the inverse Fourier transform of eqn (28)

$$\hat{D}\{i_n(z,t)\} = 2\ln(2h/a)\, i_n(z,t)$$
$$- \int_0^L \left[\frac{i_n\left(z', t-\sqrt{(z-z')^2+a^2}\,/c\right)}{\sqrt{(z-z')^2+a^2}} - \frac{i_n\left(z', t-\sqrt{(z-z')^2+4h^2}\,/c\right)}{\sqrt{(z-z')^2+4h^2}}\right] \mathrm{d}z' \tag{76}$$

After some mathematical manipulations, eqn (76) can be written in the following form more suitable for a numerical integration:

$$\hat{D}\{i_n(z,t)\} = i_n(z,t)\ln\left[\frac{\left(L-z+\sqrt{(L-z)^2+4h^2}\right)\left(z+\sqrt{z^2+4h^2}\right)}{\left(L-z+\sqrt{(L-z)^2+4a^2}\right)\left(z+\sqrt{z^2+a^2}\right)}\right]$$
$$+ \int_0^L \left\{\frac{i_n(z,t) - i_n\left(z', t-\sqrt{(z-z')^2+a^2}\,/c\right)}{\sqrt{(z-z')^2+a^2}}\right. \tag{77}$$
$$\left. - \frac{i_n(z,t) - i_n\left(z', t-\sqrt{(z-z')^2+4h^2}\,/c\right)}{\sqrt{(z-z')^2+4h^2}}\right\} \mathrm{d}z'$$

It is important to note that the summation in eqn (75) has a finite number of terms since

$$\hat{D}\{i_{(n-1)}(z,t)\}\big|_{z,t} = 0 \quad \text{for } t \le 0 \tag{78}$$

Similar to the frequency-domain solutions, the zeroth iteration term is determined by using the TL approximation; the following terms $i_n(z,t)$ can be calculated as a function of the previous term $i_{n-1}(z,t)$ using relations (75) and (77), which involve only one integration along the line length.

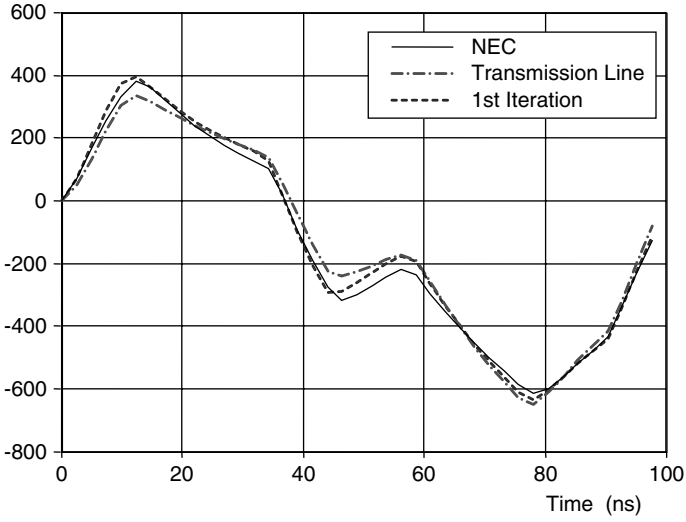

Figure 9: Comparison of the proposed iterative method with the solution obtained using NEC, for a 20 m long, 5 m high overhead wire above a perfectly conducting ground. The current is calculated for the coordinate $z = 17$ m.

The above procedure is compared with results obtained using the Numerical Electromagnetics Code (NEC) [12] for a line of finite length, considering a 20 m long, 5 m high wire above a perfectly conducting ground illuminated by an incident plane wave with an azimuth angle $\Phi = 0°$ and an elevation angle $\theta = 90°$. The incident electric field, parallel to the wire, is defined as

$$E^{\mathrm{i}}(t) = E_0(\mathrm{e}^{-a_1 t} - \mathrm{e}^{-a_2 t})\eta(t) \quad \text{with } E_0 = 65 \text{ kV/m}, a_1 = 4\times10^7 \text{ s}^{-1}, a_2 = 6\times10^8 \text{ s}^{-1} \tag{79}$$

In Fig. 9, we present the 'exact solution' obtained using NEC superimposed with the TL approximation (zero order) and the first-order solution for the induced current at $z = 17$ m. It can be observed that a noticeable improvement of the results it achieved after only one iteration. In particular, the computed peak current after the first iteration is practically identical to the NEC results, whereas the TL approximation leads to an error of more 20%.

2.6 Discussion of the convergence of the procedure for a finite line

In this section, we discuss the convergence of the developed method for the case of a finite horizontal open-circuited line, excited by a plane wave equations (45) and (46). The zero-order iteration for the induced current can be easily found by

the solution of the telegrapher's equations (32) and (33) with the boundary conditions (36):

$$I_0(j\omega,z) = I_{0,0}(j\omega)\left[\frac{e^{-j(k_i+k)L}-1}{1-e^{-2jkL}}e^{-jkz} + \frac{e^{-2jkL}-e^{-j(k_i+k)L}}{1-e^{-2jkL}}e^{jkz} + e^{-jk_iz}\right] \quad (80)$$

where $I_{0,0}(j\omega)$ is the amplitude of the current induced by the incident plane wave in the infinite horizontal wire given by eqn (58). The general solution for the current of nth iteration, $n \geq 1$, $I_n(j\omega, z)$, is given by eqns (40) and (41) already presented in Section 1.

A careful examination of the iteration series and analysis of the results allow us in making the following observations. For some frequencies, a fast convergence of the iteration procedure is observed (see e.g. results of Fig. 10). However, for values close to the resonant frequencies of the wire ($\omega_n = \pi cn/L$, $n = 1, 2, 3, \ldots$), the iterations series diverges (see Fig. 11). This phenomenon can be explained by looking closely at eqns (40) and (42). The term in the perturbation series which appears after manipulations of the first two terms in the square brackets in the zero-iteration current expression (80) contains as expansion parameter not $1/2\ln(2h/a)$, but $1/[(1-\exp(-2jkL))2\ln(2h/a)]$. It is obvious that when this parameter is about, or larger than one, the iteration series diverges.

It is, however, possible to cope with this problem. In the denominators of eqns (80) and (40), the exponent is actually multiplied by the square of the current reflection coefficient at the line terminals

$$\frac{1}{1-\exp(-2jkL)} \rightarrow \frac{1}{1-R^2\exp(-2jkL)} \quad (81)$$

In the TL approximation, this reflection coefficient is $R = -1$, resulting in eqns (40) and (80). Instead of $R = -1$, we can use the exact reflection coefficient for the semi-infinite line (eqn (61)), or the reflection coefficient with electrodynamical corrections (69), improving the convergence of the iteration series. However, near the terminal, this solution does not satisfy the boundary conditions. A consistent theory for the case of a finite-length, terminated line excited by an external plane wave is presented in Chapter 5.

Now, let us discuss the convergence of the iteration procedure in the time domain. In Fig. 12a–c, we present the zeroth, first and second iteration terms $i_0(t)$, $i_1(t)$ and $i_2(t)$ corresponding to the case of Fig. 9. As it can be seen from this figure, the current envelope for the nth iteration increases as t^n. (It can indeed be shown that the nth iteration term in the frequency domain has a term $\sim(1 - \exp(-2jkL))^{-(n+1)}$ ($n + 1$ – order pole), the inverse Fourier transform of which brings a factor t^n.) However, the accuracy of the iterative procedure can be verified by the usual perturbation theory, which requires that the present iteration must be much smaller than the previous one. Numerical calculations show that this requirement is satisfied

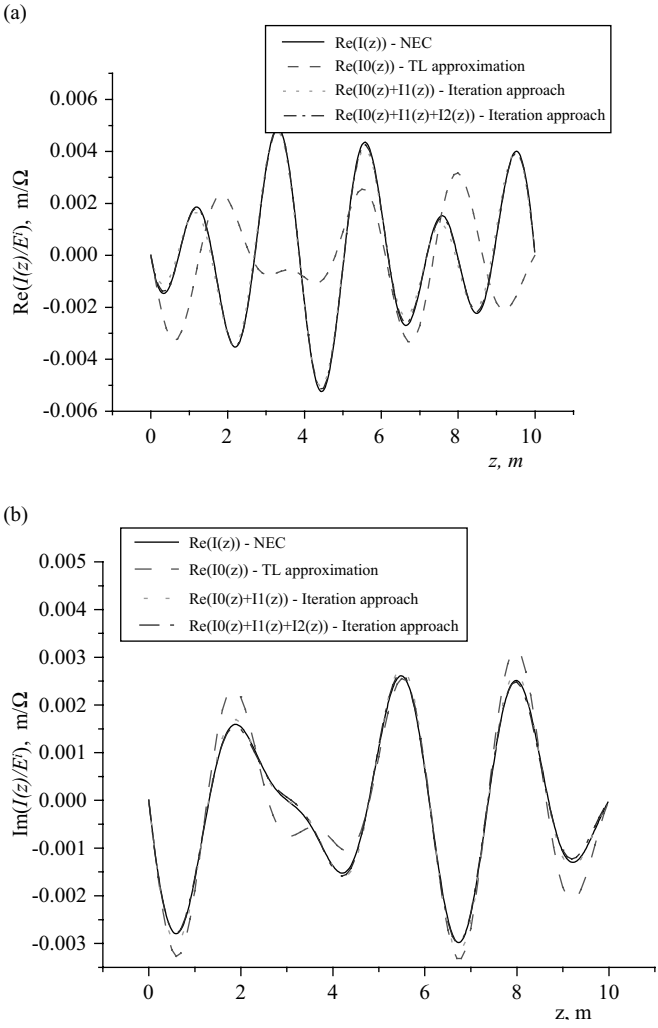

Figure 10: Convergence of the iteration series to the 'exact' NEC solutions. L = 10 m, h = 0.5 m, $a = 1 \times 10^{-3}$ m, $\theta = 45°$, $k = 3$ m^{-1}.

for the first and second terms for several early time periods, when the maximum stress occurs. In Fig. 12d, we have presented again the zeroth iteration term $i_0(t)$ (TL approximation) superimposed with the sum $i_0(t) + i_1(t) + i_2(t)$ which can be considered as the corrected solution. It can be seen that while the envelope of the TL solution $i_0(t)$ is constant due to the absence of any losses, the envelope of the corrected induced current $i_0(t) + i_1(t) + i_2(t)$ show a decrease as a function of time. This decrease corresponds to the line radiation.

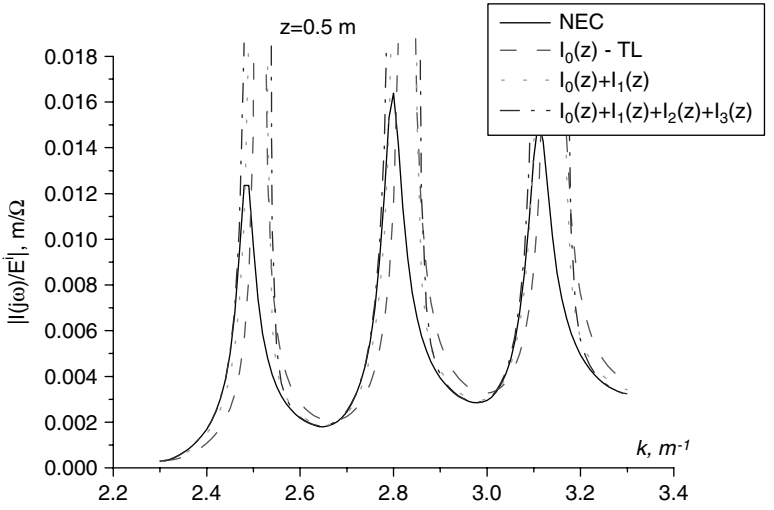

Figure 11: Frequency dependence of the 'exact' NEC solution and iterative solutions for the observation point $z = 0.5$ m. $L = 10$ m, $h = 0.5$ m, $a = 1 \times 10^{-3}$ m, $\theta = 45°$.

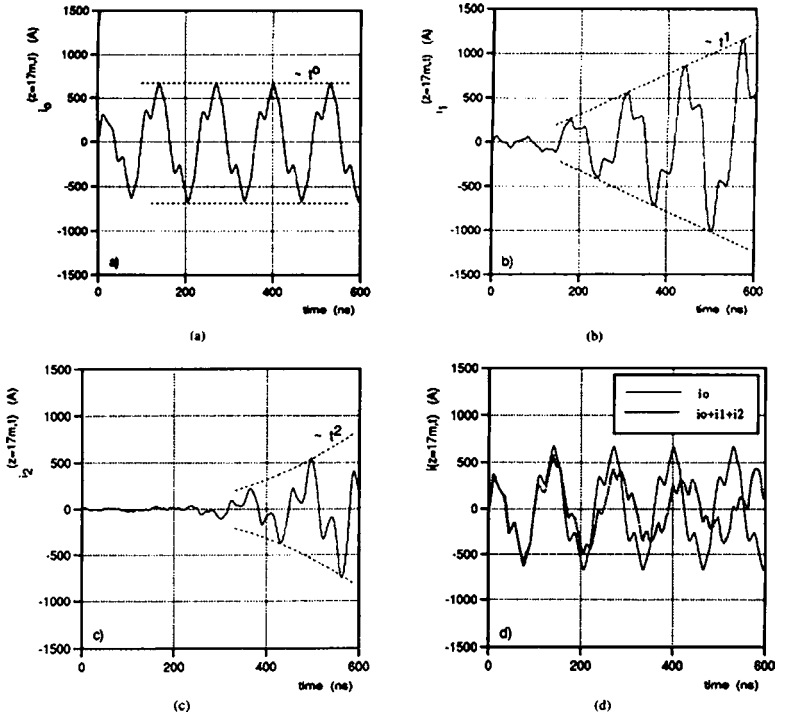

Figure 12: Zero (TL), first and second iteration terms for the case presented in Fig. 9.

3 Propagation of high-frequency current waves through a line bend

3.1 Statement of the problem

The current along a uniform TL (horizontal infinite straight wire parallel to a perfectly conducting ground) can be represented as a sum of a forward propagating wave exp(–*jkl*) and a backward propagating wave exp(*jkl*). Further, no radiation is associated with such a line [7, 11].

Radiation effects appear when the uniformity of the line is disturbed [13]. In particular, for lines of finite length, the line uniformity is disturbed near the terminals of the line. Non-uniformities also arise in presence of 'bends' in the line (see Fig. 13). This is an important problem in electromagnetic compatibility and has been the subject of many recent publications [14–18]. In this case, radiation occurs in the 'near-bend' region. Quantitatively, the current distribution along the non-uniform line, sufficiently far from the near-bend region, can be described in terms of complex asymptotical reflection and transmission coefficients R and D, associated with the bend

$$I(l) \cong \tilde{I} \begin{cases} \mathrm{e}^{-jkl} + R\,\mathrm{e}^{jkl}, & l \le -2h \\ D\,\mathrm{e}^{-jkl}, & l \le 2h \end{cases} \tag{82}$$

The total radiation of the bend can be also expressed in terms of coefficients R and D [15]. Usually, these coefficients are determined using numerical algorithms such as the method of moments (e.g. [14, 15]).

In this section, we derive analytical expressions for the reflection and transmission coefficients associated with the bend. To do this, we generalize the iteration approach developed earlier (see [19] and Section 2) to deal with a non-straight wire. First, electric field integral equations for current and voltages in the line are derived under the thin wire assumption. Again, these equations can be written in a

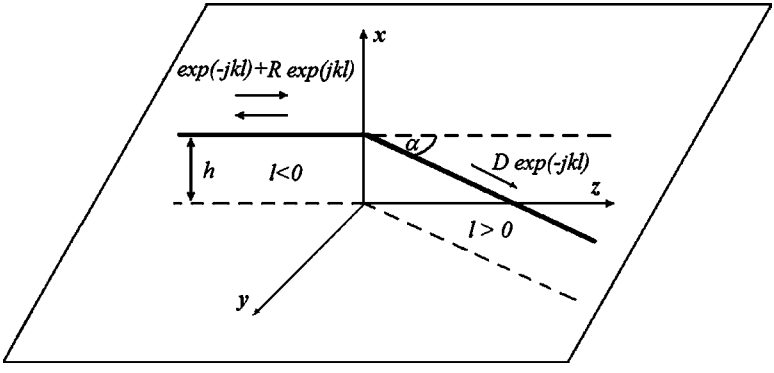

Figure 13: Configuration of the problem and the coordinate system.

TL-like form but with additional voltage and current source terms representing the electrodynamics corrections to the TL approximation. These additional source terms disappear at low frequencies $kh \to 0$. The solution of these equations by the iterative approach yields the reflection and transmission coefficients. The derived analytical expressions are compared with numerical results published in the literature. The developed analytical expressions can also be used to evaluate the radiated power associated with line bend.

3.2 Characterization of the line bend: derivation of the electric field integral equations

Consider a lossless current filament of infinite length above a perfectly conducting ground. The TL has a bend characterized by an angle α in the origin of coordinates.

We assume that the line is in presence of an external electromagnetic field.

The boundary condition on the surface of the non-rectilinear wire $\{l\}$ implies that the total tangential electric field should be equal to zero on the surface of the wire

$$(\vec{E}^{\mathrm{e}} + \vec{E}^{\mathrm{s}})\vec{e}_l\big|_{\{l\}} = 0 \tag{83}$$

In eqn (83), $\vec{E}^{\mathrm{e}}$ is the exciting electric field obtained by the sum of the incident electric field $\vec{E}^{\mathrm{i}}$ and the ground-reflected field $\vec{E}^{\mathrm{r}}$, both determined in absence of the wire; $\vec{E}^{\mathrm{s}}$ is the scattered field, which represent the reaction of the wire to the excitation field. The vector $\vec{e}_l$ in eqn (83) is a unit vector tangent to the curve $\{l\}$ along the wire axis. For the geometry of Fig. 13, the unit vector $\vec{e}_l$ is

$$\vec{e}_l(l) = \begin{cases} \vec{e}_z, & l < 0 \\ \vec{e}_y \sin\alpha + \vec{e}_z \cos\alpha, & l \geq 0 \end{cases} \tag{84}$$

where l is the current length along the wire and α is the angle of the bend (see Fig. 13). Again, we use the thin-wire approximation in which it is assumed that the current and charge densities are distributed along the wire axis and the condition (83) satisfies in the surface of the wire [7].

As for the case of a straight wire, the scattered electric field, produced by the charge and current densities ρ and $\vec{J}$, can be expressed in terms of scalar and vector retarded potentials (2). In the considered present case, to obtain the potentials integration has to be performed along a non-straight wire

$$\vec{A}(\vec{r}) = \frac{\mu_0}{4\pi} \int_{\{l\}} I(l')\vec{e}_l(l')\, g(\vec{r},\vec{r}'(l'))\, \mathrm{d}l' \tag{85a}$$

$$\Phi(\vec{r}) = \frac{1}{4\pi\varepsilon_0} \int_{\{l\}} I(l')\rho(l')\, g(\vec{r},\vec{r}'(l'))\, \mathrm{d}l' \tag{85b}$$

where l' is the natural coordinate along the wire (current length of the curve $\{l\}$), $\vec{r} = x\vec{e}_x + y\vec{e}_y + z\vec{e}_z$ is measured from the origin to the observation point, $\vec{r}'(l')$

from the point l' on the curve $\{l\}$ to the origin, $I(l')$ and $\rho(l')$ are the current and change density along the wire, and $g(\vec{r},\vec{r}')$ is the scalar Green's function (5) for the semi-infinite space bordered by the perfectly conducting plane.

For the considered case of Fig. 13, the coordinates of the axis of the wire is defined as

$$\vec{r}(l)=\begin{cases}(h,0,l), & l<0\\ (h,l\sin\alpha,l\cos\alpha), & l\geq 0\end{cases} \tag{86}$$

and the equations for the scalar and vector potentials can be written as

$$\begin{aligned}\Phi(\vec{r})=&\frac{1}{4\pi\varepsilon_0}\int_{-\infty}^{0}\mathrm{d}l'\rho(l')\left[\frac{\mathrm{e}^{-jk\sqrt{(x-h)^2+y^2+(z-l')^2}}}{\sqrt{(x-h)^2+y^2+(z-l')^2}}-\frac{\mathrm{e}^{-jk\sqrt{(x+h)^2+y^2+(z-l')^2}}}{\sqrt{(x+h)^2+y^2+(z-l')^2}}\right]\\&+\frac{1}{4\pi\varepsilon_0}\int_{0}^{\infty}\mathrm{d}l'\rho(l')\left[\frac{\mathrm{e}^{-jk\sqrt{(x-h)^2+(y-l'\sin\alpha)^2+(z-l'\cos\alpha)^2}}}{\sqrt{(x-h)^2+(y-l'\sin\alpha)^2+(z-l'\cos\alpha)^2}}\right.\\&\left.-\frac{\mathrm{e}^{-jk\sqrt{(x+h)^2+(y-l'\sin\alpha)^2+(z-l'\cos\alpha)^2}}}{\sqrt{(x+h)^2+(y-l'\sin\alpha)^2+(z-l'\cos\alpha)^2}}\right]\end{aligned} \tag{87}$$

$$\begin{aligned}\vec{A}(\vec{r})=&\frac{\mu_0}{4\pi}\int_{-\infty}^{0}\mathrm{d}l'I(l')\vec{e}_z\left[\frac{\mathrm{e}^{-jk\sqrt{(x-h)^2+y^2+(z-l')^2}}}{\sqrt{(x-h)^2+y^2+(z-l')^2}}-\frac{\mathrm{e}^{-jk\sqrt{(x+h)^2+y^2+(z-l')^2}}}{\sqrt{(x+h)^2+y^2+(z-l')^2}}\right]\\&+\frac{\mu_0}{4\pi}\int_{0}^{\infty}\mathrm{d}l'I(l')(\vec{e}_y\sin\alpha+\vec{e}_z\cos\alpha)\left[\frac{\mathrm{e}^{-jk\sqrt{(x-h)^2+(y-l'\sin\alpha)^2+(z-l'\cos\alpha)^2}}}{\sqrt{(x-h)^2+(y-l'\sin\alpha)^2+(z-l'\cos\alpha)^2}}\right.\\&\left.-\frac{\mathrm{e}^{-jk\sqrt{(x+h)^2+(y-l'\sin\alpha)^2+(z-l'\cos\alpha)^2}}}{\sqrt{(x+h)^2+(y-l'\sin\alpha)^2+(z-l'\cos\alpha)^2}}\right]\end{aligned} \tag{88}$$

After calculating the retarded scalar and vector potential, when the field point is on the wire's surface ($\vec{r}=\vec{r}(l)+a\vec{e}_x$) and making use of eqn (2), it is straightforward to obtain the following set of equations for the induced current and charge density.

For $l<0$

$$\begin{aligned}&\frac{\partial\Phi(l)}{\partial l}+j\omega\frac{\mu_0}{4\pi}\left[\int_{-\infty}^{0}g(l'-l)I(l')\,\mathrm{d}l'\right.\\&\left.+\cos\alpha\int_{0}^{\infty}g\left(\sqrt{l'^2+l^2-2l'l\cos\alpha}\right)I(l')\,\mathrm{d}l'\right]=E_l^{\mathrm{e}}(l)\end{aligned} \tag{89a}$$

$$\Phi(l)=\frac{1}{4\pi\varepsilon_0}\left[\int_{-\infty}^{0} g(l'-l)\rho(l')\,\mathrm{d}l'+\int_{0}^{\infty} g\left(\sqrt{l'^2+l^2-2l'l\cos\alpha}\right)\rho(l')\,\mathrm{d}l'\right] \tag{89b}$$

For $l>0$

$$\frac{\partial\Phi(l)}{\partial l}+j\omega\frac{\mu_0}{4\pi}\left[\cos\alpha\int_{-\infty}^{0} g\left(\sqrt{l'^2+l^2-2l'l\cos\alpha}\right)I(l')\,\mathrm{d}l'+\int_{0}^{\infty} g(l'-l)I(l')\,\mathrm{d}l'\right]=E_l^{\mathrm{e}}(l) \tag{90a}$$

$$\Phi(l)=\frac{1}{4\pi\varepsilon_0}\left[\int_{-\infty}^{0} g\left(\sqrt{l'^2+l^2-2l'l\cos\alpha}\right)\rho(l')\,\mathrm{d}l'+\int_{0}^{\infty} g(l'-l)\rho(l')\,\mathrm{d}l'\right] \tag{90b}$$

The scalar Green's function on the wire $g(z)$ is given by eqn (7).

After substituting the expression for the scalar potential equations (90b) and (89b) into eqns (90a) and (89a), and using the continuity equation for the current and charge density along the wire

$$\rho(l)=-\frac{1}{j\omega}\frac{\mathrm{d}I(l)}{\mathrm{d}l} \tag{91}$$

we obtain the following equations describing induced current along the non-uniform line.

For $l<0$

$$\left(\frac{\mathrm{d}^2}{\mathrm{d}l^2}+k^2\right)\int_{-\infty}^{0} g\left(l'-l\right)I(l')\,\mathrm{d}l'+\int_{0}^{\infty}\left(k^2\cos\alpha-\frac{\partial^2}{\partial l\partial l'}\right)\times g\left(\sqrt{l'^2+l^2-2l'l\cos\alpha}\right)I(l')\,\mathrm{d}l'=-4\pi\varepsilon_0 j\omega E_l^{\mathrm{e}}(l) \tag{92}$$

For $l>0$

$$\int_{-\infty}^{0}\left(k^2\cos\alpha-\frac{\partial^2}{\partial l\partial l'}\right)g\left(\sqrt{l'^2+l^2-2l'l\cos\alpha}\right)I(l')\,\mathrm{d}l'+\left(\frac{\mathrm{d}^2}{\mathrm{d}l^2}+k^2\right)\int_{-\infty}^{0} g(l'-l)I(l')\,\mathrm{d}l'=-4\pi\varepsilon_0 j\omega E_l^{\mathrm{e}}(l) \tag{93}$$

Consider now the equations for low-frequencies, where $2kh \ll 1$, and for the points along the line sufficiently distant from the bend, i.e. when $|l| \gg 2h$. Under these conditions, it can be shown that the second term in eqn (92) and the first

term in eqn (93) become negligible [13]. On the other hand, analyzing the function $g(l' - l)$ (see Section 2.1 and [19]), it can be shown that for $l < 0$

$$\int_{-\infty}^{0} g(l'-l)I(l')\,\mathrm{d}l' \approx \int_{-\infty}^{\infty} g(l'-l)I(l')\,\mathrm{d}l' \approx 2\ln(2h/a)\,I(l) \tag{94}$$

Also the same result is obtained for $l > 0$.

Therefore, in the low-frequency approximation, the set of eqns (92) and (93) can be put in the form of a second-order differential equation

$$\left(\frac{\mathrm{d}^2}{\mathrm{d}l^2} + k^2\right) I(l) = -j\omega \frac{2\pi\varepsilon_0}{\ln(2h/a)} E_l^{\mathrm{e}}(l) \tag{95}$$

Equation (95) is the usual form of the coupling equation for the induced current in the TL approximation [7] for which analytical solution may be obtained using well-known mathematical methods.

It is possible to show that the exact coupling equations (92) and (93) for an infinite line with a bend can be written in the TL-like form (eqn (95)) but with an additional integral term $\widehat{D}_{\mathrm{b}}\{I(l)\}$ representing the correction to the TL approximation and taking into account radiation effects. (The derivation is in analogy with the derivation of the coupling equations for the finite wire above a perfectly conducting ground in Section 2.1.) This equation reads

$$\left(\frac{\mathrm{d}^2}{\mathrm{d}l^2} + k^2\right) I(l) = -j\omega \frac{2\pi\varepsilon_0}{\ln(2h/a)} E_l^{\mathrm{e}}(l) + \widehat{D}_{\mathrm{b}}\{I(l)\} \tag{96}$$

in which

$$\widehat{D}_{\mathrm{b}}\{I(l)\} = (\mathrm{d}^2/\mathrm{d}l^2 + k^2)F_{\mathrm{b1}}(l) + F_{\mathrm{b2}}(l) \tag{97}$$

and the functions $F_{\mathrm{b1}}(l)$ and $F_{\mathrm{b2}}(l)$ are given by

$$F_{\mathrm{b1}}(\{I(l)\}) = \frac{1}{2\ln(2h/a)}\left[2\ln(2h/a)\,I(l) - \int_{-\infty}^{0} g(l'-l)I(l')\,\mathrm{d}l'\right] \tag{98}$$

$$F_{\mathrm{b2}}(\{I(l)\}) = \frac{1}{2\ln(2h/a)} \int_{0}^{\infty} \left(k^2\cos\alpha - \frac{\partial^2}{\partial l \partial l'}\right) g\left(\sqrt{l'^2 + l^2 - 2l'l\cos\alpha}\right) I(l')\,\mathrm{d}l' \tag{99}$$

for $l < 0$, and

$$F_{\mathrm{b1}}(\{I(l)\}) = \frac{1}{2\ln(2h/a)}\left[2\ln(2h/a)\,I(l) - \int_{0}^{\infty} g(l'-l)I(l')\,\mathrm{d}l'\right] \tag{100}$$

$$F_{b2}(\{I(l)\}) = \frac{1}{2\ln(2h/a)} \int_{-\infty}^{0} \left(k^2 \cos\alpha - \frac{\partial^2}{\partial l \partial l'} \right) g\left(\sqrt{l'^2 + l^2 - 2l'l\cos\alpha} \right) I(l')\, dl' \tag{101}$$

for $l > 0$.

3.3 Iterative solutions of the electric field integral equation

As in the case of straight wire (see Section 2.2), the quantity $1/2\ln(2h/a)$ appearing in eqns (96)–(101) is much smaller than 1 for thin wires and it is convenient to solve the derived eqn (96) using the perturbation theory around this small expansion parameter. Thus, the unknown induced current is decomposed into the following series

$$I(l) = I_0(l) + I_1(l) + I_2(l) + \cdots \tag{102}$$

where the zeroth iteration term $I_0(l)$ is determined from the TL approximation (95). Every next term $I_n(l)$ is the solution of the TL-like eqn (96), but with a source term $\widehat{D}_b$ corresponding to the previous iteration I_{n-1}, in other words,

$$\left(\frac{d^2}{dl^2} + k^2 \right) I_n(l) = \widehat{D}_b\{I_{n-1}(l)\}, \quad n \geq 1 \tag{103}$$

Therefore, the magnitude of the nth iteration will be proportional to $I_n(l) \sim (1/2\ln(2h/a))$.

Previously in this chapter, it has been shown that the above iterative method for the case of straight infinite and semi-infinite wires yields excellent approximation to the exact solutions after only one iteration and for high frequencies (kh up to several unities).

Now, the developed method will be applied to evaluate the current reflection and transmission coefficients associated with the line bend. In this case the external electromagnetic field is assumed to be absent

$$E_l^e(l) = 0, \quad -\infty < l < \infty \tag{104}$$

If the source is located at $-\infty$, the current wave travelling from $-\infty$ is partially reflected from the bend and partially transmitted to $+\infty$. The complex amplitudes of the reflected and transmitted waves are described by the coefficients $R(j\omega)$ and $D(j\omega)$. Using the perturbation theory and eqn (102) for the induced current, the reflection and transmission coefficients can be decomposed to

$$R = R_0 + R_1 + R_2 + \cdots \tag{105a}$$

$$D = D_0 + D_1 + D_2 + \cdots \tag{105b}$$

The zeroth iteration term, solution of eqn (95) is

$$I_0(l) = \tilde{I} e^{-jkl} \tag{106}$$

and the reflection and transmission coefficients have the trivial values

$$R_0 = 0, \quad D_0 = 1 \tag{107}$$

The first iteration is given by the solution of the non-homogeneous differential equation (103) with $n = 1$ and a source term given by eqns (97)–(101), (106). It is convenient to solve the differential equations separately in the $l < 0$ and $l > 0$ regions and join the obtained solutions afterward.

The general solutions of eqn (103) for negative and positive values of l, which take into account the correct boundary conditions at infinity (82), read

$$I_1(l) = \tilde{I}\left\{F_{b1}\{\tilde{I}e^{-jkl}\} - \frac{j}{2k}\int_{-\infty}^{0} e^{-jk|l'-l|}F_{b2}\{\tilde{I}e^{-jkl}\}\,dl' + C_1 e^{jkl}\right\} \tag{108}$$

for $l < 0$, and

$$I_1(l) = \tilde{I}\left\{F_{b1}\{\tilde{I}e^{-jkl}\} - \frac{j}{2k}\int_{0}^{\infty} e^{-jk|l'-l|}F_{b2}\{\tilde{I}e^{-jkl}\}\,dl' + C_2 e^{-jkl}\right\} \tag{109}$$

for $l > 0$. In eqns (108) and (109), the solutions of homogeneous differential equations e^{-jkl} for $l < 0$ and e^{jkl} for $l > 0$ can be dropped since the bend can generate only outward current waves.

Using the fact that in infinity [19]

$$\lim_{l\to\pm\infty} F_{b1}\{I(l)\} = 0 \tag{110}$$

it is possible to obtain the following expressions for the first-order corrections to the reflection and transmission coefficients R_1 and D_1 through unknown coefficients C_1 and C_2

$$R_1 = C_1 - \frac{j}{2k}\int_{-\infty}^{0} e^{-jk|l'-l|}F_{b2}\{\tilde{I}e^{-jkl}\}\,dl' \tag{111}$$

$$D_1 = C_2 - \frac{j}{2k}\int_{0}^{\infty} e^{-jk|l'-l|}F_{b2}\{\tilde{I}e^{-jkl}\}\,dl' \tag{112}$$

To determine the coefficients C_1 and C_2, it is necessary to impose that the solutions (108) and (109), as well as their derivatives (which are, up to the factor, charges per-unit length), are continuous at $l = 0$. After some straightforward mathematical manipulations, we obtain the following expressions for the first-order corrections R_1, D_1, to the reflection and transmission coefficients R_0 and D_0. These expressions are

$$R_1 = \frac{j}{2\ln(2h/a)}\left[2\int_0^{\infty}\sin kl\, g(l)\,dl - k(1+\cos\alpha)\right.$$
$$\left.\times\int_0^{\infty}dl\int_{-\infty}^{0}dl'\cos(k(l+l'))\,g\left(\sqrt{l'^2+l^2-2l'l\cos\alpha}\right)\right] \tag{113}$$

$$D_1 = \frac{j}{2\ln(2h/a)} k(1-\cos\alpha) \int_0^{\infty} \mathrm{d}l \int_{-\infty}^{0} \mathrm{d}l' \cos(k(l'-l)) g\left(\sqrt{l'^2 + l^2 - 2l'l\cos\alpha}\right) \tag{114}$$

Finally, the expression for the reflection and transmission coefficients R and D (including the zero and the first iterative terms) read

$$R \approx R_0 + R_1 = R_1 \tag{115a}$$

$$D \approx D_0 + D_1 = 1 + D_1 \tag{115b}$$

From eqn (114), it is obvious that for $\alpha = 0$, $D_1 = 0$. Making a change of variables ($x_1 = l + l'$, $x_2 = l' - l$) in eqn (115a), it is possible to show that for $\alpha = 0$, $R_1 = 0$.

3.4 Validation of the proposed method

The analytical expressions (113)–(115) obtained in Section 3.3 for the coefficients R and D are not convenient for a numerical integration because of the double integration over infinite intervals. It is, however, possible to find a more convenient form of these equations by making the following change of variables:

$$kl = \frac{\eta}{2}\left(\frac{\cos\varphi}{\sin(\alpha/2)} - \frac{\sin\varphi}{\cos(\alpha/2)}\right) \tag{116a}$$

$$kl' = \frac{\eta}{2}\left(\frac{\cos\varphi}{\sin(\alpha/2)} + \frac{\sin\varphi}{\cos(\alpha/2)}\right) \tag{116b}$$

The expressions (113) and (114) are then modified to the following forms, more suitable for a numerical integration:

$$R_1 = \frac{j}{2\ln(2h/a)}\left[2\int_0^{\infty} \sin\xi\, g(\xi/k)\,\mathrm{d}\xi - \mathrm{ct}g(\alpha/2)\int_0^{\infty} \eta\, g(\eta/k)\,\mathrm{d}\eta \int_{-\alpha/2-\pi/2}^{\alpha/2-\pi/2} \mathrm{d}\varphi \cos\left(\frac{\eta}{\sin(\alpha/2)}\cos\varphi\right)\right] \tag{117}$$

$$D_1 = \frac{j}{2\ln(2h/a)}\tan(\alpha/2)\int_0^{\infty} \eta\, g(\eta/k)\,\mathrm{d}\eta \int_{-\alpha/2-\pi/2}^{\alpha/2-\pi/2} \mathrm{d}\varphi \cos\left(\frac{\eta}{\cos(\alpha/2)}\sin\varphi\right) \tag{118}$$

Figures 14 and 15 present a comparison between our results and those obtained using the method of moments and reported in [15] for both reflection and transmission coefficients. We considered a horizontal wire with a radius $a = 5 \times 10^{-4}$ m located at a height $h = 0.3$ m above a perfectly conducting ground. The bend angle is $\alpha = 90°$. It can be seen that a very good agreement is found between the numerical method and our proposed approach, over a wide range of frequency for which the TL approximation looses its validity.

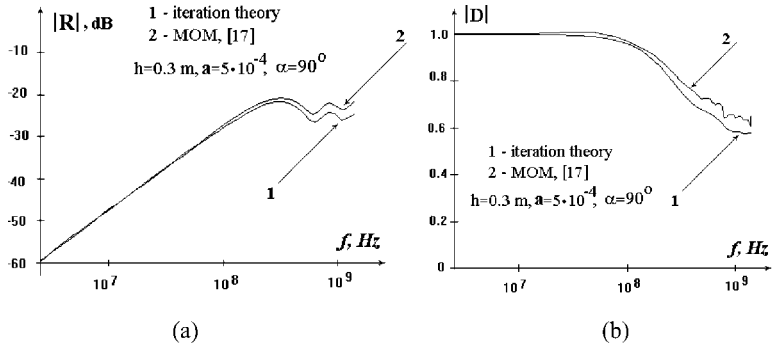

Figure 14: Reflection (a) and transmission (b) coefficients (magnitude) as function of frequency.

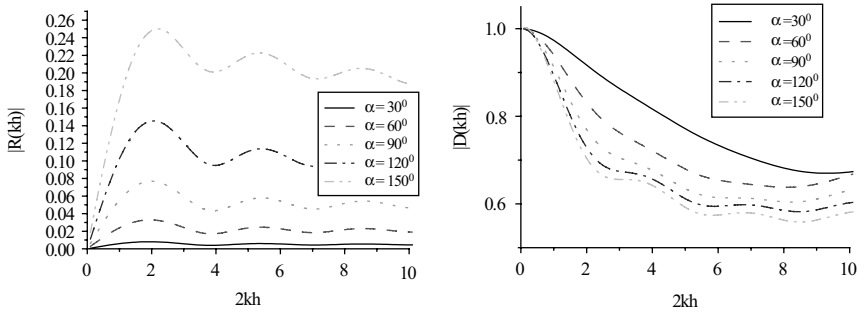

Figure 15: Reflection (a) and transmission (b) coefficients for the straight line bend (h = 0.5 m, a = 1 mm) as a function of frequency for the different bend angles.

In Fig. 15, we present frequency and angle dependence of the magnitude of the reflection and transmission coefficients, corresponding different bend angles $\alpha = 30°, 60°, 90°, 120°, 150°$.

As one would expect, the reflection and transmission coefficients are close to their TL values ($R \approx 0$, $D \approx 1$) for the low frequencies $kh << 1$, and for small bend angles $\alpha << 1$. For higher frequencies and larger bend angles, one can observe oscillations in the frequency dependencies of these coefficients, which are connected to the excitation of current eigen modes (leaky modes). These exponentially decaying eigen modes υ appear together with spreading out TEM modes and radiation modes near any non-uniformity of the wire, where the pure TEM wave is scattered. The eigen modes have the form $\exp(-jk_v|l|)$, where $\mathrm{Im}(k_v) < 0$. The detailed analytical investigation of these different types of modes can be carried out analytically for the case of infinitely long, straight wires near the ground excited by a lumped source [20, 21].

3.5 Radiated power

The knowledge of reflection and transmission coefficients allows also the evaluation of the radiated power associated with line bend. The radiated power P_{rad} can be expressed as

$$P_{\text{rad}} = P_{\text{inc}} - P_{\text{tr}} - P_{\text{ref}} \tag{119}$$

in which P_{inc}, P_{tr} and P_{ref} are, respectively, the incident, the transmitted and the reflected power at the discontinuity and are given by [15, 22]

$$P_{\text{inc}} = \frac{Z_{\text{C}} \left| I_{\text{inc}} \right|^2}{2} = \frac{Z_{\text{C}} \left| \tilde{I} \right|^2}{2} \tag{120a}$$

$$P_{\text{tr}} = \frac{Z_{\text{C}} \left| I_{\text{tr}} \right|^2}{2} = \frac{Z_{\text{C}} \left| \tilde{I} D \right|^2}{2} \tag{120b}$$

$$P_{\text{ref}} = \frac{Z_{\text{C}} \left| I_{\text{ref}} \right|^2}{2} = \frac{Z_{\text{C}} \left| \tilde{I} R \right|^2}{2} \tag{120c}$$

where $\tilde{I}$ is the amplitude of the initial current, $Z_{\text{C}} = \sqrt{\mu_0 / \varepsilon_0} \big/ 2\pi \ln(2h/a)$ is the line characteristic impedance.

Inserting eqn (120) into eqn (119) yields

$$P_{\text{rad}} / P_{\text{inc}} = 1 - \left| R^2 \right| - \left| D \right|^2 \tag{121}$$

In Fig. 16, we have represented the radiated power computed analytically using eqns (121), (115), (117) and (118) as a function of frequency, for the same configuration as in Fig. 14. On the same figure, we have plotted numerical values obtained using the method of moments in [14]. It can be seen that the proposed analytical approach yields results which are in reasonable agreement with 'exact' numerical values. However, due to the square dependence in eqn (121), the agreement is less good for the radiated power than for the reflection and transmission coefficients. To improve the agreement, higher-order iterations need to be considered in the perturbation theory.

For a quantitative characterization of radiation losses in the bend, we introduce the 'radiation resistance of the bend' R_{rad} as

$$P_{\text{rad}} = R_{\text{rad}} \left| \tilde{I} \right|^2 / 2 \tag{122}$$

then from eqns (120)–(122), we have

$$R_{\text{rad}} = Z_{\text{C}} (1 - \left| R^2 \right| - \left| D \right|^2) \tag{123}$$

The radiation resistance for a straight line bend for different angles of the bend is presented in Fig. 17 in comparison with the characteristic impedance of the line. We can observe that no significant radiation occurs at low frequencies and small bend angles. For higher frequencies, however, radiation of the bend becomes significant compared to the full power of the initial current.

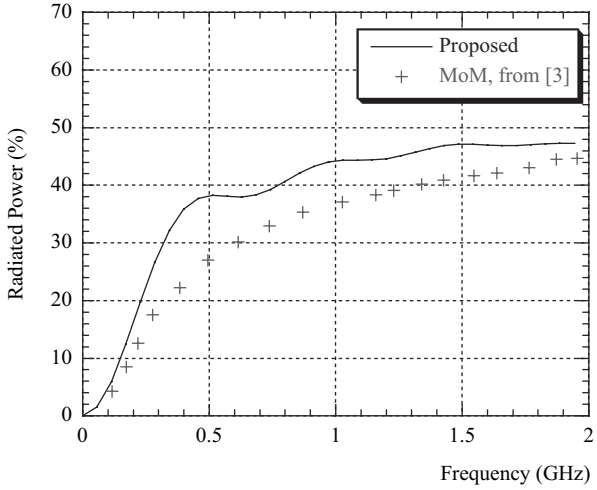

Figure 16: Radiated power as a function of frequency.

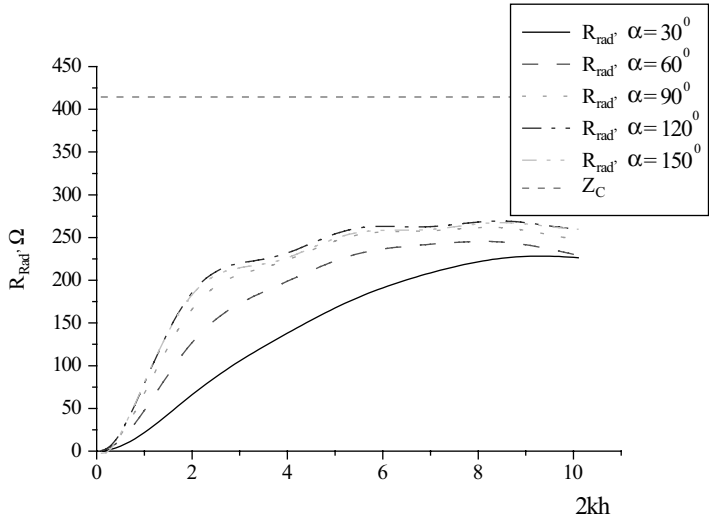

Figure 17: Radiation resistance for a straight line bend (h = 0.5 m, a = 1 mm) as a function of frequency for different bend angles.

4 Conclusion

The iteration approach described in this chapter allowed the taking into account of electrodynamics corrections to the results of TL approximation for high-frequency electromagnetic fields coupling with transmission lines of different geometric

form. The method is based on the electric field integral equation for the pair current–potential which is written in a TL-like form, but with addition integral terms accounting for electrodynamics corrections. This form is convenient for iterative solution, where the zeroth iteration term is determined by using the TL theory. The perturbation expansion is based on the small parameter $1/2\ln(2h/a)$. In the case of a straight wire, the corrections can be obtained in an explicit form. As the parameter of decomposition is frequency independent, it is possible to make a simple transformation of the obtained results in time domain.

One of the limitations of the method in the present formulation is that it does not take into account the vertical elements and loads of the line at its two ends. This can be done, if we use a more general electric field integral equation for the loaded wire of arbitrary geometric form [23] and generalize the iteration approach [24].

Another disadvantage of the method is the divergence of the perturbation series for high quality-factor systems near the resonant frequencies. This problem can be coped with if we use general equations for the reflection coefficient (instead of the TL approximation), which take into account radiation losses. The corresponding theory will be described in Chapter 5. In the same time, the method yields good results for semi-infinite lines (when re-reflections are absent), as well as in non-resonant frequency regions for finite systems. Often, only one iteration is enough to obtain an excellent agreement with the exact solutions.

Finally, it is also worth mentioning that the choice of the solution of the classical TL approximation with constant parameters as zeroth iteration for the perturbation solution of the electric field integral equation in this chapter is quite arbitrary. An important question is: could one minimize the correction term in the TL-like integral equations by an appropriate choice of the parameters of the zeroth iteration? An attempt to answer this question was made in [25], where the integral equation was reduced to the non-homogeneous TL equations with real l-dependent anti-diagonal parameters (real per-unit-length inductance and capacitance) and only zero-order iteration was considered. On the other hand, in [26], it was proved that the electric field integral equation for a wiring system excited by two independent sources (lumped voltages, lumped impedance, etc.), could be reduced to a non-homogeneous TL equations with anti-diagonal as well as diagonal parameters. These parameters depend upon the coordinate along the line, are complex valued and their imaginary part is connected with radiation of the system (see also [23, 27, 28]).

References

[1] Vance, E.F., *Coupling to Shielded Cables*, Wiley InterScience: New York, 1978.

[2] Tesche, F.M., Comparison of the transmission line and scattering models for computing the NEMP response of overhead cables. *IEEE Trans. Electromagn. Compat.*, **34(2)**, pp. 93–99, 1992.

[3] Bridges, G.E.J. & Shafai, L., Plane wave coupling to multiple conductor transmission lines above a lossy earth. *IEEE Trans. Electromagn. Compat.*, **31(4)**, pp. 396–397, 1989.

[4] Agrawal, A.K., Price, H.J. & Gurbaxani, S.H., Transient response of multiconductor transmission lines excited by a nonuniform electromagnetic field. *IEEE Trans. Electromagn. Compat.*, **EMC-22(2)**, pp. 119–129, 1980.

[5] Leontovitch, M. & Levin, K., On the theory of excitation of oscillations in wire antennas. *J. Tech. Phys.*, **XIV(9)**, pp. 481–506, 1946 (in Russian).

[6] Collin, R.E. & Zucker, F.J., *Antenna Theory*, McGraw-Hill: New York, 1969.

[7] Tesche, F.M., Ianoz, M. & Karlsson, T., *EMC Analysis Methods and Computational Models*, John Wiley and Sons: New York, 1997.

[8] Weinstein, L.A., *The Theory of Diffraction and the Factorization Method*, Golem Press, Chapter V, 1969.

[9] Prudnikov, A.P., Brychkov, Yu.A. & Marichev, O.I., *Integrals and Series, Vol. 1: Elementary Functions*, Gordon and Breach Science Publishers: New York, 1986.

[10] Abramowitz, M. & Stegun, I., *Handbook of Mathematical Functions*, Dower Publications: New York, 1970.

[11] Collin, R.E., *Field Theory of Guided Waves*, IEEE Press: New York, 1991.

[12] Burke, G.J., Poggio, A.J., Logan, J.C. & Rockway, J.W., Numerical electromagnetics code – a program for antenna system analysis. *Proc. 3rd Int. Symp. Tech. Exhibition EMC*, Rotterdam, 1–3 May 1979.

[13] Tkachenko, S., Rachidi, F., Ianoz, M. & Martynov, L., An asymptotic approach for the calculation of electromagnetic field coupling to long terminated lines. *Int. Symp. on EMC, EMC'98 ROMA*, Italy, pp. 605–609, 14–18 September 1998.

[14] Reineix, A. & Jecko, B., Radiation losses in the time domain transmission line method. *Int. Symp. on EMC, EMC'94 ROMA*, Italy, pp. 402–407, 13–16 September 1994.

[15] Girard, C., Thomas, B., Reineix, A. & Jecko, B., Introduction of discontinuities effects in transmission line method. Emission problem. *Int. Symp. on EMC, EMC'96 ROMA*, Italy, pp. 54–58, 17–20 September 1996.

[16] Wendt, D.O. & ter Haseborg, J.L., Representation of the effects caused by inhomogeneities of transmission lines in the TLT. *Int. Symp. on EMC, EMC'96 ROMA*, Italy, pp. 48–53, 17–20 September 1996.

[17] Pezin, F., Kone, L., Demoulin, B., Girard, C., Reinex, A. & Jecko, B., Experimental characterization of the attenuation and radiation due to bended transmission lines. *Int. Symp. On EMC, EMC'98 ROMA*, Rome, Italy, pp. 626–631, 14–18 September 1998.

[18] Ishibashi, N., Lee, S.K. & Hayakawa, M., Numerical study on the radiation from a bend in a transmission line. *13th International Zurich Symposium Electromagnetic Compatibility*, pp. 635–638, February 1999.

[19] Tkatchenko, S., Rachidi, F. & Ianoz, M., Electromagnetic field coupling to a line of finite length: theory and a fast iterative solutions in frequency and time domains. *IEEE Trans. Electromagn. Compat.*, **37(4)**, pp. 509–518, 1995.

[20] Olsen, R.G., Young, G.L. & Chang, D.C., Electromagnetic wave propagation on a thin wire above earth. *IEEE Transaction on Antennas and Propagation*, **AP-48(9)**, pp. 1413–1419, 2000.

[21] Leviatan, Y. & Adams, A.T., The response of two-wire transmission line to incident field and voltage excitation, including the effects of higher order modes. *IEEE Tran. Ant. Prop.*, **AP-30(5)**, pp. 998–1003, September 1982.

[22] Tkachenko, S., Rachidi, F. & Nitsch, J., Analytical characterization of a line bend. *Proceedings of International Symposium ELECTROCOMP 2005*, FL, USA, pp. 599–608, 16–18 March 2005.

[23] Nitsch, J.B. & Tkachenko, S.V., Global and modal parameters in the generalized transmission line theory and their physical meaning. *Radio Sci. Bull.*, **312**, pp. 21–31, March 2005.

[24] Tkachenko, S., Rachidi, F. & Nitsch, J., High frequency wave propagation along non-uniform transmission lines: a direct iteration approach. *CD Proceedings of the GA URSI*, New Delhi, October 2005.

[25] Korovkin, N.V., Kochetov, S.V., Selina, E.E., Tkachenko, S.V. & Ianoz, M., A model for a finite length transmission line considering skin and radiation effect. *14th Int. Zurich Symposium on EMC*, pp. 108–112, 20–22 February 2001.

[26] Haase, H. & Nitsch, J., Full-wave transmission line theory (FWTLT) for the analysis of three-dimensional wire-like structures. *Proc. 14th Int. Zurich Symposium on EMC*, pp. 235–240, February 2001.

[27] Haase, H., Steinmetz, T. & Nitsch, J., New propagation models for electromagnetic waves along uniform and nonuniform cables. *IEEE Trans. Electromagn. Compat.*, **EMC-47(3)**, pp. 345–352, 2004.

[28] Haase, H., Nitsch, J. & Steinmetz, T., Transmission-line super theory: a new approach to an effective calculation of electromagnetic interactions. *Radio Sci. Bull.*, **307**, pp. 33–60, 2003.

CHAPTER 5

High-frequency electromagnetic field coupling to long loaded non-uniform lines: an asymptotic approach

S.V. Tkachenko[1], F. Rachidi[2] & J.B. Nitsch[1]
[1]*Otto-von-Guericke-University Magdeburg, Magdeburg, Germany.*
[2]*Ecole Polytechnique Federale de Lausanne, Lausanne, Switzerland.*

Abstract

In this chapter, we present and validate an efficient hybrid method to compute high-frequency electromagnetic field coupling to long loaded lines, when the transmission line approximation is not applicable. The line can contain additional discontinuities (either a lumped impedance or a lumped source) in the central region. In the proposed method, the induced current along the line can be expressed using closed form analytical equations. These expressions involve current waves scattering coefficients at the line non-uniformities, which can be determined using either approximate analytical solutions, numerical methods (for the scattering in the line near-end regions), or exact analytical solutions (for the scattering at the lumped impedance in the central region). The proposed approach is compared with numerical simulations and excellent agreement is found.

1 Introduction

The present study considers the important electromagnetic compatibility (EMC) problem of high-frequency electromagnetic field coupling to long transmission lines (TLs). We assume that the frequency spectrum of the exciting field and the transverse dimensions of the line are such that the TL approximation is not applicable. To solve such a problem, one generally resorts to the use of numerical methods (e.g. method of moments) based on the antenna theory. However, a pure numerical method allows to have a general physical picture of the phenomena, only after large series of calculations. Moreover, a systematic use of such methods usually needs prohibitive computer time and storage requirements, especially when analyzing long transmission lines.

Exact analytical expressions of induced current have been developed for the case of infinite overhead lines [1, 2]. Using those expressions, it has been shown that corrections to TL approximation can be considerable under certain circumstances.

In [3, 4] (see also Chapter 4), a system of equations is derived under the thin-wire approximation describing the electromagnetic field coupling to a horizontal wire of *finite arbitrary* length above the ground plane. The derived equations are in the form of telegrapher's equations in which the electrodynamics corrections to the TL approximation appear as additional voltage and current source terms. Based on perturbation theory, an efficient iterative procedure has been proposed to solve the derived coupling equations, where the zeroth iteration term is determined by using the TL approximation (see Chapter 4). However, this method (as formulated in [3, 4]) does not take into account the vertical elements and loads of the wire. Another disadvantage of the method is the divergence of the perturbation series for high-quality-factor systems (e.g. a horizontal open-circuited wire) near the resonant frequencies.

In this chapter, we consider the case of a *long* line, excited by a plane electromagnetic wave. The line can be terminated at each end by arbitrary impedances (with vertical elements), a configuration that requires taking into account the interactions between wire sections with different directions. The line can contain an additional discontinuity (in the form of a lumped impedance or a lumped source) in the central region.

The proposed hybrid method to compute high-frequency electromagnetic field coupling with a long line will be based on the specific features of wave propagation along long wires, as described next. An exciting plane wave generates fast current waves (i.e. with phase velocities larger than the speed of light) along an infinite straight wire parallel to a perfectly conducting ground. This current wave radiates uniformly along the line [5–10]. When the homogeneity of the line is disturbed by a discontinuity (lumped impedance or lumped source, vertical elements of the line, bend, etc.), the current distribution near the discontinuity becomes more complex, involving different propagation modes, namely transverse electromagnetic (TEM) modes, leaky modes (which are attenuated exponentially with the distance), and radiation modes (which are attenuated as $1/r^n$, r being the distance). The exact analytical solution of this problem is known only for the case of a lumped source (lumped impedance) in an infinite wire (see, e.g. [11–13]), or for the case of a semi-infinite open-circuited wire [14]. At distances large enough from the discontinuity, in the so-called 'asymptotic region', only TEM modes 'survive', which propagate along the line without producing any radiation [8, 15, 16]. The amplitude associated with the TEM modes can be expressed in terms of scattering coefficients. These TEM modes, in turn, will scatter when reaching line discontinuities, near which, again different type of modes will be present; however, enough distant from the discontinuities in the line asymptotic region, the only 'surviving' mode is TEM, and the scattering process can be described by the reflection and transmission coefficients. To obtain the global solution, we have to consider the scattering associated with each line

discontinuity and join the solutions in the asymptotic region(s). As a result, we will obtain a closed form analytical expressions for the induced current along the line [5, 6, 17, 18]. These expressions involve scattering coefficients for different types of current waves on the line discontinuities, which can be determined using either approximate analytical solutions, numerical methods (for the scattering in the line near–end regions), or exact analytical solutions (for the scattering near a lumped impedance in the central region [18]). The proposed approach will be compared with numerical simulations.

2 High-frequency electromagnetic field coupling to a long loaded line

2.1 Asymptotic approach

Consider a long current filament of finite length above a perfectly conducting ground, in presence of an external plane wave (see Fig. 1). The line is loaded at its terminals by impedances Z_1 and Z_2.

2.1.1 Solution for the induced current in the asymptotic region

The exact spatial dependence of the induced current can be determined by the solution of the one-dimensional (thin wire approximation) Pocklington's electric field integral equation [19]. The examination of this equation for long lines

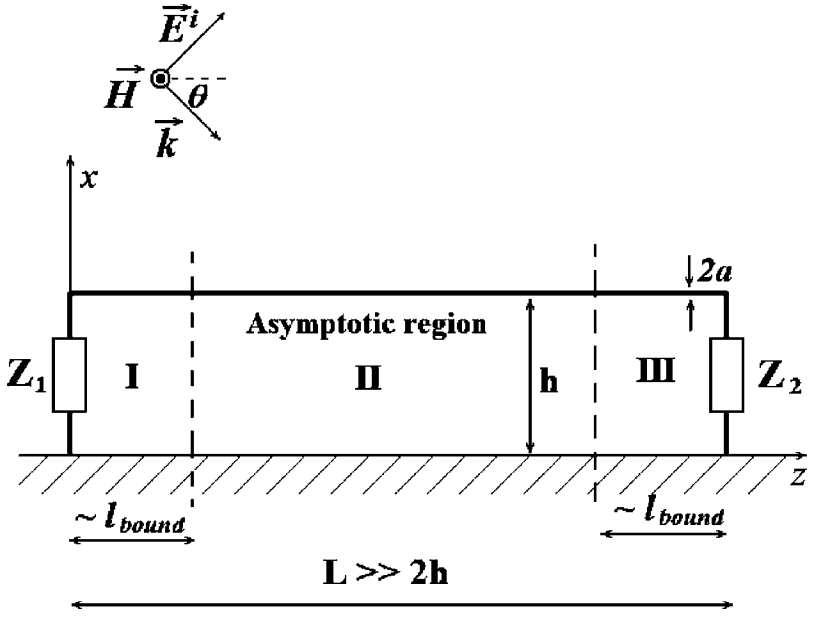

Figure 1: Geometry of the long terminated line excited by an external plane wave.

($L >> 2h$) has shown that the current distribution along the line may be divided into three regions as illustrated in Fig. 1 [5]. Regions I and III are located near the terminal loads. The main region II is constituted by portions of the wire sufficiently far from the terminations, i.e. $l_{\text{bound}} << z << L\text{-}l_{\text{bound}}$. In this central region, called hereafter *the asymptotic region*, the influence of electromagnetic fields arising from the load currents may be neglected in comparison with the fields generated by the currents along the wire [5]. The value l_{bound} depends rigorously upon the modes generated near the line discontinuities, i.e. lumped loads and vertical elements. However, for most cases of practical interest when $kh <\cong 1$, a value l_{bound} equal to about $2h$ can be adopted.

Therefore, we postulate that the general solution for the current along the asymptotic region can expressed as a sum of three distinct terms

$$I(z) = I_0 \exp(-jk_1 z) + I_1 \exp(jkz) + I_2 \exp(-jkz) \tag{1}$$

where $k = \omega/c$, and $k_1 = k \cos\theta$, where θ is the elevation angle of the incident field (the azimuth angle $\varphi = 0$).

The first term is a forced response wave, which corresponds to the induced current on an infinitely long wire. The second and the third terms are positive and negative travelling waves and the coefficients I_1 and I_2 depend upon the respective geometric wire configuration and loads at the two line terminals.

The coefficient I_0 of the forced response wave is determined from the solution of the Pocklilngton's equation for the case of an infinitely long wire [19]

$$(\mathrm{d}^2/\mathrm{d}z^2 + k^2) \int_{-\infty}^{\infty} g(z'-z) I(z')\,\mathrm{d}z' = -4\pi\varepsilon_0 j\omega E_z^{\mathrm{e}}(h,z), \quad ka << 1 \tag{2}$$

in which $I(z)$ is the induced current, and $g(z)$ is the scalar Green's function given by

$$g(z) = \frac{\mathrm{e}^{-jk\sqrt{z^2+a^2}}}{\sqrt{z^2+a^2}} - \frac{\mathrm{e}^{-jk\sqrt{z^2+4h^2}}}{\sqrt{z^2+4h^2}} \tag{3}$$

The term $E_z^{\mathrm{e}}(h,z)$ is the tangential exciting E-field at the line height, which, for the case of a vertically polarized plane wave is given by

$$E_z^{\mathrm{e}}(h,z) = E^i \mathrm{e}^{-jk_1 z}(1 - \mathrm{e}^{-2jkh\sin\theta})\sin\theta = E_z^{\mathrm{e}}(h, j\omega)\mathrm{e}^{-jk_1 z} \tag{4}$$

The analytical solution for the coefficient of the forced wave for the case of a vertically polarized exciting field is given by [20] (see also Section 4.2.3)

$$I_0 = \frac{1}{j\omega\eta_0 \sin^2\theta} \frac{4\pi c E_z^{\mathrm{e}}(h, j\omega)}{2\ln(2/\gamma ka\sin\theta) - j\pi + j\pi H_0^{(2)}(2kh\sin\theta)}, \quad ka << 1 \tag{5}$$

In order to determine the coefficients I_1 and I_2 of the positive and negative travelling waves for an arbitrary frequency of the exciting field, it is necessary to know the exact solutions for the induced current in regions I and III, which may be

obtained by solving Pocklington's equations in these regions using a numerical method (e.g. method of moments). It is worth nothing that Pocklington's equation uses as source term the tangential component of the exciting electric field along the wire and along the conductors of the load impedances.

To obtain the coefficients from the numerical solutions near the line ends, it is necessary to consider an intermediary step, which consists of defining two semi-infinite lines as shown in Fig. 2. (The semi-infinite line configurations will also

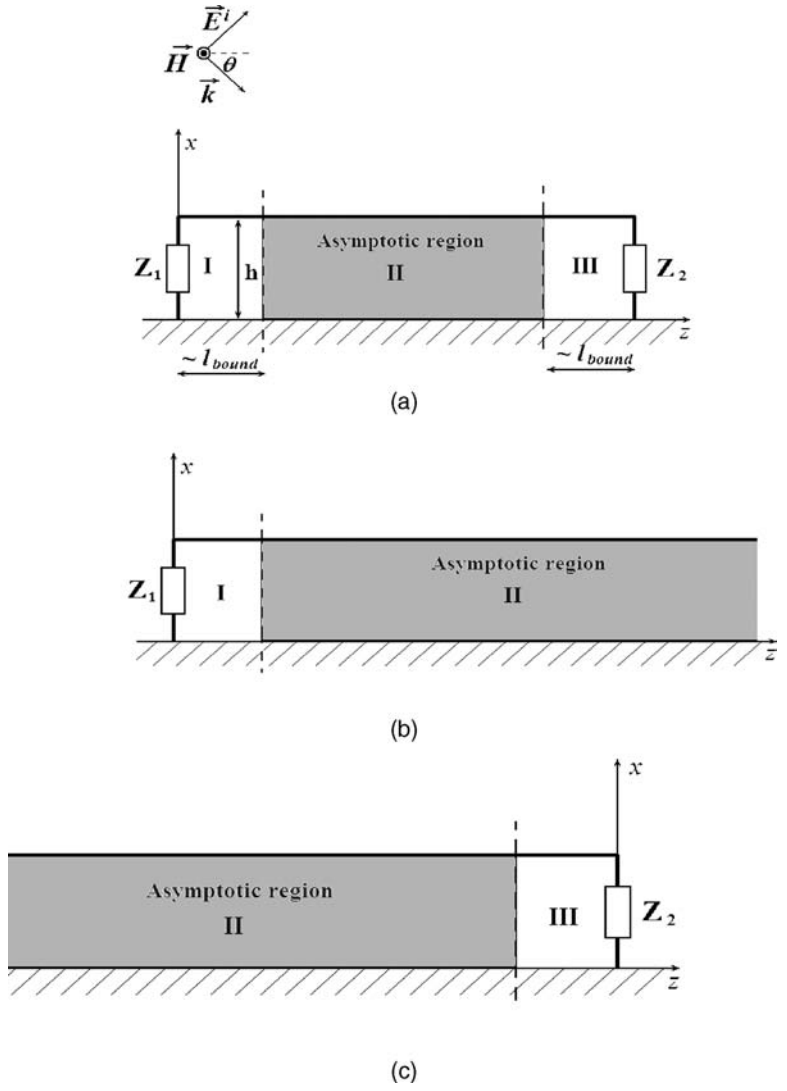

Figure 2: Geometry for the original line (a), the right semi-infinite line (b), and the left semi-infinite line (c).

allow us to obtain analytical expressions for the induced current near and at the two extremities of the long line, as we shall see in Section 2.1.2.) The right semi-infinite line extends from the line left-end to +∞ (Fig. 2b), and the left semi-infinite line extends from −∞ to the line right-end (Fig. 2c). The general solution to this problem can be expressed as a linear combination of the solutions for non-homogeneous (with external field excitation) and homogeneous (no external excitation) problems.

The non-homogeneous solution for the right semi-infinite line ($0 \le z < \infty$) and for left semi-infinite line ($-\infty \le z \le 0$) can be expressed respectively as

$$I_+^{\mathrm{e}}(z) = I_0 \Psi_+^{\mathrm{e}}(z) \tag{6}$$

$$I_-^{\mathrm{e}}(z) = I_0 \Psi_-^{\mathrm{e}}(z) \tag{7}$$

in which

$$\Psi_+^{\mathrm{e}}(z) = \begin{cases} \text{exact solution in the region,} & 0 \le z \le l_{\mathrm{bound}} \\ \exp(-jk_1 z) + C_+ \exp(-jkz), & z >> l_{\mathrm{bound}} \end{cases} \tag{8}$$

and

$$\Psi_-^{\mathrm{e}}(z) = \begin{cases} \text{exact solution in the region,} & -l_{\mathrm{bound}} \le z \le 0 \\ \exp(-jk_1 z) + C_- \exp(jkz), & z << -l_{\mathrm{bound}} \end{cases} \tag{9}$$

In eqns (8) and (9), C_+ and C_- are scattering coefficients, which depend on the frequency and the angle of incidence of the exciting electromagnetic field $C_+ = C_+(k,\theta)$, $C_- = C_-(k,\theta)$.

The homogeneous solution (no external excitation) is given by

$$I_+^{0}(z) = \Psi_+^{0}(z) \tag{10}$$

$$I_-^{0}(z) = \Psi_-^{0}(z) \tag{11}$$

in which

$$\Psi_+^{0}(z) = \begin{cases} \text{exact solution in the region,} & 0 \le z \le l_{\mathrm{bound}} \\ \exp(jk\, z) + R_+ \exp(-jkz), & z >> l_{\mathrm{bound}} \end{cases} \tag{12}$$

and

$$\Psi_-^{0}(z) = \begin{cases} \text{exact solution in the region,} & -l_{\mathrm{bound}} \le z \le 0 \\ \exp(-jk\, z) + R_- \exp(jkz), & z << -l_{\mathrm{bound}} \end{cases} \tag{13}$$

In eqns (12) and (13), R_+ and R_- are the reflection coefficients, which depend on the frequency ($R_+ = R_+(k)$, $R_- = R_-(k)$). It is important to note that both reflection coefficients and scattering coefficients are independent of the line length.

Coefficients I_1 and I_2 can be expressed as a function of the coefficients C_+, C_-, R_+, and R_- by considering that the induced current in the asymptotic region of the

initial line is identical to the current in the asymptotic region for the semi-infinite lines (see Fig. 2). The general solution for the current in the right semi-infinite line is given by the sum of homogeneous and non-homogeneous solution

$$I_+(z) = I_0 \Psi_+^{\mathrm{e}}(z) + \tilde{I}_1 \Psi_+^0(z) \tag{14}$$

in which I_0 and $\tilde{I}_1$ are constant coefficients.

In the asymptotic region of the line, using eqns (8) and (12), the above solution can be written as

$$\begin{aligned} I_+(z >> l_{\mathrm{bound}}) &= I_0 \exp(-jk_1 z) + I_0 C_+ \exp(-jkz) + \tilde{I}_1 \exp(jkz) + \tilde{I}_1 R_+ \exp(-jkz) \\ &= I_0 \exp(-jk_1 z) + \tilde{I}_1 \exp(jkz) + [I_0 C_+ + \tilde{I}_1 R_+] \exp(-jkz) \end{aligned} \tag{15}$$

Similarly, the general solution for the current in the left semi-infinite line can be written as the sum of non-homogeneous and homogeneous solutions, but considering appropriate argument shifts caused by the new coordinate origin which is shifted by a length L (see Fig. 2c)

$$I_-(z) = I_0 \exp(-jk_1 L) \Psi_-^{\mathrm{e}}(z - L) + \tilde{I}_2 \Psi_-^0(z - L) \tag{16}$$

Also in the asymptotic region, we have

$$\begin{aligned} I_-(z << -l_{\mathrm{bound}}) &= I_0 \exp(-jk_1 z) + I_0 C_- \exp(jkz - jkL - jk_1 L) \\ &\quad + \tilde{I}_2 \exp(-jk\, z + jkL) + \tilde{I}_2 R_- \exp(jk\, z - jkL) \\ &= I_0 \exp(-jk_1 z) + \left\lfloor I_0 C_- \exp(-jkL - jk_1 L) + \tilde{I}_2 R_- \exp(-jkL) \right\rfloor \\ &\quad \times \exp(jk\, z) + \tilde{I}_2 \exp(-jk\, z + jkL) \end{aligned} \tag{17}$$

As it can be seen by eqns (15) and (17), the solution in the asymptotic region is given in the form of the proposed three-term approximation (1). By imposing that the coefficients for the terms exp(*jkz*) and exp(*–jkz*) are identical in eqns (15) and (17), we obtain a linear system for the unknown coefficients $\tilde{I}_1$ and $\tilde{I}_2$, which yields the following solutions:

$$\tilde{I}_1 = I_0 \frac{C_- \exp(-jkL - jk_1 L) + C_+ R_- \exp(-2\,jkL)}{1 - R_+ R_- \exp(-2\,jkL)} \tag{18}$$

$$\tilde{I}_2 = I_0 \frac{C_+ \exp(-jkL) + C_- R_+ \exp(-2\,jkL - jk_1 L)}{1 - R_+ R_- \exp(-2\,jkL)} \tag{19}$$

And, therefore, the coefficients I_1 and I_2 in eqn (1) are given by

$$I_1 = \tilde{I}_1 = I_0 \frac{C_- \exp(-jkL - jk_1 L) + C_+ R_- \exp(-2\,jkL)}{1 - R_+ R_- \exp(-2\,jkL)} \tag{20}$$

$$I_2 = \tilde{I}_2 \exp(jkL) = I_0 \frac{C_+ + C_- R_+ \exp(-jkL - jk_1 L)}{1 - R_+ R_- \exp(-2jkL)} \tag{21}$$

In this way, the induced current in the asymptotic region II is expressed analytically by eqn (1), in which the coefficients, I_0, I_1, and I_2 are given by eqns (5), (20), and (21). The coefficients I_1 and I_2 are expressed in terms of the asymptotic coefficients C_+, C_-, R_+, and R_-, which are independent of the line length (for a line length larger than a few times its height) and are characterized only by the current scattering near the loads.

For simple line terminal configurations such as an open-circuit without vertical elements, these coefficients may be obtained analytically using the iteration method presented in Chapter 4. For the general case of arbitrary terminal loads, these coefficients have to be determined numerically (using the method of moments, for instance). Since the asymptotic coefficients are independent of the line length, they can be evaluated using the numerical solutions for significantly shorter lines. In this way, the proposed method makes it possible to compute the response of TL to exciting electromagnetic field with a reasonable computation time, regardless of the line length.

In order to determine the scattering coefficients, it is indispensable to consider two lines because we have to determine four unknowns (C_+, C_-, R_+, and R_-), and for each line we have a set of two eqns (20) and (21). Starting from eqns (20) and (21), written for two lines with similar configurations (by which we mean the same wire radius, height above ground, terminal impedances, and exciting electromagnetic field), but with significantly shorter lengths L_1 and L_2, the following expressions for the scattering coefficients C_+, C_-, R_+, and R_- and can be derived (see Appendix 1)

$$R_+ = \frac{I_2(L_2) - I_2(L_1)}{I_1(L_2) - I_1(L_1)} \tag{22}$$

$$C_+ = \frac{1}{I_0} \frac{I_2(L_1) I_1(L_2) - I_2(L_2) I_1(L_1)}{I_1(L_2) - I_1(L_1)} \tag{23}$$

$$R_- = \frac{I_1(L_2) \exp[j(k + k_1) L_2] - I_1(L_1) \exp[j(k + k_1) L_1]}{I_2(L_2) \exp[j(k_1 - k) L_2] - I_2(L_1) \exp[j(k_1 - k) L_1]} \tag{24}$$

$$C_- = \frac{1}{I_0} \frac{I_1(L_1) I_2(L_2) \exp(2jkL_1) - I_1(L_2) I_2(L_1) \exp(2jkL_2)}{I_2(L_2) \exp[j(k - k_1) L_1] - I_2(L_1) \exp[j(k - k_1) L_2]} \tag{25}$$

2.1.2 Expression for the induced current at the line terminals (regions I and III)

Starting from numerical solutions for the two short line configurations $I(z,L_1)$ and $I(z,L_2)$, it is also possible to derive analytical expressions for the current at the terminals of the original line. The solution in the left-end region (region I in Fig. 1) for the two short lines can be expressed as (from eqn (14))

$$I_+(z, L_1) = I_0 \Psi_+^{\mathrm{e}}(z) + \tilde{I}_1(L_1) \Psi_+^0(z) \tag{26}$$

$$I_+(z,L_2) = I_0\Psi_+^{\mathrm{e}}(z) + \tilde{I}_1(L_2)\Psi_+^0(z) \tag{27}$$

Note that in the above two equations, the length dependence is contained only in the coefficients $\tilde{I}_1(L_1)$ and $\tilde{I}_1(L_2)$, which can be calculated by eqn (18). From these two equations, it is possible to infer the functions $\Psi_+^{\mathrm{e}}(z)$ and $\Psi_+^0(z)$. After some straightforward mathematical manipulations, we get

$$\Psi_+^0(z) = \frac{I(z,L_2) - I(z,L_1)}{\tilde{I}_1(L_2) - \tilde{I}_1(L_1)} \tag{28}$$

$$\Psi_+^{\mathrm{e}}(z) = \frac{1}{I_0}\frac{I(z,L_1)\tilde{I}_1(L_2) - I(z,L_2)\tilde{I}_1(L_1)}{\tilde{I}_1(L_2) - \tilde{I}_1(L_1)} \tag{29}$$

Inserting the relations (28) and (29) into eqn (14) and considering that $I_1 = \tilde{I}_1$, we get the solution for the induced current in the left-end region

$$I_+(z,L)\big|_{\text{left end}} = \frac{I(z,L_1)I_1(L_2) - I(z,L_2)I_1(L_1)}{I_1(L_2) - I_1(L_1)} + I_1(L)\frac{I(z,L_2) - I(z,L_1)}{I_1(L_2) - I_1(L_1)} \tag{30}$$

Similarly, in the right-end region (region III in Fig. 1), the solution for the two short configurations can be expressed as (from eqn (16))

$$I_-(z,L_1) = I_0\exp(-jk_1L_1)\Psi_-^{\mathrm{e}}(z-L_1) + \tilde{I}_2(L_1)\Psi_-^0(z-L_1) \tag{31}$$

$$I_-(z,L_2) = I_0\exp(-jk_1L_2)\Psi_-^{\mathrm{e}}(z-L_2) + \tilde{I}_2(L_2)\Psi_-^0(z-L_2) \tag{32}$$

Again in the above two equations, the length-dependence is contained only in coefficients $\tilde{I}_2(L_1)$ and $\tilde{I}_2(L_2)$, which can be calculated by eqn (19). After some mathematical manipulations, it is possible to inter from these two equations the functions $\Psi_-^{\mathrm{e}}(z)$ and $\Psi_-^0(z)$

$$\Psi_-^0(z) = \frac{\exp(jk_1L_1)I(z+L_1,L_1) - \exp(jk_1L_2)I(z+L_2,L_2)}{\exp(jk_1L_1)\tilde{I}_2(L_1) - \exp(jk_1L_2)\tilde{I}_2(L_2)} \tag{33}$$

$$\Psi_-^{\mathrm{e}}(z) = \frac{1}{I_0}\frac{I(z+L_1,L_1)\tilde{I}_2(L_2) - I(z+L_2,L_2)\tilde{I}_2(L_1)}{\exp(-jk_1L_1)\tilde{I}_2(L_2) - \exp(-jk_1L_2)\tilde{I}_2(L_1)} \tag{34}$$

Inserting the expressions (33) and (34) into eqn (16) and taking into account that $I_2 = \tilde{I}_2\exp(jkL)$, we get the solution for the induced current in the right-end region

$$\begin{aligned} I_-(z,L)\big|_{\text{right end}} &= \exp(-jk_1L)\frac{\exp(-jkL_2)I_2(L_2)I(z-L+L_1,L_1) - \exp(-jkL_1)I_2(L_1)I(z-L+L_2,L_2)}{I_2(L_2)\exp(-jk_1L_1 - jkL_2) - I_2(L_1)\exp(-jk_1L_2 - jkL_1)} \\ &\quad + I_2(L)\exp(-jkL)\frac{\exp(jk_1L_1)I(z-L+L_1,L_1) - \exp(jk_1L_2)I(z-L+L_2,L_2)}{\exp(j(k_1-k)L_1)I_2(L_1) - \exp(j(k_1-k)L_2)I_2(L_2)} \end{aligned} \tag{35}$$

2.1.3 Summary of the proposed procedure to determine the induced current along the line and at the line terminals

The procedure for the determination of the coefficients of the analytical expressions for the induced current along a long line (Fig. 2a) can be summarized as follows:

1. Apply a numerical method (e.g. method of moments) to compute the response of two equivalent lines having the same configuration as the initial line, but with shorter lengths $L_1 << L$ and $L_2 << L$. Typically, it is enough to consider L_1 equal to about $5h$ and in order to avoid numerical instability, it is desirable to take L_2 frequency dependent, for example $L_2 = L_1 + \lambda/2$.

   Starting from the numerical solutions for the induced current on the two above-mentioned lines, we determine the coefficients $I_1(L_1)$, $I_2(L_1)$, $I_1(L_2)$, $I_2(L_2)$ using the least-square method.
2. The scattering coefficients C_+, C_-, R_+, R_- are then computed using eqns (22)–(25).
3. The coefficients C_+, C_-, R_+, R_-, which are independent of the line length, are used to compute the coefficients $I_1(L)$, $I_2(L)$, for any length L using (20) and (21). The analytical expressions for the induced current along the asymptotic region of the line (1) and at the line ends (30), (35) can be applied for the any line length.

Note that only the first step of the above procedure requires numerical computations, which is to be performed not for the whole line structure but on two significantly shorter lines. Therefore, the computation time can be drastically reduced for long lines. Additionally, once the numerical solutions for the two short line configurations are known, it is possible to compute analytically the solution for any similar line configuration, but with any different line length.

2.2 Accuracy of the proposed three-term expression for the induced current along the asymptotic region of the line

In order to validate our assumption on the analytical form of the induced current in the asymptotic central region II, we have developed a code for the determination of the coefficients I_0, I_1, I_2 in expression (1), starting from numerical solutions obtained using Numerical Electromagnetics Code (NEC) [21]. The real and imaginary parts of coefficients I_0, I_1, I_2 were determined separately using the least-square method. It has been shown, considering several load conditions, that the proposed expression (1) approximates very well the spatial dependence of the induced current [6]. An example of comparison between the numerical solutions obtained using NEC with the proposed approximate expression (1) is presented in Fig. 3. The line is characterized by a length $L = 16$ m, a conductor radius $a = 10$ mm, and a height above ground $h = 0.5$ m, and is short-circuited at both ends ($Z_1 = 0$, $Z_2 = 0$). The exciting field is a plane wave with $f = 358$ MHz ($\lambda = 0.84$ m), $\theta = 45°$, $E_0 = 50$ kV/m. Note that, the TL approximation is not applicable to this case because the wavelength of the exciting field is practically equal to the height of the conductor above ground. In this figure, the abscissa l represents the coordinate

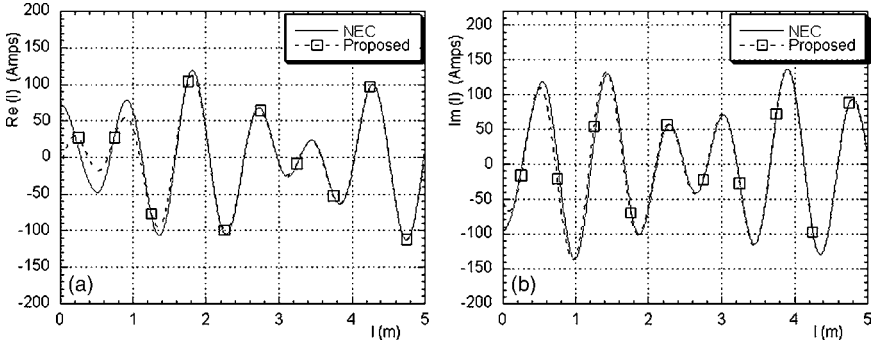

Figure 3: Comparison of the induced current flowing along the line using the NEC solution and the proposed approximate formula (1), with coefficients determined using the least-square method. Angle of incidence θ = 45°. (a) Real part and (b) imaginary part of the current.

along the whole wire length including the vertical risers, $l = 0$ corresponding to the point where the vertical conductor touches the ground and $l = h$ to the beginning of the horizontal part of the line. The total number of segments along the line considered in the NEC code was $N_{seg} = 245$.

It can be seen that an excellent approximation is found in the asymptotic region of the line.

According to our hypothesis, the coefficient I_0 in the three-term spatial dependence (1) should be equal to the expression (5), corresponding to the current induced by an external plane wave for the case of an infinitely long line. Comparisons between the real and imaginary parts of I_0 obtained from a least-square approximation from the NEC solution and those obtained using relation (5) have also shown an excellent agreement [6]. The results of comparison for the same case of a horizontal wire short-circuited at its both ends are presented in Fig. 4 as a function of the frequency and angle of incidence of the exciting field. Note that the results are practically identical within the resolution accuracy of the drawings.

Other successful tests of the proposed theory were presented in [6] by comparing the results to analytical solutions for the case of simple line configurations, such as an open-circuit semi-infinite line.

2.3 Application: response of a long terminated line to an external plane wave

The solution of the coupling equations for long terminated lines using the proposed asymptotic theory is illustrated here by two examples.

First, let us consider an open-circuited wire of finite length above a perfectly conducting ground (see Fig. 1 in Chapter 4). In this case the exact expressions for the asymptotic coefficients can be obtained analytically using the Wiener–Hopf solution [14] (for the coefficients $R_+ = R_- = R$). They can also be determined using

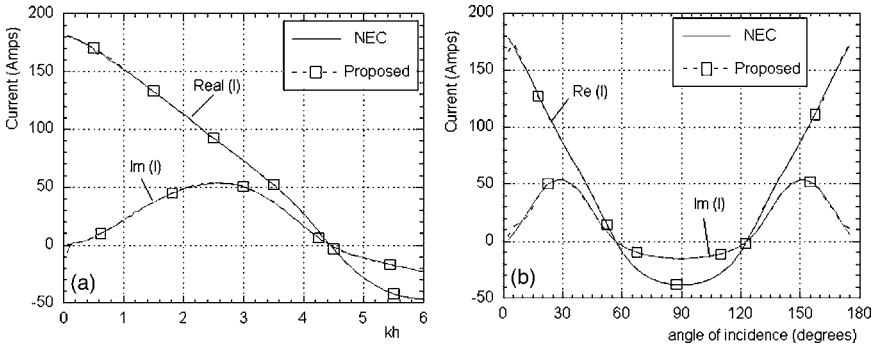

Figure 4: Comparison between the real and imaginary parts of I_0 obtained by a least-square approximation from the NEC solution and those obtained using relation (5), as a function of (a) frequency and (b) the angle of incidence.

the iterative approach of Chapter 4 (see Section 2.4 in Chapter 4 for the coefficients $R_+ = R_- = R$, and Appendix 2 for coefficients C_+ and C_-).

In Fig. 5, we present a comparison between calculation results obtained by the developed asymptotic approach and those obtained numerically using the method of moment (MoM). The height of the wire is 0.5 m, its length L = 16 m, its radius a = 10 mm. The wire is illuminated by a vertically polarized plane wave with amplitude E_0 = 50 kV/m, angle of incidence θ = 45° (φ = 0), and a frequency f = 100 MHz ($kh \approx 1$).

Figure 5 shows a very good agreement between the proposed analytical solution and numerical simulation obtained using the MoM code CONCEPT [22]. On the same figure, we have also plotted the results obtained using TL theory, which does not provide accurate results.

For the general case of arbitrary terminal loads and geometrical configurations, the asymptotic coefficients R and C are determined using a procedure based on the exact solutions of the integral equations for two similar wire configurations, but having a significantly shorter length (as described in Section 2.1). The knowledge of the asymptotic coefficients R and C permits the computation of the current coefficients I_1 and I_2 for any terminal line having the same terminal loads and geometry. In other words, the numerical solution obtained for a relatively short line permits the analytical determination of the solution for any longer line having the same configuration. The aim of the second numerical example is to illustrate the use of the proposed procedure to compute the induced current by an external field on a long loaded line.

Consider a 50 m long line with a radius a = 10 mm, and a height above ground h = 0.5 m. The line is short-circuited at both ends ($Z_1 = 0$, $Z_2 = 0$). The exciting field is a plane wave with E_0 = 50 kV/m, $\theta = 45°$.

Starting from the numerical solutions for the induced current on two similar line configurations with L_1 = 16 m and $L_2 = L_1 + \lambda/2$, we determine the coefficients

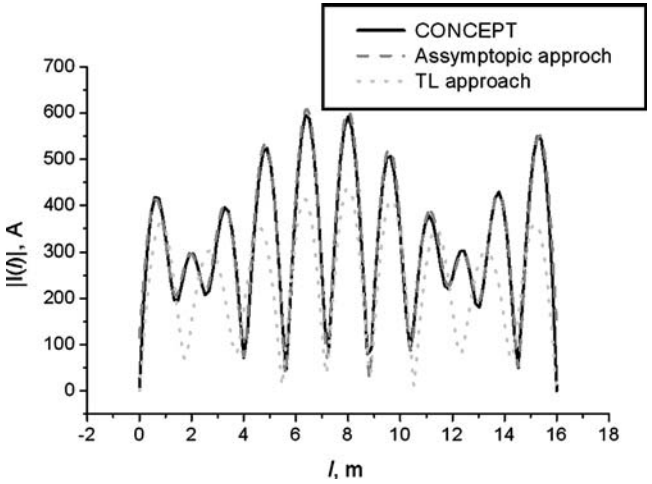

Figure 5: Current induced along an open-circuited line.

$I_1(L_1)$, $I_2(L_1)$, $I_1(L_2)$, $I_2(L_2)$ using the least square method. The scattering coefficients $C_+(j\omega)$, $C_-(j\omega)$, $R_+(j\omega)$, $R_-(j\omega)$, are then computed using eqns (22)–(25) as a function frequency. The results are shown in Fig. 6.

It can be seen that for low frequencies ($kh \ll 1$), the reflection coefficients R_+ and R_- tend to 1, which is the TL current reflection coefficient associated with a short-circuit termination. Additionally the scattering coefficients C_+ and C_- tend to zero at low frequencies.

Let us now define the current distribution, for example, for the frequency $f \cong 358$ MHz ($\lambda = 0.84$ m, $kh = 3.75$). Note that at the considered frequency, the TL approximation is not valid since the wavelength has the same order of magnitude as the line height.

The scattering coefficients C_+, C_-, R_+, R_- for this frequency are as follows:

$$R_+ = R_- = 0.292 - 0.327\,j \tag{36a}$$

$$C_+ = 1.250 - 0.291\,j \tag{36b}$$

$$C_- = -1.004 + 0.402\,j \tag{36c}$$

Using eqns (20) and (21) the coefficients I_1 and I_2 for a 50 m long line can be determined as

$$I_1(L = 50\text{m}) = -65.91 + 16.1\,j \tag{37a}$$

$$I_2(L = 50\text{m}) = 26.25 + 24.28\,j \tag{37b}$$

On the other hand, the coefficient I_0 calculated using eqn (5) is given by

$$I_0 = -48.43 - 4.72\,j \tag{38}$$

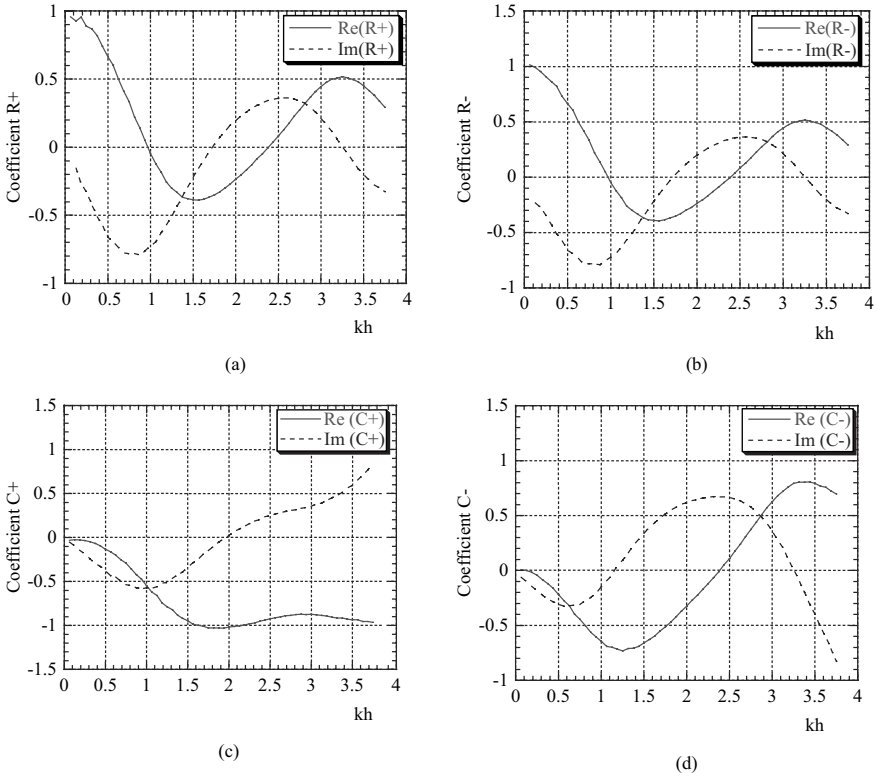

Figure 6: Variation of the coefficients R_+, R_-, C_+, C_-, for the horizontal wire short-circuited by vertical risers, as function of frequency.

The current along the 50 m long line is simply given by eqn (1) with numerical values for the coefficients given by eqns (37) and (38). The results for the induced current in the near end and in the central regions of the line are presented in Fig. 7.

It can be seen that the agreement between the proposed approach and the exact numerical solutions obtained using NEC is very satisfactory. Note that in this figure, as in Figs 3 and 4, the abscissa l corresponds to the coordinate along the whole wire systems, including the vertical risers.

3 Asymptotic approach for a non-uniform transmission line

The asymptotic approach presented in Section 2.4 can be generalized to calculate the current induced by an incident plane wave along a long line, which has a local discontinuity represented by a series lumped impedance Z_L at some intermediate point (see Fig. 8). This problem can describe, for example, a cable with a damaged shield or a shield discontinuity [23].

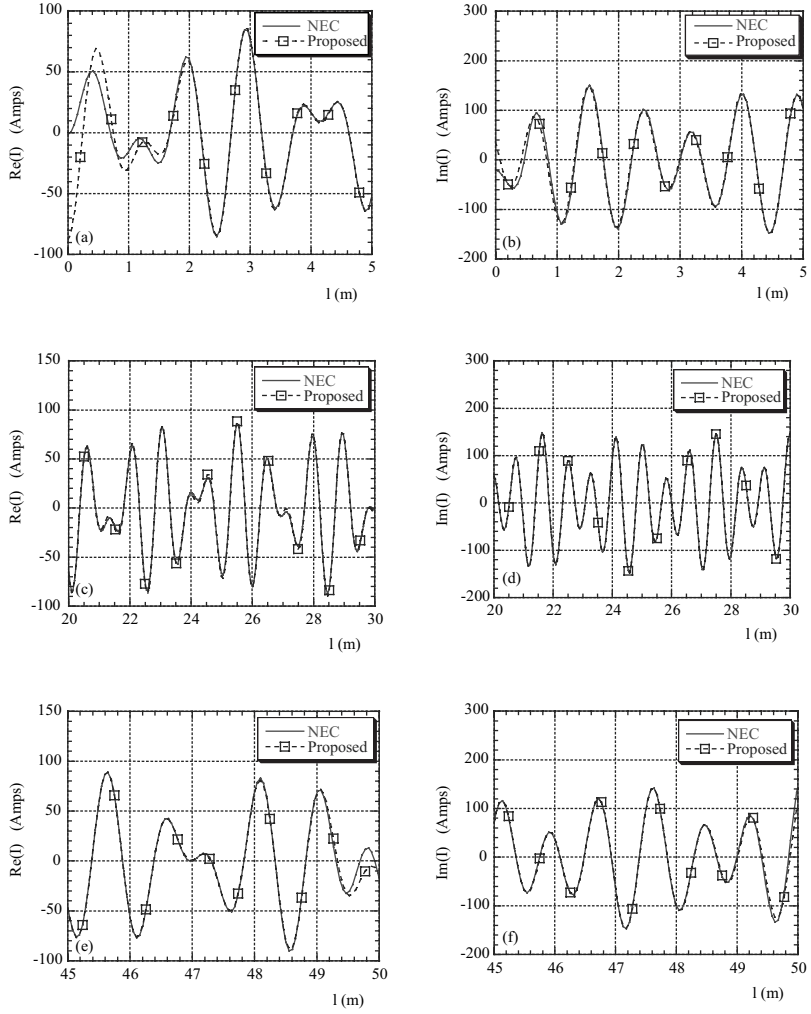

Figure 7: Current spatial distribution along a short-circuited horizontal wire (L = 50 m). Comparison between NEC solutions (solid line) and the proposed asymptotic approach (dashed line): (a and b) current in the left-end region; (c and d) current in the central region; (e and f) current in the right-end region. Left columns: real part; right columns: imaginary part.

Let us first consider an auxiliary problem represented by Fig. 9, where the line is infinitely long. The Pocklington's integral equation, assuming the lumped impedance is placed at the coordinate origin $z = 0$, is given by

$$\frac{1}{4\pi\varepsilon_0 j\omega}\left(\frac{\mathrm{d}^2}{\mathrm{d}\,z^2}+k^2\right)\int_{-\infty}^{\infty} g(z'-z)I(z')\mathrm{d}z' = -E_z^{\mathrm{e}}(h,z)+Z_L I(0)\delta(z) \qquad (39)$$

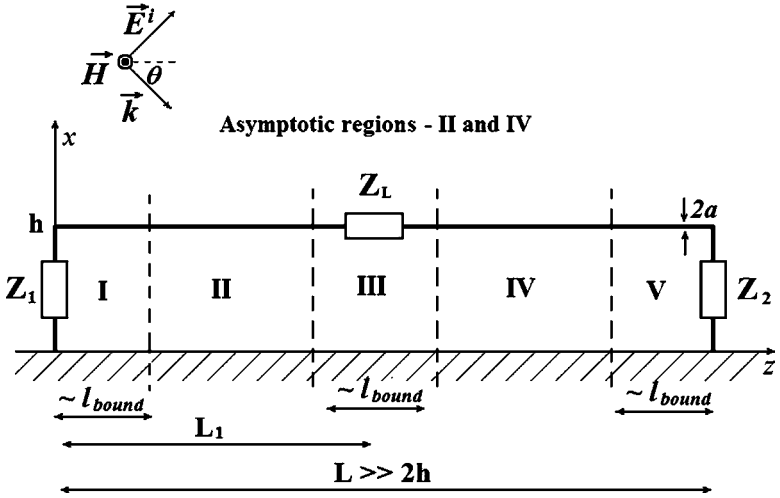

Figure 8: Geometry of the long terminated line with an addition lumped impedance.

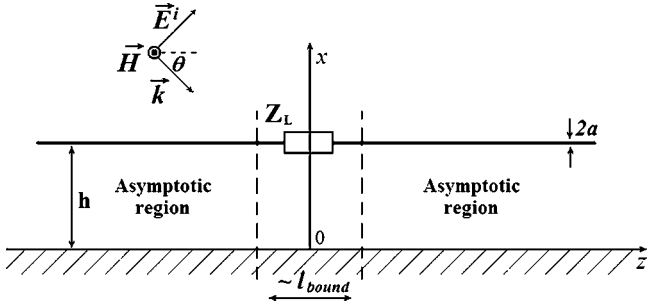

Figure 9: Infinitely long line with additional lumped impedance.

where $g(z)$ is the scalar Green's function given by eqn (3). The lumped impedance, which is usually considered through a boundary condition, is taken into account in eqn (39) as an additional term in the total exiting tangential field E_z^{t}, accounting for the discontinuity at $z = 0$ [24]

$$E_z^{\mathrm{t}} = E_z^{\mathrm{e}} - Z_{\mathrm{L}} I(0)\delta(z) \tag{40}$$

where $I(0)$ is the current in the impedance.

Considering that the integration in eqn (39) is carried out over an infinite interval and that the kernel of the integral-differential equation (39) depends on the difference of arguments $z - z'$, it is possible to find a solution using the spatial Fourier transform.

The general solution for an incident plane wave can be written in the form $I_{\mathrm{m}}^{\mathrm{e}}(z) = I_0\, \psi_{\mathrm{m}}^{\mathrm{e}}(z)$. The subscript m indicates that the scatterer is placed in the main

central region of the line. $\psi_{\mathrm{m}}^{\mathrm{e}}(z)$ is the solution of the non-homogeneous scattering problem in the main central region of the line. Let us also define:

- $\psi_{\mathrm{m},+}^{0}(z)$ as the solution in the central region of the homogeneous (no exciting field) scattering problem for a current (TEM) wave $\exp(jkz)$ incident to the load from ∞; and
- $\psi_{\mathrm{m},-}^{0}(z)$ as the solution in the central region of the homogeneous scattering problem for a current (TEM) wave $\exp(jkz)$ incident to the load from $-\infty$.

Using the spatial Fourier transform and after mathematical manipulations, it can be shown that

$$\psi_{\mathrm{m}}^{\mathrm{e}}(z) = \exp(-jk_1 z) + F_2(z) \tag{41}$$

$$\psi_{\mathrm{m},+}^{0}(z) = \exp(jkz) + F_2(z) \tag{42}$$

$$\psi_{\mathrm{m},-}^{0}(z) = \exp(-jkz) + F_2(z) \tag{43}$$

in which, the function $F_2(z)$ is

$$F_2(z) = -\frac{Z_{\mathrm{L}}[\mathrm{e}^{-jk|z|} + F_1(a/2h, 2kh, z/2h)]}{2Z_{\mathrm{C}} + Z_{\mathrm{L}}[1 + F_1(a/2h, 2kh, 0)]} \tag{44}$$

and $Z_{\mathrm{c}} = \sqrt{\mu_0/\varepsilon_0}(1/2\pi)\ln(2h/a)$ is the characteristic impedance of the line, and the function F_1 is

$$F_1(a, y_0, \xi) = \frac{2y_0}{\pi j}\int_0^{2k_{\max}h}\left[\frac{2\ln(1/a)}{G\left(a, \sqrt{y_0^2 - y^2}\right)} - 1\right]\frac{\cos(y\xi)}{y_0^2 - y^2}\,\mathrm{d}y \tag{45}$$

and

$$G\left(a, \sqrt{y_0^2 - y^2}\right) = \begin{cases} -\pi j\left[H_0^{(2)}\left(a\sqrt{y_0^2 - y^2}\right) - H_0^{(2)}\left(\sqrt{y_0^2 - y^2}\right)\right], & y < y_0 \\ 2\ln(1/a), & y = y_0 \\ 2\left[K_0^{(2)}\left(a\sqrt{y^2 - y_0^2}\right) - K_0^{(2)}\left(\sqrt{y^2 - y_0^2}\right)\right], & y > y_0 \end{cases} \tag{46}$$

It is important to note that the delta-function in eqns (39) and (40) is a mathematical idealization. In reality, the resistive region along the wire has a finite length $\Delta(\Delta \geq a)$. As far as we are not interested here in the detailed structure of this region, it is possible to limit the integration at the corresponding wave number $k_{\max} \approx \pi/2\Delta$. In this way, the integration convergence is ensured.

The z-dependence of the second term in eqns (41)–(43) is similar to that of the current induced by a point voltage source in an infinite wire above a perfectly conducting ground. The corresponding solution can also be easily obtained by the spatial Fourier transform. This problem is a special case of the well-known problem of an infinite wire above a ground of finite conductivity. In [11], a number of papers on this topic were reviewed. Using methods of complex variable functions, it was shown that $F_2(z)$ can be represented as the sum of three terms: a main TEM mode, the sum of eigen modes (or leaky modes), and the so-called radiation mode (the anti-symmetrical current modes in the two wire system are presented and investigated in [12, 13]). An investigation of the z-dependence for the function $F_2(z)$ shows that for distances from the load larger than about $2h$(for $kh <\sim 1$), the transmission line TEM mode $\exp(-jk|z|)$ predominates. Other modes decay with the distance from the scattering load as an inverse power of z (radiation mode) or exponentially (eigen modes), i.e. $F_1(a/2h, 2kh, z/2h) \underset{|z|\to\infty}{\to} 0$.

As a consequence, we can write

$$\psi^{\mathrm{e}}_{\mathrm{m}}(z) = \exp(-jk_1 z) + R_{\mathrm{m}} \exp(-jk\,|z|) \tag{47}$$

$$\psi^{0}_{\mathrm{m},+}(z) = \exp(jkz) + R_{\mathrm{m}} \exp(-jk\,|z|) \tag{48}$$

$$\psi^{0}_{\mathrm{m},-}(z) = \exp(-jkz) + R_{\mathrm{m}} \exp(-jk\,|z|) \tag{49}$$

where R_{m} is the reflection coefficient given by

$$R_{\mathrm{m}} = -\frac{Z_{\mathrm{L}}}{2Z_{\mathrm{C}} + Z_{\mathrm{L}}[1 + F_1(a/2h, 2kh, 0)]} \tag{50}$$

In the low-frequency limit, when $kh << 1$, $F_1(a/2h, 2kh, 0) \to 0$ (see Fig. 10) and the reflection coefficient reduces to the well-known TL approximation, that is $R_{\mathrm{m}} = -Z_{\mathrm{L}}/(2Z_{\mathrm{C}} + Z_{\mathrm{L}})$.

Figure 11 shows the variation of the reflection coefficient as a function of kh. It can be seen that at low frequencies ($kh << 1$), it reduces to the TL value.

Coming back to the finite system of Fig. 8, and according to the asymptotic approach, we will search for a solution for the induced current in the following form.

In regions I and II:

$$I(z) = I_0 \psi^{\mathrm{e}}_{+}(z) + \tilde{I}_1 \psi^{0}_{+}(z) \tag{51}$$

In regions II–IV:

$$I(z) = I_0 \mathrm{e}^{-jk_1 L_1} \psi^{\mathrm{e}}_{\mathrm{m}}(z - L_1) + \tilde{I}_2 \psi^{0}_{\mathrm{m},-}(z - L_1) + \tilde{I}_3 \psi^{0}_{\mathrm{m},+}(z - L_1) \tag{52}$$

where L_1 is the distance from the line left-end to the impedance Z_{L}.

Also, in regions IV and V:

$$I(z) = I_0 \mathrm{e}^{-jk_1 L} \psi^{\mathrm{e}}_{-}(z - L) + \tilde{I}_4 \psi^{0}_{-}(z - L) \tag{53}$$

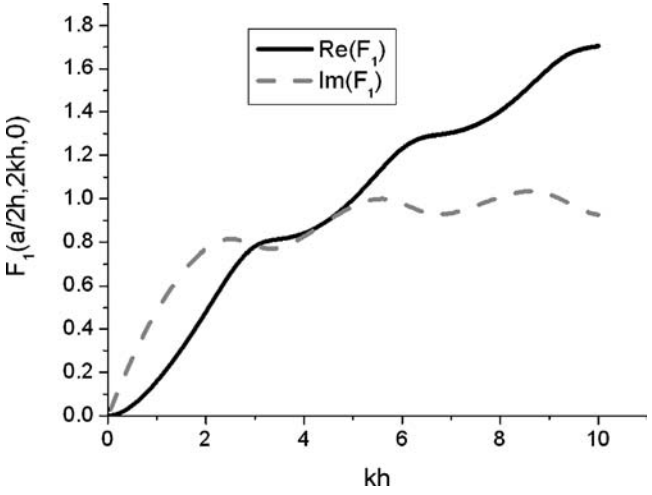

Figure 10: Frequency dependence of the function F_1 ($a/2h$, $2kh$, 0) for $h = 0.5$ m, $a = 0.01$ m, $\Delta = 0.04$ m.

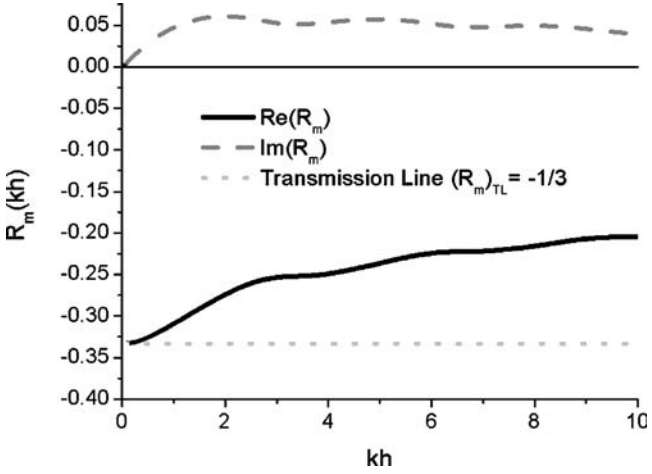

Figure 11: Frequency dependence of the reflection coefficient R_m (kh), eqn (50), for $a/2h = 0.01$, $\Delta = 4a$, $Z_L = Z_C$.

Coefficients $\tilde{I}_1$, $\tilde{I}_2$, $\tilde{I}_3$, $\tilde{I}_4$ in the above equations can be determined considering an asymptotic view of these solutions in regions II, IV by formulas (8), (9), (12), (13), and (47)–(49) and taking into account that in these regions, the solution can be written using the three-term form (eqn (1)). In this way, approximate analytical solutions for the problem of Fig. 8 can be obtained (see Appendix 3).

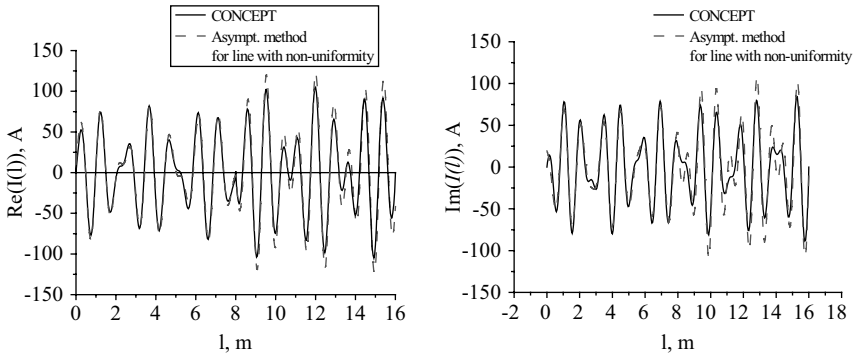

Figure 12: Real and imaginary parts of the induced current along the line. Comparison between the proposed approach and numerical results obtained using MoM.

To illustrate the proposed asymptotic method, let us consider a simple model of an open-end straight wire above a perfectly conducting ground. The height of the wire is $h = 0.5$, its length $L = 16$ m, its radius $a = 10$ mm. The wire is illuminated by a vertically polarized plane wave with an amplitude $E_0 = 50$ kV/m, angle of incidence $\theta = 45°$ ($\varphi = 0$), and a frequency $f = 358$ MHz. The wire contains an impedance at its centre equal to the characteristic impedance of the line, $Z_L = Z_C$. The length of the impedance region is $\Delta = 40$ mm. In Fig. 12, we show a comparison between the proposed asymptotic method (eqns (51)–(53) with asymptotic formulas (8), (9), (12), (13), and (47)–(49)) and numerical results obtained using the MoM code CONCEPT [22], for the real and imaginary parts of the induced current.

The reflection coefficients for the current wave at the ends of the line $R_+ = R_- = R$, C_+, and C_- are obtained using an iterative approach (see Chapter 4 and Appendix 2).

It can be seen that the results obtained using the proposed approach are in excellent agreement with 'exact' numerical results.

4 Conclusion

We presented in this chapter an efficient hybrid method to compute electromagnetic field coupling to a long terminated line. The line can also have a discontinuity in the form of a lumped impedance in its central region. The method is applicable for high-frequency excitation for which the TL approximation is not valid.

In the proposed method, the induced current along the line can be expressed using closed form analytical expressions. These expressions involve scattering coefficients at the line non-uniformities, which can be determined using either approximate analytical solutions, numerical methods (for the scattering in the line near–end regions), or exact analytical solutions (for the scattering at the lumped

impedance in the central region). The proposed approach has been compared with numerical simulations and excellent agreement is found.

Appendix 1: Determination of coefficients R_+, R_-, C_+, C_- as a function of coefficients I_1 and I_2

We start from eqns (20) and (21) re-written below

$$I_1(L) = I_0 \frac{C_- \exp(-jkL - jk_1L) + C_+R_- \exp(-2jkL)}{1 - R_+R_- \exp(-2jkL)} \tag{A1.1}$$

$$I_2(L) = I_0 \frac{C_+ + C_-R_+ \exp(-jkL - jk_1L)}{1 - R_+R_- \exp(-2jkL)} \tag{A1.2}$$

We will first 'decouple' the above equations to obtain the separate equations for R_+, C_+, and for R_-, C_-. To do that, lets us consider the quantities $I_2(L)$–$R_+I_1(L)$ and $I_1(L)$–$R_-I_2(L)\exp(-2jkL)$. After straightforward mathematics, it can easily be shown that

$$I_2(L) - R_+I_1(L) = I_0C_+ \tag{A1.3}$$

$$I_1(L) - R_-I_2(L)\exp(-2jkL) = I_0C_- \exp[-j(k + k_1)L] \tag{A1.4}$$

Now, let us write eqn (A1.3) for two different line lengths

$$I_2(L_1) - R_+I_1(L_1) = I_0C_+ \tag{A1.5}$$

$$I_2(L_2) - R_+I_1(L_2) = I_0C_+ \tag{A1.6}$$

It is easy now to express R_+ and C_+ in terms of I_1 and I_2

$$R_+ = \frac{I_2(L_2) - I_2(L_1)}{I_1(L_2) - I_1(L_1)} \tag{A1.7}$$

$$C_+ = \frac{1}{I_0} \frac{I_2(L_1)I_1(L_2) - I_2(L_2)I_1(L_1)}{I_1(L_2) - I_1(L_1)} \tag{A1.8}$$

Writing eqn (A1.4) for two different line lengths yields

$$I_1(L_1) - R_-I_2(L_1)\exp(-2jkL_1) = I_0C_- \exp[-j(k + k_1)L_1] \tag{A1.9}$$

$$I_1(L_2) - R_-I_2(L_2)\exp(-2jkL_2) = I_0C_- \exp[-j(k + k_1)L_2] \tag{A1.10}$$

And consequently

$$R_- = \frac{I_1(L_2)\exp[j(k + k_1)L_2] - I_1(L_1)\exp[j(k + k_1)L_1]}{I_2(L_2)\exp[j(k_1 - k)L_2] - I_2(L_1)\exp[j(k_1 - k)L_1]} \tag{A1.11}$$

$$C_- = \frac{1}{I_0}\frac{I_1(L_1)I_2(L_2)\exp(2jkL_1) - I_1(L_2)I_2(L_1)\exp(2jkL_2)}{I_2(L_2)\exp[j(k-k_1)L_1] - I_2(L_1)\exp[j(k-k_1)L_2]} \quad \text{(A1.12)}$$

Appendix 2: Derivation of analytical expressions for the coefficients C_+ and C_- for a semi-infinite open-circuited line, using the iterative method presented in Chapter 4

In this appendix, we use the iterative procedure presented in Chapter 4 to derive an approximate analytical expression of the zeroth and the first iteration terms of the asymptotic coefficients C_+ and C_-, for the case of semi-infinite open-circuited line (for a right semi-infinite line (Fig. 2b), the geometry is identical to the one shown in Fig. 1 of Chapter 4, with $L \to \infty$). The system is excited by a vertically polarized external electromagnetic wave with an elevation angle θ. The azimuth angle of incidence is assumed to be zero, $\varphi = 0$. For the right semi-infinite line the solution in the asymptotic region $z >> 2h$ can be expressed as (see Section 2.1.1)

$$I_+^e(z) \underset{z>>2h}{\approx} I_0(\exp(-jk_1z) + C_+\exp(-jkz)) \quad \text{(A2.1)}$$

where $k = \omega/c$, $k_1 = k\cos\theta$ and I_0 is the current induced on an infinite line, given by the expression (A2.2), which can easily be derived (see eqn (53) in Chapter 4)

$$I_0(j\omega) = \frac{4cE_z^e(j\omega)}{\eta_0\omega\sin^2\theta(H_0^{(2)}(ka\sin\theta) - H_0^{(2)}(2kh\sin\theta))} \quad \text{(A2.2)}$$

where $E_z^e(j\omega)$ is the total exciting (incident + ground-reflected) tangential electric field, $H_0^{(2)}(x)$ is the zero order Hankel function of the second kind [25], $\eta_0 = \sqrt{\mu_0\varepsilon_0}$.

The zeroth iteration term of the perturbation theory, which is determined by the TL approximation and which satisfies the open-circuit boundary condition for $z = 0$, is given by

$$I_{+,0}^e(z) = I_{0,0}(\exp(-jk_1z) - \exp(-jkz)) \quad \text{(A2.3)}$$

in which $I_{0,0}$ is the induced current on an infinite line calculated using TL approximation [20] (eqn (58) in Chapter 4)

$$I_{0,0} = \frac{E_z^e(h,\omega)}{\mu_0/2\pi\ln(2h/a)j\omega}\frac{1}{\sin^2\theta} \quad \text{(A2.4)}$$

We will derive now an expression for the first iteration term $I_1(z)$ using the general equation of the perturbation theory for the nth iteration term (eqn (40) from Chapter 4) which reduces, for the right semi-infinite line ($0 \le z < \infty$, $k \to k - j\delta$, $\delta \to 0$), to the following expression:

$$I_{+,n}^e(z) = F_{n-1}(z) - F_{n-1}(0)\exp(-jkz) \quad \text{(A2.5)}$$

Using the general equation for the function $F_n(z)$ (eqn (41) from Chapter 4) and making use of eqn (A2.3), we can obtain the expression for the function $F_0(z)$ for the first iteration

$$F_0(z) = I_{0,0}[\mathrm{e}^{-jk_1 z} - \mathrm{e}^{-jkz}] - \frac{I_{0,0}}{2\ln(2h/a)} \int_0^{\infty} \left[\frac{\mathrm{e}^{-jk\sqrt{(z-z')^2+a^2}}}{\sqrt{(z-z')^2+a^2}} - \frac{\mathrm{e}^{-jk\sqrt{(z-z')^2+4h^2}}}{\sqrt{(z-z')^2+4h^2}} \right] \left[\mathrm{e}^{-jk_1 z'} - \mathrm{e}^{-jkz'} \right] \mathrm{d}z' \tag{A2.6}$$

For small arguments, eqn (A2.6) yields

$$F_0(0) = -I_{0,0} D_1 \tag{A2.7}$$

in which

$$D_1 \approx \frac{1}{2\ln(2h/a)} \int_0^{\infty} \left[\frac{\exp(-jk\xi)}{\xi} - \frac{\exp\left(-jk\sqrt{\xi^2+4h^2}\right)}{\sqrt{\xi^2+4h^2}} \right] \left[\mathrm{e}^{-jk_1\xi} - \mathrm{e}^{-jk\xi} \right] \mathrm{d}\xi \tag{A2.8}$$

And, for large arguments $z \to \infty$, we get

$$F_0(z) \underset{z\to\infty}{=} I_{0,0} \exp(-jk_1 z) D_2 \tag{A2.9}$$

where

$$D_2 = \frac{\pi j}{2\ln(2h/a)} \left[1 - \frac{2j}{\pi} \ln(\gamma kh \sin\theta) - H_0^{(2)}(2kh\sin\theta) \right] \tag{A2.10}$$

To obtain the large argument expressions (A2.9) and (A2.10), we have used the integral (eqn (51)) from Chapter 4 and the well-known formula from the theory of Bessel functions [25]

$$H_0^{(2)}(z) \underset{z\to 0}{\approx} 1 - \frac{2j}{\pi} \ln(\gamma z/2), \quad \text{where } \gamma = 1.781\ldots \tag{A2.11}$$

The knowledge of function F_0 for $z = 0$ and $z \to \infty$ makes it possible to obtain a closed-form solution in the asymptotic region $z >> 2h$ for the first iteration term of the induced current $I_1(z)$. Using eqns (A2.5), (A2.7), and (A2.9), we get

$$I_{+,1}^{\mathrm{e}}(z) \underset{z\to\infty}{\approx} I_{0,0}[D_2 \exp(-jk_1 z) + D_1 \exp(-jkz)] \tag{A2.12}$$

The total induced current in the asymptotic region is then given by

$$\begin{aligned} I_{+}^{\mathrm{e}}(z) &\approx I_{+,0}^{\mathrm{e}}(z) + I_{+,1}^{\mathrm{e}}(z) \underset{z\to\infty}{\approx} I_{0,0}\{(1+D_2)\exp(-jk_1 z) + (D_1 - 1)\exp(-jkz)\} \\ &= I_{0,0}(1+D_2)\{\exp(-jk_1 z) + (D_1 - 1)(1+D_2)^{-1}\exp(-jkz)\} \end{aligned} \tag{A2.13}$$

Now using eqns (A2.2) and (A2.11), and assuming $D_2 << 1$ we can write for the current amplitude

$$I_0 \approx I_{0,0}\frac{1}{1-D_2} \approx I_{0,0}(1+D_2) \tag{A2.14}$$

and eqn (A2.13) becomes

$$I_+^{\mathrm{e}}(z) \cong I_0\{\exp(-jk_1z) + (D_1-1)(1+D_2)^{-1}\exp(-jkz)\} \tag{A2.15}$$

Expanding in terms of $[2\ln(2h/a)]^{-1}$ and taking the two first terms, the coefficient $(D_1 - 1)(1 + D_2)^{-1}$ in eqn (A2.15) reduces to $(D_1 + D_2 - 1)$, and eqn (A2.15) becomes

$$I_+^{\mathrm{e}}(z) \cong I_0\{\exp(-jk_1z) + (D_1+D_2-1)\exp(-jkz)\} \tag{A2.16}$$

The coefficient C_+ may be obtained by identification of eqns (A2.1) and (A2.16)

$$C_+ \approx -1 + D_1 + D_2 \tag{A2.17}$$

The coefficient C_- can be determined in a similar way considering a semi-infinite line $-\infty < z \le 0$, for which the current in the asymptotic region $z << -2h$ is given by

$$I_-^{\mathrm{e}}(z) \underset{z<<2h}{\approx} I_0(\exp(-jk_1z) + C_-\exp(jkz)) \tag{A2.18}$$

It can be easily shown, following similar mathematical development, that the expression for C_- is the same as for C_+, eqn (A2.17), but replacing k_1 by $-k_1$ in eqns (A2.8) and (A2.10).

A comparison of the frequency dependence of the asymptotic current coefficient $C(j\omega)$ for an open-circuit semi-infinite line under normal incidence ($C_+ = C_- = C$) obtained by the proposed asymptotic method (Section 2.1.1) and the one derived by iteration method (eqn (A2.17)) is presented in Fig. A2.1, and again, a very good agreement is found.

Appendix 3: Analytical expression for the induced current along the asymptotic region of the line containing a lumped impedance

Let us consider the solution for the current in the asymptotic regions II and IV (see Fig. 7).

In region II, starting from the left end of the line, using the expression (51) and taking into account the asymptotic representation (eqns (8) and (12)), we will get

$$\begin{aligned} I(z) &= I_0\psi_+^{\mathrm{e}}(z) + \tilde{I}_1\psi_+^0(z) \\ &\underset{z>>2h}{\cong} I_0[\exp(-jk_1z) + C_+\exp(-jkz)] + \tilde{I}_1[\exp(jkz) + R_+\exp(-jkz)] \\ &= I_0\exp(-jk_1z) + \tilde{I}_1\exp(jkz) + [C_+ + \tilde{I}_1R_+]\exp(-jkz) \end{aligned} \tag{A3.1}$$

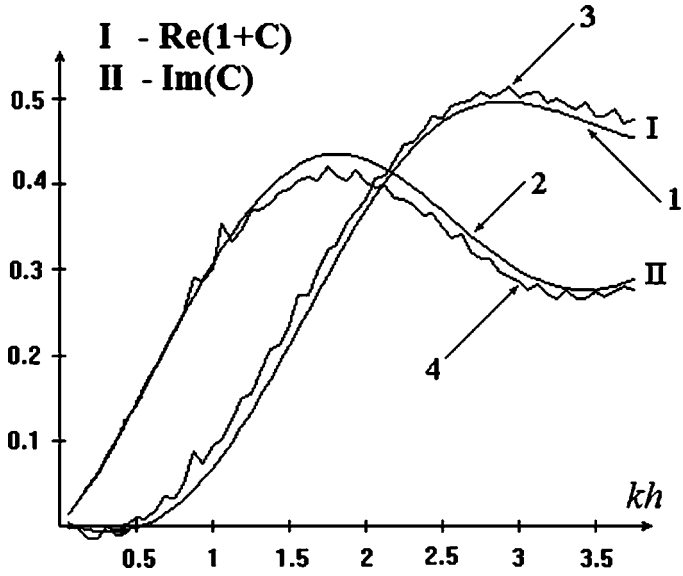

Figure A2.1: Comparison of asymptotic coefficient for an open-circuit semi-infinite line obtained by iteration theory (curves 1 and 2) and the one derived by the asymptotic theory (curves 3 and 4). Normal incidence.

Now, starting from the centre of the line, using expression (52), and taking into account the asymptotic representation (eqns (47)–(49)), we will get

$$
\begin{aligned}
I(z) &= I_0 \mathrm{e}^{-jk_1 L} \psi_{\mathrm{m}}^{\mathrm{e}}(z-L_1) + \tilde{I}_2 \psi_{\mathrm{m},-}^{0}(z-L_1) + \tilde{I}_3 \psi_{\mathrm{m},+}^{0}(z-L_1) \\
&\underset{L_1 - z \gg 2h}{\cong} I_0 \mathrm{e}^{-jk_1 L_1} [\mathrm{e}^{-jk_1(z-L_1)} + R_{\mathrm{m}} \mathrm{e}^{jk(z-L_1)}] + \tilde{I}_2 \, [\mathrm{e}^{-jk(z-L_1)} + R_{\mathrm{m}} \mathrm{e}^{jk(z-L_1)}] \\
&\quad + \tilde{I}_3 \, [\mathrm{e}^{jk(z-L_1)} + R_{\mathrm{m}} \, \mathrm{e}^{jk(z-L_1)}] \\
&= I_0 \mathrm{e}^{-jk_1 z} + [I_0 R_{\mathrm{m}} \mathrm{e}^{-jk_1 L_1} + \tilde{I}_2 R_{\mathrm{m}} + \tilde{I}_3 (1 + R_{\mathrm{m}})] \, \mathrm{e}^{jk(z-L_1)} + \tilde{I}_2 \mathrm{e}^{-jk(z-L_1)}
\end{aligned}
\tag{A3.2}
$$

As it can be seen from eqns (A3.1) and (A3.2), the solution in the asymptotic region is given in the form of the proposed three-term approximation (1). By imposing that the coefficients for the terms exp(*jkz*) and exp(–*jkz*) are identical in eqns (A3.1) and (A3.2), we obtain two equations to determine the unknown coefficients $\tilde{I}_1$, $\tilde{I}_2$, and $\tilde{I}_3$

$$
\tilde{I}_1 = I_0 R_{\mathrm{m}} \mathrm{e}^{-j(k+k_1)L_1} + \tilde{I}_2 R_{\mathrm{m}} \mathrm{e}^{-jkL_1} + \tilde{I}_3 (1 + R_{\mathrm{m}}) \mathrm{e}^{-jkL_1} \tag{A3.3}
$$

$$
I_0 C_+ + \tilde{I}_1 R_+ = \tilde{I}_2 \mathrm{e}^{jkL_1} \tag{A3.4}
$$

In a similar way, using the expressions for region IV, we can obtain two other equations for the unknown coefficients $\tilde{I}_1$, $\tilde{I}_2$, $\tilde{I}_3$, and $\tilde{I}_4$

$$\tilde{I}_3 e^{-jkL_1} = I_0 C_- e^{-j(k+k_1)L} + \tilde{I}_4 R_- e^{-jkL} \tag{A3.5}$$

$$I_0 R_m e^{j(k-k_1)L_1} + \tilde{I}_2 e^{jkL_1}(1+R_m) + \tilde{I}_3 e^{jkL_1} R_m = \tilde{I}_4 e^{jkL} \tag{A3.6}$$

The final solutions for the system of eqns (A3.3)–(A3.6) are given by

$$\begin{aligned}\tilde{I}_2 = I_0\{&(1-R_-R_m e^{-2jkL_2})(C_+ e^{-jkL_1} + R_+ R_m e^{-jk_1L_1-2jkL_1}) \\ &+ R_+(1+R_m)e^{-2jkL_1}(C_- e^{-jk_1L-jkL_2} + R_- R_m e^{-jk_1L_1-2jkL_2})\} \\ &\times\{(1-R_+R_m e^{-2jkL_1})(1-R_-R_m e^{-2jkL_2}) - R_+R_-(1+R_m)^2 e^{-2jkL}\}^{-1}\end{aligned} \tag{A3.7}$$

$$\begin{aligned}\tilde{I}_3 = \tilde{I}_0\{&(1-R_+R_m e^{-2jkL_1})(C_- e^{-jk_1L-jkL_2} + R_- R_m e^{-jk_1L_1-2jkL_2}) \\ &+ R_-(1+R_m)e^{-2jkL_2}(C_+ e^{-jkL_1} + R_+ R_m e^{-jk_1L_1-2jkL_1})\} \\ &\times\{(1-R_+R_m e^{-2jkL_1})(1-R_-R_m e^{-2jkL_2}) - R_+R_-(1+R_m)^2 e^{-2jkL}\}^{-1}\end{aligned} \tag{A3.8}$$

$$\tilde{I}_1 = (\tilde{I}_2 e^{jkL_1} - I_0 C_+)A_+^{-1} \tag{A3.9}$$

$$\tilde{I}_4 = (\tilde{I}_3 e^{jkL_2} - I_0 C_- e^{-jk_1L})A_+^{-1} \tag{A3.10}$$

where $L_2 = L - L_1$ in eqns (A3.7) and (A3.8).

Using the above coefficients, the induced current in the asymptotic regions will be given by

In region II:

$$I(z) = I_0 e^{-jk_1z} + I_1 e^{jkz} + I_2 e^{-jkz} \tag{A3.11}$$

In region IV:

$$I(z) = I_0 e^{-jk_1z} + I_3 e^{jkz} + I_4 e^{-jkz} \tag{A3.12}$$

where

$$I_1 = \tilde{I}_1 \tag{A3.13}$$

$$I_2 = I_0 C_+ + \tilde{I}_1 R_+ \tag{A3.14}$$

$$I_3 = I_0 C_- e^{-jk(k+k_1)L} + \tilde{I}_4 R_- e^{-jkL} \tag{A3.15}$$

$$I_4 = \tilde{I}_4 e^{jkL} \tag{A3.16}$$

References

[1] Tesche, F.M., Comparison of the transmission line and scattering models for computing the NEMP response of overhead cables. *IEEE Trans. on Electromagnetic Compatibility*, **34(2)**, pp. 93–99, 1992.

[2] Bridges, G.E.J. & Shafai, L., Plane wave coupling to multiple conductor transmission line above lossy earth. *IEEE Trans. on Electromagnetic Compatibility*, **31(1)**, pp. 21–33, February 1989.

[3] Tkatchenko, S., Rachidi, F. & Ianoz, M., A time domain iterative approach to correct the transmission line approximation for lines of finite length. *Int. Symposium on Electromagnetic Compatibility, EMC '94 Roma*, 13–16 September 1994.

[4] Tkatchenko, S., Rachidi, F. & Ianoz, M., Electromagnetic field coupling to a line of finite length: theory and fast iterative solutions in frequency and time domains. *IEEE Trans. on Electromagnetic Compatibility*, **37**(4), pp. 509–518, 1995.

[5] Tkatchenko, S., Rachidi, F., Ianoz, M. & Martynov, L.M., Exact field-to-transmission line coupling equations for lines of finite length. *Int. Symposium on Electromagnetic Compatibility*, *EMC '96 Roma*, 17–20 September 1996.

[6] Tkatchenko, S., Rachidi, F., Ianoz, M. & Martynov, L., An asymptotic approach for the calculation of electromagnetic field coupling to long terminated lines. *Int. Symposium on Electromagnetic Compatibility, EMC'98 ROMA*, pp. 605–609, 14–18 September 1998.

[7] Agrawal, A.K., Price, H.J. & Gurbaxani, S.H., Transient response of multiconductor transmission lines excited by a nonuniform electromagnetic field. *IEEE Trans. on Electromagnetic Compatibility*, **EMC-22(2)**, pp. 119–129, 1980.

[8] Markov, G.T. & Chaplin, A.F., *The Excitation of Electromagnetic Waves*, Radio i Sviaz: Moscow, 1983 (in Russian).

[9] Nitsch, J. & Tkachenko, S., Complex-valued transmission-line parameters and their relation to the radiation resistance. *IEEE Transaction on Electromagnetic Compatibility*, **EMC-47**(3), pp. 477–487, 2004.

[10] Nitsch, J. & Tkachenko, S., Telegrapher equations for arbitrary frequencies and modes-radiation of an infinite, lossless transmission line. *Radio Science*, **39**, RS2026, doi:10.1029/2002RS002817, 2004.

[11] Olsen, R.G., Young, G.L. & Chang, D.C., Electromagnetic wave propagation on a thin wire above earth. *IEEE Transaction on Antennas and Propagati*on, **AP-48**(9), pp. 1413–1419, 2000.

[12] Marin, L., Transient electromagnetic properties of two parallel wires. *Sensor and Simulation Notes*, Note 173, March 1973.

[13] Leviatan, Y. & Adams, A.T., The response of two-wire transmission line to incident field and voltage excitation including the effects of higher order modes. *IEEE Transactions on Antennas and Propagation*, **AP-30(5)**, pp. 998–1003, September 1982.

[14] Weinstein, L.A., *The Theory of Diffraction and the Factorization Method*, Chapter VI, Golem, 1969.
[15] Collin, R.E., *Field Theory of Guided Waves*, IEEE Press: New York, 1991.
[16] Nitsch, J. & Tkachenko, S., Source dependent transmission line parameters – plane wave vs TEM excitation. *IEEE International Symposium on Electromagnetic Compatibility*, Istanbul, Turkey (CD), 11–16 May 2003.
[17] Tkachenko, S., Rachidi, F. & Ianoz, M., High-frequency electromagnetic field coupling to long terminated lines. *IEEE Transaction on Electromagnetic Compatibility*, **43(2)**, pp. 117–129, 2001.
[18] Tkachenko, S., Rachidi, F., Nitsch, J. & Steinmetz, T., Electromagnetic field coupling to non-uniform transmission lines: treatment of discontinuities. *15th Int. Zurich Symposium on EMC*, Zurich, pp. 603–607, 2003.
[19] Tesche, F.M., Ianoz, M. & Karlsson, T., *EMC Analysis Methods and Computational Models*, John Willey and Sons: New York, October 1996.
[20] Vance, E.F., *Coupling to Shielded Cables*, Wiley: New York, 1978.
[21] Burke, G.J., Poggio, A.J., Logan, I.C. & Rockway, J.W., Numerical electro-magnetics code – a program for antenna system analysis. *International Symposium on Electromagnetic Compatibility*, Rotterdam, May 1979.
[22] Singer, H., Brüns, H.-D., Mader, T., Freiberg, A. & Bürger, G.: CONCEPT II User Manual. *TUHH*, 1997.
[23] Rachidi, F., Tesche, F.M. & Ianoz, M., Electromagnetic coupling to cables with shield interruptions. *12th Int. Symp. on EMC*, Zurich, February 1997.
[24] Leontovich, M. & Levin, K. On the theory of excitation of oscillations in wire antennas. *Journal of Technical Physics*, **XIV(9)**, pp. 481–506, 1946 (in Russian).
[25] Abramowitz, M. & Stegun, I., *Handbook of Mathematical Functions*, Dower publications: New York, 1970.

CHAPTER 6

Transmission line models for high-speed conventional interconnects and metallic carbon nanotube interconnects

A.G. Chiariello[1], A. Maffucci[2], G. Miano[1] & F. Villone[2]
[1]*DIEL, Università di Napoli Federico II, Italy.*
[2]*DAEIMI, Università di Cassino, Italy.*

Abstract

The transmission line is a powerful model to describe in a simple and accurate way the propagation of electric signals along interconnects of different kind. The 'standard' transmission line (STL) model is derived under a series of assumptions involving both the physical structures and the carried signals, which are satisfied for a large amount of cases of practical interest. Nowadays the signal speed is growing rapidly due to market requirements and progress in technology. As the velocity of the electrical signals increases, high-frequency effects due to dispersion and radiation losses, which the STL model is unable to describe, are no more negligible.

In the future large scale integration electronics the interconnect cross-sections will become smaller and smaller down to nanometric dimensions. As interconnect sizes shrink copper resistivity increases due to grain and surface scattering effects and wires become more and more vulnerable to electro-migration due to the higher current densities that must be carried. In order to overcome these limitations the use of metallic carbon nanotubes (CNTs) as interconnects has been proposed and discussed recently.

Here both an 'enhanced' transmission line model able to describe the high-frequency effects due to dispersion and radiation losses in conventional high-speed interconnects and a new transmission line model for metallic CNT interconnects are reviewed. Some applications to interconnects of particular interest in present high-speed electronics and in future nanoelectronics are presented.

1 Introduction and historical background

The transmission of electric signals through metallic wires is one of the most important contributions to the development of modern technology. S.F.B. Morse

invented the electric telegraph in 1838 and the first commercial telegraph line was erected in 1844, between New York, Baltimore and Washington. Nevertheless, at that time the theory of electric circuits was still at its dawn and hardly anything was known about the transmission of electric signals along conducting wires. The paper in which G. Kirchhoff formulated his well-known laws has been published in 1845.

The rapid development of telegraphic signal transmission by means of overland lines and undersea cables (the first undersea cable was laid between France and England in 1851 and in 1853 the first transatlantic cable was installed) gave rise to a long series of theoretical investigations on the transmission of electrical signals through conducting wires.

Lord Kelvin (1855) studied the effects of transients in telegraphic signal transmission through long cables and formulated the first distributed parameter model for an electric cable. He assumed that the effects of magnetic field were negligible, and modeled the effects of electric induction by means of the per-unit-length (p.u.l.) capacitance of the cable and the lossy effects by means of the p.u.l. resistance, so deriving the well-known voltage diffusion equation (Lord Kelvin, 1855).

Shortly after Kirchhoff (1857), using Weber's electromagnetic theory [1], analyzed the transmissions of electric signals through two wires with finite conductivity, including the effects of the magnetic field, and obtained what we can define as the first transmission line model [2]. He deduced that the electric signals propagate along the conductors with the same velocity as that which light propagates in the vacuum, several years before Maxwell published his fundamental paper demonstrating the electromagnetic nature of light [3]. Unfortunately, for reasons that are still not fully clear, Kirchhoff's work has never been widely acknowledged and is even today largely unknown. There is an interesting work by Ferraris in which Kirchhoff's model is reviewed and studied in depth [4].

O. Heaviside (1881–87) was the first to study the 'guided' propagation of electric signals along couples of rectilinear and parallel conducting wires, with finite conductivity, immersed in a lossy homogeneous dielectric, using Maxwell's electromagnetic theory. He developed the transmission line theory as it is still known today [5]. Hereafter, the Heaviside transmission line model is called the 'standard' transmission line (STL) model.

Kirchhoff obtained his transmission line model starting with an integral formulation of the problem based on Weber's theory of electromagnetism. This theory is based on interaction at distance, described by two variables that can be considered as a forerunner of the electric scalar potential and the magnetic vector potential. Heaviside, instead, obtained his transmission line model starting from a formulation based directly on Maxwell's field theory under the assumption that the configuration of the electromagnetic field is quasi-transverse electromagnetic (TEM).

The STL model has since been extended to interconnects, even non-uniform ones, with many wires, in the presence of conducting planes and non-homogeneous dielectrics. The reader is referred to many excellent books and reviews existing in the literature for a complete and comprehensive treatment of the subject [5–8].

The STL model for conventional interconnects is based on the assumptions that:

- The interconnect quasi-parallel wires are metals, whose electrical behavior is governed by Ohm's law;
- The structure of the electromagnetic field surrounding the wires is of quasi-TEM type with respect to the wire axis;
- The total current flowing through each transverse section is equal to zero.

A TEM field structure is one in which the electric and magnetic fields in the space surrounding the conductors are transverse to the wire axis. The TEM fields are the fundamental modes of propagation of ideal multiconnected guiding structures, i.e. guiding structures with transverse section uniform along the wire axis, made by perfect conductors and embedded in a homogeneous medium [6, 8]. In actual interconnects the electromagnetic field is never exactly of the TEM type. In ideal shielded guiding structures, high-order non-TEM modes with discrete spectra can propagate as well as the TEM fundamental modes. In unshielded guiding structures there are also non-TEM propagating modes with continuous spectra. Actual guiding structures are most frequently embedded in a transversally non-homogeneous medium, and thus TEM modes cannot exist. However, even if the medium were homogeneous, due to the losses, the guiding structure could not support purely TEM modes. Furthermore, the field structure is complicated by the influence of non-uniformities present along the axis of the guiding structures (bends, crossovers, etc.). However, when the cross-sectional dimensions of the guiding structure are smaller than the smallest characteristic wavelength of the electromagnetic field propagating along it, the transverse components of the electromagnetic field give the 'most significant' contribution to the overall field and to the resulting terminal voltages and currents [9]. In other words, we have that the structure of the electromagnetic field is said to be of quasi-TEM type.

Nowadays, the speed of electronic signals is growing rapidly due to market requirements and to progress in technology, e.g. allowing switching times below 1 ns. Because of such high-speed signals the distance between the wires of interconnects existing at various levels in an electronic circuit may become comparable with the smallest characteristic wavelength of the signal themselves. As a consequence high-frequency effects such as dispersion and radiation losses are no more negligible and there is the need of a new model to describe the propagation of the signals along the interconnects.

Several efforts have been made to obtain generalized transmission line models from a full-wave analysis based on integral formulations to overcome the restrictions of the STL model [10–17]. Recently, the authors [18–20] have proposed an 'enhanced' transmission line (ETL) model derived from a full-wave analysis based on an integral formulation of the electromagnetic field equations, which has the same simplicity and structure as the STL model. The ETL model describes the propagation along interconnects in frequency ranges where the STL model fails, taking into account the shape effects of the transverse cross-section of the interconnect wires. It reduces to the STL model in the frequency ranges, where the distance between wires is electrically short. Specifically, the ETL model allows to

forecast phenomena that the STL model cannot foresee, such as the distortion introduced by the non-local nature of the electromagnetic interaction along the conductors, and the attenuation due to radiation losses in the transverse direction. Furthermore, the ETL model describes adequately both the propagation of the differential mode and the propagation of the common mode and the mode conversion. The ETL model considers thick quasi-perfect conducting wires and evaluate correctly the kernel that shows the logarithmic singularity that is typical of the surface distributions. Such a singularity plays a very important role in the radiation problems, e.g. it may regularize the numerical models [21, 22]. The approach on which the ETL model is based bears a resemblance to the Kirchhoff approach [2].

The STL model can be easily enhanced so to describe non-perfect conductors, provided that they satisfy Ohm's law, as for instance copper does. Unfortunately, in future ultra-large-scale integrated circuits some problems will arise from the behavior of the copper interconnects. As the cross-section shrinks to nanometric dimensions, due to surface scattering, grain boundary scattering and electromigration, the copper resistivity rises to values higher than its bulk value. Because of heating, these high values will limit the maximum allowed current density. Nanometric copper conductors also suffer from the additional problem of mechanical stability. Carbon nanotubes (CNTs) are allotropes of carbon that have been discovered fairly recently [23] and are considered as an alternative to conventional technology for future nanoelectronic applications such as transistors, antennas, filters and interconnects [24, 25]. Metallic CNTs have been suggested to replace copper in nano-interconnects [26–28], due to their unique electrical, mechanical and thermal properties, such as the high-current density allowed (up to 10^{10} A/cm^2) which is three order of magnitude higher than the one of copper, the thermal conductivity as high as that of diamond, and the long mean free path (ballistic transport along the tube axis). Recently, the authors [29–31] have proposed a transmission line model to describe the propagation of electrical signals along metallic single wall CNT interconnects.

In this chapter, both the ETL model and the transmission line model for metallic CNT interconnects are reviewed. In Section 2, the derivation of transmission line models from a general integral formulation of the electromagnetic problem is presented. Section 3 is devoted to the transmission line model representation of conventional interconnects, like wire pairs or microstrips. In Section 4, the transmission line model for the propagation along metallic CNTs is presented. Finally, in Section 5 some case-studies are carried out showing either qualitative or quantitative analysis of the behavior of conventional and CNT interconnects.

2 General integral formulation and derivation of transmission line models

2.1 Integral formulation

Let us consider an interconnect made of N conductors of generic cross-sections, with parallel axis $\hat{x}$ and total length l, as depicted in Fig. 1, where the y–z plane

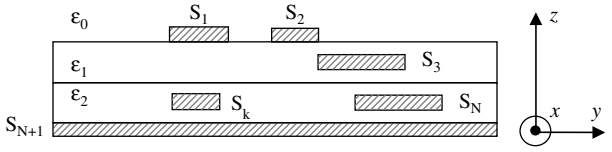

Figure 1: Generic cross-section of a multilayered interconnect.

is shown. A perfect conductor ground is located at $x = 0$ and a stratified inhomogeneous dielectric is considered, made by several dielectric layers with relative permittivity ε_k. Let S_k be the boundary surface of the kth conductor, and l_k be its contour at any given cross-section x = const. (s_k is the curvilinear abscissa along l_k). We assume that a sinusoidal steady state is reached, and that the operating frequencies and the geometrical dimensions are such that the current density is mainly located on the conductor surfaces S_j. In the frequency domain, the Faraday–Neumann law relates the electric to the magnetic field as:

$$\nabla \times \mathbf{E} = -i\omega\mathbf{B}, \tag{1}$$

where ω is the radian frequency. In order to automatically solve (1) and to impose the solenoidality of $\mathbf{B}$, implied by eqn (1) itself, we can introduce the *magnetic vector potential* $\mathbf{A}$ and the *electric scalar potential* φ such that:

$$\mathbf{E} = -i\omega\mathbf{A} - \nabla\varphi, \quad \mathbf{B} = \nabla \times \mathbf{A}. \tag{2}$$

The potentials $\mathbf{A}$ and φ are not uniquely defined, unless a suitable gauge condition is imposed. In the present derivation we will use the so-called *Lorenz gauge*

$$\nabla \cdot \mathbf{A} + i\omega\varepsilon\mu\varphi = 0, \tag{3}$$

which is imposed in homogeneous regions, i.e. in regions where the dielectric permittivity ε and the magnetic permeability μ are constant. Note that at the interfaces between homogeneous regions we have to impose the continuity of the tangential components of the fields.

The sources of the electromagnetic field are the (superficial) current and charge densities $\mathbf{J}_s$ and σ_s, which must satisfy the charge conservation law:

$$\nabla_s \mathbf{J}_s + i\omega\sigma_s = 0, \tag{4}$$

where (∇_s) is the surface divergence operator. These sources may be related to the potentials through the *Green functions* defined for the domain of interest:

$$\mathbf{A}(\mathbf{r}) = \mu_0 \iint_S G_A(\mathbf{r},\mathbf{r}')\mathbf{J}_s(\mathbf{r}')\,\mathrm{d}S, \tag{5}$$

$$\varphi(\mathbf{r}) = \frac{1}{\varepsilon_0} \iint_S G_\varphi(\mathbf{r},\mathbf{r}')\sigma_s(\mathbf{r}')\,\mathrm{d}S, \tag{6}$$

where ε_0 and μ_0 are the dielectric constant and the magnetic permeability in the vacuum space, S represents the union of all the N conductor surfaces S_j. Note that the Green function G_A is in general dyadic.

In order to derive a multiport representation of the interconnect, we assume that it would be possible to characterize it regardless of the actual devices on which it is terminated. In other words, the terminal elements are taken into account only through the relations that they impose on the terminal currents and voltages, but the sources located on their surfaces are neglected in computing the potentials (5) and (6). This is a crucial point in the field/circuit coupling problem. This condition is approximately satisfied if the characteristic dimensions of the terminal devices are small compared to the interconnect length. Anyway, as a consequence of this approximation, the potentials in eqns (5) and (6) do not wholly satisfy the Lorenz gauge condition. Conversely, when the assumption does not hold, there is no way to separate the behavior of the interconnect from that of terminal devices and the electromagnetic system has to be analyzed as a whole.

2.2 Transmission line equations

The first fundamental assumption is that the surface current density is mainly directed along $\hat{x}$: $\mathbf{J}_s = J_s(\mathbf{r})\hat{x}$. In other words, we neglect any transverse component of the current density, taking into account only the longitudinal one. This assumption is well-founded when the interconnect length is infinite and only the fundamental mode is excited. Even with an infinite length, high-order propagation modes may exhibit non-longitudinal current density components; hence this assumption defines an upper limit in the frequency range.

The first consequence of this assumption is a drastic simplification of eqns (5) and (6). Indeed, the magnetic vector potential (eqn (5)) is directed only along $\hat{x}$, and so the magnetic field is of Transverse Magnetic (TM) type. In this condition, it is uniquely defined the voltage between any couple of points lying on a plane x = constant.

A second assumption is that the current and charge densities have a spatial dependence of separable type:

$$J_s(\mathbf{r})\big|_{\mathbf{r}\in S_k} = I_k(x)F_k'(s_k), \quad \sigma(\mathbf{r})\big|_{\mathbf{r}\in S_k} = Q_k(x)F_k''(s_k), \tag{7}$$

where $I_k(x)$ and $Q_k(x)$ are the total current and p.u.l. charge associated with the conductor and F' and F'' are shape functions dimensionally homogeneous with m^{-1}, describing the distribution of currents and charges along the contour l_k. In other words, we are assuming that only the total current $I_k(x)$ and p.u.l. charge $Q_k(x)$ vary along x, whereas the spatial distributions of current and charge densities are independent on x.

Imposing the charge conservation law (4) on the kth conductor and using eqn (7), we obtain

$$\frac{dI_k(x)}{dx}F_k'(s_k) + i\omega Q_k(x)F_k''(s_k) = 0, \tag{8}$$

which yields:

$$F_k'(s_k) = F_k''(s_k) = F_k(s_k), \tag{9}$$

$$\frac{\mathrm{d}I_k(x)}{\mathrm{d}x} + i\omega Q_k(x) = 0. \tag{10}$$

The shape functions for the charge and current distributions must be the same. If we impose the following normalization condition:

$$\oint_{l_k} F_k(s_k) ds_k = 1 \tag{11}$$

then the current and the p.u.l. charge are obtained by integrating eqn (7) along l_k.

With the position (7), the problem may be solved by separating the transverse and longitudinal behavior of the current and charge distributions. When the characteristic transverse dimensions of the conductors are electrically short and the interconnect is geometrically long, the transverse behavior is obtained by solving once for all a quasi-static 2D problem in the transverse plane. This assumption imposes the high-frequency validity limit for the ETL model.

Equation (10) may be written for every conductor, introducing the numerical vectors $\mathbf{I}(x) = \{I_k(x)\}_{k=1,\ldots,N}$ and $\mathbf{Q}(x) = \{Q_k(x)\}_{k=1,\ldots,N}$:

$$\frac{\mathrm{d}\mathbf{I}(x)}{\mathrm{d}x} + i\omega\mathbf{Q}(x) = 0. \tag{12}$$

This is the first of the two governing equations for any transmission line model. In order to derive the second one, we must impose the boundary conditions. Assuming an ohmic behavior, on the surface of the kth conductor the boundary condition may be written as

$$\mathbf{E}(\mathbf{r}) \times \hat{n}\big|_{\mathbf{r}\in S_k} = \varsigma_k \mathbf{J}_s(\mathbf{r}) \times \hat{n}\big|_{\mathbf{r}\in S_k}. \tag{13}$$

This assumption will be removed in Section 4, when dealing with CNTs. In eqn (13) the *surface impedance* ς_k takes into account the ohmic losses inside the conductor. For high-frequency operating conditions, for instance, it reduces to the well-known Leontovich expression

$$\varsigma_k = \eta_k \frac{1+i}{\delta_k}, \tag{14}$$

where η_k and δ_k are, respectively, the conductivity and the penetration depth of the kth conductor.

Let us now focus on the relation between the voltage and p.u.l. magnetic flux. Let a_k indicates a characteristic dimension of the cross-section of the kth conductor and let $a = \max_k(a_k)$: assuming operating conditions such that a is electrically small it is possible to approximate at any abscissa x the values of $A(x,y,z)$ and

$\varphi(x,y,z)$ on the surfaces S_1 and S_2 with their average values along the conductor cross-sections contours, say $\hat{A}_k(x)$ and $\hat{\varphi}_k(x)$. As already pointed out, it is possible to define uniquely the voltage between any two pair of points lying on a plane x = const. We may then introduce the *grounded mode* voltage of the kth conductor as follows:

$$V_k(x) = \hat{\varphi}_k(x) - \hat{\varphi}_{N+1}(x). \tag{15}$$

The p.u.l. magnetic flux linked to a closed loop connecting the kth conductor and the ground one in the plane x–z may be expressed as

$$\Phi_k(x) = \hat{A}_k(x) - \hat{A}_{N+1}(x). \tag{16}$$

Let us introduce the vectors $\mathbf{V}(x) = \{V_k(x)\}_{k=1\ldots N}$ and $\mathbf{\Phi}(x) = \{\Phi_k(x)\}_{k=1\ldots N}$: by using eqns (15) and (16) in eqn (13) it is easy to obtain

$$-\frac{\mathrm{d}\mathbf{V}(x)}{\mathrm{d}x} = i\omega\mathbf{\Phi}(x) + Z_s(i\omega)\mathbf{I}(x), \tag{17}$$

where $Z_s(i\omega)$ is a diagonal matrix with $Z_s^{kk}(i\omega) = \varsigma/\pi a_k$.

Equations (12) and (17) must be now augmented with the relation between the p.u.l. flux and the current and that between the voltage and the p.u.l. charge. In the above assumptions these relations may be obtained from eqns (5) and (6):

$$\mathbf{\Phi}(x) = \mu_0 \int_0^l H_I(x-x')\mathbf{I}(x')dx', \tag{18}$$

$$\mathbf{V}(x) = \frac{1}{\varepsilon_0}\int_0^l H_Q(x-x')\mathbf{Q}(x')dx'. \tag{19}$$

These *constitutive* relations are spatial convolutions, hence their meaning is straightforward: in the general case the value of the p.u.l. magnetic flux (the voltage) at a given abscissa x depends on the whole distribution of the current intensity (p.u.l. electric charge) along the line. The kernels in eqns (18) and (19) are $N \times N$ matrices whose entries are:

$$H_I^{ik}(\zeta) = \frac{1}{c_i}\oint_{l_i} ds_i \oint_{l_k} G_A(s_i, s_k'; \zeta) F_i(s_k')ds_k' \tag{20}$$

$$H_Q^{ik}(\zeta) = \frac{1}{c_i}\oint_{l_i} ds_i \oint_{l_k} G_\varphi(s_i, s_k'; \zeta) F_i(s_k')ds_k' \tag{21}$$

The system of equations (12) and (17)–(19) represents a *generalized transmission line model*: in the following we will refer to it as the ETL model. The 3D

full-wave problem has been recast in a transverse quasi-static 2D problem and a 1D propagation problem. The first problem is solved once for all and provides the source distributions $F_k(s_k)$ along the conductor contours. The 1D propagation problem provides, instead, the distributions of voltages, currents, p.u.l. charge and magnetic flux along the line axis.

Letting the frequency go to zero and the interconnect length go to infinity, it is possible to prove that the kernels in eqns (18) and (19) tend to spatial Dirac pulses [21]:

$$H_I(x-x') \to H_{I_0}\delta(x-x'), \quad H_Q(x-x') \to H_{Q_0}\delta(x-x'). \tag{22}$$

Hence eqns (18) and (19) reduce to *local* relations:

$$\Phi(x) = \mu_0 H_{I_0}\mathbf{I}(x), \quad \mathbf{V}(x) = \frac{1}{\varepsilon_0} H_{Q_0}\mathbf{Q}(x), \tag{23}$$

which along with eqns (12) and (17) provide the classical expression of the telegraphers' equations in frequency domain

$$-\frac{\mathrm{d}\mathbf{V}(x)}{\mathrm{d}x} = Z(i\omega)\mathbf{I}(x), \quad -\frac{\mathrm{d}\mathbf{I}(x)}{\mathrm{d}x} = Y(i\omega)\mathbf{V}(x), \tag{24}$$

where the p.u.l. impedance and admittance matrices are given by:

$$Z(i\omega) = i\omega\mu_0 H_{I_0}(\omega) + Z_s(i\omega), \quad Y(i\omega) = i\omega\varepsilon_0 H_{Q_0}^{-1}(\omega). \tag{25}$$

For the ideal case of a lossless transmission line $Z(i\omega) = i\omega L$, $Y(i\omega) = i\omega C$, where L and C are, respectively, the p.u.l. inductance and capacitance matrices.

This means that the ETL model (eqns (12) and (17)–(19)) contains the STL model (eqn (24)) as a particular case, obtained when the interconnect is enough long to neglect the effect of the finite length and the frequency is enough low to make the transverse dimensions electrically small.

It is worth noting that, as all the transmission line models, the STL model is based on the separation between a transverse quasi-static 2D problem and a 1D propagation problem. The difference with respect to the ETL model is in the fact that the transverse 2D problem, solved once for all, provides the p.u.l. parameters (eqn (25)), whereas, as for all the transmission line models, the distributions of voltages and currents are the solutions of a 1D propagation problem (eqn (24)).

3 Transmission line model for conventional conductors

3.1 A cylindrical pair

Let us study the simple case of a straight pair in the vacuum space, made by two cylindrical perfect conductors of radius a. Let h_c be the center to center distance in the transverse plane (see Fig. 2a) and the total length. The example can be also

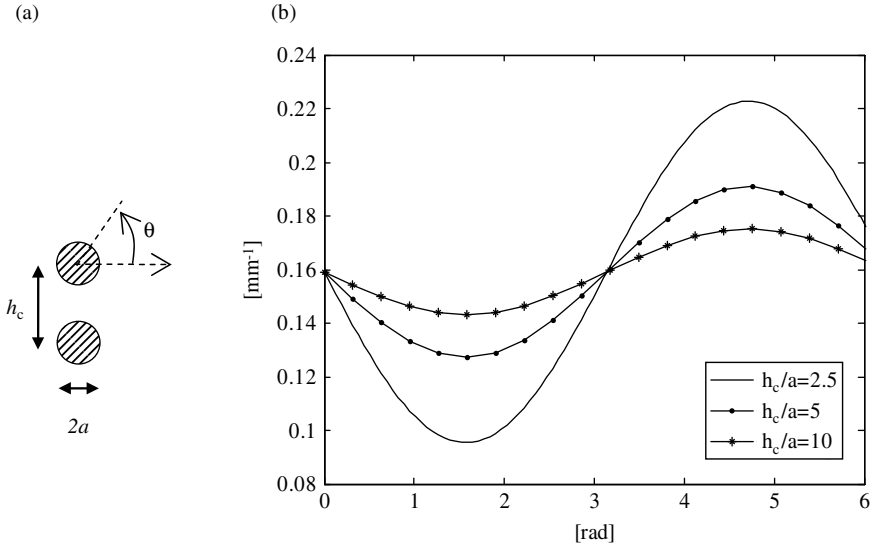

Figure 2: Cylindrical pair: (a) cross-section and (b) shape function $F(\theta)$.

used to analyze the case of a cylindrical conductor above a perfect ground plane. In vacuum the Green functions in eqns (4) and (5) reduce to the function

$$G(r) = \frac{\exp(-ikr)}{4\pi r}, \tag{26}$$

where r is the distance between the source and field points and $k = \omega\sqrt{\varepsilon\mu}$ is the propagation constant.

The static distribution of the sources along the conductor contours may be expressed in closed form as a function of the angle (see Fig. 2a) [19]:

$$F(\theta) = \frac{1}{2\pi a}\left(1 - \frac{a}{h_c}\sin\theta\right), \quad \theta \in [0, 2\pi]. \tag{27}$$

Figure 2b shows the behavior of $F(\theta)$ for a = 1 mm and for different values of the ratio h_c/a: for small values of h_c/a (say <10) this distribution differs significantly from the uniform case because of the proximity effect.

When considering widely separated conductors it results $F(\theta) = 1/2\pi a$ and it is possible to give a closed-form expression to the kernel (eqns (20) and (21)), which may be split as the sum of a *static* and a *dynamic* term, $H = H_{\text{stat}} + H_{\text{dyn}}$:

$$H_{\text{stat}}(\zeta) = \frac{1}{\pi^2}\frac{\kappa[m(\zeta)]}{R_s(\zeta)} - \frac{1}{2\pi}\frac{1}{R_m(\zeta)}, \tag{28}$$

$$H_{\text{dyn}}(\zeta) = -\frac{ik}{\pi}\exp\left[-\frac{ikR_m(\zeta)}{2}\right]\sin c\left[\frac{kR_m(\zeta)}{2}\right]. \tag{29}$$

Here $\kappa(m)$ is the *complete elliptic integral* of the first type, and

$$m(\zeta) = \frac{\zeta^2}{(4a^2 + \zeta^2)}, \quad R_m(\zeta) = \sqrt{h_c^2 + \zeta^2}, \quad R_s(\zeta) = \sqrt{4a^2 + \zeta^2}. \tag{30}$$

The dynamic term depends on the frequency and vanishes as $\omega \to 0$. The static term is independent on frequency but shows a singularity of logarithmic type:

$$H_s(\zeta) \approx -\frac{1}{2a\pi^2}\ln(\zeta) \quad \text{for } \zeta \to 0. \tag{31}$$

As already pointed out, if we consider infinitely long lines and assume frequency operating conditions such that $h_C/\lambda << 1$, λ being the characteristic signal wavelength, $H(\zeta)$ reduces to a spatial Dirac pulse $H(\zeta) \to H_0\delta(\zeta)$, where

$$H_0 = \int_{-\infty}^{\infty} H(x)\mathrm{d}x = \frac{1}{\pi}\ln\left(\frac{h_c}{a}\right). \tag{32}$$

In this case the cylindrical pair is described by the classical telegrapher's equations for ideal two-conductor lines, namely by eqn (24) with $Z(i\omega) = i\omega\mu_0 H_0 = i\omega L$ and $Y(i\omega) = i\omega\varepsilon_0/H_0 = i\omega C$.

3.2 A coupled microstrip

A structure of great interest for high-speed electronic applications is the microstrip line: Fig. 3 shows a simple example of a three conductor microstrip, made by two signal conductors on a dielectric layer and a ground plane. Figure 3a shows the references for the voltages and currents (note that the grounded modes are considered).

From a qualitative point of view, the results highlighted in Section 3.1 still hold: the kernels (20) and (21) show a singularity of logarithmic type and the STL model may be obtained as a limit case of the generalized one.

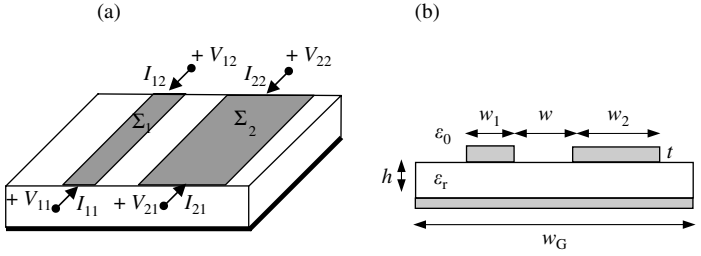

Figure 3: A coupled microstrip: reference for terminal voltages and currents (a); schematic of the cross-section (b).

The first difference is in the fact that the shape functions are no longer known in analytical form. However, they may be easily numerically computed by solving the electrostatic problem in the cross-section: for instance Fig. 4 shows the computed behavior of the shape function for the signal conductor of a single microstrip with $w_1 = 5$ mm, $t = 1.25$ mm, $h = 8.7$ mm and $\varepsilon_r = 4$. It is here evident the effect due to the sharp edges of the rectangular section.

A second difference is due to the influence of the dielectric. In this case the kernels (20) and (21) are different, since we have to consider two different Green functions in eqns (5) and (6). As already pointed out, the Green function involved in eqn (5) is in general dyadic. Since the layers properties are assumed to change only along $\hat{z}$ (see Fig. 1), G_A has the structure

$$G_A = \begin{bmatrix} G_{xx} & 0 & G_{zx} \\ 0 & G_{yy} & G_{zy} \\ G_{zx} & G_{zy} & G_{zz} \end{bmatrix}. \tag{33}$$

In many practical applications the thickness of conductors t is small compared to their width w. If we assume zero-thickness for the signal conductors, since the current density $\mathbf{J}_s$ directed along $\hat{x}$ we have the simple expression $G_A = G_{xx}$.

For the considered structure the Green functions may be evaluated in closed form in the spectral domain: let $\tilde{G}_{xx}(k_\rho)$ and $\tilde{G}_\varphi(k_\rho)$ be their transforms in such a

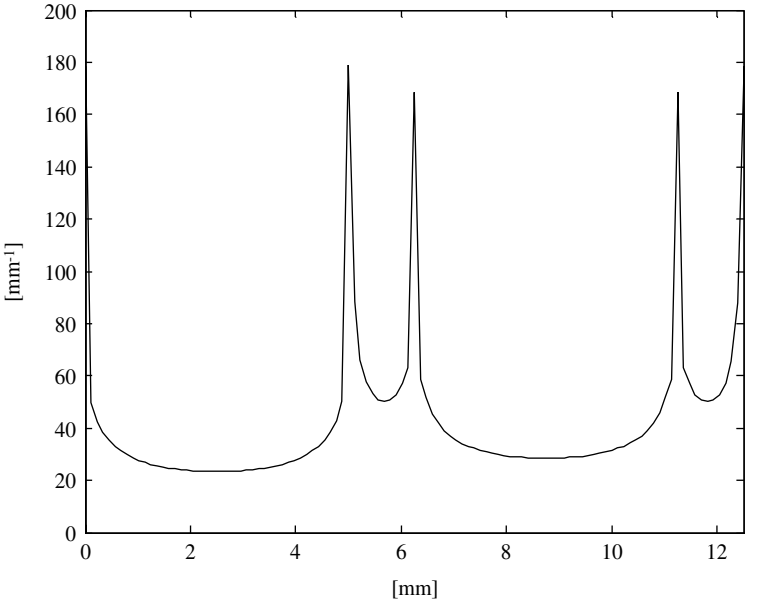

Figure 4: Computed shape function $F(s)$ for the signal conductor of a microstrip.

domain, where k_ρ is the spectral domain variable. The spatial domain functions are obtained by evaluating the Sommerfeld integrals [32]:

$$G_{xx}(r) = \frac{1}{4\pi}\int_{-\infty}^{+\infty} \tilde{G}_{xx}(k_\rho) H_0^{(2)}(k_\rho r) k_\rho \, \mathrm{d}k_\rho, \tag{34}$$

$$G_{\varphi}(r) = \frac{1}{4\pi}\int_{-\infty}^{+\infty} \tilde{G}_{\varphi}(k_\rho) H_0^{(2)}(k_\rho r) k_\rho \, \mathrm{d}k_\rho, \tag{35}$$

where $H_0^{(2)}$ is the Hankel function. Such integrals are hard to compute practically, due to the slowly decaying and oscillating nature of the kernels. The cost for computing such integrals is extremely high because of the slow decay of the integrands. A way to overcome this problem is to extract analytically the terms which are dominant in the low-frequency range, referred to as the *quasi-static terms*. For the single-layer microstrip structure of Fig. 3b they may be expressed as follows [33]:

$$G_{xx}^0(r) = \frac{\mathrm{e}^{-ik_0\sqrt{x^2+y^2}}}{4\pi\sqrt{x^2+y^2}} - \frac{\mathrm{e}^{-ik_0\sqrt{x^2+y^2+(2h)^2}}}{4\pi\sqrt{x^2+y^2+(2h)^2}}, \tag{36}$$

$$G_{\varphi}^0(r) = (1+K)\frac{\mathrm{e}^{-ik_0\sqrt{x^2+y^2}}}{4\pi\sqrt{x^2+y^2}} + (K^2-1)\sum_{n=1}^{\infty} K^{n-1}\frac{\mathrm{e}^{-ik_0\sqrt{x^2+y^2+(2nh)^2}}}{4\pi\sqrt{x^2+y^2+(2nh)^2}}, \tag{37}$$

where $K = (1 - \varepsilon_\mathrm{r})/(1 + \varepsilon_\mathrm{r})$ and k_0 is the vacuum space wavenumber.

Once these terms have been extracted, the remainders (*dynamic terms*) may be evaluated in an efficient way by approximating the corresponding expressions in the spectral domain [34]. The quasi-static terms are associated to the fundamental mode, are the only terms left when $f \to 0$ and dominate the local range interactions. The dynamic terms are associated to parasitic waves (surface waves, leaky waves), vanish as $f \to 0$ and dominate the long-range interactions.

Figure 5 gives an example of scalar potential Green function G_φ computed at 2.1 GHz for a single microstrip with $\varepsilon_\mathrm{r} = 4.9$, $h = 0.7$ mm.

The quasi-static term dominates the near-field region, whereas for increasing distances the dynamic terms become the principal ones.

Unless very high frequencies are considered, in practical interconnects the quasi-static terms are dominant, hence the approximation of the remainder is usually satisfactorily pursued by a low-order model. A reliable criterion [35] states that the Green functions are accurately represented by the quasi-static terms when $k_0 h\sqrt{\varepsilon_\mathrm{r} - 1} < 0.1$.

4 Transmission line model for CNT interconnects

CNTs are allotropes of carbon that have been discovered fairly recently [23] and are considered as an alternative to conventional technology for future nanoelectronic

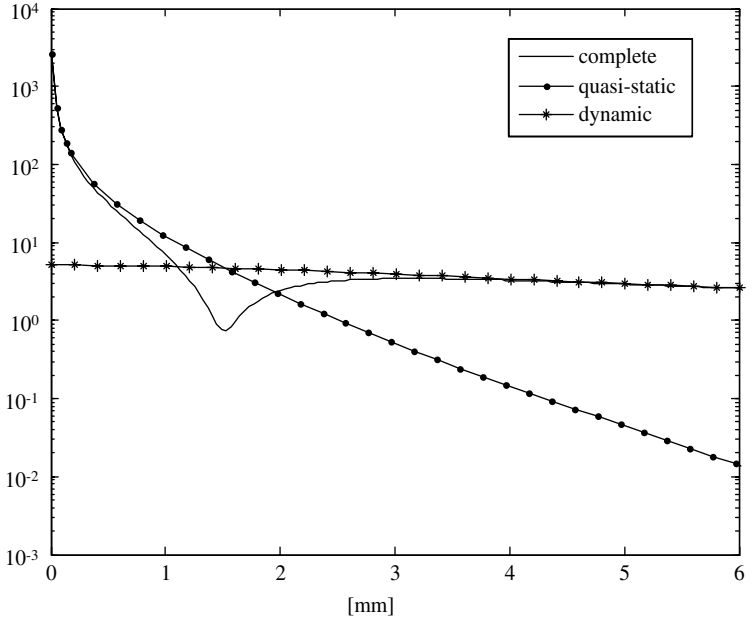

Figure 5: Typical high-frequency behavior of the scalar potential Green function: contributions of the quasi-static and dynamic terms.

applications such as transistors, antennas, filters and interconnects [24, 25]. Metallic CNTs have been suggested to replace copper in nano-interconnects, due to their unique electrical, mechanical and thermal properties [26–28]. Table 1 shows typical values for current density allowed, thermal conductivity and mean free path [28].

A single wall carbon nanotube (SWCNT) is a single sheet of a mono-atomic layer of graphite rolled-up (Fig. 6a). It possesses four valence electrons for each carbon atom: three of these form tight bonds with the neighboring atoms in the plane, whereas the fourth electron is free to move across the positive ion lattice. When the sheet is rolled up it may become either metallic or semiconducting, depending on the way it is rolled up.

To describe the electrodynamics of CNTs we need to model the interaction of the free electrons with the fixed positive ions and the electromagnetic field produced by the electrons themselves and the external sources. This requires, in principle, a quantum mechanical approach, because the electrical behavior of the electrons depends strongly on the interaction with the positive ion lattice. However, under suitable assumption the problem may be modeled by using a linearized fluid model to describe the dynamics of the effective conduction electrons, and by coupling the fluid equations to the Maxwell equations through the Lorentz force.

Table 1: Properties of CNTS compared to copper.

Property	CNT	Cu
Maximum current density [A/cm^2]	~10^{10}	~10^6
Thermal conductivity [W/mK]	~6000	~400
Mean free path [nm]	~1000	~40

(a) (b)

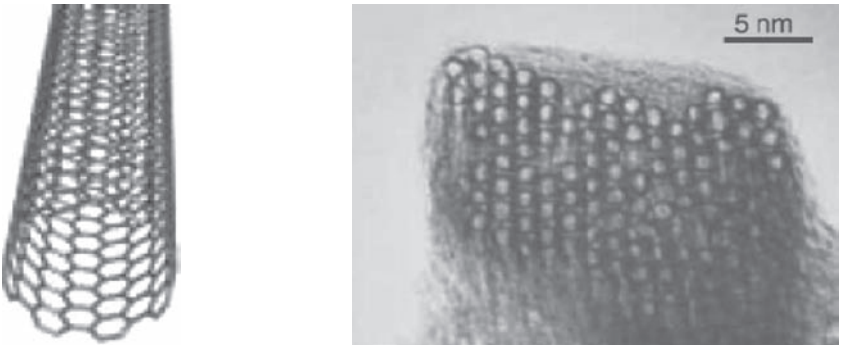

Figure 6: Schematic representation of a CNT (a); picture of a CNT bundle (b) [28].

4.1 A fluid model for CNTs

We model a SWCNT as an infinitesimally thin cylinder shell with radius r_c and length l. The graphene has valence electrons (π-electrons) whose dynamics depends on the electric field due to interactions with ions and other electrons (atomic field), with the other π-electrons (collective field) and with external fields. If the atomic field is much stronger than the collective and the external fields (the sum of these two is denoted with $\mathbf{e}(\mathbf{r}; t)$) and if $\mathbf{e}(\mathbf{r}; t)$ varies slowly compared to the atomic time-space scale, the π-electron may be described as a quasi-classical particle: the dynamics is the same as for a classical particle with the same charge and an *effective mass* (which takes into account quantum effects) moving under the action of $\mathbf{e}(\mathbf{r}; t)$.

In these conditions the conduction electrons (distributed on the cylinder surface S) may be described as an electron fluid with surface number density $n(\mathbf{r}; t)$, velocity $\mathbf{V}(\mathbf{r},t) = u(\mathbf{r},t)\,\hat{x}$ and 2D hydro-dynamical pressure $p = p(\mathbf{r}; t)$, of quantum nature [29]. We have assumed the velocity to be directed along the CNT axis $\hat{x}$. Assuming small perturbations around equilibrium condition (n_0, p_0), i.e. expressing the conduction electron density and the pressure as $n = n_0 + \delta n$, and $p = p_0 + \delta p$, the interaction between $\mathbf{e}(\mathbf{r}; t)$ and the electron fluid is assumed to be governed by the *linearized Euler's equation*

$$m_{\text{eff}} n_0 \frac{\partial u}{\partial t} = -\frac{\partial \delta p}{\partial x} + e n_0 e_x - m_{\text{eff}} n_0 \upsilon_c u \tag{38}$$

where m_{eff} and e denote, respectively, the effective mass and the charge of the electron and υ is a parameter which accounts for the collisions. Equation (38) is augmented with a 'state equation' relating δp to δn

$$\delta p = m_{\text{eff}} c_s^2 \delta n \tag{39}$$

where c_s is the thermodynamic speed of sound. The continuity condition imposes the following relation:

$$\frac{\partial \delta n}{\partial t} = -\frac{\partial (n_0 u)}{\partial x}. \tag{40}$$

Introducing in eqns (38) and (40) the charge density $\sigma = -e\delta n$ and the current density $j = -en_0 u$ on the surface S, we obtain the following system:

$$\frac{\partial j}{\partial t} + c_s^2 \frac{\partial \sigma}{\partial x} + \upsilon j = \frac{e^2 n_0}{m_{\text{eff}}} e_x \tag{41}$$

$$\frac{\partial \sigma}{\partial t} = -\frac{\partial j}{\partial x}. \tag{42}$$

To complete the fluid model, we have to fix the values of the parameters n_0/m_{eff}, c_s and υ. First of all, the equilibrium number density n_0 is determined by requiring that the longitudinal electric conductivity obtained from this model agreed with the expression obtained from a semi-classical transport theory for a sufficient small CNT radius [36]:

$$\frac{n_0}{m_{\text{eff}}} \cong \frac{4\upsilon_F}{\pi h} \frac{1}{r_c} \tag{43}$$

where h is the Planck constant and υ_F is the Fermi velocity. Next, c_s is assumed to be equal to υ_F and finally for the collision frequency υ we use the expression

$$\upsilon = \alpha \frac{\upsilon_F}{l_{\text{mfp}}}, \tag{44}$$

where l_{mfp} is the *mean free path* and α is a correction factor, which can be used as a 'tuning' factor able to take into account, for instance, the slight dependence of l_{mfp} from the CNT radius [37].

4.2 A transmission line model for a SWCNT above a ground plane

Let us consider a SWCNT above a perfect conducting plane, as schematically represented in Fig. 7; h_c is the distance between the axis nanotube and the plane. We assume the same operating conditions used for the general formulation introduced

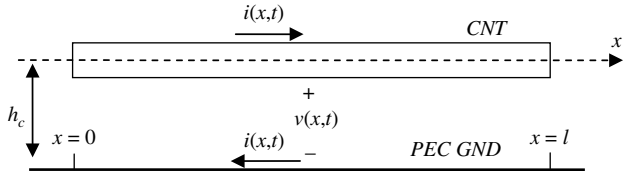

Figure 7: An SWCNT transmission line.

in Section 3, hence the governing equations in the frequency domain are still given by eqns (12) and (17), which read for this case:

$$\frac{\mathrm{d}I(x)}{\mathrm{d}x} + i\omega Q(x) = 0, \quad -\frac{\mathrm{d}V(x)}{\mathrm{d}x} = i\omega\Phi(x) + E(x). \tag{45}$$

Note that in this case the longitudinal component of the electric field $E(x)$ appearing in the RHS of the second of eqn (45) is not expressed through the simple ohmic relation as in eqn (17), but should be derived from eqn (41) assuming all the above mentioned conditions on the sources:

$$E(x) = \upsilon L_{\mathrm{k}} I(x) + i\omega L_{\mathrm{k}} I(x) + \frac{1}{C_{\mathrm{q}}}\frac{\mathrm{d}Q(x)}{\mathrm{d}x}, \tag{46}$$

where and L_{k} and C_{q} are, respectively, the *kinetic inductance* and the *quantum capacitance*, given by

$$L_{\mathrm{k}} = \frac{h}{8e^2\upsilon_{\mathrm{F}}}, \qquad C_{\mathrm{q}} = \frac{1}{L_{\mathrm{k}}c_{\mathrm{s}}^2} = \frac{8e^2}{h\upsilon_{\mathrm{F}}}. \tag{47}$$

The parameters and L_{k} and C_{q} derived here agree with those obtained in literature starting from different models (e.g. in [27], using a phenomenological approach based on Luttinger liquid theory).

Equations (45) and (46) must be augmented with the constitutive relations (18) and (19). Assuming a quasi-TEM approximation, in this case they reduce to the simple relations (23):

$$\Phi(x) = L_{\mathrm{m}} I(x), \qquad V(x) = \frac{Q(x)}{C_{\mathrm{e}}}, \tag{48}$$

where L_{M} and C_{e} are the classical p.u.l. magnetic inductance and electrical capacitance for a single wire above a ground plane:

$$L_{\mathrm{m}} = \frac{\mu_0}{2\pi}\ln\left(\frac{2h_{\mathrm{c}}}{r_{\mathrm{c}}}\right), \qquad C_{\mathrm{e}} = \frac{2\pi\varepsilon_0}{\ln\left(2h_{\mathrm{c}}/r_{\mathrm{c}}\right)}. \tag{49}$$

By using eqns (46) and (48) in eqn (45), we obtain that the interconnect is described by a simple lossy RLC transmission line model:

$$-\frac{\mathrm{d}V(x)}{\mathrm{d}x} = (R + i\omega L)I(x), \quad -\frac{\mathrm{d}I(x)}{\mathrm{d}x} = i\omega CV(x), \tag{50}$$

where the p.u.l. parameters are given by:

$$L = \frac{L_\mathrm{m} + L_\mathrm{k}}{1 + C_\mathrm{e}/C_\mathrm{q}}, \quad C = C_\mathrm{e}, \quad R = \frac{L_\mathrm{k}\upsilon}{1 + C_\mathrm{e}/C_\mathrm{q}}. \tag{51}$$

As will be shown in the case-studies analyzed in Section 5, the behavior of this particular transmission line is strongly affected by the influence of the kinetic inductance and quantum capacitance. For instance, assuming, $\upsilon_\mathrm{F} \approx 8.8 \times 10^5$ m/s, $l_\mathrm{mfp} \approx 1$ μm, and $h_\mathrm{c}/r_\mathrm{c} = 5$ we have $L_\mathrm{k}/L_\mathrm{m} = 8 \times 10^3$ and $C_\mathrm{e}/C_\mathrm{q} = 7 \times 10^{-2}$. The result on the inductances is quite insensitive to variation of the geometry of the line: the kinetic inductance always dominates over the magnetic one. As for the capacitance, if different dielectrics are considered the quantum capacitance may be comparable to the electrostatic one. As a consequence, the *propagation speed* and the *lossless characteristic impedance*

$$c_\mathrm{CNT} = \frac{1}{\sqrt{LC}}, \quad Z_\mathrm{0CNT} = \sqrt{\frac{L}{C}}, \tag{52}$$

may be well different from those theoretically obtained using the same geometry for the transmission line and replacing the CNT with a perfect conductor, say c_0 and Z_0. Typical values are $c_\mathrm{NT}/c_0 \approx 10^{-2}$ and $Z_\mathrm{0CNT}/Z_0 \approx 10^2$.

As for the resistance, by using eqns (51) and (44) with the same parameters as above and with $a = 1$, we obtain $R \approx 3$ kΩ/ km. The high values of this p.u.l. resistance and of the characteristic impedance in eqn (52) suggest using as interconnect stacks or bundles of CNTs rather than single CNT [31, 37–39].

In order to analyze multiconductor structures such as bundles, it is useful to extend the model to interconnects made by n CNTs over a ground plane. Following the same steps described above, the relation between voltage $\mathbf{v}(x,t) = [\upsilon_1(x,t), ..., \upsilon_n(x,t)]^\mathrm{T}$ and current $\mathbf{i}(x,t) = [i_1(x,t), ..., i_n(x,t)]^\mathrm{T}$ is given by the multiconductor transmission line equations

$$-\frac{\partial \mathbf{v}}{\partial x} = \underline{\underline{L}}\frac{\partial \mathbf{i}}{\partial t} + \underline{\underline{R}}\mathbf{i}, \quad -\frac{\partial \mathbf{i}}{\partial x} = \underline{\underline{C}}\frac{\partial \mathbf{v}}{\partial t}, \tag{53}$$

where the p.u.l. parameter matrices are given by

$$\underline{\underline{L}} = (\underline{\underline{I}} + \underline{\underline{C_\mathrm{e}}}/C_\mathrm{q})^{-1}(\underline{\underline{L_\mathrm{m}}} + L_\mathrm{k}\underline{\underline{I}}), \quad \underline{\underline{C}} = \underline{\underline{C_\mathrm{e}}}, \quad \underline{\underline{R}} = (\underline{\underline{I}} + \underline{\underline{C_\mathrm{e}}}/C_\mathrm{q})^{-1}R_\mathrm{c}, \tag{54}$$

$\underline{\underline{I}}$ being the identity matrix.

Finally, we have to remark that given the assumptions at its basis, the transmission line model introduced here describes the propagation in the low-bias voltage condition (corresponding to a longitudinal field less than 0.1 V/μm) and assuming $l \geq l_{mfp}$. In high-bias condition this model should be modified with the insertion of a non-linear resistance [30].

5 Examples and applications

5.1 Finite length and proximity effect

A first simple application (Case 1) of the ETL model is the high-frequency analysis of a simple cylindrical pair as in Fig. 2, with a = 1 mm, h_c = 1 cm and total length l = 0.1 m. The conductors are ideal and the pair is in the vacuum space. Although simple, this example exhibits a lot of phenomena, which can be found also in more complex applications.

Figure 8 shows the spatial current distributions when the line is fed at the near-end and is left open at the far-end: $I(x = 0)$ = 1 a.u. and $I(x = l) = 0$. The prediction of the ETL model is compared to those provided by the STL model and by a full-wave numerical solution obtained by means of Numerical Electromagnetics Code (NEC), a full-wave commercial simulator based on the method of moment technique [40]. The agreement between the ETL solution and the full-wave one is very satisfactorily. As expected, for $kh_c > 0.1$ the full-wave solution starts to deviate from the STL one: Fig. 8a refers to an operating frequency of f = 1 GHZ, which means $kh_c \approx 0.21$. For higher frequencies the STL solution is completely inadequate to describe the real full-wave solution, whereas the ETL model is still accurate. Figure 8b refers to f = 5 GHZ, which means $kh_c \approx 1.05$.

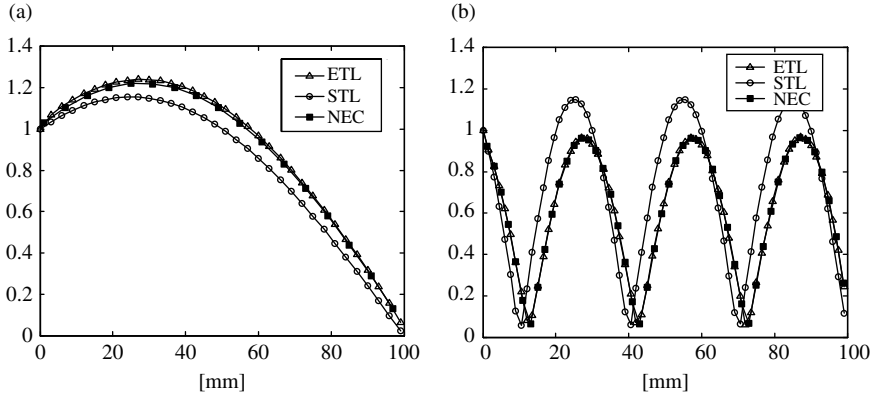

Figure 8: Case 1, amplitude (in arbitrary units) of the current distribution for the mismatched case, computed at 1 GHz (a) and 5 GHz (b).

To investigate the phenomena which are at the basis of such a behavior, it is useful to exploit the possibility given in eqns (28) and (29) to split the static and dynamic terms in the kernels. Let us consider the same conditions as above, except for the far end, which is now assumed to be *matched* (it is loaded by the characteristic impedance $Z_0 = \sqrt{L/C} = 276.2\ \ \Omega$ of the STL case).

Figure 9 shows the STL solution, the ETL complete solution and the ETL solution due only to the static kernel. The main contribution to the difference is given, at low frequencies, by the static part H_s, while for high frequencies also the dynamic part H_d provides a significant contribution. This means that, when entering the high-frequency range $kh_c > 0.1$, the first effect experienced by the solution is due to the finite length of the structure, whereas the effect due to unwanted radiation in the transverse plane starts acting for higher frequencies.

Finally, Fig. 10 shows the frequency behavior of the input impedance of the line (normalized to $Z_0 = 276\ \Omega$), when the far-end is left open.

The ETL model is able to predict the shift of the resonance frequencies toward lower values. Note that the shift to lower frequencies with respect to those of STL model means that the interconnect is electrically shorter than it actually is. Besides, the ETL model well predicts the amplitudes at the resonance frequencies that are finite and decreasing with increasing frequency, which is typical of a lossy line with frequency-dependent losses.

In very large-scale integration (VLSI) applications it is of great interest the study of the proximity effect, because of the short distances between the signal traces. Case 1 referred to a condition of widely separated wires, with $h_c/a = 10$. For such a condition the distribution of the sources along the wire contours may assumed to be uniform (see Fig. 2b). For a cylindrical pair, we may assume as a rule of thumb that the proximity effect should be considered for $h_c/a = 2.5$. Let us study again a wire pair, with $a = 2.5$ mm, $h_c = 5.7$ mm and total length $l = 1$ m

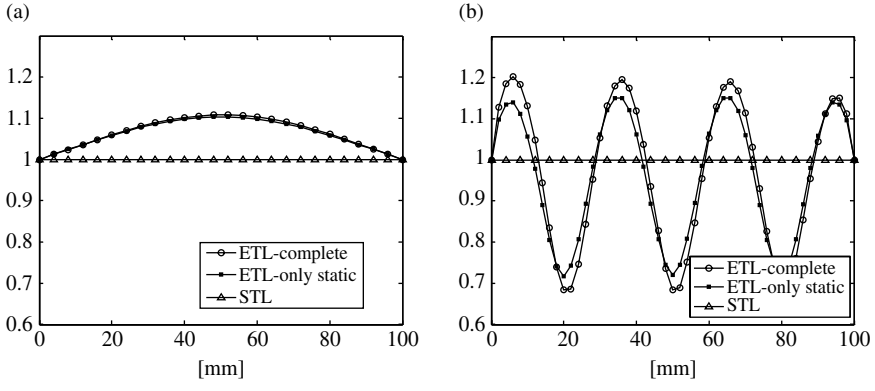

Figure 9: Case 1, amplitude (in arbitrary units) of the current distribution for the matched case, computed at 1 GHz (a) and 5 GHz (b).

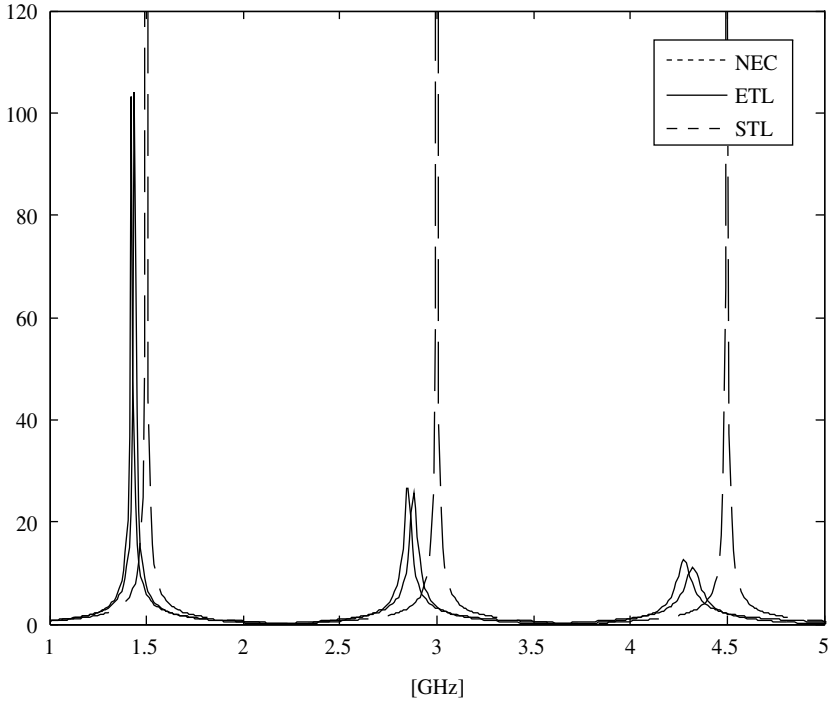

Figure 10: Case 1, amplitude of the self-impedance, normalized to Z_0.

(Case 2). The line is fed at one end by a voltage source of 1 V and is terminated on a short circuit at the other end. This case has been analyzed in [14], where a full-wave solution is provided by using the wire antenna theory. The proximity effect is there taken into account by introducing a set of 'equivalent' wires, whose artificial electrical axes are positioned so to satisfy the static problem in the transverse plane.

Figure 11 shows the current distribution at 1.2 GHz for this case, computed by means of ETL and STL models and compared to the quoted full-wave solution. An approximated ETL solution is also plotted, obtained by disregarding the proximity effect and hence assuming uniform distributions.

5.2 High-frequency losses

In high-speed integrated circuit technology losses play a crucial role in the overall system performance. With respect to a full-wave solution provided by brute-force numerical simulators, one of the most important advantages in using the ETL solution is the possibility to have a qualitative insight on the lossy phenomena affecting the high-frequency solution. We can distinguish at least three different lossy

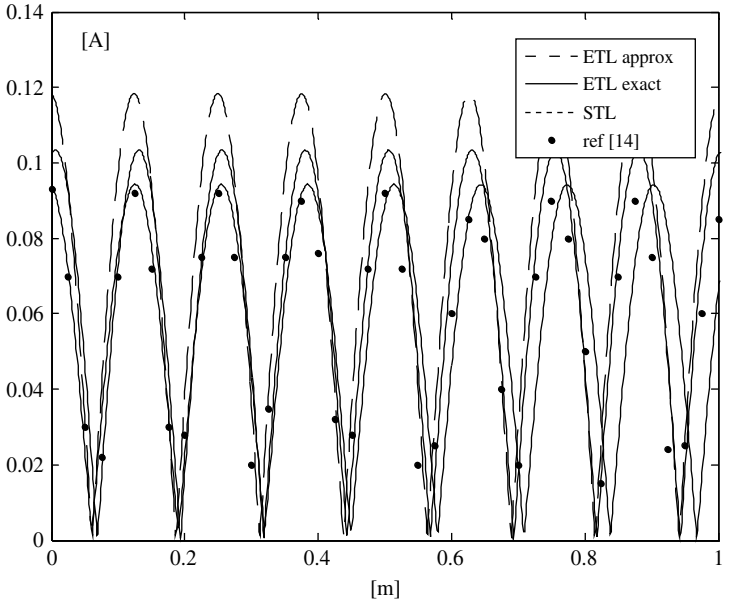

Figure 11: Case 2, amplitude of the current distribution computed at 1.2 GHz.

mechanisms: (i) conductor losses; (ii) dielectric losses; (iii) excitation of parasitic modes (leaky waves, surface waves); (iv) radiation.

Let us consider the same pair of Case 1, assuming the conductors to be real, with a conductor resistivity $\eta = 1.7 \times 10^{-8}\ \Omega$m (Case 3). These losses are very sensitive to the frequency because of the skin-effect and this may be taken easily into account by using a suitable definition of surface impedance as in eqn (14). The line is fed by a unitary current source (arbitrary units) and is opened at the other end. We consider the frequencies $0.1\, f_0 - 2.5 f_0$ ($f_0 = 1.5$ GHz), corresponding to a range where the STL model fails. We have evaluated the difference between the values of the mean power absorbed at $x = 0$

$$P_{\text{in}}(\omega) = \frac{1}{2}\text{real}\{V(\omega)I^*(\omega)\}, \tag{55}$$

evaluated with ideal and real conductors. In the first case the ohmic losses are not considered, whereas in the second case they add to the radiation losses. Figure 12a shows the radiated mean power computed in these two conditions. In the low-frequency range the absorbed power is dominated by the ohmic losses whereas the radiation losses are more relevant in the high-frequency range. The ratio between ohmic and radiated mean power is plotted in Fig. 12b. The effect of a finite resistivity is relevant for frequency ranges where the STL model may be still used. For frequencies where the ETL model should be used, the losses are mainly due to radiation.

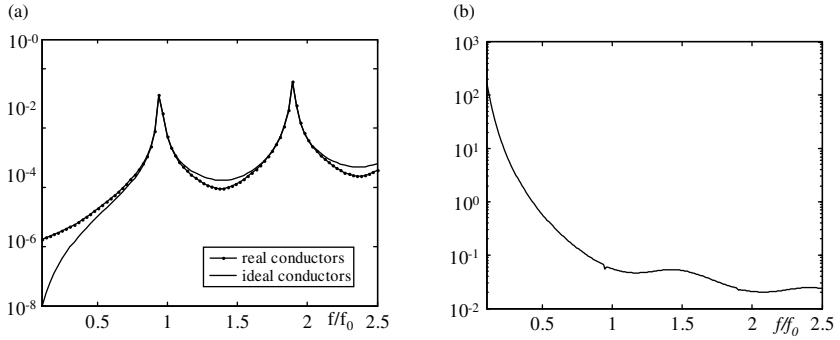

Figure 12: Case 3, dissipated mean power in arbitrary units (a); ratio between ohmic and radiated mean power (b).

Let us now consider a printed circuit board microstrip, with the geometry of Fig. 3, assuming a single signal conductor above a ground plane and a length of 36 mm (Case 4). The signal conductor has zero thickness, width w_1 = 1.8 mm, and lies on a FR-4 dielectric layer of thickness h = 1.016 mm, dielectric constant ε_r = 4.9 and magnetic permeability $\mu = \mu_0$. The conductors and dielectric are assumed ideal.

The ETL model solution is compared to the STL one and to two 3D full-wave solutions, one provided by the commercial finite element method code *HFSS* [41] and the other by the tool *SURFCODE*, which is based on the *electric field integral equation* formulation [42]. Assuming for this case $h_c = h$, since $\varepsilon_{r,eff}$ = 3.65 we have $kh_c \approx 0.1$ at 1.4 GHz, which is in agreement with the results shown in Fig. 13, where it is plotted the absolute value of the input impedance of the line with the far-end left open. Indeed, the results of all the models agree satisfactorily in the low-frequency range (Fig. 13a), whereas in the high-frequency range the full-wave solutions start to deviate significantly from the ideal STL solution.

As for the previous case-studies, since the conductors and the dielectric are assumed to be ideal, the finite amplitude of the peak is only due to the lossy effects related to the presence of unwanted parasitic modes (surface waves, leaky waves). In this condition a small but not negligible amount of power is associated with radiation in the transverse plane. Using eqn (55), the real power absorbed by the interconnect fed at one end by a sinusoidal current of r.m.s. value I_0 and left open at the other end is given by $P_{in}(\omega) = \text{real}\{Z_{in}(\omega)\} I_0^2/2$. Figure 14a shows the absorbed real power computed with I_0 = 1 mA. The ETL solution is in good agreement with the full-wave one around the peak, whereas there is a deviation in the other ranges (where, however the values of power are very low). Note that, since we are in the ideal case, the STL input impedance is strictly imaginary, hence the absorbed real power predicted by the STL model is always zero.

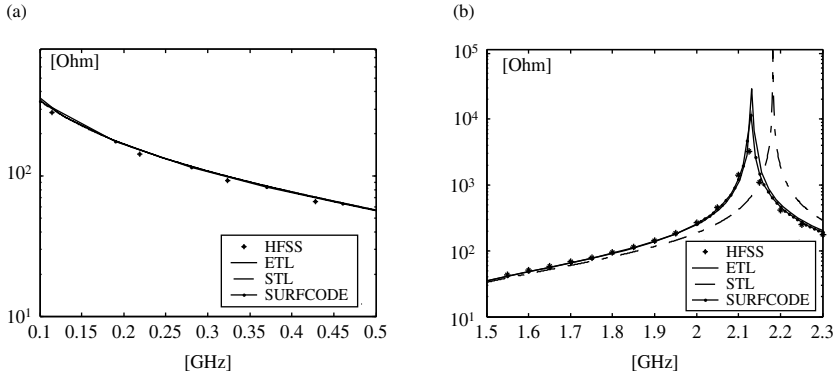

Figure 13: Case 4, absolute value of the input impedance in the low (a) and high (b) frequency range.

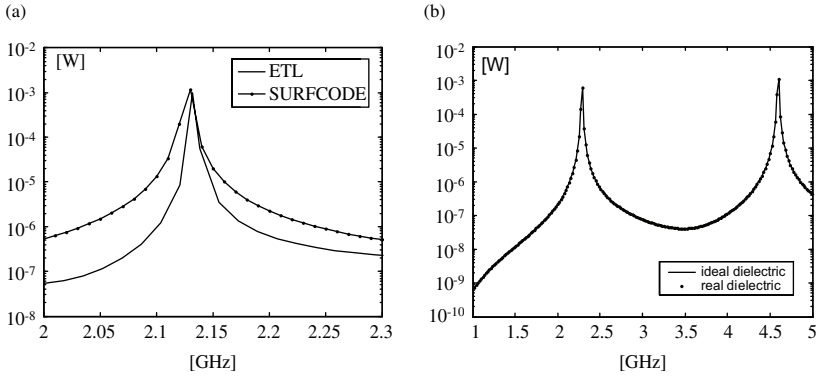

Figure 14: Case 4, absorbed power for ideal (a) and real (b) dielectrics.

Next, let us assume the dielectric to be real, i.e. let us introduce frequency-dependent dielectric losses by using, for instance, a simple Debye model [43]

$$\varepsilon_r(\omega) = \varepsilon_{r_\infty} + \frac{\varepsilon_{r_0} - \varepsilon_{r_\infty}}{1 + i\omega\tau}, \tag{56}$$

where ε_{r_0} and ε_{r_∞} are, respectively, the low- and high-frequency limit, whereas τ is a relaxation time constant. For the considered case, we assume $\varepsilon_{r_0} = 4.178$, $\varepsilon_{r_\infty} = 4.07$ and $\tau = 1.15$ ps.

Figure 14b shows the power dissipated in the high-frequency range assuming again $I_0 = 1$ mA and comparing the real dielectric described by (56) to the ideal one with $\varepsilon_r = 4.178$. It is clear that in this case the dielectric losses are negligible with respect to the losses associated to the other high-frequency phenomena.

5.3 High-frequency crosstalk and mode-conversion

In VLSI applications the crosstalk noise and the differential to common mode conversion are unwanted phenomena, which may lower dramatically the performances. The crosstalk between adjacent traces may cause false signaling and is a serious bottleneck in the miniaturizing process for incoming scaled technologies. A correct evaluation of the common-mode currents is a crucial point in the analysis of systems like printed circuit boards, because of their remarkable effect on the overall electromagnetic interference performance. Although they may be even some order of magnitude lower than the differential mode currents, their effects may be comparable, for instance in terms of radiated emissions. Both phenomena may be analyzed by studying a simple three-conductor structure, like the one depicted in Fig. 3b.

Case 5 refers to a coupled microstrip in air (Fig. 3), with w_1 = 5 mm, w_2 = 10 mm, w = 2.5 mm, h = 8.7 mm, t = 1.25 mm, and a total length of 50 mm. For such a structure, we assume h_c = 9.35 mm, and investigate the frequency range 0.1–3 GHz, corresponding to $kh_c \in (0.02 - 0.59)$.

The line is assumed to be in the free space and to be open at the far end: $I_{12} = I_{22} = 0$ (see Fig. 3a for references). Figure 15 shows the frequency behavior of the self and mutual terms of the input impedance, computed, respectively, as $Z_{11} = V_{11}/I_{11}$ and $Z_{21} = V_{21}/I_{11}$ when $I_{21} = 0$. The three models agree in the low-frequency range, up to 0.5 GHz, corresponding to $kh_c \approx 0.1$. For higher frequencies the full-wave and ETL solutions deviate from the STL one, capturing not only the frequency shift that has been already observed in the previous cases, but also the additional small peaks due to the resonance in the transverse plane. The impedance Z_{12} is an index for the crosstalk noise: it would be the near-end crosstalk voltage assuming I_{11} = 1 A and all the other currents equal to zero. Figure 15b clearly shows that above 1.5 GHz the crosstalk noise level predicted by the STL model is well below the full-wave solution.

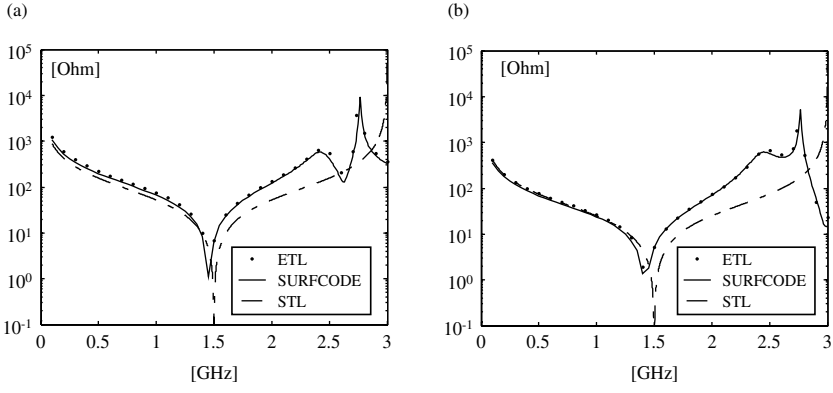

Figure 15: Case 5, amplitude of self (a) and mutual (b) impedance at the near end.

Let us analyze, for the same structure, the problem of the common mode excitation. Usually the common-mode currents are due to unwanted effects, as the presence of external fields, asymmetric conductor cross-sections and non-ideal behavior of the ground. In the *differential signaling* technique, however, a signal is defined as the difference between the signals of two conductors with respect to a third reference one and hence, due to the presence of the ground, a common-mode solution propagate. In order to study this 'mixed-mode' propagation it is convenient to introduce the common-mode variables: assuming the references as in Fig. 3a, the differential and common-mode variables are

$$I_{\mathrm{d}}(z) \equiv \frac{I_1(z) - I_2(z)}{2}, \quad V_{\mathrm{d}}(z) \equiv V_1(z) - V_2(z), \tag{57}$$

$$I_{\mathrm{C}}(z) \equiv I_1(z) + I_2(z), \quad V_{\mathrm{C}}(z) \equiv \frac{V_1(z) + V_2(z)}{2}. \tag{58}$$

In order to study the mode conversion, let us assume the line to be excited by a pure differential mode current at the near end, with the far end left open: $I_{\mathrm{d1}} = 1$ (arbitrary units) and $I_{\mathrm{c1}} = 0$. Figure 16 shows the distribution of the excited common mode currents computed at 1.7 and 2.5 GHz. For low frequencies the mode conversion due to asymmetric signal conductors may be neglected, whereas for frequencies above 1 GHz the excited common mode current starts to be relevant.

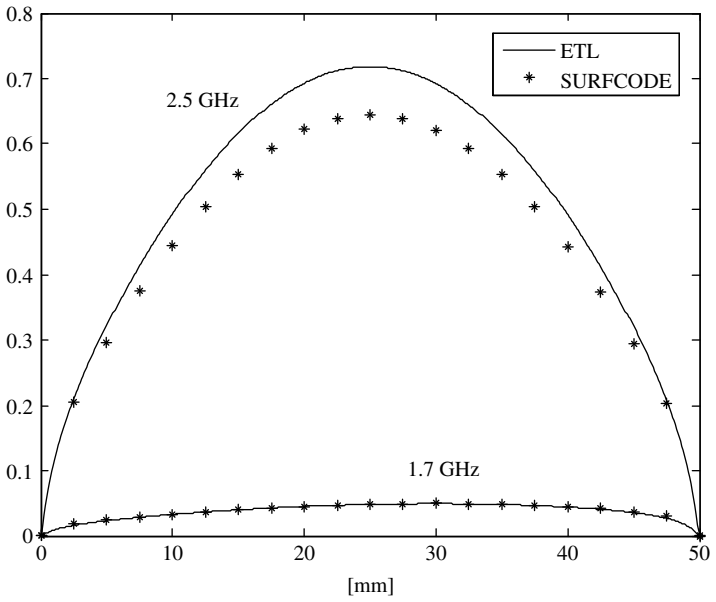

Figure 16: Case 5, common-mode current distribution for a pure differential excitation.

5.4 A comparison between CNT and copper interconnects for nanoelectronic applications

In future ultra-large-scale integrated circuits the use of copper nano-interconnects will be seriously limited by the strong degradation of its performances. The main challenge for Cu nano-interconnects is the trade-off between the request for increasing current density and the steep increase of the resistivity which, at nanometric dimensions, rises to values higher than its bulk value of $\rho = 1.7$ μΩ/cm. Because of heating, this high value will limit the maximum allowed current density. For 45 nm node technology, the International Technology Roadmap for Semiconductors (ITRS) [44] foresees, for instance, a request of a current density in local vias of 8×10^6 A/cm^2, whereas the maximum allowed current density for copper will be about 4.5×10^6 A/cm^2. This limitation suggests considering the use of metallic CNTs, given their excellent electrical and thermal properties (see Table 1 in Section 4).

As first case-study, we consider the simple interconnect structure of Fig. 7, made by a single CNT of radius $r_c = 2.712$ nm at a distance $h = 20$ nm from a perfect ground, and compare its performances to those which would be in principle obtained by scaling the copper technology to the same dimensions (Case 6). For this case, we assume $l = 1$ μm and $\upsilon = 3.33 \times 10^{11}$ s^{-1}. To investigate the validity limits of the transmission line model equation (50), its predictions have been compared to those provided by a full-wave three-dimensional electromagnetic numerical model based on the same fluid description of the conduction [29]. Figure 17 shows the absolute value of the input admittance of the interconnect terminated on a short circuit: the transmission line model provides accurate results up to 1–2 THz.

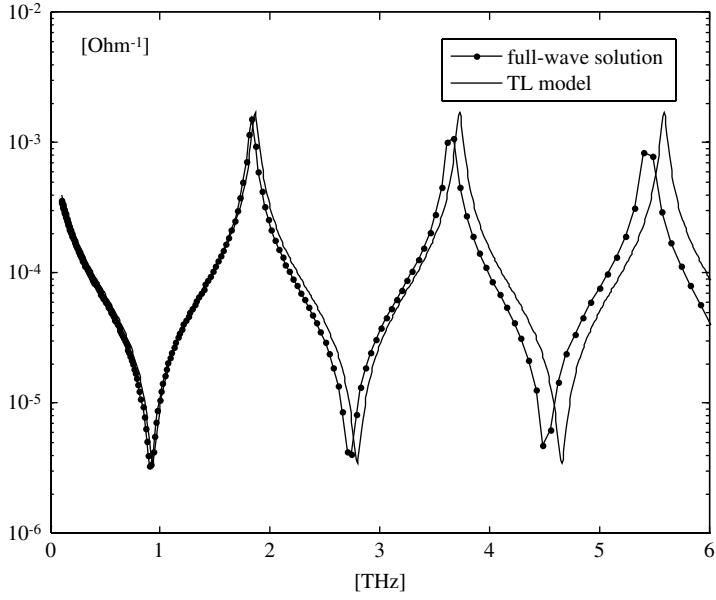

Figure 17: Case 6, absolute value of the input admittance.

Let us first consider lossless interconnects. For the considered case using the definition in eqn (52), we have $c_{CNT} \approx 0.0120 c_0$, hence the *electrical length* of CNT interconnects is completely different from that of the copper one interconnect. Figure 18a shows the frequency behavior of the absolute value of the input impedance compared to that of the equivalent copper interconnect, assuming an interconnect length of l = 10 μm. The CNT interconnect shows resonances at much lower frequencies. Resonances are extremely undesirable for interconnects, hence the above result seems to limit to short lengths (<1 μm) the possibility to use CNT interconnects in high-speed circuits. However, if we take into account the damping effect due to the huge p.u.l. resistance R predicted by eqn (51) this conclusion may change. For the considered case it is $R \approx 1.16$ kΩ/μm: it introduces a strong damping effect able to cancel out the resonance peaks, as shown in Fig. 18b, where the absolute value of the input impedance for CNT interconnect is computed both considering (real CNT) and disregarding (ideal CNT) the effect of R. This result agrees with experimental evidence [16].

In order to compare the performances between CNT and Cu interconnects, it is useful to investigate the behavior of the scattering parameters. Figure 19a and b shows the absolute value of S_{11} and S_{12} computed for line lengths of 1 and 10 μm, respectively. For Cu interconnect, we disregard the increase of copper resistivity, assuming a constant value of $\rho_{Cu} \cong 1.7 \times 10^{-8}$ Ωm. The reference impedance for the definition of all the S-parameters is chosen equal to the lossless characteristic impedance of the CNT interconnect, $Z_{0CNT} \approx 13$ kΩ for this case (this is the reason for the particular behavior of such parameters for the copper case).

As a conclusion, provided that it would be possible to load the line with such an impedance, it is clear that CNT interconnect are suitable for short and intermediate lengths, while they introduce a strong attenuation for longer lines. In addition, for high frequencies they seem to outperform the ideally scaled conventional technology.

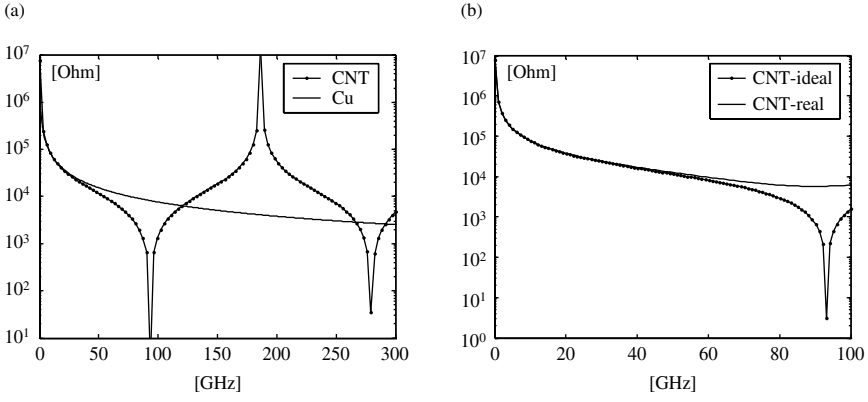

Figure 18: Case 6, absolute value of the input impedance for the ideal (a) and real (b) cases.

The high values of characteristic impedance, the p.u.l. resistance and the presence of huge parasitic resistance due to imperfect metal-CNT contacts make impossible the use of a single CNT as an interconnect. A more realistic condition should consider bundles of CNTs and compare their performance with that of copper, taking into account the increase of copper resistivity too at nanometric scale. Case 7 will refer to a microstrip, where the signal trace is made by a bundle of CNTs (Fig. 20), compared to a Cu conductor with the same cross-section tw. For the dimensions and the values of the parameters, we refer to the indications proposed by the ITRS for the 45 nm technology (year 2010) [44]. Let us consider a 200 (10 × 20) CNT bundle, assuming r_c = 1.35 nm, $d = 2r_c$ (hence w = 27 nm, $t = 2w$), $h = 2t$ and $\varepsilon_{r,eff} = 2.2$.

The propagation speed along CNTs is 3.2×10^7 m/s, whereas for the Cu interconnect it is 2×10^8 m/s. Note that at 30 GHz the wavelength is 1.6 mm for CNT and 10 mm for Cu interconnects: therefore up to lengths of 100 μm (local and intermediate level) the interconnects are electrically short. The effects of propagation should be taken into account only for global level (order of mm).

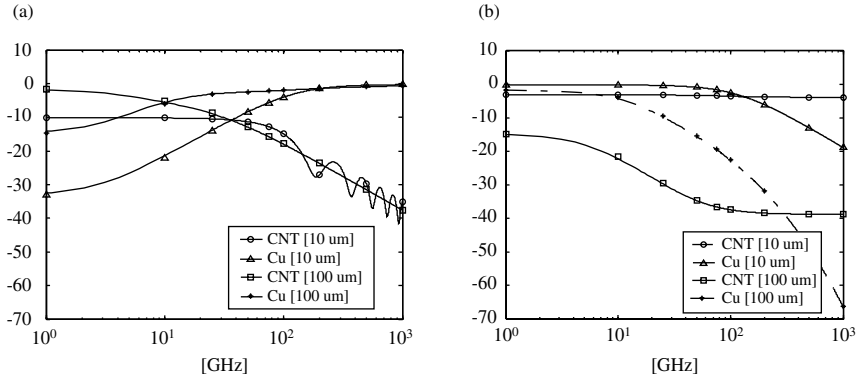

Figure 19: Case 6, absolute value of S_{11} (a) and S_{12} (b).

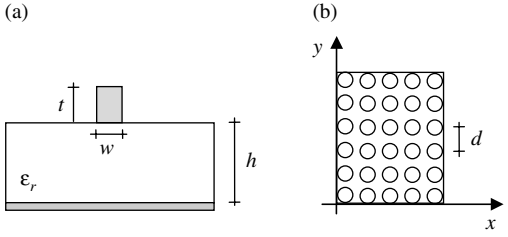

Figure 20: Case 7, the considered microstrip structure (a); realization of the signal trace with a CNT bundle (b).

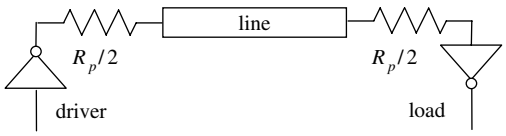

Figure 21: Case 7, the considered signaling system.

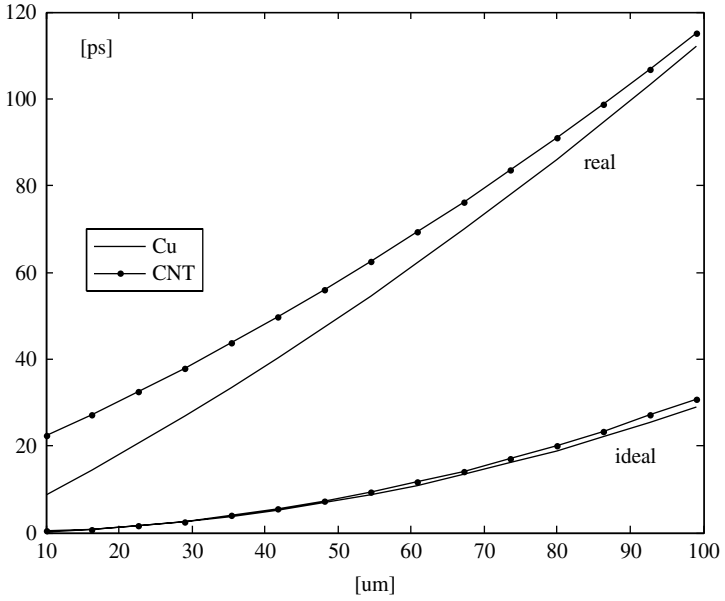

Figure 22: Case 7, computed switching delays.

Let us refer to the simple signaling system depicted in Fig. 21, where R_p is a generic parasitic resistance. As a consequence of the above considerations, the interconnect delay in this system is strongly dominated by the resistance. Let us compare the delay introduced by the CNT bundle to that produced by an equivalent Cu line, with resistivity $\rho = 4.08$ μΩ/cm [44]. Figure 22 shows the results obtained for an ideal case (ideal drivers and contacts, ideal load: $C_{load} = 0$) and for a real case (ideal drivers, $R_p = 100$ kΩ and $C_{load} = 0.01$ pF). The performances of the two interconnects are very close and an accurate control of the parasitic contact resistance for CNT bundles would lead to CNT delays comparable to the Cu ones. The result suggests considering CNT interconnects as possible alternative to Cu ones at least for local and intermediate level, since they provide similar delays but much better performances in terms of current density allowed, heating dissipation and mechanical properties.

6 Conclusions

In this chapter, the extension of the popular transmission line model to high-speed interconnects and to CNT nano-interconnects is discussed. Starting from a full-wave integral formulation, an ETL model is derived, able to describe interconnects with transverse dimensions comparable to the characteristic wavelength of the propagating signals. The model allows us to describe, with a computational cost typical of a transmission line model, the phenomena which are not included in the solution of the classical transmission line model but could be only taken into account by a full-wave solution. It is not only possible to obtain the correct behavior of high-speed interconnects in high-frequency ranges, but also to distinguish between the phenomena affecting the solution at such frequencies: finite size, radiation, mode conversion, frequency-dependent losses in conductors and dielectrics, excitation of parasitic modes.

Starting from a fluid model, a transmission line model is also derived to describe the propagation along interconnects made by metallic CNTs. Although simple, this model takes into account complex phenomena related to the quantistic behavior of such nanostructures, with a suitable definition of the transmission line model parameters. This tool is extremely useful to compare the performances of CNT interconnects and conventional ones for future nanoelectronic applications.

Acknowledgements

The authors wish to thank Dr. Walter Zamboni for useful support in performing the SURFCODE simulations.

References

[1] Whittaker, E., *A History of the Theories of Aether & Electricity*, Harper & Brothers: New York, 1960.
[2] Kirchhoff, G., On the motion of electricity in wires. *Philosophical Magazine XIII*, p. 393, 1857.
[3] Maxwell, J.C., A dynamical theory of the electromagnetic field. *Proc. Roy. Soc.*, **13**, pp. 531–536, 1864.
[4] Ferraris, G., *Sulla Teoria Matematica della Propagazione dell'Elettricità nei Solidi Omogenei*, Stamperia Reale: Torino, Italy, 1872.
[5] Heaviside, O., *Electromagnetic Theory*, E&FN Spon Ltd: London, 1951.
[6] Collin, R.E., *Foundation of Microwave Engineering*, McGraw-Hill: New York, 1992.
[7] Paul, C.R., *Analysis of Multiconductor Transmission Lines*, John Wiley & Sons: New York, 1994.
[8] Franceschetti, G., *Electromagnetics*, Plenum Press: New York, 1997.
[9] Lindell, I.V. & Gu, Q., Theory of time-domain quasi-TEM modes in inhomogeneous multiconductor lines. *IEEE Transactions on Microwave Theory and Techniques*, **35**, pp. 893–897, 1987.

[10] Tkatchenko, S., Rachidi, F. & Ianoz, M., Electromagnetic field coupling to a line of finite length: theory and fast iterative solutions in the frequency and time domain. *IEEE Transactions on Electromagnetic Compatibility*, **37**, pp. 509–518, 1995.

[11] Larrabee, D.A., Interaction of an electromagnetic wave with transmission lines, including reradiation. *Proc. of IEEE Intern. Symp. Electromagnetic Compatibility*, **1**, pp. 106–111, 1998.

[12] Haase, H. & Nitsch, J., Full-wave transmission-line theory (FWTLT) for the analysis of three-dimensional wire like structure. *Proc. of Intern. Symposium on Electromagnetic Compatibility*, Zurich, pp. 235–240, 2001.

[13] Tkatchenko, S., Rachidi, F. & Ianoz, M., High-frequency electromagnetic field coupling to long terminated lines. *IEEE Transactions on Electromagnetic Compatibility*, **43**, pp. 117–129, 2001.

[14] Cui, T.J. *et al.*, Full-wave analysis of complicated transmission-line circuits using wire models. *IEEE Transactions on Antennas and Propagation*, **50**, pp. 1350–1359, 2002.

[15] Cui, T.J. & Chew, W.C., A full-wave model of wire structures with arbitrary cross-sections. *IEEE Transactions on Electromagnetic Compatibility*, **45**, pp. 626–635, 2003.

[16] Haase, H., Nitsch, J. & Steinmetz, T., Transmission-line super theory: a new approach to an effective calculation of electromagnetic interactions. *URSI Bulletin*, pp. 33–59, 2003.

[17] Poljak, D. & Doric, V., Time-domain modeling of electromagnetic field coupling to finite-length wires embedded in a dielectric half-space. *IEEE Transactions on Electromagnetic Compatibility*, **47**, pp. 247–253, 2005.

[18] Maffucci, A., Miano, G. & Villone, F., Full-wave transmission line theory. *IEEE Transactions on Magnetics*, **39**, pp. 1593–1597, 2003.

[19] Maffucci, A., Miano, G. & Villone, F., An enhanced transmission line for conducting wires. *IEEE Transactions on Electromagnetic Compatibility*, **46(4)**, pp. 512–528, 2004.

[20] Maffucci, A., Miano, G. & Villone, F., An enhanced transmission line model for conductors with arbitrary cross-sections. *IEEE Transactions on Advanced Packaging*, **28(2)**, pp. 174–188, 2005.

[21] Peterson, A.F., Ray, S.L. & Mittra, R., *Computational Methods for Electromagnetics*, IEEE Press: New York, 1998.

[22] King, R.W.P., Fikioris, G.J. & Mack, R.B., *Cylindrical Antennas and Arrays*, Cambridge University Press: New York, 2002.

[23] Iijima, S., Helical microtubules of graphitic carbon. *Nature*, **354**, pp. 56–58, 1991.

[24] Avouris, P., Appenzeller, J., Marte, R. & Wind, S.J., Carbon nanotube electronics. *Proceedings of IEEE*, **91(11)**, pp. 1772–1784, 2003.

[25] Hoenlein, W. *et al.*, Carbon nanotube applications in microelectronics. *IEEE Trans. on Comp. and Packaging Techn.*, **27(4)**, pp. 629–634, 2004.

[26] Kreupl, F. *et al.*, Carbon nanotubes in interconnect applications. *Microelectronic Engineering*, **64**, pp. 399–408, 2002.

[27] Burke, P.J., An RF circuit model for carbon nanotubes. *IEEE Trans. on Nanotechnology*, **2**, pp. 55–58, 2003.

[28] Anantram, M.P. & Léonard, F., Physics of carbon nanotube electronic devices. *Reports on Progress in Physics*, **69**, pp. 507–561, 2006.

[29] Miano, G. & Villone, F., An integral formulation for the electrodynamics of metallic carbon nanotubes based on a fluid model. *IEEE Transactions on Antennas and Propagation*, **54**, pp. 2713–2724, 2006.

[30] Maffucci, A., Miano, G. & Villone, F., A transmission line model for metallic carbon nanotube interconnects. *International Journal of Circuit Theory and Applications*, published on line, DOI: 10.1002/cta.396. 2006.

[31] Chiariello, A.G., Maffucci, A., Miano, G., Villone, F. & Zamboni, W., Electromagnetic models for metallic carbon nanotube interconnects. *COMPEL, International Journal for Computation and Mathematics in Electrical and Electronic Engineering*, **26(3)**, pp. 571-585, 2007.

[32] Michalski, K.A. & Mosig, J.R., Multilayered media Green's functions in integral equation formulations. *IEEE Transactions on Antennas and Propagation*, **45(3)**, pp. 508–519, 1997.

[33] Chow, Y.L., Yang, J.J., Fang, D.G. & Howard, G.E., A closed-form spatial Green's function for the thick microstrip substrate. *IEEE Trans on Microwave Theory and Techniques*, **39**, pp. 588–592, 1991.

[34] Kourkoulos, V.N. & Cangellaris, A.C., Accurate approximation of Green's functions in planar stratified media in terms of a finite sum of spherical and cylindrical waves. *IEEE Transactions on Antennas and Propagation*, **54**, pp. 1568–1576, 2006.

[35] Chiariello, A.G., Maffucci, A., Miano, G., Villone, F., & Zamboni, W, Full-wave numerical analysis of single-layered substrate planar interconnects. *Proc. of SPI 2006, IEEE Work. on Signal Propagation on Interconnects*, Berlin, Germany, pp. 57–60, 2006.

[36] Slepyan, G.Y., Maksimenko, S.A., Lakhtakia, A., Yevtushenko, O. & Gusakov, A.V., Electrodynamics of carbon nanotubes: dynamics conductivity, impedance boundary conditions, and surface wave propagation. *Physical Review B*, **60**, pp. 17136–17149, 1999.

[37] Nieuwoudt, A. & Massoud, Y., Evaluating the impact of resistance in carbon nanotube bundles for VLSI interconnect using diameter-dependent modeling techniques. *IEEE Transactions on Electron Devices*, **53(10)**, pp. 2460–2466, 2006.

[38] Raychowdhury, A. & Roy, K., Modelling of metallic carbon-nanotube interconnects for circuit simulations and a comparison with Cu interconnects for scaled technologies. *IEEE Transactions on Computer-Aided Design for Integrated Circuits and Systems*, **25**, pp. 58–65, 2006.

[39] Banerjee, K. & Srivastava, N., Are carbon nanotubes the future of VLSI interconnections. *Proc. Design Automation Conference DAC*, San Francisco, CA, USA, pp. 809–814, 2006.

[40] Burke, G.J. & Poggio, A.J., Numerical electromagnetic code (NEC) – method of moments. Naval Ocean Systems Center, Technical Document 116, 1981.
[41] HFSS™ 3D Full-wave Electromagnetic Field Simulation, Ansoft Corporation. http://www.ansoft.com/products/hf/hfss/.
[42] Miano, G. & Villone, F., A surface integral formulation of Maxwell equations for topologically complex conducting domains. *IEEE Transactions on Antennas and Propagation*, **53(12)**, pp. 4001–4014, 2005.
[43] Miano, G. & Maffucci, A., *Transmission Lines and Lumped Circuits*, Academic Press: New York, 2001.
[44] International Technology Roadmap for Semiconductors, Edition 2005, http://public.itrs.net.

CHAPTER 7

The electromagnetic field coupling to buried wires: frequency and time domain analysis

D. Poljak
Department of Electronics, FESB, University of Split, Split, Croatia.

Abstract

This chapter deals with the transient analysis of buried cables using the wire antenna theory and applying both the frequency and the time domain approach. On one hand, if the solution for a large number of incident waves arriving from various directions is of interest then the frequency domain approach is appropriate. On the other hand, for some electromagnetic compatibility applications in which accurate frequency data are required, the frequency samples obtained by the use of Fourier transform do not ensure accurate results and the time domain approach would be a better choice. Particularly, the direct time domain approach is convenient if the transient response is required only for the early time behavior, since the frequency domain approach requires computing of the frequency response up to the maximum effective frequency and the entire range of frequency spectrum has to be transformed. The frequency domain model is based on the Pocklington integral equation while the time domain formulation deals with the Hallen integral equation approach. Both the Pocklington and the Hallen equation are handled via the appropriate Galerkin–Bubnov scheme of the indirect boundary element method. The strengths and weaknesses of both approaches are discussed.

1 Introduction

The electromagnetic field coupling to lines buried in a lossy medium is of great practical interest for many electromagnetic compatibility (EMC) applications [1–4], such as transient analysis of power and communications cables. Basically, the buried wire can represent a telephone cable, power cable, or a cylindrical antenna operating at a very low frequency. Some important applications are also related to submarine communication (long dipoles submerged in water), geophysical

probing and electromagnetic stimulation of biological tissue. In the past, the transient excitation of buried wires, as one of the major causes of malfunction of telecommunication and power lines, has been mostly related to the lightning discharge problems [3].

Generally, the electromagnetic field coupling to underground wires configurations [1, 2] has been investigated to a somewhat lesser extent than coupling to above-ground lines [3–11].

The studies related to buried wires are usually based on an approximate transmission line approach [3]. The transmission line approach can be considered as a compromise between a quasi-static approximation and a full wave (wire antenna) model, and it is mostly related to infinite or at least very long buried wires.

However, the effects at the line ends cannot be taken into account utilizing the transmission line approach [12]. Also, the effect of the earth–air interface has usually been neglected featuring the assumption that the wire is buried at a very large depth [1].

The transmission line approach, though sufficient approximation if long lines with electrically small cross sections are considered, fails if one deals with the lines of finite length and high-frequency excitations.

Namely, the transmission line model fails to predict resonances, fails to take into account the presence of a lossy ground and the effects at the line ends [3–7]. Consequently, when the lines of the finite length are of interest the full wave model based on the receiving antenna (scattering) theory has to be used.

Thus, the wave-like behavior of the induced responses at higher frequencies requires a more general approach which is based on integral equations arising from the wire antenna theory. On the other hand, the principal restriction of the wire antenna model applied to overhead lines is often related to the long computational time required for the calculations pertaining to the long lines.

The transient analysis of buried cables using the wire antenna theory can be carried out in either frequency or time domain. Essentially, there is no definitive advantage that could be gained using the indirect frequency domain approach or the direct time domain solution method.

Generally, if the solution for a large number of incident waves arriving from various directions is of interest then the frequency domain approach is appropriate.

On the other hand, for some EMC applications in which accurate frequency data are required, the frequency samples obtained by the use of Fourier transform do not ensure accurate results. The time domain approach would be a better choice if the transient response is required only for the early time behavior, since the frequency domain approach requires computing of the frequency response up to the maximum effective frequency and the entire range of frequency spectrum has to be transformed.

This chapter deals with both approaches. The frequency domain model is based on the Pocklington integral equation while the time domain formulation deals with the Hallen integral equation approach. The strengths and weaknesses of both approaches are discussed.

2 The frequency domain approach

The frequency domain antenna theory approach provides one to take into account the earth–air interface effects via rigorous Sommerfeld integral formulation. However, the Sommerfeld integrals cannot be evaluated analytically, while the corresponding numerical solution is rather demanding and very time consuming [13–17]. Consequently, some authors prefer to use a simplified approach based on the reflection coefficient approximation [1, 4].

The wire antenna approach to the analysis of the plane wave coupling to the buried cable of finite length, with the effect of the half space included via the reflection coefficient approximation, has been proposed in [18]. This approach has been extended to the more complex case of a plane wave excitation with an arbitrary angle of incidence [19].

The frequency domain formulation presented in this chapter is based on the Pocklington integro-differential equation. The reflection coefficient by which the earth–air interface is taken into account is included in the integral equation kernel.

This integral equation is solved via the Galerkin–Bubnov scheme of the indirect boundary element method (GB-IBEM) [20]. Furthermore, the transient response of the wire is computed using the inverse Fourier transform [21].

2.1 Formulation in the frequency domain

The horizontal line of length L and radius a, buried in a lossy ground at depth d, is shown in Fig. 1. The current distribution along the buried wire is governed by the corresponding Pocklington integro-differential equation. This integro-differential equation can be derived by enforcing the interface conditions for the tangential electric field components.

Assuming the wire to be perfectly conducting, the total field along the wire surface vanishes, i.e.:

$$\vec{e}_x \vec{E}^{\,\mathrm{tot}} = 0 \tag{1}$$

where the total field $\vec{E}^{\,\mathrm{tot}}$ is composed from the excitation $\vec{E}^{\,\mathrm{exc}}$ and scattered field $\vec{E}^{\,\mathrm{sct}}$ field components, respectively:

$$\vec{E}^{\,\mathrm{tot}} = \vec{E}^{\,\mathrm{exc}} + \vec{E}^{\,\mathrm{sct}} \tag{2}$$

where the excitation field component represents the sum of the incident field $\vec{E}^{\,\mathrm{inc}}$ and field reflected from the lossy ground $\vec{E}^{\,\mathrm{ref}}$:

$$\vec{E}^{\,\mathrm{exc}} = \vec{E}^{\,\mathrm{inc}} + \vec{E}^{\,\mathrm{ref}} \tag{3}$$

The scattered field component is given by:

$$\vec{E}^{\,\mathrm{sct}} = -j\omega\vec{A} - \nabla\varphi \tag{4}$$

where $\vec{A}$ is the magnetic vector potential and φ is the electric scalar potential.

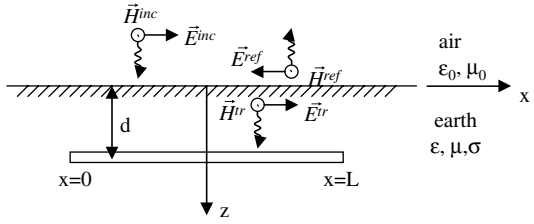

Figure 1: A straight wire of finite length buried in a dissipative medium.

According to the widely used thin wire approximation [3, 4] only the axial component of the magnetic potential differs from zero and eqn (4) becomes:

$$E_x^{\text{sct}} = -j\omega A_x - \frac{\partial \varphi}{\partial x} \tag{5}$$

where the magnetic vector potential and electric scalar potential are, respectively, defined as:

$$A_x = \frac{\mu}{4\pi}\int_0^L I(x')g(x,x')\,\mathrm{d}x' \tag{6}$$

$$\varphi(x) = \frac{1}{4\pi\varepsilon_{\text{eff}}}\int_0^L q(x')g(x,x')\mathrm{d}x' \tag{7}$$

where ε_{eff} is the complex permittivity of the lossy ground given by:

$$\varepsilon_{\text{eff}} = \varepsilon_{\text{r}}\varepsilon_0 - j\frac{\sigma}{\omega} \tag{8}$$

while $q(x)$ is the charge distribution along the line, $I(x')$ denotes the induced current along the line and $g(x, x')$ stands for the Green's function given by:

$$g(x,x') = g_0(x,x') - R_{\text{TM}}g_i(x,x') \tag{9}$$

and $g_0(x, x')$ denotes the lossy medium Green function:

$$g_0(x,x') = \frac{\mathrm{e}^{-jk_2R_1}}{R_1} \tag{10}$$

while $g_i(x, x')$ is, in accordance to the image theory, given by:

$$g_i(x,x') = \frac{\mathrm{e}^{-jk_2R_2}}{R_2} \tag{11}$$

where k_2 is the propagation constant of the lower medium and R_1 and R_2 are distances from the source point in the ground and from the corresponding image in the air to the observation point defined by:

$$R_1 = \sqrt{(x-x')^2 + a^2}, \quad R_2 = \sqrt{(x-x')^2 + 4d^2} \tag{12}$$

The influence of a nearby ground interface is taken into account by means of the Fresnel plane wave reflection coefficient:

$$R_{\mathrm{TM}} = \frac{\frac{1}{\underline{n}}\cos\theta - \sqrt{\frac{1}{\underline{n}} - \sin^2\theta}}{\frac{1}{\underline{n}}\cos\theta + \sqrt{\frac{1}{\underline{n}} - \sin^2\theta}}, \quad \theta = \operatorname{arctg}\frac{|x-x'|}{2d}, \quad \underline{n} = \frac{\varepsilon_{\mathrm{eff}}}{\varepsilon_0} \tag{13}$$

The linear charge density and the current distribution along the line are related through the equation of continuity [7]:

$$q = -\frac{1}{j\omega}\frac{\mathrm{d}I}{\mathrm{d}x} \tag{14}$$

Substituting eqn (14) into eqn (7) yields:

$$\varphi\,(x) = -\frac{1}{j4\pi\omega\varepsilon_{\mathrm{eff}}}\int_0^L \frac{\partial I(x')}{\partial x'} g(x,x')\mathrm{d}x' \tag{15}$$

Combining eqns (5), (6) and (15) results in the following integral relationship for the scattered field:

$$E_x^{\mathrm{sct}} = -j\omega\frac{\mu}{4\pi}\int_0^L I(x')g(x,x')\mathrm{d}x' + \frac{1}{j4\pi\omega\varepsilon_{\mathrm{eff}}}\frac{\partial}{\partial x}\int_0^L \frac{\partial I(x')}{\partial x'} g(x,x')\mathrm{d}x' \tag{16}$$

Finally, eqns (3) and (16) result in the following integral equation for the unknown current distribution induced along the line:

$$E_x^{\mathrm{exc}} = j\omega\frac{\mu}{4\pi}\int_0^L I(x')g(x,x')\mathrm{d}x' - \frac{1}{j4\pi\omega\varepsilon_{\mathrm{eff}}}\frac{\partial}{\partial x}\int_0^L \frac{\partial I(x')}{\partial x'} g(x,x')\mathrm{d}x' \tag{17}$$

Integral equation (17) is well-known in antenna theory and represents one of the most commonly used variants of the Pocklington's integro-differential equation.

The electric field transmitted into the lossy ground and illuminating the buried line is given by:

$$E_x^{\mathrm{exc}} = E_x^{\mathrm{tr}} = E_0(\Gamma_{\mathrm{TE}}\sin\phi - \Gamma_{\mathrm{TM}}\cos\theta_t\cos\phi)\,\mathrm{e}^{-jk_2\vec{n}_i\vec{r}} \tag{18}$$

where α is the angle between *E-field* vector while the plane of incidence and θ_{t} is defined by the Snell's law [1]:

$$k_1\sin\theta = k_2\sin\theta_{\mathrm{t}} \tag{19}$$

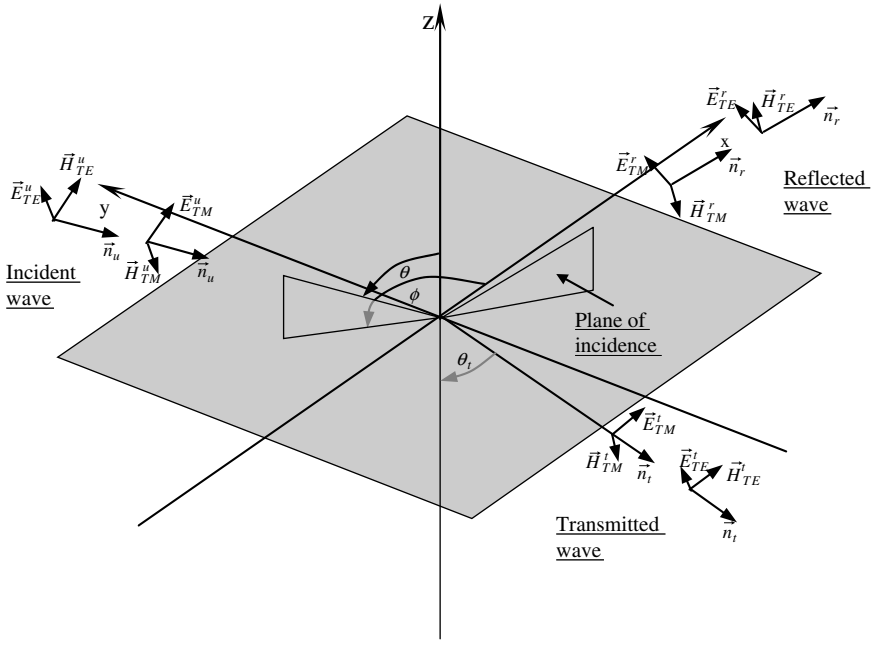

Figure 2: Incident, reflected and transmitted wave from an air–earth interface.

where k_1 is the propagation constant in the free space.

Quantities Γ_{TM} and Γ_{TE} denote the vertical and horizontal Fresnel transmission coefficients, respectively, at the air–earth interface (Fig. 2) given by [1]:

$$\Gamma_{\mathrm{TM}} = \frac{2\sqrt{\underline{n}}\cos\theta}{\underline{n}\cos\theta + \sqrt{\underline{n} - \sin^2\theta}} \tag{20}$$

$$\Gamma_{\mathrm{TE}} = \frac{2\cos\theta}{\cos\theta + \sqrt{\underline{n} - \sin^2\theta}} \tag{21}$$

and $\vec{n}_t\vec{r}$ is distance from the origin point to the observation point at the wire surface.

$$\vec{n}_t\vec{r} = -x\sin\theta_t\cos\phi - y\sin\theta_t\sin\phi - z\cos\theta_t \tag{22}$$

Solving the Pocklington integro-differential equation (17) the current distribution at the operating frequency is obtained.

2.2 Numerical solution of the integro-differential equation

The numerical solution of eqn (17) is obtained via GB-IBEM, which is outline below. More detailed description of the method can be found in [13].

An operator form of the Pocklington integro-differential equation (18) can be, for convenience, symbolically written as:

$$KI = E \tag{23}$$

where K is a linear operator and I is the unknown function to be found for a given excitation E.

The unknown current is expanded into a finite sum of linearly independent basis functions $\{f_i\}$ with unknown complex coefficients α_i:

$$I \cong I_n = \sum_{i=1}^{n} \alpha_i f_i \tag{24}$$

Substituting eqn (24) into eqn (23) yields:

$$KI \cong KI_n = \sum_{i=1}^{n} \alpha_i K f_i = E_n = P_n(E) \tag{25}$$

where $P_n(E)$ is called a projection operator [13].

Now the residual R_n is formed as follows:

$$R_n = KI_n - E = P_n(E) - E \tag{26}$$

According to the definition of the scalar product of functions in Hilbert function space the error R_n is weighted to zero with respect to certain weighting functions $\{W_j\}$, i.e.:

$$\left\langle R_n, W_j \right\rangle = 0, \quad j = 1, 2, ..., n \tag{27}$$

where the expression in brackets stands for a scalar product of functions given by:

$$\left\langle R_n, W_j \right\rangle = \int_{\Omega} R_n W_j^* \, \mathrm{d}\Omega \tag{28}$$

where Ω denotes the actual calculation domain.

Since the operator K is linear, a system of linear equations is obtained by choosing $W_j = f_j$, which implies the Galerkin–Bubnov procedure. Thus, it can be written as:

$$\sum_{i=1}^{n} \alpha_i \left\langle K f_i, f_j \right\rangle = \left\langle E, f_j \right\rangle, \quad j = 1, 2, ..., n \tag{29}$$

Equation (29) is the strong Galerkin–Bubnov formulation of the Pocklington integral equation (18). Utilizing the integral equation kernel symmetry and taking into

account the Dirichlet boundary conditions for the current at the wire ends of the cylinder, after integration by parts eqn (29) becomes:

$$\sum_{j=1}^{n} a_i \frac{1}{j4\pi\omega\varepsilon_{\text{eff}}}\left[\int_0^L \frac{\partial f_j(x)}{\partial x}\int_0^L \frac{\partial f_i(x')}{\partial x'} g(x,x')\mathrm{d}x'\,\mathrm{d}x + k_2^2 \int_0^L f_j(x)\int_0^L f_i(x')g(x,x')\mathrm{d}x'\,\mathrm{d}x\right]$$
$$= \int_0^L E_x^{\text{exc}}(x) f_j(x)\,\mathrm{d}x, \quad j = 1,2,\ldots n \tag{30}$$

Equation (30) represents the weak Galerkin–Bubnov formulation of the integral equation (23).

The resulting system of algebraic equations arising from the boundary element discretization of eqn (30) is given by:

$$\sum_{j=1}^{M} [Z]_{ji}\{I\}_i = \{V\}_j, \quad j = 1,2,\ldots,M \tag{31}$$

where $[Z]_{ji}$ is the local matrix representing the interaction of the *i*th source boundary element with the *j*th observation boundary element:

$$[Z]_{ji} = \frac{1}{j4\pi\omega\varepsilon_{\text{eff}}}\left[\int_0^L \{D\}_j \int_0^L \{D\}^{\mathrm{T}} g(x,x')\mathrm{d}x'\,\mathrm{d}x + k_2^2 \int_0^L \{f\}_j \int_0^L \{f'\}^{\mathrm{T}} g(x,x')\mathrm{d}x'\,\mathrm{d}x\right] \tag{32}$$

The vector $\{I\}$ contains the unknown coefficients of the solution, and it represents the local voltage vector. Matrices $\{f\}$ and $\{f'\}$ contain the shape functions while $\{D\}$ and $\{D'\}$ contain their derivatives, M is the total number of line segments, and Δl_i, Δl_j are the widths of *i*th and *j*th segment.

Functions $f_k(z)$ are the Lagrange's polynomials and $\{V\}_j$ is the local right-side vector for the *j*th observation segment,

$$\{V\}_j = \int_{\Delta l_j} E_x^{\text{exc}}\{f\}_j\,\mathrm{d}z \tag{33}$$

representing the local voltage vector.

Linear approximation over a boundary element is used as it has been shown that this choice provides accurate and stable results [13].

2.3 The calculation of a transient response

Calculating the current distribution along a buried wire in a wide frequency spectrum one obtains the transfer function of the system, $H(f)$ is obtained.

To analyze the transient response of the buried wire, an incident field in a form of a single exponentially decaying function is used:

$$e_x^{\mathrm{tr}}(t) = E_0 e^{-at} \tag{34}$$

which Fourier transform is given by:

$$E_x^{\mathrm{tr}}(f) = \frac{E_0}{a + j2\pi f} \tag{35}$$

Now, the current distribution $I(f)$, i.e. the frequency response of the wire to the particular excitation (35) is obtained by multiplying the frequency spectrum of the excitation function with the corresponding transfer function of the linear system $H(f)$:

$$I(f) = H(f)E_x^{\mathrm{tr}}(f) \tag{36}$$

Applying the inverse Fourier transform is to be applied to the function $I(f)$ yields the transient current induced along the buried transmission line [21]:

$$i(t) = \int_{-\infty}^{\infty} I(f)e^{j2\pi ft}\mathrm{d}\omega \tag{37}$$

As the system transfer function $H(f)$ is represented by the discrete set of values, and the actual frequency response $I(f)$ is also represented by a discrete set of values, the integral equation (37) thus cannot be solved analytically and one has to deal with the Discrete Fourier transform (or in this case Fast Fourier Transform), i.e.:

$$i(t) = \mathrm{IFFT}(I(f)) \tag{38}$$

Thus, the discrete set of the time domain current values is defined by [21]:

$$i(n\Delta t) = F\sum_{k=0}^{N-1} I(k\,\Delta f)e^{jk\,\Delta f\,n\,\Delta t} \tag{39}$$

where F is the highest frequency taken into account, N is the total number of frequency samples, Δf is sampling interval and Δt is the time step.

2.4 Numerical results

For the comparison purposes, first the current distribution induced along a wire conducting cylinder, immersed in sea water, is computed assuming a unit incident field. The water parameters are $\varepsilon_r = 80$ and $\sigma = 4$ S/m, and the operating frequency is $f = 1$ MHz. The cylinder length is $L = 120$ and 160 m, respectively, with a radius of $a = 0.6$ and 0.8 m, respectively, while in Fig. 3 the calculated current distributions are compared to the analytical results available from [22]. Agreement is found to be satisfactory.

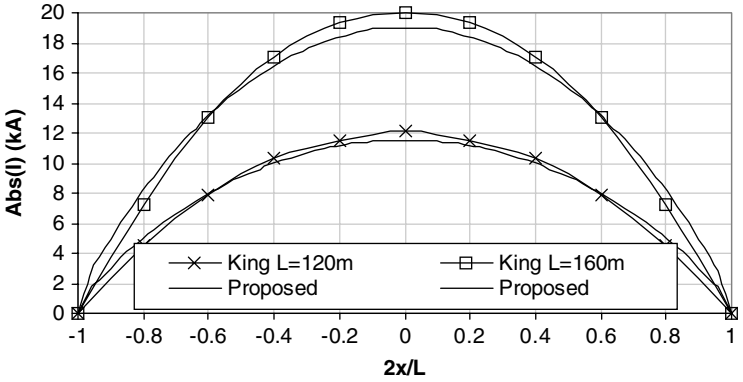

Figure 3: Comparison of numerical results obtained with different solution methods.

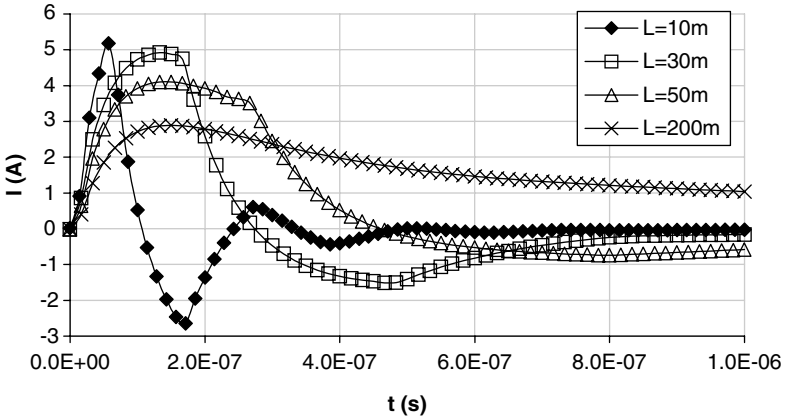

Figure 4: Transient response for different wire lengths.

Further numerical examples are related to the transmission lines buried in a lossy ground with permittivity $\varepsilon_r = 10$ and conductivity $\sigma = 0.001$ S/m. Conductor radius is $a = 1$ cm wire length L and burial depth d are varied. The wire is excited by the transmitted plane wave with a single exponential decaying form eqn (35). The parameters of the exponential function are, as follows: $E_0 = 1$ V/m, $a = (7.854 \times 10^{-8}\ \text{s})^{-1}$.

The transient response, i.e. the current induced at the center of the wires having various lengths for the normal incidence is shown in Fig. 4. The burial depth is $d = 1$ m. The current wave reflections from the wire ends are clearly visible, particularly for the shorter wires. Figure 5 shows the influence of the burial depth on the induced current at the center of the 200 m long wire.

The both time shift and the attenuation of the signal seems to be increased with the depth. The only exception occurs for $d = 0.1$ m, where the induced current is lower then for $d = 1$ m. This happens due to the vicinity of the nearby ground–air interface.

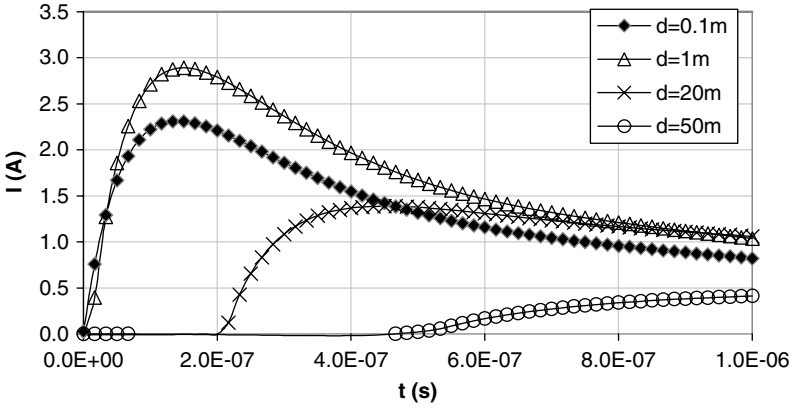

Figure 5: Transient response for different burial depths.

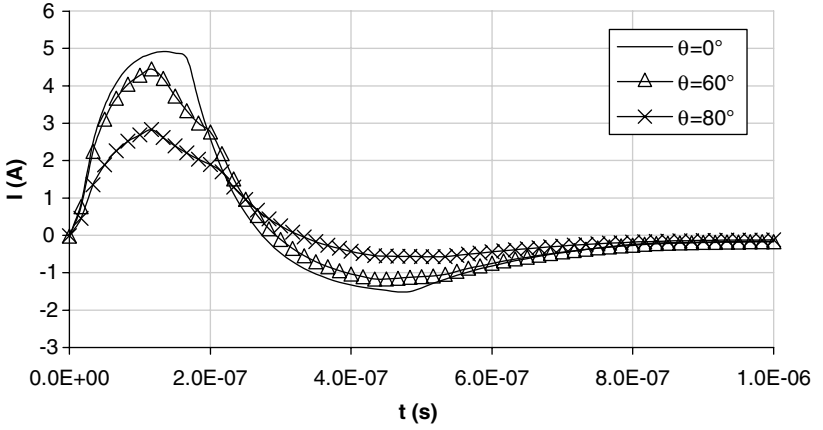

Figure 6: Transient response for different angles of incidence.

The transient response of the wire of the transmission line of length $L = 30$ m buried at depth $d = 1$ m for various angles of incidence $\theta = 0°$, $60°$ and $80°$ is shown in Fig. 6.

The transient response of the wire of the transmission line of length $L = 30$ m buried at depth $d = 1$ m for various angles of incidence $\theta = 0°$, $60°$ and $80°$ is shown in Fig. 6. For the higher angle θ, amplitude of the induced current at the wire center is smaller, since the tangential component of the transmitted electric field is also decreased.

3 Time domain approach

This section deals with a time domain study of a single straight wire embedded in a dielectric half-space and illuminated by a non-uniform transient electric field.

This topic is very important as a starting point in the transient analysis of wires buried in a lossy medium which is of great practical interest for many EMC applications [1–4].

The analysis presented in this section is based on the wire antenna theory and is carried out directly in the time domain. Dealing with a rather simple geometry of a single wire embedded in a dielectric half-space this section aims to introduce some basic ideas on the subject. The method can be also applied to a case of arbitrary wire configurations, which is of much more practical importance in EMC applications.

The time domain formulation presented in this section is based on the space–time Hallen integral equation for half-space problems [23]. The effects of the two-media configuration are taken into account via the corresponding reflection coefficient and the transmission coefficient. The transient current along the straight wire embedded in a dielectric half-space is obtained by solving the corresponding Hallen integral equation via the time domain variant of the GB-IBEM [13].

Once calculating the space–time current distribution along the wire, to further evaluate the obtained transient response, the time domain energy measures can be computed by spatially integrating the squared current and charge along the wire [24–27].

Furthermore, a simplified version of space–time reflection/transmission coefficient has been promoted in [28], while an alternative formulation for a finite length wire placed within the dielectric half-space featuring the simplified form of the reflection/transmission coefficient, instead of use of Fresnel coefficients has been proposed in [29].

This alternative approach to the time domain analysis of buried wires is presented in this section, as well.

3.1 Formulation in the time domain

A perfectly conducting straight thin wire of length L and radius a, immersed in a dielectric medium at depth d is considered, as shown in Fig. 7. The wire is illuminated by a horizontally polarized transient electric field tangential along its

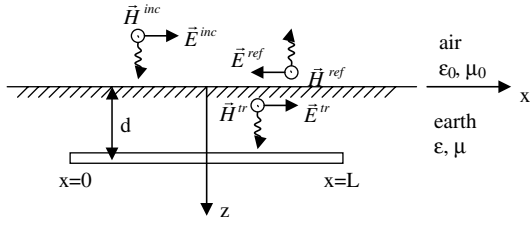

Figure 7: A straight wire embedded in a dielectric half-space.

surface, i.e. the case of normal incidence is considered only.

The mathematical framework of the problem is based on the wire antenna theory and thin wire approximation [3, 4].

The transient induced current flowing along the straight wire embedded in a dielectric half-space is governed by the corresponding space–time integral equation. The time domain formulation for the single wire problem in terms of the Pocklington or the Hallen integral equation type can be readily obtained as an extension of the wire in homogeneous dielectric medium.

The time domain Pocklington type integral equations often suffer from numerical instabilities, i.e. from the non-physical, rapidly growing oscillations at later instants of time [30].

On the other hand, the time domain Hallen integral equation does not contain either space or time derivatives within its kernel, which are found to be the origin of numerical instabilities. Consequently, the Hallen equation has been proven to be attractive from the computational point of view [4, 30–32].

The Hallen integral equation approach, also used for the transient analysis of straight wire configuration above-ground [8–11], is applied to the problem of wires embedded in a dielectric half-space in this section. The Hallen integral equation for the straight wire in unbounded lossless medium can be readily derived from the corresponding Pocklington integro-differential equation type.

Since the wire is perfectly conducting the tangential component of the total field vanishes on the antenna surface, i.e.:

$$E_x^{\text{inc}} + E_x^{\text{sct}} = 0 \tag{40}$$

where E_x^{inc} is the incident and E_x^{sct} scattered field on the metallic wire surface. From the first Maxwell equation:

$$\nabla x \, \vec{E} = -\frac{\partial \vec{B}}{\partial t} \tag{41}$$

and using the vector magnetic potential $\vec{A}$:

$$\vec{B} = \nabla x \, \vec{A} \tag{42}$$

it follows:

$$\vec{E}^{\text{inc}}\big|_{\text{tan}} = \left(\frac{\partial \vec{A}}{\partial t} + \nabla \varphi \right)_{\text{tan}} \tag{43}$$

where $\vec{A}$ and φ are space–time-dependent magnetic vector and electric scalar potential, respectively. These two potentials are to satisfy the Lorentz gauge:

$$\frac{\partial \varphi}{\partial t} + \frac{1}{\mu \varepsilon} \nabla \vec{A} = 0 \tag{44}$$

Differentiating eqn (43) and taking into account the Lorentz gauge equation (44) yields in the wave equation for magnetic vector potential $\vec{A}$:

$$\left(\frac{\partial^2 \vec{A}}{\partial t^2} - \frac{1}{\mu\varepsilon}\nabla(\nabla\vec{A})\right)_{|_{\tan}} = \frac{\partial \vec{E}^{\,\mathrm{inc}}}{\partial t}_{|_{\tan}} \tag{45}$$

In accordance to the thin wire approximation, only the axial component of the vector potential exists, so it can be written:

$$\frac{\partial^2 A_x}{\partial x^2} - \frac{1}{v^2}\frac{\partial^2 A_x}{\partial t^2} = -\frac{\partial E_x^{\mathrm{inc}}}{\partial t} \tag{46}$$

where v is the velocity of wave propagation in a homogeneous dielectric medium, defined as follows:

$$v = \frac{1}{\sqrt{\mu\varepsilon_{rg}\varepsilon_0}} \tag{47}$$

where $\varepsilon_{\mathrm{rg}}$ is the lower medium relative permittivity where c denotes the velocity of light.

Equation (46) is valid on the surface of the perfect conductor and the solution can be represented by a sum of the homogeneous equation solution and particular solution of the inhomogeneous equation:

$$A_x(x,t) = A_x^{\mathrm{h}}(x,t) + A_x^{\mathrm{p}}(x,t) \tag{48}$$

In addition, the solution of the homogeneous wave equation is given as a superposition of incident and reflected wave [13]:

$$A_x^{\mathrm{h}}(x,t) = F_1\left(t - \frac{x}{v}\right) + F_2\left(t + \frac{x}{v}\right) \tag{49}$$

The particular solution is given by the integral [13]:

$$A_x^{\mathrm{p}}(x,t) = \frac{\varepsilon v}{2}\int_{-\infty}^{x}\int_{-\infty}^{t-\frac{(x-x')}{c}} \frac{\partial E_x^{\mathrm{inc}}(x',t')}{\partial t}\mathrm{d}t'\,\mathrm{d}x' + \frac{\varepsilon v}{2}\int_{-\infty}^{x}\int_{-\infty}^{t+\frac{(x-x')}{c}} \frac{\partial E_x^{\mathrm{inc}}(x',t')}{\partial t}\mathrm{d}t'\,\mathrm{d}x' \tag{50}$$

Since the differential equation is related to the wire antenna surface eqn (50) simplifies into:

$$A_x^{\mathrm{p}}(x,t) = \frac{1}{2Z_{\mathrm{g}}}\int_0^L E_x^{\mathrm{inc}}\left(x', t - \frac{|x-x'|}{v}\right)\mathrm{d}x' \tag{51}$$

where Z_{g} is the corresponding impedance of a dielectric medium given by:

$$Z_{\mathrm{g}} = \sqrt{\frac{\mu}{\varepsilon_{rg}\varepsilon_0}} \tag{52}$$

On the other hand, the magnetic vector potential on the metallic wire surface on the left-hand side of eqn (48) may be also obtained as a solution of the wave equation:

$$\nabla^2\vec{A} - \mu\varepsilon\frac{\partial^2\vec{A}}{\partial t^2} = -\mu\vec{J}(r,t) \tag{53}$$

where $\vec{J}(r,t)$ denotes the surface current density.

The solution of differential equation (53) is usually obtained via the Green function theory by introducing the auxiliary equation:

$$\nabla^2 g - \mu\varepsilon\frac{\partial^2 g}{\partial t^2} = \delta(\vec{r}-\vec{r}', t-t') \tag{54}$$

The solution is given in the form of retarded Dirac impulse:

$$g(\vec{r}-\vec{r}', t-t') = \frac{\delta(t-t'-(R/v))}{4\pi R} \tag{55}$$

where R is a distance from the source to the observation point.

Then the solution of eqn (53) using the Green function approach may be written in the form:

$$\vec{A}(r,t) = \frac{\mu}{4\pi}\int_{-\infty}^{t}\int_{S}\vec{J}_s(\vec{r}',t)\frac{\delta(t-t'-R/v)}{R}\,\mathrm{d}S'\,\mathrm{d}t' \tag{56}$$

Performing the time domain integration one obtains:

$$\vec{A}(r,t) = \frac{\mu}{4\pi}\iint_{S}\frac{\vec{J}_s(r',t-R/v)}{R}\,\mathrm{d}S' \tag{57}$$

According to the thin wire approximation, the equivalent current along the wire is assumed to flow in the axis, while the observation points are located on the antenna surface, i.e. it follows:

$$I(x,t) = 2\pi a J_z(x,t) \tag{58}$$

and the axial component of the magnetic vector potential is given by:

$$A_x(x,t) = \frac{\mu}{4\pi}\int_{0}^{L}\frac{I(x',t-R/v)}{R}\,\mathrm{d}x' \tag{59}$$

Combining the relations (46) and (59) yields the Pocklington integro-differential equation:

$$\left[\frac{\partial^2}{\partial x^2} - \frac{1}{v^2}\frac{\partial^2}{\partial t^2}\right]\int_0^L \frac{I(x',t-R/v)}{4\pi R}\,\mathrm{d}x' = \frac{\partial E_x^{\mathrm{inc}}}{\partial t} \tag{60}$$

while relations (48), (49), (51) and (59) leads to the space–time Hallen integral equation:

$$\int_0^L \frac{I(x',t-R/v)}{4\pi R}\,\mathrm{d}x' = F_0\left(t-\frac{x}{v}\right)+F_L\left(t-\frac{L-x}{v}\right)+\frac{1}{2Z_\mathrm{g}}\int_0^L E_x^{\mathrm{inc}}\left(x',t-\frac{|x-x'|}{v}\right)\mathrm{d}x' \tag{61}$$

Equations (60) and (61) are both related to the straight, finite length wire in an unbounded dielectric medium, where the distance from the observation point is given by:

$$R=\sqrt{(x-x')^2+a^2} \tag{62}$$

The multiple reflections of the current at the free ends of the wire are taken into account by the unknown functions $F_0(t)$ and $F_L(t)$.

The Hallen integral equation for a homogeneous lossless medium can be also derived directly from the Pocklington equation by performing the straight-forward convolution [10].

The corresponding Hallen integral equation for the wire embedded in a dielectric half-space can be derived gradually.

As a first step, the Hallen integral equation for an unbounded medium equation (61) is transferred into the frequency domain:

$$\int_0^L \frac{I(x',s)\mathrm{e}^{-sR/v}}{4\pi R}\,\mathrm{d}x' = F_0(s)\mathrm{e}^{-sX/v}+F_L(s)\mathrm{e}^{-s(L-X)/v}+\frac{1}{2Z_\mathrm{g}}\int_0^L E_x^{\mathrm{inc}}(x',s)\,\mathrm{e}^{-s(|x-x'|/v)}\,\mathrm{d}x' \tag{63}$$

where $s=j\omega$ denotes the Laplace variable.

The frequency domain Hallen integral equation for a straight wire in a dielectric half-space is obtained by extending the integral equation (63) with an additional term due to an image wire in the air located at height d above interface. This term contains the reflection coefficient Γ_{ref} for the transverse magnetic (TM) polarization multiplied by the Green function of the image wire in the air. In addition, the incident field E_x^{inc} appearing in the last term in eqn (61) has to be replaced by the corresponding transmitted field E_x^{tr}.

Thus, the resulting space frequency Hallen integral equation for the straight wire embedded in a dielectric medium becomes:

$$\begin{aligned}&\int_0^L \frac{I(x',s)\,\mathrm{e}^{-\frac{sR}{v}}}{4\pi R}\,\mathrm{d}x' - \int_0^L \Gamma_{\mathrm{ref}}(\theta)\frac{I(x',s)\,\mathrm{e}^{-\frac{sR^*}{v}}}{4\pi R^*}\,\mathrm{d}x' \\ &\quad = F_0(s)\,\mathrm{e}^{-\frac{sx}{v}}+F_L(s)\,\mathrm{e}^{-s\frac{(L-x)}{v}}+\frac{1}{2Z_\mathrm{g}}\int_0^L E_x^{\mathrm{tr}}(x',s)\,\mathrm{e}^{-s\frac{|x-x'|}{v}}\mathrm{d}x'\end{aligned} \tag{64}$$

where R^* is the distance from the source point located at the image wire in the air to the observation point located at the wire immersed in a dielectric medium:

$$R^* = \sqrt{(x - x')^2 + 4d^2} \tag{65}$$

The space dependent reflection coefficient, by which the ground–air interface effects are taken into account, is defined by the relation [1]:

$$\Gamma_{\text{ref}}(\theta) = \frac{\dfrac{1}{\varepsilon_{\text{rg}}}\cos\theta - \sqrt{\dfrac{1}{\varepsilon_{\text{rg}}} - \sin^2\theta}}{\dfrac{1}{\varepsilon_{\text{rg}}}\cos\theta + \sqrt{\dfrac{1}{\varepsilon_{\text{rg}}} - \sin^2\theta}}, \quad \theta = \text{arctg}\frac{|x - x'|}{2d} \tag{66}$$

Finally, the electric field transmitted into the dielectric medium E_x^{tr} is given as follows:

$$E_x^{\text{tr}} = \Gamma_{\text{tr}}(\theta_{\text{tr}}) E_x^{\text{inc}} \tag{67}$$

where E_x^{inc} is the incident field in the air and $\Gamma_{\text{tr}}(\theta_{\text{tr}})$ is the corresponding transmission coefficient by which the air–ground interface effects are taken into account.

The space dependent transmission coefficient, for the case of normal incidence considered in this work, is given by [23]:

$$\Gamma_{\text{tr}}(\theta_{\text{tr}}) = \left.\frac{2\sqrt{\varepsilon_{\text{rg}}}\cos\theta_{\text{tr}}}{\varepsilon_{\text{rg}}\cos\theta_{\text{tr}} + \sqrt{\varepsilon_{\text{rg}} - \sin^2\theta_{\text{tr}}}}\right|_{\theta_{\text{tr}}=0} = \frac{2}{\sqrt{\varepsilon_{\text{rg}}} + 1} \tag{68}$$

where θ_{tr} is the angle of transmission.

The time domain Hallen equation for a straight thin wire in a dielectric half-space now can be obtained applying the inverse Laplace transform and the convolution theorem to the integral equation (64).

Therefore, it follows:

$$\int_0^L \frac{I(x', t - R/v)}{4\pi R}\,\mathrm{d}x' - \int_{-\infty}^{t}\int_0^L \Gamma_{\text{ref}}(\theta, \tau)\frac{I(x', t - R^*/v - \tau)}{4\pi R^*}\,\mathrm{d}x'\,\mathrm{d}\tau$$
$$= F_0\left(t - \frac{x}{v}\right) + F_L\left(t - \frac{L - x}{v}\right) + \frac{1}{2Z_{\text{g}}}\int_0^L E_x^{\text{tr}}\left(x', t - \frac{|x - x'|}{v}\right)\mathrm{d}x' \tag{69}$$

where the time domain counterpart of the Fresnel reflection coefficient $\Gamma_{\text{ref}}(\theta, t)$ is:

$$\Gamma_{\text{ref}}(\theta, t) = \Gamma_{\text{ref}}(\theta)\delta(t) \tag{70}$$

and $\delta(t)$ stands for the Dirac impulse.

The transmitted electric field in the dielectric medium E_x^{tr} represents a time domain counterpart of the relation (67) and can be obtained from the convolution integral:

$$E_x^{\mathrm{tr}}(x,t) = \int_{-\infty}^{t} E_x^{\mathrm{inc}}(x,t-\tau)\Gamma_{\mathrm{tr}}(\theta_{\mathrm{tr}},\tau)\mathrm{d}\tau \tag{71}$$

where $\Gamma_{\mathrm{tr}}(\theta_{\mathrm{tr}}, t)$ is the time domain transmission coefficient counterpart of the expression (68):

$$\Gamma_{\mathrm{tr}}(\theta,t) = \Gamma_{\mathrm{tr}}(\theta)\delta(t) \tag{72}$$

Substituting the relations (72) and (68) into eqn (71), for the case of normal incidence ($\theta_{\mathrm{tr}} = 0$), it follows:

$$E_x^{\mathrm{tr}} = \frac{2}{\sqrt{\varepsilon_{\mathrm{rg}}}+1} E_x^{\mathrm{inc}}(t-t_0) \tag{73}$$

where $t_0 = d/v$ denotes the time delay.

It should be stated that a field reference point ($x = 0$, $z = 0$) has been used throughout this analysis.

Finally, combining the relations (66)–(73) the resulting integral equation for the wire immersed in a dielectric medium becomes:

$$\int_0^L \frac{I(x',t-R/v)}{4\pi R}\mathrm{d}x' - \int_0^L \frac{\dfrac{1}{\varepsilon_{\mathrm{rg}}}\cos\theta - \sqrt{\dfrac{1}{\varepsilon_{\mathrm{rg}}}-\sin^2\theta}}{\dfrac{1}{\varepsilon_{\mathrm{rg}}}\cos\theta + \sqrt{\dfrac{1}{\varepsilon_{\mathrm{rg}}}-\sin^2\theta}} \frac{I(x',t-R^*/v)}{4\pi R^*}\mathrm{d}x'$$

$$= F_0\left(t-\frac{x}{v}\right) + F_L\left(t-\frac{L-x}{v}\right) + \frac{1}{2Z_{\mathrm{g}}}\int_0^L \frac{2}{\sqrt{\varepsilon_{\mathrm{rg}}}+1} E_x^{\mathrm{inc}}\left(x', t-t_0-\frac{|x-x'|}{v}\right)\mathrm{d}x' \tag{74}$$

The problem of a straight wire embedded in a dielectric medium governed by the space–time Hallen integral equation (74) can be solved by prescribing, without any loss of generality, the zero edge $I(0, t) = I(L, t) = 0$ and initial conditions $I(x, 0) = 0$.

The use of a convolution approach through eqns (69)–(72) to handle the reflection and transmission coefficients is not necessary for the case of dielectric half-space as they are only functions of angle. This integral equation formulation is used as it can serve as a starting point in deriving the model for the wire buried in a medium with finite conductivity.

3.2 Time domain energy measures

The transient response of a straight thin wire embedded in a dielectric half-space can be postprocessed by the time domain energy measures based on spatial integrals of the squared current and charge induced along the wire.

The time domain energy measures represented by the current and charge induced on an object yield insight into where and how much the object radiates as a function of time. These measures were originally proposed in [24], for wires in free space, and re-examined in [10, 25] and recently in [26]. The concept of the time domain energy measures is extended to the case of buried wires in [27].

Upon solving the set of Hallen integral equations (74) for the transient current along the wire located in a dielectric medium, the charge distribution along the wire can be determined from the continuity equation [10]:

$$q = -\int_0^t \frac{\partial I(x',t)}{\partial x'} \mathrm{d}t \tag{75}$$

where q is the linear charge distribution along the embedded wire in a dielectric half-space.

Having found the current and charge, measures of the H-field (kinetic) and the E-field (static) energy densities are expressed as proposed in [27].

The H-field energy is represented by the relation:

$$W_I = \frac{\mu_0}{4\pi} \int_0^L I^2(x',t) \mathrm{d}x' \tag{76}$$

while the E-field energy is measured by the following integral:

$$W_q = \frac{1}{4\pi\varepsilon_r\varepsilon_0} \int_0^L q^2(x',t) \mathrm{d}x' \tag{77}$$

The total energy stored in the near field is proportional to the sum of W_I and W_q [27].

Numerical procedures for the calculation of the current, charge and time domain energy are outlined in Section 2.3.

3.3 Time domain numerical solution procedures

Time domain modeling is a more demanding task than is the frequency domain approach however the former provides not only a better insight into the physical transient phenomena, but also some computational advantages [4, 10, 14]. The time domain version of the GB-IBEM applied to the solution of various Hallen integral equation types provides the stable numerical results [8–11] and it is used for numerical handling of the straight thin wire in a dielectric half-space in [23].

As the time domain solution procedure for the Hallen integral equation is stable for an arbitrary time interval, it does not require any smoothing procedure, contrary to the most of the known techniques [30]. The space–time discretization is performed carefully, so that within one time increment the propagation on at least one space segment is considered, thus satisfying the inequality:

$$\Delta t \le \frac{\Delta z}{c} \tag{78}$$

Through the marching-on-in-time procedure it is possible to obtain the solution for the current at a present time for each space node as a function of currents at previous instants, without requiring matrix inversion. It is also necessary to prescribe the initial values of current at the wire ends to start the stepping procedure.

According to the usual space–time discretization procedure, the local approximation for unknown current can be expressed in the form:

$$I(x',t') = \{f\}^{\mathrm{T}}\{I\} \tag{79}$$

where $\{f\}$ is a vector containing shape functions, and $\{I\}$ is the time-dependent solution vector. In addition, applying the weighted residual approach, the space boundary discretization of integral equation (74) leads to the local equation system for *i*th source and *j*th observation boundary element:

$$\begin{aligned}
&\int_{\Delta l_j}\int_{\Delta l_i} \{f\}_j\{f\}_i^{\mathrm{T}} \frac{1}{4\pi R}\,\mathrm{d}x'\,\mathrm{d}x\{I\}\Big|_{t-\frac{R}{v}} \\
&\quad - \int_{\Delta l_j}\int_{\Delta l_i} \{f\}_j\{f\}_i^{\mathrm{T}} \frac{\dfrac{1}{\varepsilon_{\mathrm{rg}}}\cos\theta - \sqrt{\dfrac{1}{\varepsilon_{\mathrm{rg}}} - \sin^2\theta}}{\dfrac{1}{\varepsilon_{\mathrm{rg}}}\cos\theta + \sqrt{\dfrac{1}{\varepsilon_{\mathrm{rg}}} - \sin^2\theta}} \frac{1}{4\pi R^*}\,\mathrm{d}x'\,\mathrm{d}x\{I\}\Big|_{t-\frac{R^*}{v}} \\
&= \int_{\Delta l_j} F_0\left(t - \frac{x}{v}\right)\{f\}_j\,\mathrm{d}x + \int_{\Delta l_j} F_L\left(t - \frac{L-x}{v}\right)\{f\}_j\,\mathrm{d}x \\
&\quad + \frac{1}{2Z_{\mathrm{g}}}\int_{\Delta l_j}\int_{\Delta l_i} \frac{2}{\sqrt{\varepsilon_{\mathrm{rg}}}+1} E_x^{\mathrm{inc}}\left(x', t - t_0 - \frac{|x-x'|}{c}\right)\{f\}_j\,\mathrm{d}x'\,\mathrm{d}x
\end{aligned} \tag{80}$$

Expression (80) can be written in the matrix form given by:

$$\begin{aligned}
&[A]\{I\}\Big|_{t-\frac{R}{c}} - [A_1^*]\{I\}\Big|_{t-\frac{R^*}{c}} = [B]\{E\}\Big|_{t-\frac{|x-x'|}{c}} + [C]\left\{\sum_{n=0}^{\infty} I^n\right\}\Big|_{t-\frac{x}{c}-\frac{2nL}{c}-\frac{R_0}{c}} \\
&\quad - [C_1^*]\left\{\sum_{n=0}^{\infty} I^n\right\}\Big|_{t-\frac{x}{c}-\frac{2nL}{c}-\frac{R_0^*}{c}} - [B]\left\{\sum_{n=0}^{\infty} E^n\right\}\Big|_{t-\frac{x}{c}-\frac{2nL}{c}-\frac{x'}{c}} - [D]\left\{\sum_{n=0}^{\infty} I^n\right\}\Big|_{t-\frac{x}{c}-\frac{2n+1}{c}L-\frac{R_L}{c}} \\
&\quad + [D_1^*]\left\{\sum_{n=0}^{\infty} I^n\right\}\Big|_{t-\frac{x}{c}-\frac{2n+1}{c}L-\frac{R_L^*}{c}} + [B]\left\{\sum_{n=0}^{\infty} E^n\right\}\Big|_{t-\frac{x}{c}-\frac{2n+1}{c}L-\frac{L-x'}{c}} + [D]\left\{\sum_{n=0}^{\infty} I^n\right\}\Big|_{t-\frac{L-x}{c}-\frac{2nL}{c}-\frac{R_L}{c}}
\end{aligned}$$

$$-[D_1^*]\left\{\sum_{n=0}^{\infty} I^n\right\}\Bigg|_{t-\frac{L-x}{c}-\frac{2nL}{c}-\frac{R_L^*}{c}} -[B]\left\{\sum_{n=0}^{\infty} E^n\right\}\Bigg|_{t-\frac{L-x}{c}-\frac{2nL}{c}-\frac{L-x'}{c}} -[C]\left\{\sum_{n=0}^{\infty} I^n\right\}\Bigg|_{t-\frac{L-x}{c}-\frac{2n+1}{c}L-\frac{R_0}{c}}$$
$$+[C_1^*]\left\{\sum_{n=0}^{\infty} I^n\right\}\Bigg|_{t-\frac{L-x}{c}-\frac{2n+1}{c}L-\frac{R_0^*}{c}} +[B]\left\{\sum_{n=0}^{\infty} E^n\right\}\Bigg|_{t-\frac{L-x}{c}-\frac{2n+1}{c}L-\frac{x'}{c}} \tag{81}$$

where $\{E\}$ vector denotes the excitation function and the space–time dependent matrices are given, as follows:

$$[A] = \int_{\Delta l_j}\int_{\Delta l_i} \frac{1}{4\pi R}\{f\}_j\{f\}_i^{\mathrm{T}}\,\mathrm{d}x'\,\mathrm{d}x \tag{82}$$

$$[A_1^*] = \int_{\Delta l_j}\int_{\Delta l_i} \frac{\dfrac{1}{\varepsilon_{\mathrm{rg}}}\cos\theta - \sqrt{\dfrac{1}{\varepsilon_{\mathrm{rg}}} - \sin^2\theta}}{\dfrac{1}{\varepsilon_{\mathrm{rg}}}\cos\theta + \sqrt{\dfrac{1}{\varepsilon_{\mathrm{rg}}} - \sin^2\theta}} \frac{1}{4\pi R^*}\{f\}_j\{f\}_i^{\mathrm{T}}\,\mathrm{d}x'\,\mathrm{d}x \tag{83}$$

$$[B] = \frac{1}{2Z_0}\int_{\Delta l_j}\int_{\Delta l_i} \{f\}_j\{f\}_i^{\mathrm{T}}\,\mathrm{d}x'\,\mathrm{d}x \tag{84}$$

$$[C] = \int_{\Delta l_j}\int_{\Delta l_i} \frac{1}{4\pi R_0}\{f\}_j\{f\}_i^{\mathrm{T}}\,\mathrm{d}x'\,\mathrm{d}x \tag{85}$$

$$\left[C_1^*\right] = \int_{\Delta \mathrm{l}_j}\int_{\Delta \mathrm{l}_i} \frac{\dfrac{1}{\varepsilon_{\mathrm{rg}}}\cos\theta - \sqrt{\dfrac{1}{\varepsilon_{\mathrm{rg}}} - \sin^2\theta}}{\dfrac{1}{\varepsilon_{\mathrm{rg}}}\cos\theta + \sqrt{\dfrac{1}{\varepsilon_{\mathrm{rg}}} - \sin^2\theta}} \frac{1}{4\pi R_0^*}\{f\}_j\{f\}_i^{\mathrm{T}}\,\mathrm{d}x'\,\mathrm{d}x \tag{86}$$

$$[D] = \int_{\Delta \mathrm{l}_j}\int_{\Delta \mathrm{l}_i} \frac{1}{4\pi R_L}\{f\}_j\{f\}_i^{\mathrm{T}}\,\mathrm{d}x'\,\mathrm{d}x \tag{87}$$

$$[D_1^*] = \int_{\Delta \mathrm{l}_j}\int_{\Delta \mathrm{l}_i} \frac{\dfrac{1}{\varepsilon_{\mathrm{rg}}}\cos\theta - \sqrt{\dfrac{1}{\varepsilon_{\mathrm{rg}}} - \sin^2\theta}}{\dfrac{1}{\varepsilon_{rg}}\cos\theta + \sqrt{\dfrac{1}{\varepsilon_{\mathrm{rg}}} - \sin^2\theta}} \frac{1}{4\pi R_L^*}\{f\}_j\{f\}_i^{T}\,\mathrm{d}x'\,\mathrm{d}x \tag{88}$$

Having completed the space discretization procedure, the weighted residual approach is used for the time discretization procedure, as well.

Assuming that solution in time on the *i*th space segment can be expressed as:

$$I_i(t') = \sum_{k=1}^{N_t} I_i^k T^k(t') \tag{89}$$

where I_i^k are the unknown coefficients and T^{k} are the time domain shape functions, and choosing the Dirac impulses as test functions, the recurrence formula for the space–time varying current can be written as:

$$I_{j}\Big|_{t_k} = \frac{-\sum_{i=1}^{N_g}\left(\bar{A}_{ji} I_{i}\Big|_{t_k-\frac{R}{c}} - A^*_{ji_1} I_{i}\Big|_{t_k-\frac{R^*}{c}}\right) + g_{j_1}^*\Big|_{\text{all retarded times}}}{A_{jj}} \tag{90}$$

where N_{g} denotes the total number of global nodes A_{ji} are the global matrix terms, g_{jl}* is the whole right ride of the expression (81) containing the excitation and the currents at previous instants, while the overbar denotes that the self term is omitted.

Once the current distribution is obtained by solving the integral equation (74) via the GB-IBEM, the energy-measure integrals (76) and (77) can be evaluated.

First, the charge distribution is determined by solving the integral:

$$q = -\sum_{i=1}^{M}\sum_{k=1}^{N_t}\int_{\Delta t_k} \frac{\partial}{\partial x'}\{f\}_i^{\mathrm{T}}\{I\}_i \,\mathrm{d}t \tag{91}$$

where M denotes the total number of segments, while N_{t} stands for the total number of time steps.

The solution of integral in eqn (91) is carried out analytically, and given in the form:

$$q = -\frac{1}{2v}\sum_{i=1}^{M}\sum_{m=1}^{N_t}(I_{i+1}^m + I_{i+1}^{m+1} - I_i^m - I_i^{m+1}) \tag{92}$$

The H-field energy measure is obtained by evaluating the integral:

$$W_I = \frac{\mu_0}{4\pi}\sum_{i=1}^{M}\int_{\Delta t_k}\frac{\partial}{\partial x'}(\{f\}_i^{\mathrm{T}}\{I\}_i)^2 \,\mathrm{d}x' \tag{93}$$

The solution is available in the closed form and is given by:

$$W_I = 10^{-7}\frac{\Delta x}{3}\sum_{i=1}^{M}\left[(I_i^k)^2 + I_i^k I_{i+1}^k + (I_{i+1}^k)^2\right], \quad k = 1, 2, \ldots, N_{\mathrm{t}} \tag{94}$$

The *E*-field energy is obtained from the integral:

$$W_q = \frac{1}{4\pi\varepsilon_r\varepsilon_0}\sum_{i=1}^{M}\int_{\Delta t_k}\frac{\partial}{\partial x'}(\{f\}_i^{\mathrm{T}}\{q\}_i)^2\,\mathrm{d}x' \tag{95}$$

for which the solution is then:

$$W_q = \frac{1}{4\pi\varepsilon_r\varepsilon_0}\frac{\Delta x}{3}\sum_{i=1}^{M}[(q_i^k)^2 + q_i^k q_{i+1}^k + (q_{i+1}^k)^2], \quad k = 1,2,\ldots,\ N_t \tag{96}$$

and the total energy measure is given by sum of W_I and W_q.

3.4 Alternative time domain formulation via a simplified reflection/transmission coefficient

A transient analysis of a finite length wire embedded in a dielectric half-space and illuminated by the electromagnetic pulse (EMP) using a simplified reflection coefficient approach. A direct time domain formulation is based on the wire antenna theory and on the corresponding Hallen integral equations for half-space problems. The presence of a dielectric half-space is taken into account via the simplified reflection/transmission coefficient arising from the modified image theory. The Hallen equation is solved via the time-domain GB-IBEM and some illustrative numerical results are presented in this section.

The transient response obtained using the simplified reflection/transmission coefficient approach is compared to the results obtained via the Fresnel coefficients approach.

A simplified form of the earth–air reflection coefficient, based on the modified image theory, and proposed in [28] is given by:

$$\Gamma_{\mathrm{MOT}}^{\mathrm{ref}}(t) = \Gamma_{\mathrm{MOT}}^{\mathrm{ref}}\delta(t) \tag{97}$$

where $\Gamma_{\mathrm{MOT}}^{\mathrm{ref}}$ depends on the permittivity of the dielectric medium, only:

$$\Gamma_{\mathrm{MOT}}^{\mathrm{ref}} = \frac{1-\varepsilon_{\mathrm{rg}}}{1+\varepsilon_{\mathrm{rg}}} \tag{98}$$

A simplified form of the transmission coefficient, based on the modified image theory, proposed in [28] can be written, as follows:

$$\Gamma_{\mathrm{MOT}}^{\mathrm{tr}}(t) = \Gamma_{\mathrm{MOT}}^{\mathrm{tr}}\delta(t) \tag{99}$$

where $\Gamma_{\mathrm{MOT}}^{\mathrm{tr}}$, dependent only on the permittivity of the dielectric medium, is given by:

$$\Gamma_{\mathrm{MOT}}^{\mathrm{tr}} = \frac{2\varepsilon_{\mathrm{rg}}}{1+\varepsilon_{\mathrm{rg}}} \tag{100}$$

Substituting the relations (99) and (100) into eqn (71), for the case of normal incidence, it follows:

$$E_x^{\mathrm{tr}}(t) = \frac{2\varepsilon_{\mathrm{rg}}}{1+\varepsilon_{\mathrm{rg}}} E_x^{\mathrm{inc}}(t - t_0) \tag{101}$$

where $t_0 = d/v$ denotes the time delay.

Also, substituting eqns (97) and (98) into eqn (69), the resulting integral equations for the straight wire immersed in a dielectric medium becomes:

$$\int_0^L \frac{I(x', t - R/v)}{4\pi R}\,\mathrm{d}x' - \int_0^L \frac{1-\varepsilon_{\mathrm{rg}}}{1+\varepsilon_{\mathrm{rg}}} \frac{I(x', t - R^*/v)}{4\pi R^*}\,\mathrm{d}x'$$
$$= F_0\left(t - \frac{x}{v}\right) + F_L\left(t - \frac{L-x}{v}\right) + \frac{1}{2Z_{\mathrm{g}}} \int_0^L \frac{2\varepsilon_{\mathrm{rg}}}{1+\varepsilon_{\mathrm{rg}}} E_x^{\mathrm{inc}}\left(x',\ t - t_0 - \frac{|x - x'|}{v}\right)\mathrm{d}x' \tag{102}$$

The numerical solution of the space–time Hallen integral equation is obtained using the procedure presented in Section 2.3.

3.5 Computational examples

The first example is related to the straight wire of length $L = 5$ m and radius $a = 1$ cm embedded in the dielectric half-space with $\varepsilon_{\mathrm{r}} = 10$ at the depth $d = 1$ m. The wire is illuminated by the transmitted part of the EMP incident waveform:

$$E^{\mathrm{inc}}(t) = E_0(\mathrm{e}^{-at} - \mathrm{e}^{-bt}) \tag{103}$$

where the EMP parameters are: $E_0 = 52.5$ kV/m, $a = 4 \times 10^6$ s^{-1} and $b = 4.78 \times 10^8$ s^{-1}.

The transient current induced at the wire center is shown in Fig. 8

The transient response obtained using the direct time domain approach seems to be in a satisfactory agreement with the results computed via the indirect frequency domain approach. The multiple reflections of the transient current from the wire ends are due to the reflected waves. This effect can be also observed in Figs 9–11.

Figure 9 shows the transient response of the same wire buried at various depths.

The curves shown in Fig. 9 for the transient current induced at the center of the wire embedded in the dielectric half-space at depth $d = 1$, 10 and 20 m represent time delayed waveforms due to the propagation delay necessary for the incident electric field to reach the wire. A slight amplitude and waveform variation as a function of depth indicate the minimal interface effect.

A slight proximity effect of the ground–air interface is visible for the case of the transient current induced along the wire placed at depth $d = 1$ m below ground, while only the time delay is noticeable for the curves related to the wires located at depth $d = 10$ and 20 m, respectively.

The initial delay of the first peak is caused by the arrival time of the incident field and strongly depends on the depth d. After that time the transient behavior of the incident current is the same.

Furthermore, Fig. 10 shows the transient current induced of the center of $L = 5$ m long wire buried at $d = 1$ m below the interface for the various values of permittivity. Thus, three typical values of relative dielectric constant are chosen; $\varepsilon_r = 10$ (ground), $\varepsilon_r = 55$ (brain permittivity at GSM (Global System for Mobile Communications) frequencies), $\varepsilon_r = 80$ (sea water). It can be observed from Fig. 10 that permittivity of the medium strongly affects the transient response of the wire embedded in the dielectric medium.

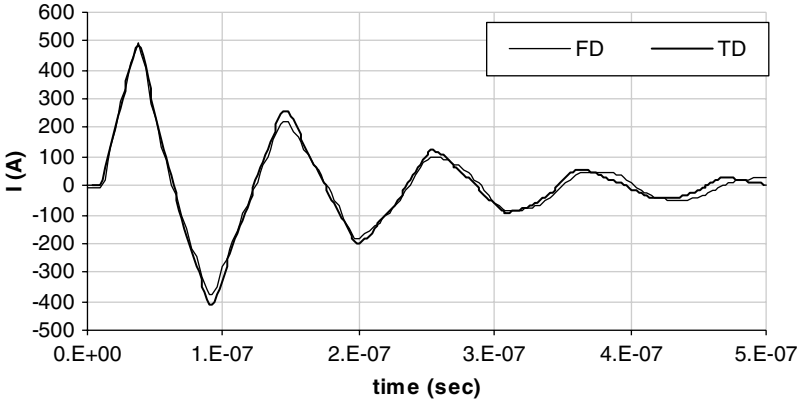

Figure 8: Transient current induced at the center of the straight wire ($L = 5$ m, $a = 1$ cm, $\varepsilon_r = 10$, $d = 1$ m).

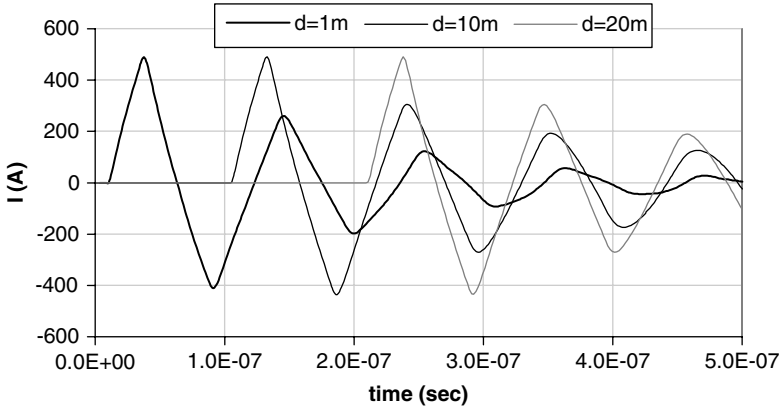

Figure 9: Transient current induced at the center of the straight wire ($L = 5$ m, $a = 1$ cm, $\varepsilon_r = 10$) for various depths.

As shown in Fig. 10 the initial delay of the transient waveform first peak is significantly influenced by the relative permittivity of a dielectric semi-infinite medium ε_{rg}. Also, time delay of the reflections from the wire free ends is influenced by the velocity of the propagation in the dielectric medium. Smaller the value of ε_{rg}, the greater is the velocity v while the oscillation period is decreased.

Figure 11 shows the transient response of the straight thin wire of length $L = 50$ m and radius $a = 1$ cm embedded in the dielectric half-space with $\varepsilon_r = 10$ at the depth $d = 1$ m. The wire is illuminated by the EMP waveform (97). This transient response has been computed by means of the direct time domain and the indirect

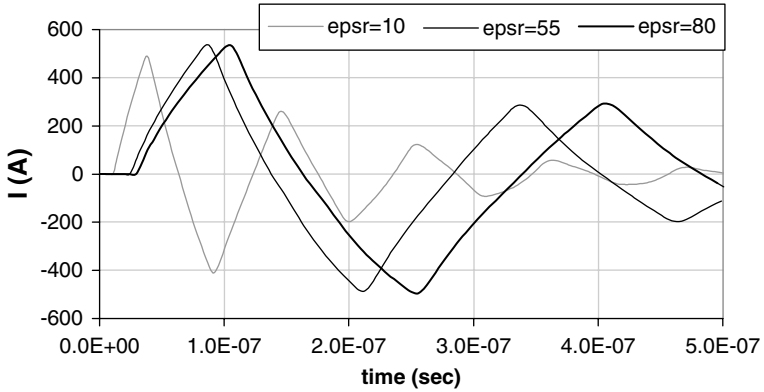

Figure 10: Transient response of the straight wires ($L = 5$ m, $a = 1$ cm) for various permittivity values.

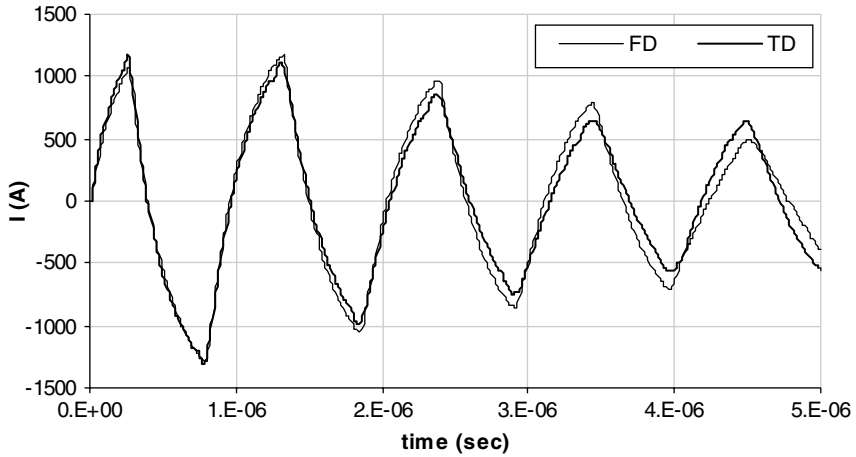

Figure 11: Transient current induced at the center of the straight buried wire ($L = 50$ m, $a = 1$ cm, $\varepsilon_r = 10$, $d = 1$ m).

frequency domain method, respectively. The numerical results obtained by the different approaches agree favorably again.

Comparison of the transient current from Fig. 11 with the current waveform from Fig. 8 clearly shows the influence of the wire length on the transient behavior.

It is also evident from Fig. 5 that the dominant effect to the transient behavior of the induced current along the line is due to the multiple reflections of the current wave from the line open ends.

There is a slight frequency shift in Figs 8 and 11 between the time domain and the frequency domain results, particularly for later time instants. Consequently, there are some points regarding the frequency domain modeling to be clarified.

The transients of highly resonant structures have very long duration while their related frequency spectra contain sharp peaks. Coarse frequency resolution cannot resolve the resonant points accurately thus resulting in errors in transient waveforms.

The problem of analyzing transients of highly resonant structures in the frequency domain is the inability to know beforehand the frequency resolution required for sampling the spectrum. Dynamic adaptive sampling can be used to overcome this problem and more details can be found in [4, 33]. An equivalent problem in analyzing transients in time domain is the inability to know the time duration of the waveform.

The related frequency spectrum of the impulse and the transient response of a 50 m long line immersed in a dielectric medium, with $\varepsilon_r = 10$ at depth $d = 1$ m is shown in Figs 12 and 13, respectively.

As it is visible from Figs 12 and 13, the frequency response spectra contain a number of peaks decreasing with frequency. Although the frequency range of these spectra is infinite, signal amplitudes for the frequencies higher than 50 MHz are low enough to be neglected. On the other hand, the location and the amplitude values of the first two peaks strongly affect the obtained transient waveform.

Therefore, it is very important for frequency samples to contain exact frequencies of the first two peaks. This could be achieved using the sufficiently fine frequency step (resulting in large number of samples) or by means of the dynamic

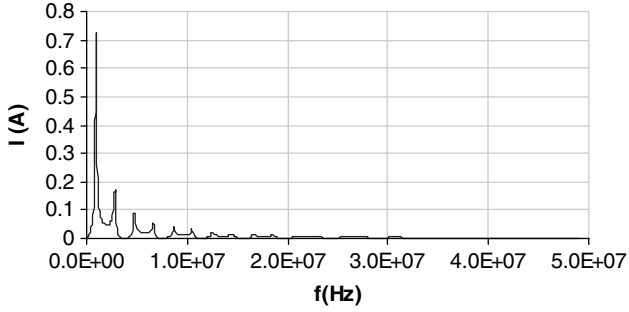

Figure 12: Frequency spectrum of the impulse response at the center of the straight wire ($L = 50$ m, $a = 1$ cm, $\varepsilon_r = 10$, $d = 1$ m).

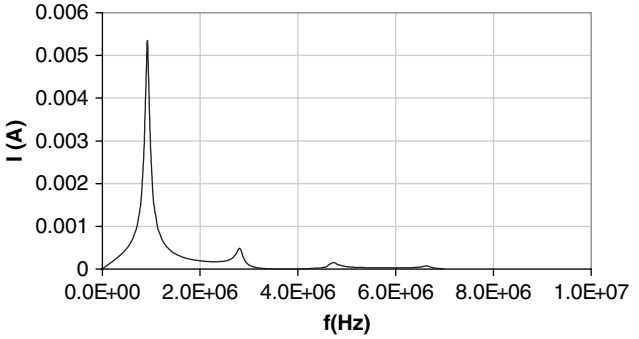

Figure 13: Frequency spectrum of the transient response at the center of the straight wire ($L = 50$ m, $a = 1$ cm, $\varepsilon_r = 10$, $d = 1$ m).

adaptive sampling technique presented in [31]. In this section a number of $N = 2^{15}$ samples over the frequency range of 50 MHz have been used in order to obtain a satisfactory convergence rate.

Since the current distribution evaluation for a single frequency takes around 30 s (depending on the computer speed), the calculation of current amplitude for each sample is obviously impossible. Thus, about 150 samples over the 50 MHz frequency range have been evaluated, while the rest of the samples have been interpolated using cubic splines.

The effect of the interface and the validity of the Fresnel reflection coefficient approximation in modeling the interface should be discussed, as well.

A relatively short wire ($L = 0.5$ m) is chosen to describe the earth–air interface effect. Figure 14 shows the transient current induced at the center of 0.5 m long wire for various depths. As is obvious from Fig. 14, there is a slight variation in amplitude and waveform and time shift for depths $d = 0.25$, 1 and 2 m. Only the curve for $d = 0.1$ m clearly demonstrates the influence of the earth–air interface in both the amplitude and waveform of the actual transient response.

Figure 15 shows the behavior of the energy stored in the near field of the wire, i.e. it represents the decrease of the wire total energy with time, once the exciting pulse vanishes.

Figure 15 also demonstrates the absorbing effect of the dielectric half-space when the wire is brought closer to the interface.

The evaluation of the validity of the proposed model is not an easy task, even in the frequency domain, and even for the simplified case of a dielectric half-space. Generally, the validity of various approximations depends on the relationship between; the spectral content and the direction of the incident field, the electrical properties of the earth, and to a lesser extent the burial depth of the line. The computational aspects in the frequency domain modeling of thin wire antennas in the presence of a lossy half-space have been reported in a number of papers and among the most cited ones are references [15, 16].

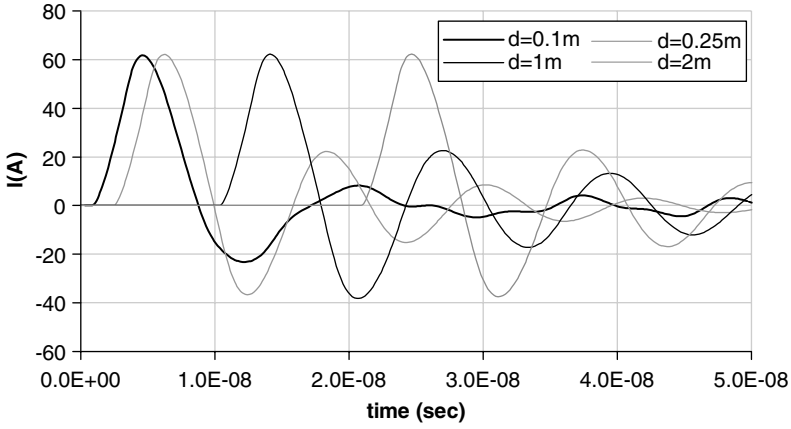

Figure 14: Transient current induced at the center of the straight wire (L = 0.5 m, a = 1 cm, ε_r = 10) for various depths.

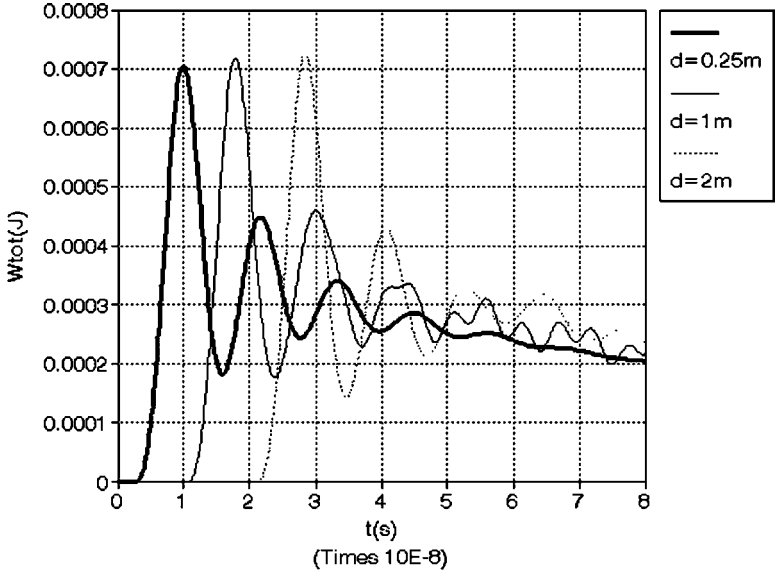

Figure 15: The measure of total energy (W_{tot}) as a function of time for various depths.

The frequency domain analysis of the buried wire scatterer has been carried out via the rigorous Sommerfeld integral [17], and via the approximate reflection coefficient approach [18], respectively, to account for the influence of the earth–air interface reflected field upon the straight wire scatterer current distribution.

The Sommerfeld integral approach has been found to be numerically stable and reliable for straight horizontal line brought to within 10^{-6} wavelengths of the interface [16, 17]. The rigorous and approximate results are in a very good agreement for depths greater or at least equal to [23]:

$$d \geq \frac{\lambda_0}{4\sqrt{\varepsilon_r}}, \quad \lambda_0 = \frac{c}{f} \tag{104}$$

As a rough guideline, the Fresnel reflection coefficient approach to account for the reflection from the earth–air interface has been found to produce results generally within 10% of those obtained using rigorous, but computationally very expensive, Sommerfeld integral approach.

Furthermore, for wire depths:

$$d \leq \frac{\lambda_0}{10\sqrt{\varepsilon_r}} \tag{105}$$

the qualitative dependence of the input admittance (obtained by using the reflection coefficient approach) upon depth is found to be generally correct, but these results primarily differ from the rigorous results due to a slight shift in the maxima with respect to depth.

Essentially, from the time domain point of view this condition should be satisfied for each component of the considered frequency spectrum.

It is also necessary to make at least a general trade-off between a dielectric half-space and an imperfectly conducting half-space. The absence of the ground conductivity (or at least low values of ground conductivity) causes strong resonance effect, which is particularly noticeable in Figs 11–13.

From the findings in the frequency domain the increasing ground conductivity is expected to decrease the response rapidly. In the realistic problems such as wire immersed inside sea water, ground probing or ground penetrating radar conductivity should not be neglected. The influence of the finite conductivity reduces the external electric field and influences the behavior of the induced current. The finite conductivity can also delay the initial field. However, the corresponding Green's function, which is responsible for the second effect, is much more complicated and has to be calculated via the Sommerfeld integral approach. In that case, one would need to perform additional integration in the Hallen equation and the problem would become tremendously time consuming.

To roughly estimate whether a dielectric half-space approximation of a dissipative half space can be used the absolute value of the refractive index of the earth should be examined.

This equation is given by

$$|n| = \sqrt{\varepsilon_{rg}^2 + \left(\frac{\sigma_g}{\omega\varepsilon_0}\right)^2} \tag{106}$$

Conductivity σ should be at least an order of magnitude less than $\omega\varepsilon_0$ to be neglected.

For example, a reasonably dry earth, $\varepsilon_{rg} = 10$, in the frequency band from around 1 kHz to 1 MHz requires the conductivity σ to vary from 10^{-6} to 10^{-4} S/m.

To sum up, the numerical results obtained via the different approaches agree satisfactorily, i.e. the maximum deviation between the results is around 6%.

The transient response of the single straight wire immersed in a dielectric half-space has been found to be influenced to a greater extent by the line length and the permittivity of a dielectric medium, and to a lesser extent by the burial depth.

The last set of numerical results deals with the transient analysis of a finite length wire immersed in a dielectric half-space using a simplified reflection/coefficient approach [29].

The computational example is related to the straight thin wire of length $L = 10$ m and radius $a = 6.74$ cm embedded in the dielectric half-space ($\varepsilon_r = 9$) at a certain burial depth d. The wire is illuminated by the transmitted part of the EMP incident waveform (103) where the EMP parameters are: $E_0 = 1.05$ kV/m, $a = 4 \times 10^6$ s^{-1} and $b = 4.78 \times 10^8$ s^{-1}.

The transient current induced at the wire center, for various depths, computed via both the Fresnel and the simplified reflection/transmission coefficient is shown in Figs 16 and 17.

As in the case of the Fresnel coefficients approach, the evaluation of the validity of the proposed reflection/coefficient approximation is not an easy task, even for the case of a lossless dielectric half-space.

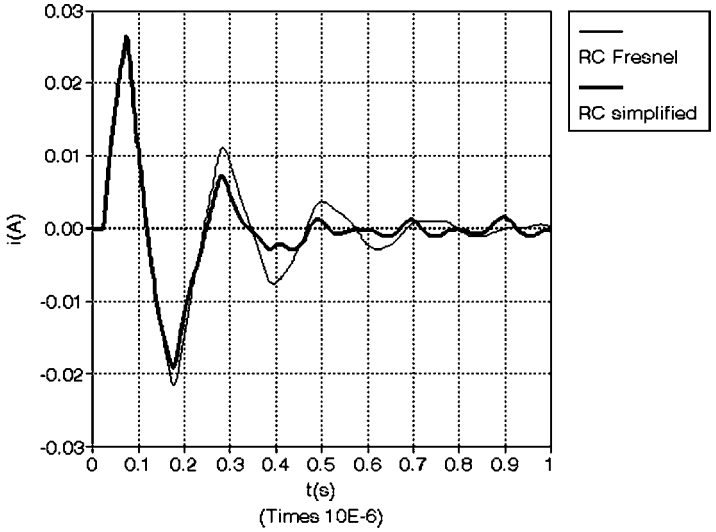

Figure 16: Transient current induced at the center of the straight wire ($L = 10$ m, $a = 6.74$ cm, $\varepsilon_r = 9$) at burial depth $d = 2.5$ m.

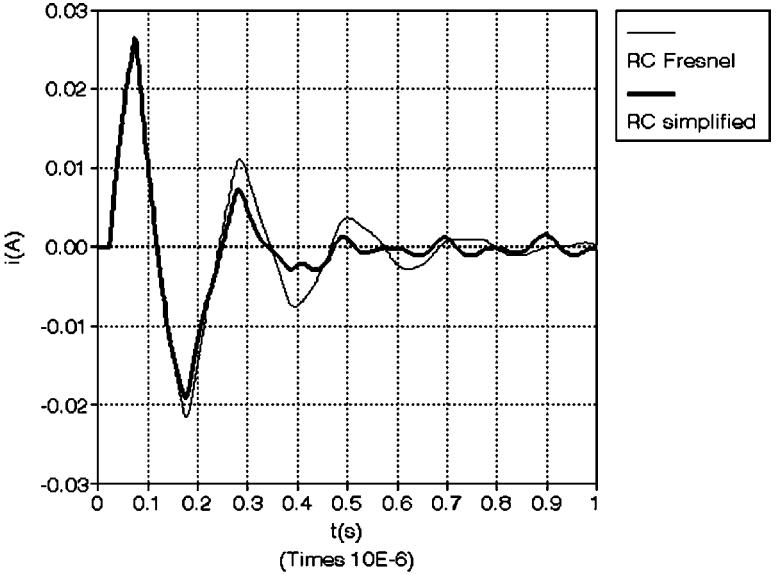

Figure 17: Transient current induced at the center of the straight wire (L = 10 m, a = 6.74 cm, ε_r = 9) at burial depth d = 5 m.

It is obvious from Figs 16 and 17 that the obtained numerical results via simplified reflection/coefficient approach agree satisfactorily with the results calculated via the Fresnel coefficients approach for earlier time instants and for increasing values of burial depth d.

References

[1] Bridges, G.E., Transient plane wave coupling to bare and insulated cables buried in a lossy half-space. *IEEE Trans. EMC*, **37(1)**, pp. 62–70, 1995.

[2] Grcev, L.D. & Menter, F.E., Transient electromagnetic fields near large earthing systems. *IEEE Trans. Magnetics*, **32**, pp. 1525–1528, 1996.

[3] Tesche, F., Ianoz, M. & Carlsson, F., *EMC Analysis Methods and Computational Models*, John Wiley & Sons: New York, 1997.

[4] Poljak, D. & Tham, C.Y., *Integral Equation Techniques in Electromagnetics*, WIT Press: Southampton and Boston, 2003.

[5] Ianoz, M., Electromagnetic field coupling to lines, cables and networks, a review of problems and solutions. *Proc. Int. Conf. on Electromagnetics in Advanced Applications, ICEAA'95*, Turin, Italy, pp. 75–80, 12–15 September 1997.

[6] Tkatchenko, S., Rachidi, F. & Ianoz, M., High frequency electromagnetic field coupling to long terminated lines. *IEEE Trans. EMC*, **43(2)**, pp. 117–129, 2001.

[7] Tkatchenko, S., Rachidi, F. & Ianoz, M., Electromagnetic field coupling to a line of a finite length: theory and fast iterative solutions in frequency and time domains. *IEEE Trans. EMC*, **37(4)**, pp. 509–518, 1995.

[8] Poljak, D. & Roje, V., Time domain modeling of electromagnetic field coupling to transmission lines. *Proc. 1988 IEEE EMC Symposium*, Denver, USA, pp. 1010–1013, August 1997.

[9] Poljak, D., Tham, C.Y., McCowen, A. & Roje, V., Electromagnetic pulse excitation of multiconductor transmission lines. *ICEAA'99*, Turin, Italy, pp. 789–792, 13–17 September 1997.

[10] Poljak, D., Miller, E.K. & Tham, C.Y., Time domain energy measures for thin-wire antennas and scatterers. *IEEE Antennas & Propagation Magazine*, **44(1)**, pp. 87–95, 2002.

[11] Poljak, D., Tham, C.Y. & McCowen, A., Transient response of nonlinearly loaded wires in a two media configuration. *IEEE Trans. EMC*, **46(1)**, pp. 121–125, 2004.

[12] Degauque, P. & Zeddam, A., Remarks on the transmission approach to determining the current induced on above-ground cables. *IEEE Trans. EMC*, **30(1)**, pp. 77–80, 1997.

[13] Poljak, D., *Electromagnetic Modelling of Wire Antenna Structures*, WIT Press: Southampton, Boston, 2001.

[14] Poljak, D., New numerical approach in analysis of thin wire radiating over lossy half-space. *International Journal for Numerical Methods in Engineering*, **38(22)**, pp. 3803–3816, 1995.

[15] Miller, E.K., Poggio, A.J., Burke, G.J. & Selden, E.S., Analysis of wire antennas in the presence of a conducting half-space, Part II. The horizontal antenna in free space. *Canadian Journal of Physiscs*, **50**, pp. 2614–2627, 1972.

[16] Burke, G.J. & Miller, E.K., Modelling antennas near to and penetrating a lossy interface. *IEEE Trans. AP*, **32(10)**, pp. 1040–1049, 1984.

[17] Poljak, D. & Roje, V., The integral equation method for ground wire input impedance. *Integral Methods in Science and Engineering, Vol. I Analytic Methods*, eds C. Constanda, J. Saranen & S. Seikkala, Longman: New York, pp. 139–143, 1997.

[18] Poljak, D., Electromagnetic modeling of finite length wires buried in a lossy half-space. *Engineering Analysis with Boundary Elements*, **26**, pp. 81–86, 2002.

[19] Doric, V., Poljak, D. & Roje, V., Transient plane wave coupling to a finite length wire buried in a conductive ground. *Boundary Elements*, **XVII**, pp. 609–617, 2005.

[20] Poljak, D. & Brebbia, C.A., Indirect Galerkin–Bubnov boundary element method for solving integral equations in electromagnetics. *Engineering Analysis with Boundary Elements*, **28(7)**, pp. 771–777, 2004

[21] Ziemer, R.E. & Tranter, W.H., *Principles of Communications*, Houghton Mifflin Company: Boston and Toronto, 1995.

[22] King, R.W.P., Sforza, P.F. & Boak, T.I.S., The current in a parasitic antenna in a dissipative medium. *IEEE Trans. AP*, **22(6)**, pp. 809–814, 1974.

[23] Poljak, D. & Doric, V., Time domain modeling of electromagnetic field coupling to finite length wires embedded in a dielectric half-space. *IEEE Trans. EMC*, **47(2)**, pp. 247–253, 2005.

[24] Miller, E.K. & Landt, J.A., Direct time-domain techniques for transient radiation and scattering from wires. *Proc. IEEE*, **168(11)**, pp. 1396–1423, 1980.

[25] Miller, E.K., PCs for AP and EM reflections. *IEEE Antennas & Propagation Magazine*, **40(1)**, pp. 96–100, 1998; **41(2)**, pp. 92–95, 1997.

[26] Poljak, D., Miller, E.K., Tham, C.Y., Yoong, C., Antonijevic, S & Doric, V., Time domain analysis of the energy stored in the near field of multiple straight-wires above dielectric half-space. *Proceedings of the ICEAA*, Turin, September 2005.

[27] Poljak, D., Time domain analysis of the energy stored in the near field of finite length wires embedded in a dielectric half-space. *Proc. Int. Symp. on EMC*, *EMC Europe 2006*, Barcelona, Spain, pp. 982–987, 4–8 September 2006.

[28] Poljak, D. & Kresic, S., A simplified calculation of transient plane waves in a presence of an imperfectly conducting half-space. *Boundary Elements XXVII*, Orlando, pp. 541–549, 2005.

[29] Poljak, D. & Kovac, N., Transient analysis of a finite length line embedded in a dielectric half-space using a simplified reflection/transmission coefficient approach. Submitted to *ICEAA 2007 Conference*, Turin, Italy, September 2007.

[30] Rao, S.M., Sarkar, T.K. & Dianat, S.A., A novel technique to the solution of transient electromagnetic scattering from thin wires. *IEEE Trans. AP*, **34**, pp. 630–634, 1986.

[31] Tijhuis, A.G., Peng, Z.Q. & Bretones, A.R., Transient excitation of a straight thin-wire segment: a new look at an old problem. *IEEE Trans. AP*, **40(10)**, pp. 1132–1146, 1992.

[32] Poljak, D., Transient response of resistively loaded straight thin wire in half-space configuration. *Journ. Elctromagn. Waves and Applic.*, **12(6)**, pp. 775–787, 1997.

[33] Tham, C.Y., McCowen, A., Towers, M.S. & Poljak, D., Dynamic adaptive sampling technique in frequency-domain transient analysis. *IEEE Trans. EMC*, **44(4)**, pp. 522–528, 2002.

Index

WIT*PRESS* ***...for scientists by scientists***

Computer Aided Design of Wire Structures

Frequency and Time Domain Analysis

D. POLJAK, V. DORIC *and* ***S. ANTONIJEVIC****, University of Split, Croatia*

As an introduction to the integral equation analysis of wire structures, this book and enclosed software package contains the user-friendly version of the boundary element software for modelling the straight thin wire arrays in both frequency and time domain. This package is designed as a step-by-step guide for postgraduate students, researchers and also practising engineers to learn CAD of wire antennas immersed in inhomogeneous media. Some electromagnetic compatibility (EMC) applications can also be handled using this package. The package contains a detailed description of antenna theory, integral equation modelling and full manuals for software packages.

Series: Advances in Electrical Engineering and Electromagnetics, Vol 3
ISBN: 978-1-85312-884-4 2007
160pp+CD-ROM
£79.00/US$139.00/€118.50

Integral Equations and their Applications

M. RAHMAN*, Dalhousie University, Canada*

For many years, the subject of functional equations has held a prominent place in the attention of mathematicians. In more recent years this attention has been directed to a particular kind of functional equation, an integral equation, wherein the unknown function occurs under the integral sign. The study of this kind of equation is sometimes referred to as the inversion of a definite integral.

While scientists and engineers can already choose from a number of books on integral equations, this new book encompasses recent developments including some preliminary backgrounds of formulations of integral equations governing the physical situation of the problems. It also contains elegant analytical and numerical methods, and an important topic of the variational principles. Primarily intended for senior undergraduate students and first year postgraduate students of engineering and science courses, students of mathematical and physical sciences will also find many sections of direct relevance.

The book contains eight chapters, pedagogically organized. This book is specially designed for those who wish to understand integral equations without having extensive mathematical background. Some knowledge of integral calculus, ordinary differential equations, partial differential equations, Laplace transforms, Fourier transforms, Hilbert transforms, analytic functions of complex variables and contour integrations are expected on the part of the reader.

ISBN: 978-1-84564-101-6 2007 384pp
£126.00/US$252.00/€189.00

WIT*Press*
Ashurst Lodge, Ashurst, Southampton, SO40 7AA, UK.
Tel: 44 (0) 238 029 3223
Fax: 44 (0) 238 029 2853
E-Mail: witpress@witpress.com

WITPRESS ...for scientists by scientists

Human Exposure to Electromagnetic Fields

***D. POLJAK**, University of Split, Croatia*

The field of computational bioelectromagnetics has grown rapidly in the last decades, but until now there has not been a comprehensive text on the many aspects of interaction between human beings and electromagnetic fields. This text fills the gap.

Partial Contents: Electrosmog-Environmental Risk of Radiation Pollution; Sources of Electromagnetic Fields and Incident Field Dosimetry; Electromagnetic Modelling of the Human Body; Thermal Modelling of the Human Body; Coupling Mechanisms Between Electromagnetic Fields and the Human Body; Safety Standards and Exposure Limits.

Series: Advances in Electrical and Electronic Engineering, Vol 6
ISBN: 1-85312-997-6 2004 200pp
£81.00/US$129.00/€121.50

Boundary Elements and Other Mesh Reduction Methods XXX

*Edited by: **C.A. BREBBIA**, Wessex Institute of Technology, UK and **L. ŠKERGET**, University of Maribor, Slovenia*

The major motivation behind the Boundary Element Method (BEM) was to reduce the dependency of analysis on the definition of meshes. This has allowed the method to expand naturally into new techniques such as Dual Reciprocity and all other Mesh Reduction Methods (MRM). MRM and BEM continue to be very active areas of research with many of the resulting techniques being successfully applied to solve increasingly complex problems.

This book contains papers presented at the much-acclaimed Thirtieth International Conference on Boundary Elements and other Mesh Reduction Methods. The proceedings contain papers on practically all major developments in Boundary Elements, including the most recent MRM techniques, grouped under the following topics: Meshless Techniques; Advances in Mesh Reduction Methods; Advanced Formulations; Advanced Structural Applications; Heat and Mass Transfer; Electrical Engineering and Electromagnetics; Fluid Flow; Computational Techniques; Dynamics and Vibrations; Damage Mechanics and Fracture; Material Characterization; Emerging Applications.

The book should be of interest to engineers and scientists within the areas of numerical analysis, boundary elements and meshless methods.

WIT Transactions on Modelling and Simulation, Vol 47
ISBN: 978-1-84564-121-4 2008
apx 400pp
apx £132.00/US$264.00/€198.00

Find us at
http://www.witpress.com

Save 10% when you order from our encrypted ordering service on the web using your credit card.

WITPRESS ...for scientists by scientists

Boundary Element Methods for Electrical Engineers

***D. POLJAK**, University of Split, Croatia and **C.A. BREBBIA**, Wessex Institute of Technology, UK*

In the last couple of decades the Boundary Element Method (BEM) has become a well-established technique that is widely used for solving various problems in electrical engineering and electromagnetics. Although there are many excellent research papers published in the relevant literature that describe various BEM applications in electrical engineering and electromagnetics, there has been a lack of suitable textbooks and monographs on the subject.

This book presents BEM in a simple fashion in order to help the beginner to understand the very basic principles of the method. It initially derives BEM for the simplest potential problems and subsequently builds on these to formulate BEM for a wide range of applications in electromagnetics.

The book aims to introduce both undergraduate and graduate students to the BEM fundamentals in a way that enables the reader to solve more complex problems on their own. In addition, it will serve as a useful text to enable professional engineers and research students to make full use of BEM in electrical engineering.

Series: Advances in Electrical Engineering and Electromagnetics Vol 4
ISBN: 1-84564-033-0 2005 208pp
£79.00/US$126.00/€118.50

Trefftz and Collocation Methods

***Z.-C. LI** and **T.-T. LU**, National Sun-sen University, Taiwan, and National Center for Theoretical Science, Taiwan, **H.-Y. HU**, Tung-Hai University, Taiwan and **A. H.-D. CHENG**, University of Mississippi, USA*

This book covers a class of numerical methods that are generally referred to as "Collocation Methods". Different from the Finite Element and the Finite Difference Method, the discretization and approximation of the collocation method is based on a set of unstructured points in space. This "meshless" feature is attractive because it eliminates the bookkeeping requirements of the "element" based methods. This text discusses several types of collocation methods including the radial basis function method, the Trefftz method, the Schwartz alternating method, and the coupled collocation and finite element method. Governing equations investigated include Laplace, Poisson, Helmholtz and bi-harmonic equations. Regular boundary value problems, boundary value problems with singularity, and eigenvalue problems are also examined. Rigorous mathematical proofs are contained in these chapters, and many numerical experiments are also provided to support the algorithms and to verify the theory. A tutorial on the applications of these methods is also provided.

ISBN: 978-1-84564-153-5 2007
apx 400pp
apx £135.00/US$240.00/€202.50

WITPRESS ...for scientists by scientists

Computational Methods and Experimental Measurements XIII

Edited by: ***C.A. BREBBIA****, Wessex Institute of Technology, UK and* ***G.M. CARLOMAGNO****, University of Naples, Italy*

Containing papers presented at the Thirteenth International conference in this well established series on Computational Methods and Experimental Measurements (CMEM), these proceedings review state-of-the-art developments on the interaction between numerical methods and experimental measurements.

Featured topics include: Computational and Experimental Methods; Experimental and Computational Analysis; Computer Interaction and Control of Experiments; Direct, Indirect and In-Situ Measurements; Particle Methods; Structural and Stress Analysis; Structural Dynamics; Dynamics and Vibrations; Electrical and Electromagnetic Applications; Biomedical Applications; Heat Transfer; Thermal Processes; Fluid Flow; Data Acquisition, Remediation and Processing and Industrial Applications

WIT Transactions on Modelling and Simulation, Vol 46

ISBN: 978-1-84564-084-2 2007 928pp £295.00/US$585.00/€442.50

Find us at http://www.witpress.com

Save 10% when you order from our encrypted ordering service on the web using your credit card.

Advanced Vector Analysis for Scientists and Engineers

Edited by: ***M. RAHMAN****, Dalhousie University, Canada*

Vector analysis is one of the most useful branches of mathematics. It is a highly scientific field that is used in practical problems arising in engineering and applied sciences. Based on notes gathered throughout the many years of teaching vector calculus, the main purpose of the book is to illustrate the application of vector calculus to physical problems. The theory is explained elegantly and clearly and there is an abundance of solved problems to manifest the application of the theory. The beauty of this book is the richness of practical applications. There are nine chapters each of which contains ample exercises at the end. A bibliography list is also included for ready reference. The book concludes with two appendices. Appendix A contains answers to some selected exercises, and Appendix B contains some useful vector formulas at a glance.

This book is suitable for a one-semester course for senior undergraduates and junior graduate students in science and engineering. It is also suitable for the scientists and engineers working on practical problems.

ISBN: 978-1-84564-093-4 2007 320pp £95.00/US$165.00/€142.50